



UNIVERSIDADE DE LISBOA
INSTITUTO SUPERIOR TÉCNICO

Characteristic formulations of general relativity
and applications

Athanasios Giannakopoulos

Supervisor: Doctor Miguel Rodrigues Zilhão Nogueira
Co-Supervisor: Doctor David Matthew Hilditch

Thesis approved in public session to obtain the PhD Degree in Physics
Jury final classification: Pass with Distinction

arXiv:2308.16001v1 [gr-qc] 30 Aug 2023



**UNIVERSIDADE DE LISBOA
INSTITUTO SUPERIOR TÉCNICO**

**Characteristic formulations of general relativity
and applications**

Athanasios Giannakopoulos

Supervisor: Doctor Miguel Rodrigues Zilhão Nogueira

Co-Supervisor: Doctor David Matthew Hilditch

Thesis approved in public session to obtain the PhD Degree in Physics

Jury final classification: Pass with Distinction

Jury

Chairperson: Doctor Vítor Manuel dos Santos Cardoso, Instituto Superior Técnico, Universidade de Lisboa

Members of the Committee:

Doctor Nigel Tempest Bishop, Faculty of Science, Rhodes University, South Africa

Doctor Filipe Artur Pacheco Neves Carteado Mena, Instituto Superior Técnico, Universidade de Lisboa

Doctor David Matthew Hilditch, Instituto Superior Técnico, Universidade de Lisboa

Doctor Edgar Gasperín Garcia, Instituto Superior Técnico, Universidade de Lisboa

Doctor Stephen Green, Max-Planck-Institut für Gravitationsphysik, Albert-Einstein-Institute, Germany

Doctor Justin L. Ripley, Department of Physics, The Grainger College of Engineering, University of Illinois Urbana-Champaign, USA

Funding Institutions:

Fundação para a Ciência e a Tecnologia Grants No. PD/BD/135425/2017,
COVID/BD/152483/2022 and BL68/2022-IST-ID

2022

Resumo

A relatividade geral descreve vários sistemas gravitacionais de relevância astrofísica, como buracos negros e estrelas de neutrões. Pode também descrever sistemas fortemente acoplados através da dualidade holográfica. Além disso, são tópicos de investigação ativa também aspectos mais formais da teoria, como a estabilidade de espaços-tempos e a formação de singularidades. Muitas vezes, soluções a problemas em aberto não são conhecidas em forma analítica e quando os métodos perturbativos são inadequados é preciso utilizar técnicas numéricas.

O problema valores iniciais (e fronteira) característicos tem muitas aplicações na relatividade geral, envolve geralmente estudos numéricos e, frequentemente, é formulado usando coordenadas de tipo Bondi. A boa-formulação dos sistemas resultantes das equações diferenciais parciais, no entanto, permanece uma questão em aberto. A resposta a esta pergunta afeta a precisão e, potencialmente, a confiabilidade das conclusões extraídas de estudos numéricos baseados em tais formulações. Uma aproximação numérica pode convergir para o limite do contínuo apenas para sistemas bem-formulados. A noção de boa-formulação está intimamente relacionada à da hiperbolicidade e inclui a especificação de uma norma.

Na primeira parte desta tese, expandimos a nossa compreensão da hiperbolicidade e da boa-formulação de sistemas de evolução livre de tipo Bondi. Mostramos que vários protótipos de formulações de tipo Bondi são apenas fracamente hiperbólicos e examinamos a causa desse resultado. Numa análise linear identificamos a gauge, as restrições e os blocos físicos na parte principal das equações de campo de Einstein nessa gauge, e mostramos que o subsistema relacionado com as variáveis de gauge é apenas fracamente hiperbólico. A hiperbolicidade fraca do sistema completo segue como consequência em vários casos. Demonstramos também isso explicitamente em através de exemplos e, portanto, argumentamos que gauge de tipo Bondi resultam em sistemas de evolução livre fracamente hiperbólicos sob condições bastante gerais. Consequentemente, o problema dos valores iniciais característicos em relatividade geral nestas gauges torna-se mal-formulado nas normas mais simples que se gostaria de utilizar. Discutimos as implicações deste resultado em métodos de modelagem precisos de sinais de ondas gravitacionais e trabalhamos para a construção de normas alternativas que possam ser mais apropriadas. Também apresentamos testes numéricos que

demonstram a hiperbolicidade fraca na prática e sublinham as características importantes para realizá-los de forma eficaz.

Na segunda parte, dirigimos a nossa atenção para aplicações dessas formulações em sistemas fortemente acoplados via holografia. O objectivo principal é perceber o comportamento qualitativo de plasmas fortemente acoplados, mas devido á fraca hiperbolicidade, não podemos realizar estimativas de erro rigorosas. Apresentamos ainda o *Jecco*, um código característico recentemente desenvolvido que nos permite simular a dinâmica de plasmas fortemente acoplados. São fornecidos também exemplos representativos das simulações que podem ser realizadas com este código, nomeadamente a dinâmica fora de equilíbrio de plasmas que sofrem transições de fase. Este pode ser um dos cenários do universo primitivo e estas simulações podem fornecer respostas sobre questões de natureza fundamental.

Palavras-chave: Relatividade geral; Ondas gravitacionais; Formulações características; Hiperbolicidade; Boa-formulação.

Abstract

General relativity can describe various gravitational systems of astrophysical relevance, like black holes and neutron stars, or even strongly coupled systems through the holographic duality. In addition, more formal aspects of the theory like the stability of spacetimes and the formation of singularities are still topics of active research. In several cases, solutions in closed analytic form are not known, and perturbative methods are inadequate, leading to the employment of numerical techniques.

The characteristic initial (boundary) value problem has numerous applications in general relativity involving numerical studies and is often formulated using Bondi-like coordinates. Well-posedness of the resulting systems of partial differential equations, however, remains an open question. The answer to this question affects the accuracy, and potentially the reliability of conclusions drawn from numerical studies based on such formulations. A numerical approximation can converge to the continuum limit only for well-posed systems. The notion of well-posedness is tightly related to that of hyperbolicity and includes the specification of a norm.

In the first part of this thesis, we expand our understanding of the hyperbolicity and well-posedness of Bondi-like free evolution systems. We show that several prototype Bondi-like formulations are only weakly hyperbolic and examine the root cause of this result. In a linear analysis we identify the gauge, constraint and physical blocks in the principal part of the Einstein field equations in such a gauge, and we show that the subsystem related to the gauge variables is only weakly hyperbolic. Weak hyperbolicity of the full system follows as a consequence in many cases. We demonstrate this explicitly in specific examples, and thus argue that Bondi-like gauges result in weakly hyperbolic free evolution systems under quite general conditions. Consequently, the characteristic initial (boundary) value problem of general relativity in these gauges is rendered ill-posed in the simplest norms one would like to employ. We discuss the implications of this result in accurate gravitational waveform modeling methods and work towards the construction of alternative norms that might be more appropriate. We also present numerical tests that demonstrate weak hyperbolicity in practice and highlight important features to perform them effectively.

In the second part, we turn our attention to applications of these formulations to strongly coupled systems via holography. We expect these studies to shed more

light on the qualitative behavior of strongly coupled plasmas, but due to weak hyperbolicity, we cannot perform rigorous error estimates to our satisfaction. We present *Jecco*, a newly developed characteristic code that allows us to simulate the dynamics of strongly coupled plasmas. Representative examples of the simulations that can be achieved with this code are provided, namely the out-of-equilibrium dynamics of said plasmas that undergo phase transitions. This is a possible scenario of the early universe and such simulations might provide insights into questions of fundamental nature.

Key-words: General relativity; Gravitational waves; Characteristic formulations; Hyperbolicity; Well-posedness.

to my parents

Acknowledgements

Reaching the end of my PhD, I realize that I have had an amazing experience during this adventure and for this I am grateful to a number of people.

Miguel and David, thank you for all the guidance, patience, teaching, and understanding all these years. I really appreciate the time you took and the effort you made, from the early days sitting next to me and helping me fix bugs and errors, to the many whiteboard calculations and the numerous online discussions later on. I have learned a lot next to you, growing both personally and professionally. I believe that the PhD is a unique experience for each person, and I definitely feel lucky to have done it under your supervision.

To all my collaborators, thank you for all the work we did together, as well as for all the scientific interaction we had. It has been very exciting and educational for me. Especially to Nigel, Denis, Yago and Mikel, thank you for the hours we spent together discussing science.

I am thankful to all the Jury members for their time and care in reading this thesis, as well as their questions, comments and suggestions.

I am grateful to all the GRIT and CENTRA members for creating a friendly and vibrant atmosphere. It has been a pleasure to be a member of this team. Especially to all my fellow PhD colleagues and office-mates, thank you for all the time we spent together and all the discussions we had. You made my time there more interesting and memorable.

To Sérgio, Manuel, João, and all the IT team of CENTRA, thank you for your constant availability and hard work. You provided crucial support, helped me with many technical problems, and allowed me to stay focused on my work. The same goes for Rita Sousa. You have always been there helping me with all sorts of bureaucratic issues that appeared and made my life easier. I really appreciate it.

Special thanks goes to Miguel Duarte for his help and suggestions with the early manuscript.

Lorenzo and Kyriako, I deeply thank you for your friendship, you took the Lisbon experience to another level for me and I will always remember our times together. Diogo, Vera, and Rebecca, it has been amazing living with you. You made me

feel at home, I am grateful to you. Isa, colega, it has been great sharing this academic path and all its challenges and frustrations, thank you. Fernanda, Arianna, Rodrigo, Francisco, Krinio, Stefano, thank you all, it has been great sharing time and experiences with you.

To my life-long friends from Greece, thank you all for your friendship, it means a lot to me. Panteli, the online coffee meetings have definitely made the pandemic period better.

To Chrysalena, my long-time partner, you have always been my constant companion all these years and in many adventures. I cannot thank you enough for all your love, understanding, and patience. I love you.

To my family, my brother and my parents, I cannot imagine how I would have done this without you. I am deeply grateful for all your support and help, all these years, in pursuing my dreams. I appreciate everything you have done for me. You are always in my heart.

Finally, I am grateful to the Fundação para a Ciência e a Tecnologia for funding this work via the grants PD/BD/135425/2017, COVID/BD/152483/2022 and BL68/2022-IST-ID and to the GWverse COST Action CA16104, “Black holes, gravitational waves and fundamental physics” for networking and partial financial support. I am also grateful to the CENTRA/IST cluster “Baltasar-Sete-Sóis”, and the MareNostrum supercomputer at the BSC, for providing computational resources and technical expertise that helped completing this work.

Contents

List of Figures	xiii
1 Introduction	1
1.1 Preliminaries	2
1.2 Motivation	6
1.3 Thesis outline and main results	9
I Hyperbolicity and well-posedness	13
2 A PDE theory toolbox	15
2.1 PDE classes and causal definitions	15
2.2 Degree of hyperbolicity	18
2.3 Well-posedness and norms	19
3 Properties of Bondi-like characteristic formulations	23
3.1 Main features of Bondi-like formulations	23
3.2 From the characteristic to the ADM equations	26
3.3 Coordinate light speeds	30
4 Gauge fixing and the principal symbol	33
4.1 FT2S Systems and their principal part	33
4.2 Pure gauge and constraint subsystems	34
4.3 Projection operators	37
4.4 Discussion	39
5 Hyperbolicity of Bondi-like PDE systems	41
5.1 The affine null gauge	44
5.1.1 Pure gauge subsystem	44
5.1.2 Pure gauge sub-block: radial direction	45
5.1.3 Pure gauge sub-block: angular direction θ	50
5.1.4 Asymptotically anti-de Sitter spacetimes	54
5.2 The Bondi-Sachs gauge proper	60
5.2.1 Pure gauge subsystem	61
5.2.2 Pure gauge sub-block: angular direction θ	62
5.2.3 Axisymmetry in characteristic variables	63
5.3 Double-null and more gauges	67

5.4	Frame independence	69
5.5	Conclusions	72
6	Well-posedness of Bondi-like PDE problems	73
6.1	Toy model PDEs	74
6.2	Algebraic determination of well-posedness	75
6.2.1	Homogeneous WH model	76
6.2.2	Inhomogeneous WH model	77
6.3	Toy CCE and CCM energy estimates	78
6.4	Energy estimates for the axisymmetric Bondi-Sachs system	82
6.5	CIBVP energy estimates for symmetric hyperbolic PDEs	86
6.5.1	Domain \mathcal{D}_1	87
6.5.2	Domain \mathcal{D}_2	90
6.6	Conclusions	93
7	Numerical Experiments	95
7.1	Toy models	95
7.1.1	Implementation	95
7.1.2	Convergence tests	96
7.2	GR in the Bondi-Sachs proper gauge	104
7.2.1	The setup	104
7.2.2	Convergence tests	108
7.3	Conclusions	111
II	Applications to holography	113
8	Numerical holography with Jecco	115
8.1	Jecco: a new characteristic code for numerical holography	117
8.1.1	Equations	117
8.1.2	Implementation	127
8.2	Testing the code	130
8.2.1	Analytical black brane	130
8.2.2	Comparison with SWECC	132
8.2.3	Convergence tests	132
8.3	Simulating strongly coupled systems	136
8.3.1	Spinodal instability	138
8.3.2	Bubbles	141
9	Final remarks	143

III	Appendix	147
A	Appendix for part I	149
A.1	The divergence theorem	149
A.2	The Grönwall inequality	149
A.3	A symmetric hyperbolic affine null PDE system	150
B	Appendix for part II	154
B.1	Radial equations	154
B.2	Apparent horizon finder	158
	References	163

List of Figures

1.1	Examples of conformal diagrams	5
1.2	CCE and CCM depiction	7
3.1	Coordinate light speeds	32
5.1	CIBVP: characteristic to auxiliary Cauchy setup	42
6.1	Model Cauchy-Characteristic extraction (CCE) and matching (CCM) setups	78
6.2	CIBVP energy estimates for symmetric hyperbolic PDEs: domain \mathcal{D}_1	87
6.3	CIBVP energy estimates for symmetric hyperbolic PDEs: domain \mathcal{D}_2	90
7.1	The final profiles of fields ϕ , ψ_v and ψ for the toy model numerical experiments	99
7.2	Pointwise convergence for toy model numerical experiments	100
7.3	The self convergence ratio in the L^2 -norm for toy model numerical experiments	101
7.4	The exact convergence ratio in the lopsided norm for the weakly hyperbolic toy model numerical experiments	103
7.5	Self and exact convergence tests with the PITTNULL code	108
7.6	Exact convergence tests with noisy data with the PITTNULL code, using only the null part of the norm	111
8.1	Illustration of Jecco 's evolution algorithm	126
8.2	Jecco relative errors for outer spectral domains	131
8.3	Jecco 's benchmark against SWEC	133
8.4	Pointwise and norm convergence tests solely with Jecco	135
8.5	Numerical violation of the total energy of gauge theory box in Jecco simulation	136
8.6	The spinodal region on phase diagrams	139
8.7	Evolution of the spinodal instability	140
8.8	Phase-separated configurations produced with Jecco	142
A.1	Divergence theorem: the orientation of the vector normal to the boundary	149

Preface

The research presented in this thesis has been carried out at the Center for Astrophysics and Gravitation (CENTRA) in the Physics department of Instituto Superior Técnico - Universidade de Lisboa.

I declare that this thesis is not substantially the same as any that I have submitted for a degree, diploma or other qualification at any other university and that no part of it has already been or is concurrently submitted for any such degree, diploma or other qualification.

The following thesis has been the result of several collaborations.

A complete list of the articles included in this thesis is displayed below:

Part I

- ◇ [1]: T. Giannakopoulos, D. Hilditch, and M. Zilhão, “Hyperbolicity of General Relativity in Bondi-like gauges”, *Phys. Rev. D* **102**, 064035 , [arXiv:2007.06419 \[gr-qc\]](#)
- ◇ [2]: T. Giannakopoulos, N. T. Bishop, D. Hilditch, D. Pollney, and M. Zilhão, “Gauge structure of the Einstein field equations in Bondi-like coordinates”, *Phys. Rev. D* **105**, 084055 , [arXiv:2111.14794 \[gr-qc\]](#)

Part II

- ◇ [3] Y. Bea, J. Casalderrey-Solana, T. Giannakopoulos, A. Jansen, S. Krippendorff, D. Mateos, M. Sanchez-Garitaonandia, and M. Zilhão, “Spinodal Gravitational Waves”, [arXiv:2112.15478 \[hep-th\]](#)
- ◇ [4]: Y. Bea, J. Casalderrey-Solana, T. Giannakopoulos, A. Jansen, D. Mateos, M. Sanchez-Garitaonandia, M. Zilhão, “Holographic Bubbles with Jecco: Expanding, Collapsing and Critical”, *J. High Energy Phys.* **2022**, 8 (2022) , [arXiv:2202.10503 \[hep-th\]](#)

The following articles include work of the author of this thesis but are not discussed here:

- ◇ [5]: Y. Bea, O. J. C. Dias, T. Giannakopoulos, D. Mateos, M. Sanchez-Garitaonandia J. E. Santos, and M. Zilhão, “Crossing a large-N phase

- transition at finite volume”, *J. High Energ. Phys.* 2021, 61 (2021) ,
[arXiv:2007.06467 \[hep-th\]](#)
- ◇ [6]: Y. Bea, J. Casalderrey-Solana, T. Giannakopoulos, D. Mateos, M. Sanchez-Garitaonandia, and M. Zilhão, “Bubble Wall Velocity from Holography”, *Phys. Rev. D* 104, L121903, [arXiv:2104.05708 \[hep-th\]](#)
- ◇ [7]: Y. Bea, J. Casalderrey-Solana, T. Giannakopoulos, D. Mateos, M. Sanchez-Garitaonandia, and M. Zilhão, “Domain Collisions”, *J. High Energ. Phys.* 2022, 25 (2022), [arXiv:2111.03355 \[hep-th\]](#)

Acronyms

AAdS	Asymptotically Anti-de Sitter
ADM	Arnowitt-Deser-Misner
AdS	Anti-de Sitter
CCE	Cauchy-Characteristic Extraction
CCM	Cauchy-Characteristic Matching
CIBVP	Characteristic Initial Boundary Value Problem
CIVP	Characteristic Initial Value Problem
DF	Dual Frame
EFE	Einstein Field Equations
GR	General Relativity
GW	Gravitational Wave
IBVP	Initial Boundary Value Problem
IVP	Initial Value Problem
ODE	Ordinary Differential Equation
PDE	Partial Differential Equation
SH	Strongly Hyperbolic
WH	Weakly Hyperbolic

CHAPTER 1

Introduction

Contents

1.1	Preliminaries	2
1.2	Motivation	6
1.3	Thesis outline and main results	9

General relativity (GR) is a theory of gravity introduced by Albert Einstein in 1915 [8, 9]. Since its creation, GR has granted us with several predictions that have been verified by experimental tests, such as the recent detections of the gravitational wave (GW) signals produced by binaries of compact objects like black holes and neutron stars [10–14], and the observation of black hole shadows [15, 16]. To make these predictions, one has to solve the equations of motion of GR, which form a system of coupled, non-linear partial differential equations (PDEs). Generically, this is a particularly difficult problem to solve and various techniques may be employed in different regimes and setups.

Fully analytical solutions to the Einstein field equations (EFE) are possible in limited cases [17], such as those with high symmetry e.g. the Minkowski, anti-de Sitter (AdS), Schwarzschild [18], and Kerr spacetimes [19]. However, many gravitational systems of interest do not fall into this category and hence different methods are needed to understand their behavior. Perturbative schemes can provide good approximations in various scenarios, for instance in the inspiral and ringdown phases during the evolution of a binary formed by compact objects. The merger phase however is highly non-linear, which makes many perturbative treatments inadequate there. A way to find solutions for gravitational systems in the highly dynamical, non-linear, strong gravity regime like the merger is by means of numerical methods. The subfield of gravitational research that exploits these methods to obtain approximate solutions to the EFE is often called *numerical relativity*.

A physical process in GR does not depend on the way we choose to describe it. Motivated by the special features and symmetries of a specific gravitational setup, we choose appropriate coordinates to express its spacetime, for example in a setup with spherical symmetry, spherical polar coordinates can be a good choice. In numerical relativity, we typically use coordinates to foliate the spacetime with hypersurfaces of a constant coordinate that we associate with

time. Quite frequently these hypersurfaces are spacelike, for instance when modeling the region near the merger of two compact objects. In other cases, it is more convenient to employ null hypersurfaces. This setup is called *characteristic* and the coordinate that labels the different hypersurfaces is the advanced or retarded time. In GR the speed of light is the upper bound at which physical signals can propagate and defines the causal structure of spacetime. This is also the speed at which GWs travel and together with light rays, they move along null hypersurfaces. Hence, characteristic formulations are particularly convenient to describe radiative processes in GR.

1.1 Preliminaries

This section is a collection of some tools that are useful in this thesis. For a more complete presentation one can consult standard textbooks of GR, e.g. [20–23].

GR adopts a geometric viewpoint for gravity and makes extensive use of differential geometry as a tool. A central object is the differentiable manifold, typically denoted by \mathcal{M} . Let us assume that \mathcal{M} is covered by a set of coordinates x^μ , where $\mu = 0, 1, 2, \dots, n - 1$ for a n -dimensional manifold. Let also V_p be the space tangent to a point p of \mathcal{M} . Then $\partial_\mu \equiv \partial/\partial x^\mu$ defines an element of a coordinate basis for V_p . A vector \mathbf{v} on V_p can be expressed in this basis via

$$\mathbf{v} = v^\mu \partial_\mu,$$

where v^μ are the n components of \mathbf{v} in the basis $\{\partial_\mu\}$. We use the Einstein summation convention throughout, i.e. repeated indices imply summation. If we use a different basis $\bar{\partial}_{\mu'}$ induced by coordinates $\bar{x}^{\mu'}$, then the components of \mathbf{v} between the two bases are related via

$$\bar{v}^{\nu'} = v^\mu \frac{\partial x^{\nu'}}{\partial x^\mu}.$$

A vector space V_p^* dual to V_p can be defined and the vectors that live on it are called dual vectors. Given a vector \mathbf{v} and a dual vector \mathbf{w} there is a bracket operation $\langle \mathbf{v}, \mathbf{w} \rangle$ that returns a number. The elements dx^μ can provide a coordinate basis for dual vectors defined via

$$\langle dx^\mu, \partial_\nu \rangle = \delta^\mu_\nu,$$

with $\delta^\mu_\nu = 1$ for $\mu = \nu$ and 0 otherwise. A dual vector \mathbf{w} can be expressed in this basis via

$$\mathbf{w} = w_\mu dx^\mu,$$

where w_μ are its components in the basis $\{dx^\mu\}$ and obey the transformation rule

$$\bar{w}_{\nu'} = w_\mu \frac{\partial x^\mu}{\partial x^{\nu'}},$$

to a different basis $\{\bar{d}x^{\mu'}\}$ induced by the coordinates $\bar{x}^{\mu'}$.

A tensor T of rank (k, l) is a generalization of vectors and dual vectors, which takes k dual vectors and l vectors and returns a number. The bases $\{\partial_\mu\}$ and $\{dx^\mu\}$ induced by the coordinates x^μ on \mathcal{M} provide a basis for tensors as well, in which the components of T are written as

$$T^{\mu_1 \dots \mu_k}_{\nu_1 \dots \nu_l}.$$

For brevity we may say that these are the components of the tensor T on the basis x^μ , implying the tensor basis induced by the coordinates. The components of the tensor T on the basis $\bar{x}^{\mu'}$ are related to those on x^μ via the following transformation rule:

$$\bar{T}^{\mu'_1 \dots \mu'_k}_{\nu'_1 \dots \nu'_l} = T^{\mu_1 \dots \mu_k}_{\nu_1 \dots \nu_l} \frac{\partial \bar{x}^{\mu'_1}}{\partial x^{\mu_1}} \dots \frac{\partial \bar{x}^{\mu'_k}}{\partial x^{\mu_k}} \frac{\partial x^{\nu_1}}{\partial \bar{x}^{\nu'_1}} \dots \frac{\partial x^{\nu_l}}{\partial \bar{x}^{\nu'_l}}.$$

A special tensor is the metric g , a symmetric tensor of rank $(0, 2)$. It allows us to measure the infinitesimal square distance ds between two points on \mathcal{M} via

$$ds^2 = g_{\mu\nu} dx^\mu dx^\nu,$$

as well as define the inner product between two vectors \mathbf{u}, \mathbf{v} through

$$\mathbf{u} \cdot \mathbf{v} \equiv g_{\mu\nu} u^\mu v^\nu.$$

The metric also allows us to raise and lower indices of any tensor e.g. given the components v^μ of a vector \mathbf{v} —which is a tensor of rank $(1, 0)$ —we can obtain the components v_μ of its dual vector

$$v_\mu = g_{\mu\nu} v^\nu.$$

Finally, given a metric we can always find a basis of V_p^* such that $g_{\mu\nu} = 0$ if $\mu \neq \nu$ and $g_{\mu\nu} = \pm 1$ if $\mu = \nu$. The number of $+$ and $-$ signs occurring in this basis is called the signature of the metric. If there are no $-$ signs, the metric is positive definite and is called Riemannian. In GR the spacetime is understood as a manifold equipped with a metric of signature $(-, +, \dots, +)$ ¹, which is called a Lorentzian manifold.

¹It can also be $(+, -, \dots, -)$ if another convention is adopted.

To understand how tensors change on a manifold, the notion of tensorial differentiation is needed. A covariant derivative ∇ takes a tensor of rank (k, l) to one of rank $(k, l + 1)$ and can be written as

$$\nabla_\lambda T^{\mu_1 \dots \mu_k}_{\nu_1 \dots \nu_l} = \partial_\lambda T^{\mu_1 \dots \mu_k}_{\nu_1 \dots \nu_l} + \Gamma^{\mu_1}_{\lambda\sigma} T^{\sigma \dots \mu_k}_{\nu_1 \dots \nu_l} + \dots - \Gamma^\sigma_{\lambda\nu_1} T^{\mu_1 \dots \mu_k}_{\sigma \dots \nu_l} - \dots,$$

in the basis x^μ , where $\Gamma^\mu_{\nu\sigma}$ is called the connection and is symmetric in ν, σ . The connection does not transform as a tensor and essentially provides a way to relate the tensor bases of different points on the manifold. There are different ways to define ∇ , but in GR we often choose a metric compatible covariant derivative, that is

$$\nabla_\sigma g_{\mu\nu} = 0.$$

Metric compatibility and the symmetry of the connection allow one to fully determine it from the metric via

$$\Gamma^\alpha_{\beta\gamma} = \frac{1}{2} g^{\alpha\delta} (\partial_\gamma g_{\delta\beta} + \partial_\beta g_{\delta\gamma} - \partial_\delta g_{\beta\gamma}).$$

This connection is called the Christoffel symbol. The metric can also help us build the Riemann curvature tensor, the components of which in the x^μ basis can be written as

$$R^\alpha_{\beta\gamma\delta} = \partial_\gamma \Gamma^\alpha_{\beta\delta} - \partial_\delta \Gamma^\alpha_{\beta\gamma} + \Gamma^\alpha_{\lambda\gamma} \Gamma^\lambda_{\beta\delta} - \Gamma^\alpha_{\lambda\delta} \Gamma^\lambda_{\beta\gamma}.$$

The Ricci tensor and scalar can be defined by the relations

$$R_{\mu\nu} \equiv R^\lambda_{\mu\lambda\nu}, \quad R \equiv g^{\mu\nu} R_{\mu\nu},$$

respectively. The EFE relate the curvature of the spacetime to its matter content via

$$G_{\mu\nu} + \Lambda g_{\mu\nu} = \kappa T_{\mu\nu},$$

where

$$G_{\mu\nu} \equiv R_{\mu\nu} - \frac{1}{2} R g_{\mu\nu},$$

is the Einstein tensor, Λ is the cosmological constant, $T_{\mu\nu}$ is the stress-energy tensor of matter, and $\kappa \equiv 8\pi G c^{-4}$, with G the Newton's constant and c the speed of light. The EFE can be derived as the Euler-Lagrange equations of the action

$$S = \int \left[\frac{1}{2\kappa} (R - 2\Lambda) + \mathcal{L}_M \right] \sqrt{-g} d^n x,$$

by varying with respect to the inverse metric, where \mathcal{L}_M is the Lagrangian density for the matter content that vanishes in vacuum.

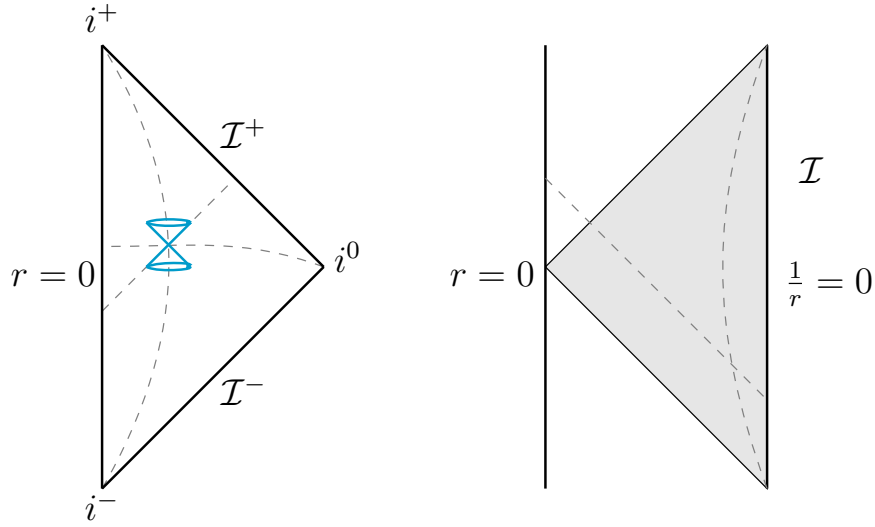


Figure 1.1: The conformal (or Carter-Penrose) diagrams for Minkowski (left), and AdS (right) spacetimes. Only two dimensions are depicted, the time and radius. If the spacetime is 4-dimensional and we use spherical polar coordinates, each point represents a two-sphere of radius r . In asymptotically flat spacetimes, there are the past and future temporal infinities, future and past null infinities and spatial infinity, denoted by i^- , i^+ , \mathcal{I}^- , \mathcal{I}^+ and i^0 , respectively. The causal structure on the conformal diagram is the same as the full spacetime it depicts and is illustrated by a light-cone on the left diagram. The asymptotic boundary \mathcal{I} of AdS is timelike. The shaded region is the Poincare patch of AdS.

The speed of light is constant for every observer in GR and is the fastest speed at which a physical signal can travel. These properties make trajectories of light and null hypersurfaces essential in understanding the causal structure of the spacetime. This is a global property of the spacetime and is better understood using conformal diagrams, introduced by Penrose [24]. Examples of such diagrams are shown in Fig. 1.1 for Minkowski (left) and a region of AdS spacetime, called the Poincare patch (see e.g. [25] for more details).

Finally, we should mention that in this work we sometimes use the abstract index notation, see for instance Sec. 2.4 of [21] for details. Briefly, in this notation, a tensor T of type (k, l) is denoted as

$$T^{a_1 \dots a_k}{}_{b_1 \dots b_l}.$$

The lowercase Latin indices here are reminders of the number and type of variables the tensor acts on and not basis components. Using the abstract index notation one can write true tensor equations that are valid in any basis.

For the rest of the thesis we adopt the geometric unit convention i.e. $G = c = 1$.

1.2 Motivation

There are several areas where characteristic formulations of GR have advantages over more standard spacelike foliations. In the next few paragraphs we attempt to provide a quick and non-exhaustive overview of some, which is meant to serve mainly as a motivation for the work of the thesis.

Precision gravitational wave astronomy

Arguably, one of the major and most timely areas where characteristic formulations of GR find use is that of accurate gravitational waveform modeling. A waveform here typically refers to the GW signal detected when a binary system of two compact objects inspirals, merges and relaxes to a final compact object. Given the increasing sensitivity of GW detectors—ground-based interferometers such as the advanced LIGO, Virgo and Kagra [26–28], future space-borne detectors like TianQin [29], Taiji [30], LISA [31], and the Einstein Telescope [32]—waveforms of high fidelity are essential to maximize the discovery potential. Collections of these waveforms form catalogues which are then compared against observational data and consequently the fundamental properties of the sources are inferred. These catalogues require high numbers of different waveforms, and so finding economic but accurate techniques to produce them is a topic of extensive research. Some of these methods are the effective-one-body formalism [33], phenomenological waveforms [34], and numerical relativity surrogates [35]. Nevertheless, numerical relativity approximations are still necessary to a large extent, e.g. to calibrate some of the aforementioned models.

In the modeling process, a GW detector is typically assumed to be infinitely far away from the source. After emission, GWs propagate towards future null infinity at the speed of light, where they can be detected. Since characteristic formulations are based on null hypersurfaces, future null infinity can be naturally included in the computational domain. This is the region where quantities such as the Bondi news function, that provides a way to determine the energy flux of gravitational radiation, are unambiguously defined. Different approaches can be exploited to compute such quantities at infinity accurately. A common one is to solve the initial boundary value problem (IBVP) for two compact object in GR using a spacelike formulation, for a finite region of spacetime. After solving the same IBVP, but placing the outer boundary of the computational domain at different radii r_{out} , an extraction process that utilizes an $1/r$ expansion can be used to compute the GW signal at null infinity. This is an extrapolation technique that allows us to understand the signal at infinity by data in a finite region, but also introduces systematic errors which contaminate the accuracy of the waveform [36].

To avoid such errors an alternative method has been proposed, which comes by the name

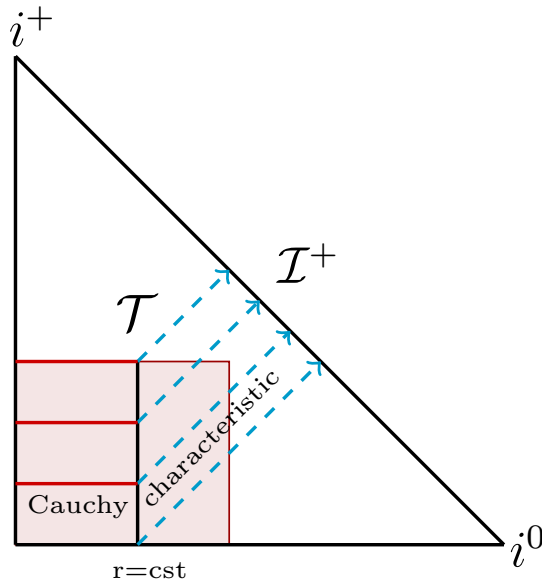


Figure 1.2: Depiction of the Cauchy-Characteristic extraction and matching setups for an asymptotically flat spacetime. The Cauchy setup is used to model the region near the GW source and the characteristic one the propagation of GW to future null infinity. The worldtube \mathcal{T} is the boundary between the Cauchy and characteristic domains. In CCE, information flows only from the Cauchy to the characteristic domain, whereas in CCM it is communicated both ways, that is the Cauchy and characteristic problems are solved simultaneously.

of *Cauchy-Characteristic Extraction* (CCE) [37–51]. The term *Cauchy*² here refers to the IBVP constructed using a more standard spacelike formulation. Once a numerical approximation is obtained for the PDE problem, the information is communicated to another domain where GR is formulated using the characteristic approach. The latter is the characteristic initial boundary value problem (CIBVP) of GR and the boundary is the outer domain of the IBVP through which information from the spacelike to the characteristic domain is communicated. In CCE the Cauchy problem is solved first and the characteristic follows i.e. the information through the boundary flows only from the Cauchy to the characteristic domain. Even though CCE improves the waveform accuracy and has even been used as a benchmark to evaluate the error from extrapolation techniques, it is still prone to errors that arise from artificial boundary conditions imposed during the evolution. The *Cauchy-Characteristic Matching* (CCM) method goes a step further and suggests a solution for these errors as well [36, 52, 53]. The way to do this is to solve the Cauchy-type and the characteristic problems simultaneously and allow for information to move via their

²Note the abuse of the term *Cauchy* here, since the data on this spacelike hypersurface cannot provide information for the whole spacetime and boundary data are necessary. To avoid possible confusion, we use the term *Cauchy-type* instead for such setups.

common boundary in both ways, and not just from the spacelike to the characteristic domain. Then, no artificial boundary conditions need to be imposed for the IBVP. In Fig. 1.2 the CCE and CCM setups are depicted for an asymptotically flat spacetime. To the best of our knowledge, CCE has been implemented for GR successfully in the sense that the relevant codes can run for large timescales, but CCM has only done so for the wave equation [54, 55].

For completeness, we should mention that characteristic formulations are not the only strategy to include null infinity in the computational domain. One alternative is the hyperboloidal approach, which uses hypersurfaces that are everywhere spacelike but become null only at infinity [56–64]. One advantage is that hyperboloids can be used both in the near and far zones of the source. On the contrary, null trajectories are expected to form caustics in the near zone, which makes the use of the characteristic approach there challenging. Another alternative is the conformal approach to the EFE [65–67]. Both strategies come with their own advantages and challenges and are topics of active research. We will not elaborate more on them however since they are beyond the scope of this thesis.

Strongly coupled systems and numerical holography

In addition to astrophysically relevant setups, numerical relativity can provide insights into strongly coupled systems when combined with holography. Holography roughly states that in certain limits a classical gravitational theory can be mapped to a non-gravitational, strongly coupled quantum field theory, that resides in one dimension less [68, 69]. A particular realization of this duality comes through the AdS/CFT conjecture, proposed by Maldacena [70]. This correspondence provides us with the ability to explore the dynamics of strongly coupled quantum field theory systems via the equations of motion of classical gravitational ones.

Typically, the gravitational theory under consideration is GR, with or without matter content. By solving the equations of motion on the gravity side one hopes to obtain qualitative results and universal relations of strongly coupled systems. One such example is the universality of the viscosity-entropy ratio for strongly coupled plasmas [71], which has been in good agreement with experimental data [72]. Characteristic formulations of GR and numerical relativity tools are often used to follow the out-of-equilibrium behavior of strongly coupled plasmas that can be formed in terrestrial heavy ion collisions [72]. They are also believed to exist in the early universe and undergo phase transitions and turbulent flows that can produce GWs [73], which may be detected by future detectors like LISA [74]. This line of research has also provided insights into the applicability of hydrodynamics in describing the near and out-of-equilibrium processes of these systems, which can be helpful for improving relevant fluid dynamics codes [75–77]. Cauchy-type setups are also used in holographic studies and can model e.g. confinement-deconfinement transitions in these plasmas [78, 79], but are not discussed in this thesis.

Mathematical relativity and more

Characteristic formulations have found extensive use in mathematical relativity as well. For example, in [80] they were used to show the instability of the AdS spacetime in spherical symmetry with reflective boundary conditions at infinity, in [81] to study the formation conditions for black holes and singularities, and in [82–84] to understand the stability properties of black hole spacetimes. In the study of gravitational collapse, codes based on null foliations offer a practical alternative to the standard spacelike foliation approach. Their advantage lies in the compactness of the system of PDEs solved [85–89] as well as the inclusion of null infinity in the computational domain. The aforementioned setups are usually considered in asymptotically flat geometries; though see [90, 91] for gravitational collapse in asymptotically AdS (AAAdS) spacetimes.

Characteristic setups have also been efficient in studying isolated gravitational objects, as e.g. relativistic stars [92, 93]. In fact, the first stable evolution of isolated black holes has been achieved in characteristic formulations [94, 95]. They have also been utilized in the study of the superradiant instability in AAAdS spacetimes [96] and even in explorations of cosmological scenarios [97]. Finally, they play an important role in the fluid/gravity correspondence [98–100].

1.3 Thesis outline and main results

In this thesis we focus on characteristic formulations of GR and their applications, and adopt the standpoint of numerical relativity. The thesis is divided in three parts, with the first and second composing the main body, while the third being appendix material.

In Part I we analyze the hyperbolicity and well-posedness of the vacuum EFE in Bondi-like characteristic coordinates. The characteristic problem of GR is commonly formulated using this type of coordinates (or gauges). Since the central interest of this part is hyperbolicity and well-posedness, these notions are introduced briefly in Chap. 2 together with other necessary textbook material of PDE analysis. The main properties of Bondi-like characteristic formulations are presented in Chap. 3, along with the mapping of the associated PDEs to the Arnowitt-Deser-Misner (ADM) formulation of GR. The latter is a tool we use to understand the pure gauge structure of Bondi-like PDEs, the notion of which was introduced in [101] and we briefly present in Chap. 4. The material presented in these three chapters is employed in an extensive hyperbolicity analysis of some common Bondi-like systems, which is the topic of Chap. 5. More specifically, we analyse the vacuum EFE in the affine null, the Bondi-Sachs proper and the double null coordinates and find that all these systems are only weakly hyperbolic (WH). We identify the pure gauge structure of the angular sector of the systems as the root cause of weak hyperbolicity. We further conjecture that PDE systems which result from the EFE and include up to second order metric derivatives are at most WH beyond spherical symmetry, if they are constructed in a Bondi-like gauge.

In light of this result we investigate the implications to the well-posedness of the CIBVP of GR in Bondi-like gauges, in Chap. 6. We start by introducing toy models and determine the conditions and norms in which their CIBVP is well-posed. We find that the CIBVP of the strongly hyperbolic (SH) toy model is well-posed in a version of the common L^2 -norm adapted to the characteristic setup, as expected. The WH model that mimics the structure of Bondi-like systems is weakly well-posed in a lopsided norm that is not equivalent to L^2 . However, this version of well-posedness is weaker than that of the SH system, since it is affected by lower order source terms. We identify the structure of the source terms that breaks this weak well-posedness. Based on the aforementioned systems, we examine well-posedness of model CCE and CCM setups. The former is weakly well-posed for the WH toy model, whereas the latter is ill-posed when the Cauchy-type setup is formulated with the SH model and the characteristic with the WH one. The associated IBVP and CIBVP for this CCM model are separately well-posed in norms that are incompatible with each other and hence the composite problem is ill-posed.

Returning our attention to GR in Bondi-like gauges, we know from textbook results that the CIBVP of GR in these gauges is ill-posed in the L^2 -norm. We thus explore alternative norms for the CIBVP of the Bondi-Sachs system linearized about flat space. We fail to find such a norm and pinpoint the structure of the system that leads to this shortcoming. Nevertheless, motivated by symmetric hyperbolic PDE systems in Bondi-like gauges which include higher than second order metric derivatives, we investigate norms for the well-posedness of their CIBVP. These systems do not fall into the class covered by our earlier conjecture and we expect a deeper understanding of their CIBVP to guide us in building appropriate lopsided norms for the CIBVP of the Bondi-like systems that are covered by our conjecture. This process is work in progress and we hope to report further results elsewhere. A possible existence of such a norm would have great implications for applications of characteristic formulations built upon Bondi-like gauges, in the case where only the characteristic setup is solved, i.e. CCE. Regarding precise GW modeling, it could help us validate the error estimates of waveforms produced via CCE.

Using discrete approximates of the aforementioned norms we demonstrate the effects of weak hyperbolicity in numerical experiments performed in the characteristic domain, in Chap. 7. We adapt well known robust stability tests to the CIBVP for both toy models and the Bondi-Sachs proper system. We find that noisy given data are necessary to identify weak hyperbolicity in practice, as well as employing norms that are suitable for the specific problem.

In principle, the aforementioned well-posedness result has implications to any numerical approximation produced with these characteristic setups, like those related to strongly coupled systems which is the topic of Part II. We recognize this fact, but due to the lack of a better alternative at the moment, we exploit these WH characteristic setups to explore strongly coupled systems via holography. With this strategy, our main goal is to advance our

understanding of their qualitative behavior, rather than describe them precisely. To pursue this line of research, we have developed `Jecco` a new modular characteristic code written in the Julia programming language. In Chap. 8 we provide details on the models that can be explored with `Jecco` and the PDE systems for which the code currently provides solutions, as well as information on the numerical implementation and algorithms. We also present performance, validation and convergence tests of the code, and provide a brief overview of some physical setups that we have modeled with `Jecco` so far. In Chap. 9 we present our final remarks and suggestions for future work.

PART I:

HYPERBOLICITY AND WELL-POSEDNESS

This part is based on Refs. [1, 2]

CHAPTER 2

A PDE theory toolbox

Contents

2.1	PDE classes and causal definitions	15
2.2	Degree of hyperbolicity	18
2.3	Well-posedness and norms	19

The goal of this chapter is to provide the reader with the necessary knowledge of PDE theory to understand the results presented in the thesis. By the end of the chapter the difference between a *weakly hyperbolic* and a *strongly hyperbolic* PDE system should be clear, as well as the notions of the *characteristic initial (boundary) value PDE problem* and of *well-posedness* of a PDE problem. A more complete discussion can be found e.g. in [102–105]. The reader familiar with these topics may prefer to skip the chapter.

2.1 PDE classes and causal definitions

A rough way to classify PDE systems is into *elliptic*, *parabolic* and *hyperbolic*. From the physical perspective, elliptic systems have no intrinsic notion of time, with the prototype elliptic example being the Laplace equation. Both parabolic and hyperbolic PDEs have an intrinsic notion of time. However, in parabolic systems the propagation of information has infinite speed, whereas in hyperbolic ones it is finite and so there is a clear notion of causality. The heat equation is the prototype parabolic example and the wave equation the model hyperbolic one. A system of PDEs may fall into more than one of the aforementioned classes e.g. mixed hyperbolic-parabolic. There are also examples of PDEs that can change classification depending on their coefficients as for example the Tricomi equation

$$\partial_x^2 u(x, y) + x \partial_y^2 u(x, y) = 0,$$

which is elliptic for $x > 0$ and hyperbolic for $x < 0$.

In this thesis we focus on hyperbolic PDE systems of the form

$$\mathcal{A}^t(\mathbf{u}, x^\mu) \partial_t \mathbf{u} + \mathcal{A}^p(\mathbf{u}, x^\mu) \partial_p \mathbf{u} + \mathcal{S}(\mathbf{u}, x^\mu) = 0, \quad (2.1)$$

where $\mathbf{u} = (u_1, u_2, \dots, u_q)^T$, is the state vector of the system,

$$\mathcal{A}^\mu = \begin{pmatrix} a_{11}^\mu & \dots & a_{1q}^\mu \\ \vdots & \ddots & \vdots \\ a_{q1}^\mu & \dots & a_{qq}^\mu \end{pmatrix}$$

denotes the principal part matrices, $\mathcal{S}(\mathbf{u}, x^\mu)$ the source terms and $x^\mu = (t, x^p)$ some local coordinate system. The causal nature of a hypersurface Σ_t of constant t is

- Spacelike if $\det(\mathcal{A}^t(\mathbf{u}, x^\mu)) \neq 0$ and $\mathcal{A}^t(\mathbf{u}, x^\mu)$ is positive-definite ¹.
- Timelike if $\det(\mathcal{A}^t(\mathbf{u}, x^\mu)) \neq 0$ and $\mathcal{A}^t(\mathbf{u}, x^\mu)$ is not positive-definite.
- Null or characteristic if $\det(\mathcal{A}^t(\mathbf{u}, x^\mu)) = 0$.

If the PDE system describes GR then the vector normal to a characteristic hypersurface is also null in the GR notion. In terms of initial data $\mathbf{u}_0 \equiv \mathbf{u}(0, x^p)$, the initial value problem (IVP) and the characteristic initial value problem (CIVP) have an important difference:

If Σ_0 is spacelike: All q elements of the initial state vector \mathbf{u}_0 have to be provided. Since \mathbf{u}_0 is known, then so is $\partial_p \mathbf{u}_0$ and

$$\mathcal{A}^t(0, x^p, \mathbf{u}_0) \partial_t \mathbf{u}_0 + \mathcal{A}^p(0, x^p, \mathbf{u}_0) \partial_p \mathbf{u}_0 = -\mathcal{S}(0, x^p, \mathbf{u}_0), \quad (2.2)$$

provides a system of q PDEs for the q unknowns $(\partial_0 \mathbf{u}_0)$, that lead to a time-dependent solution \mathbf{u} for the system.

If Σ_0 is characteristic: Not all q elements of \mathbf{u}_0 are freely specifiable on Σ_0 and some of them satisfy constraint equations on it. For $m \equiv \text{rank}(\mathcal{A}^t(x^\mu, \mathbf{u}))$ with $m < q$, there are only m linearly independent rows in \mathcal{A}^t and the remaining $q - m$ rows can be eliminated resulting in a system of the form

$$\bar{\mathcal{A}}^t(0, x^p, \mathbf{u}_0) \partial_t \mathbf{u}_0 + \bar{\mathcal{A}}^p(0, x^p, \mathbf{u}_0) \partial_p \mathbf{u}_0 = -\bar{\mathcal{S}}(0, x^p, \mathbf{u}_0), \quad (2.3)$$

¹A real valued symmetric matrix is positive-definite if all its eigenvalues are real and positive.

with

$$\bar{\mathcal{A}}^t = \begin{pmatrix} a_{11}^t(0, x^p, \mathbf{u}_0) & \cdots & a_{1q}^t(0, x^p, \mathbf{u}_0) \\ \vdots & \ddots & \vdots \\ a_{m1}^t(0, x^p, \mathbf{u}_0) & \cdots & a_{mq}^t(0, x^p, \mathbf{u}_0) \\ 0 & \cdots & 0 \\ \vdots & \ddots & \vdots \\ 0 & \cdots & 0 \end{pmatrix}, \quad \bar{\mathcal{S}} = \begin{pmatrix} S_1(0, x^p, \mathbf{u}_0) \\ \vdots \\ S_m(0, x^p, \mathbf{u}_0) \\ S_{m+1}(0, x^p, \mathbf{u}_0) \\ \vdots \\ S_q(0, x^p, \mathbf{u}_0) \end{pmatrix}.$$

Since there are $q - m$ zero rows in $\bar{\mathcal{A}}^t$, then there are $q - m$ equations that do not involve derivatives transversal to Σ_0 , the *intrinsic equations*. The state vector can be split in transversal and intrinsic to Σ_0 components $\mathbf{u}_0 = (\mathbf{u}_0^{\text{tr}}, \mathbf{u}_0^{\text{int}})^T$. The same decomposition holds for the principal matrices as well as the source terms, namely:

$$\bar{\mathcal{A}}^\mu(0, x^p, \mathbf{u}_0) = \begin{pmatrix} \bar{\mathcal{A}}_{\text{tr}}^\mu(0, x^p, \mathbf{u}_0) \\ \bar{\mathcal{A}}_{\text{int}}^\mu(0, x^p, \mathbf{u}_0) \end{pmatrix}, \quad \bar{\mathcal{S}}(0, x^p, \mathbf{u}_0) = \begin{pmatrix} \bar{\mathcal{S}}_{\text{tr}}(0, x^p, \mathbf{u}_0) \\ \bar{\mathcal{S}}_{\text{int}}(0, x^p, \mathbf{u}_0) \end{pmatrix},$$

with

$$\begin{aligned} \text{size}(\bar{\mathcal{A}}_{\text{tr}}^\mu) &= m \times q, & \text{size}(\bar{\mathcal{A}}_{\text{int}}^\mu) &= (q - m) \times q, \\ \text{length}(\bar{\mathcal{S}}_{\text{tr}}) &= m, & \text{length}(\bar{\mathcal{S}}_{\text{int}}) &= (q - m). \end{aligned}$$

From the system of intrinsic equations

$$\bar{\mathcal{A}}_{\text{int}}^p(0, x^p, \mathbf{u}_0) \partial_p \mathbf{u}_0 = -\bar{\mathcal{S}}_{\text{int}}(0, x^p, \mathbf{u}_0), \quad (2.4)$$

let us analyze one equation (the analysis of the rest is identical):

$$a_{q1}^p \partial_p u_{01}^{\text{tr}} + \cdots + a_{qm}^p \partial_p u_{0m}^{\text{tr}} + a_{q(m+1)}^p \partial_p u_{0(m+1)}^{\text{int}} + \cdots + a_{qq}^p \partial_p u_{0q}^{\text{int}} = -S_q, \quad (2.5)$$

where

$$a_{qj}^p = a_{qj}^p(0, x^p, \mathbf{u}_0^{\text{tr}}, \mathbf{u}_0^{\text{int}}), \quad S_q = S_q(0, x^p, \mathbf{u}_0^{\text{tr}}, \mathbf{u}_0^{\text{int}}).$$

This is a constraint equation that the initial data have to satisfy on Σ_0 . In other words, the behavior of the chosen data \mathbf{u}_0 that is intrinsic to the initial hypersurface has to comply with the above equation and all the rest of the constraint (intrinsic) equations. Note that if $m = 0$, then the hypersurface is a *total characteristic* of the system and there are q constraint equations i.e. no element of \mathbf{u}_0 is freely specifiable.

Regarding the transversal part of the system (2.3)

$$\bar{\mathcal{A}}_{\text{tr}}^0(0, x^p, \mathbf{u}_0) \partial_t \mathbf{u}_0 + \bar{\mathcal{A}}_{\text{tr}}^p(0, x^p, \mathbf{u}_0) \partial_p \mathbf{u}_0 = -\bar{\mathcal{S}}_{\text{tr}}(0, x^p, \mathbf{u}_0), \quad (2.6)$$

let us analyze one equation (the rest are identical):

$$\begin{aligned} & a_{11}^t \partial_t u_{01}^{\text{tr}} + \cdots + a_{1m}^t \partial_t u_{0m}^{\text{tr}} + a_{1(m+1)}^t \partial_t u_{0m+1}^{\text{int}} + \cdots + a_{1q}^t \partial_t u_{0q}^{\text{int}} + \\ & a_{11}^p \partial_p u_{01}^{\text{tr}} + \cdots + a_{1m}^p \partial_p u_{0m}^{\text{tr}} + a_{1(m+1)}^p \partial_p u_{0m+1}^{\text{int}} + \cdots + a_{1q}^p \partial_p u_{0q}^{\text{int}} = -S_1, \end{aligned} \quad (2.7)$$

where

$$a_{1j}^\mu = a_{1j}^\mu(0, x^p, \mathbf{u}_0^{\text{tr}}, \mathbf{u}_0^{\text{int}}), \quad S_1 = S_1(0, x^p, \mathbf{u}_0^{\text{tr}}, \mathbf{u}_0^{\text{int}}).$$

The quantities a_{1j}^μ , \mathbf{u}_0 and $\partial_p \mathbf{u}_0$ are known for $t = 0$ provided that the intrinsic equations are satisfied. However, there are the q unknowns $(\partial_t \mathbf{u}_0^{\text{tr}}, \partial_t \mathbf{u}_0^{\text{int}})$ for the m transversal equations (with $m < q$). One can formally build a system of q equations for these q unknowns from the intrinsic equations. Acting from the left with ∂_t on (2.5) and permuting the derivatives, one can obtain:

$$\begin{aligned} & \partial_t a_{q1}^p \partial_p u_{01}^{\text{tr}} + \cdots + \partial_t a_{qm}^p \partial_p u_{0m}^{\text{tr}} + \partial_t a_{q(m+1)}^p \partial_p u_{0m+1}^{\text{int}} + \cdots + \partial_t a_{qq}^p \partial_p u_{0q}^{\text{int}} + \\ & a_{q1}^p \partial_p \partial_t u_{01}^{\text{tr}} + \cdots + a_{qm}^p \partial_p \partial_t u_{0m}^{\text{tr}} + a_{q(m+1)}^p \partial_p \partial_t u_{0m+1}^{\text{int}} + \cdots + a_{qq}^p \partial_p \partial_t u_{0q}^{\text{int}} = -\partial_t S_q, \end{aligned}$$

where

$$\partial_t a_{qj}^p = \partial_t a_{qj}^p(0, x^p, \mathbf{u}_0^{\text{tr}}, \mathbf{u}_0^{\text{int}}, \partial_t \mathbf{u}_0^{\text{tr}}, \partial_t \mathbf{u}_0^{\text{int}}), \quad \partial_t S_q = \partial_t S_q(0, x^p, \mathbf{u}_0^{\text{tr}}, \mathbf{u}_0^{\text{int}}, \partial_t \mathbf{u}_0^{\text{tr}}, \partial_t \mathbf{u}_0^{\text{int}}).$$

By demanding that the constraint equations are satisfied at later times i.e. they are solved by $\mathbf{u}_0 + \partial_t \mathbf{u}_0$, one ends up with $q - m$ equations of the form:

$$\partial_t a_{q1}^p \partial_p u_{01}^{\text{tr}} + \cdots + \partial_t a_{qm}^p \partial_p u_{0m}^{\text{tr}} + \partial_t a_{q(m+1)}^p \partial_p u_{0m+1}^{\text{int}} + \cdots + \partial_t a_{qq}^p \partial_p u_{0q}^{\text{int}} = 0, \quad (2.8)$$

where $(\partial_p \mathbf{u}_0^{\text{tr}}, \partial_p \mathbf{u}_0^{\text{int}})$ are known from the given data on Σ_0 . The q unknowns $(\partial_t \mathbf{u}_0^{\text{tr}}, \partial_t \mathbf{u}_0^{\text{int}})$ still appear in the terms $\partial_t a_{qj}^p$ and so the union of the $q - m$ equations of the form (2.8) with the m transversal equations of the form (2.7) provides with q equations for these unknowns, while simultaneously assuring that the constraint equations are satisfied at later times.

2.2 Degree of hyperbolicity

Within the hyperbolic class of PDEs there are sub-classes characterized by their degree of hyperbolicity. The standard way to perform this characterization is by constructing the

principal symbol

$$\mathbf{P}^s = (\mathcal{A}^t)^{-1} \mathcal{A}^p s_p, \quad (2.9)$$

where s^i is an arbitrary unit spatial vector. Here, the explicit dependence of the principal part matrices on \mathbf{u} and x^μ is suppressed. To characterize a PDE system with variable coefficients \mathbf{P}^s has to be constructed everywhere in the domain of interest. To build \mathbf{P}^s the principal part matrix \mathcal{A}^t associated with time derivatives has to be invertible i.e. $\det(\mathcal{A}^t) \neq 0$.

We may refer to a PDE system with $\det(\mathcal{A}^t) = 0$ as a *characteristic PDE system*. For such a system, \mathbf{P}^s cannot be constructed directly in the chosen coordinates. In this case a convenient coordinate transformation is utilized to write the system with an invertible time principal part matrix. Crucially, this transformation does not alter the degree of hyperbolicity of the system, but is merely a tool to form \mathbf{P}^s .

If \mathbf{P}^s has real eigenvalues for all s^i , then the PDE system is called *weakly hyperbolic*, whereas if in addition \mathbf{P}^s is diagonalizable for all s^i , and there exists a constant K independent of s^i such that

$$|\mathbf{T}_s| + |\mathbf{T}_s^{-1}| \leq K,$$

with \mathbf{T}_s the similarity matrix that diagonalizes \mathbf{P}^s , it is called *strongly hyperbolic*. If all eigenvalues of \mathbf{P}^s are distinct for all s^i then the system is called *strictly hyperbolic*. Strict hyperbolicity implies strong hyperbolicity. Finally, a PDE system is called *symmetric hyperbolic* if all the matrices \mathcal{A}^μ are Hermitian, or symmetric for purely real-valued setups. If not all the \mathcal{A}^μ matrices are Hermitian (symmetric) in their original form, but there exists one matrix \mathbf{H} which can symmetrize them all via a similarity transformation, then the system is still symmetric hyperbolic.

2.3 Well-posedness and norms

Well-posedness is a property of a PDE problem which states that the PDE problem has a unique solution that depends continuously on the given data, in some appropriate norm. The PDE problem consists of the PDE system, the domain in which we seek a solution, as well as the given data (initial and possibly boundary data). The degree of hyperbolicity of the PDE system is tightly connected to well-posedness. More specifically, assuming there exists a unique solution of the problem, the degree of hyperbolicity of the system affects the existence and the form of the norm in which the problem can be well-posed.

Consider the Cauchy problem for the linear, constant coefficient system,

$$\partial_t \mathbf{u} = \mathcal{B}^p \partial_p \mathbf{u} + \mathcal{B} \mathbf{u}. \quad (2.10)$$

The initial value problem (IVP) for a SH system is well-posed in the L^2 -norm

$$\|\mathbf{u}\|_{L^2} = \left(\int_{\Sigma_t} \mathbf{u}^\dagger \mathbf{u} \right)^{1/2}, \quad (2.11)$$

where \int_{Σ_t} denotes the integral over a spacelike hypersurface Σ_t . To be well-posed in the L^2 -norm means that there exist real constants $K \geq 1$ and $\alpha \in \mathbb{R}$ such that

$$|e^{\mathbf{P}(i\omega)t}| \leq K e^{\alpha t}, \quad (2.12)$$

for all $t \geq 0$ and all $\omega \in \mathbb{R}^n$. Here

$$\mathbf{P}(i\omega) = i\omega_p \mathbf{B}^p + \mathbf{B} \quad (2.13)$$

is the constant-coefficient symbol of the PDE after Fourier transforming in space, with $i\omega_p \mathbf{B}^p$ the principal symbol and $\mathbf{B} \mathbf{u} = -\mathcal{S}$ the lower order term related to sources. Essentially, inequality (2.12) states that the solution of the PDE has to be bounded at each time by an exponential that is independent of the Fourier mode ω_p . In this manner one can obtain an estimate of the solution \mathbf{u} at all times by the initial data f

$$\|\mathbf{u}(\cdot, t)\|_{L^2} = \|e^{\mathbf{P}(i\omega)t} \hat{f}(\omega)\|_{L^2} \leq K e^{\alpha t} \|\hat{f}\|_{L^2} = K e^{\alpha t} \|f\|_{L^2}.$$

Crucially, the form of the source terms does not affect well-posedness for a SH system [102, 106]. This result provides the basis to show well-posedness for the IVP of variable-coefficient SH systems, as well as non-linear systems with a SH linearization.

In the terminology of [102], if a Cauchy problem instead satisfies only

$$|e^{\mathbf{P}(i\omega)t}| \leq K_1 e^{\alpha t} (1 + |\omega|^q), \quad (2.14)$$

with q some natural number, it is called weakly well-posed. This type of estimate is weaker than (2.12), because the explicit appearance of ω on the right-hand-side makes it impossible to bound the solution by an exponential independent of ω . If, rather than insisting on L^2 we allow also some *specific* derivative, determined by the system, within the norm, we can nevertheless obtain the estimate

$$\|\mathbf{u}(\cdot, t)\|_q \leq K_2 e^{\alpha t} \|f\|_q,$$

for the solution \mathbf{u} . This would not be terrible, except that if the PDE is only weakly well-posed, then perturbations to the system by generic lower order terms can lead to frequency dependent exponential growth of the solution, that is $|e^{\mathbf{P}(i\omega)t}|$ grows faster than any polynomial in $|\omega|$, and the resulting perturbed problem is ill-posed in any sense. In Sec. 6.2 we show this explicitly for our WH models. More examples can be found in subsection

2.2.3 of [102] and Example 10 of [106].

Practically, to understand if a weakly well-posed PDE problem becomes ill-posed due to lower order perturbations, one can focus on the large ω behavior of the eigenvalues of $\mathbf{P}(i\omega)$. If there is an eigenvalue with positive real part in this limit, then it gives rise to solutions that grow exponentially with ω , for fixed t . This becomes more clear when considering how the matrix norm $|e^{\mathbf{P}(i\omega)t}|$ can be computed. For completeness, we briefly present a way to perform this computation, as given in [106]. Let us denote as \mathbf{M}^* the transposed and complex conjugate of a $k \times l$ matrix \mathbf{M} . Then, the matrix norm $|\mathbf{M}|$ can be computed as

$$|\mathbf{M}| = \sqrt{\rho(\mathbf{M}^*\mathbf{M})},$$

where $\rho(\mathbf{M}^*\mathbf{M})$ is the spectral radius of the square matrix $\mathbf{M}^*\mathbf{M}$. The spectrum of this matrix is the set of all its eigenvalues and the spectral radius is their greatest absolute value.

CHAPTER 3

Properties of Bondi-like characteristic formulations

Contents

3.1	Main features of Bondi-like formulations	23
3.2	From the characteristic to the ADM equations	26
3.3	Coordinate light speeds	30

In this chapter we review the main features of Bondi-like formulations and map the corresponding equations and variables to the ADM language. To the best of our knowledge, such a mapping has been performed only in spherical symmetry so far [107]. To achieve this map, we employ a coordinate transformation between generalized Bondi-like coordinates and coordinates adapted to the ADM setup. We may refer to the latter as the ADM coordinates. The gauge, and thus the PDE character of the system are fixed by the Bondi-like coordinates. This choice determines for instance which metric components and/or derivatives thereof vanish. The subsequent transformation to the ADM coordinates merely results in relabeling variables and expressing directional derivatives of the Bondi-like basis in terms of those of the ADM basis. A more geometric description of the main properties of Bondi-like formulations is provided in terms of coordinate light speeds in Sec. 3.3.

3.1 Main features of Bondi-like formulations

To demonstrate relevant features common to all Bondi-like gauges we work with the generalized Bondi-Sachs formulation of [108] with line element

$$ds^2 = g_{uu}du^2 + 2g_{ur}du dr + 2g_{u\theta}du d\theta + 2g_{u\phi}du d\phi + g_{\theta\theta}d\theta^2 + 2g_{\theta\phi}d\theta d\phi + g_{\phi\phi}d\phi^2. \quad (3.1)$$

We consider a four dimensional spacetime and identify the coordinates θ, ϕ with the usual spherical polar angles on the two-sphere. All seven nontrivial metric components of (3.1) are functions of the characteristic coordinates $x^{\mu'} = (u, r, \theta, \phi)$, with the hypersurfaces of constant u null and henceforth denoted by \mathcal{N}_u . The null vector $(\partial/\partial r)^a$ is both tangent and normal to \mathcal{N}_u and hence orthogonal to the spatial vectors $(\partial/\partial\theta)^a$ and $(\partial/\partial\phi)^a$ that lie

within \mathcal{N}_u . This vector basis guarantees that

$$g^{uu} = g^{u\theta} = g^{u\phi} = 0, \quad (3.2)$$

and every distinct null geodesic in \mathcal{N}_u can be labeled by θ, ϕ . The characteristic hypersurface \mathcal{N}_u can be either outgoing or ingoing. If the formulation incorporates both types of null hypersurfaces, then the double null gauge [109] is imposed. In this case $g^{rr} = 0$ and the coordinates u, r correspond to the advanced and retarded time rather than an advanced (or retarded) time and the radial coordinate.

For convenience here we use the trace-reversed form of the EFE, but the rest of the analysis is equivalent in the standard form. A free evolution PDE system for the vacuum EFE in an asymptotically flat spacetime in a Bondi-like gauge consists of

$$R_{rr} = R_{r\theta} = R_{r\phi} = R_{\theta\theta} = R_{\theta\phi} = R_{\phi\phi} = 0, \quad (3.3)$$

which is often called the main system. The equation $R_{ur} = 0$ is commonly referred to as the trivial equation, because solutions to the main system automatically satisfy it, as shown in [108, 110] via the contracted Bianchi identities. The supplementary equations

$$R_{uu} = R_{u\theta} = R_{u\phi} = 0,$$

are guaranteed to be satisfied in \mathcal{N}_u if they are satisfied on a cross-section [108, 110].

Regarding terminology, notice that in a standard spacelike foliation, the constraint equations are intrinsic to the spacelike hypersurfaces of the foliation. In a free evolution scheme, the data chosen on the initial hypersurface should satisfy the constraint equations, in order for the solution of the PDE problem to be a solution to the EFEs. If the constraint equations are satisfied initially, they are satisfied also at later times, due to the Bianchi identities. Therefore, they are not explicitly solved in a free evolution scheme, but mostly their violation by a given approximate solution is examined at some stages of the evolution. The supplementary and trivial equations for a characteristic free evolution scheme are treated as the aforementioned constraints for the spacelike free evolution scheme. In a characteristic setup however, the actual constraint equations—in the PDE sense as described in Sec. 2.1—are intrinsic to null hypersurfaces and are part of the evolution scheme, meaning they are solved at each step of a time evolution. To avoid possible confusion, we call the characteristic constraint equations *intrinsic*.

The intrinsic equations of the main system can often acquire a nested structure. Given a certain subset of unknowns as initial data on a null hypersurface, the nested equations can be integrated in a specific sequence to obtain a solution to the characteristic PDE problem. In this case, each nested equation can be integrated requiring knowledge only of the initial data and the functions obtained by integrating the previous nested equations. This special

structure becomes apparent in the systems analyzed in the following chapters, is common in most Bondi-like setups used for numerical studies, and results in reduced computational cost and time. In numerical implementations, these nested equations are often treated as a system of *effectively* ordinary differential equations (ODEs) in the radial direction. By “effectively” here we mean that even though formally these are partial differential equations, provided that the necessary functions are given on the computational domain, each equation can be solved as a standard ODE for one function since the rest of the elements of the equation are known quantities. Regarding its hyperbolic properties however the system is still treated as an actual PDE system. In fact, this viewpoint of a sequential system of effective ODEs may be misleading about the well-posedness of the respective PDE problem. In other words, the notion of sources in the numerical implementation can refer to quantities that are known during the integration of an equation. Regarding hyperbolicity however, for first order linear PDEs with constant coefficients, sources are only terms with no derivatives. So, a partial derivative of a function obtained from the previous nested equation can be viewed as a source for the numerical integration of the next nested equation, but not from the perspective of the hyperbolicity analysis.

The main system provides six evolution equations for the seven unknown metric functions. Usually, a definition for the determinant of the induced metric on the two-spheres is made, namely

$$g_{\theta\theta} g_{\phi\phi} - g_{\theta\phi}^2 = \hat{R}^4 \sin^2 \theta, \quad (3.4)$$

where \hat{R} is taken to be a function of the coordinates, and reduces to the areal radius of the two-sphere in spherical symmetry.

The aforementioned are common to all Bondi-like gauges. There is a residual gauge freedom which corresponds to the choice of the coordinate labeling the position within the null geodesic. This is done differently in the various Bondi-like gauges. We focus on three common choices:

Affine null [86, 111] The final choice of equations is achieved by setting $g^{ur} = -1$ for outgoing \mathcal{N}_u and $g^{ur} = 1$ for ingoing \mathcal{N}_u . \hat{R} is then taken to be an unknown of the problem.

Bondi-Sachs proper [110] The radial coordinate matches the areal radius $\hat{R} = r$ and so the definition (3.4) reduces the number of unknowns to six.

Double null [109] The residual gauge freedom is fixed by the condition $g^{rr} = 0$.

3.2 From the characteristic to the ADM equations

We now map from the characteristic to the ADM variables and present the system equivalent to (3.3) in ADM formalism. We assume that \mathcal{N}_u are outgoing, but an analogous analysis can be performed for ingoing null hypersurfaces. To begin, we choose the ADM coordinates $x^\mu = (t, \rho, \theta, \phi)$. They are related to the characteristic coordinates via

$$u = t - f(\rho), \quad r = \rho. \quad (3.5)$$

As in [107], the quantity $-df/dr$ determines the slope of the constant t spacelike hypersurface Σ_t on the u, r plane. The angular coordinates θ, ϕ are unchanged and in this subsection we may label them with the Latin indices A, B .

The lapse of proper time between Σ_t and Σ_{t+dt} along their normal observers is $d\tau = \alpha(t, x^i)dt$, with the lapse function defined by

$$\alpha^{-2}(t, x^i) \equiv -g^{\mu\nu} \nabla_\mu t \nabla_\nu t.$$

The relative velocity between the trajectory of those observers and the lines of constant spatial coordinates is given by $\beta^i(t, x^j)$, where $x^i_{t+dt} = x^i_t - \beta^i(t, x^j)dt$. The quantity β^i is called the shift vector. The future directed unit normal 4-vector on Σ_t is

$$n^\mu \equiv -\alpha \nabla^\mu t = \alpha^{-1} (1, -\beta^i),$$

and its covector form is

$$n_\mu = g_{\mu\nu} n^\nu = (-\alpha, 0, 0, 0).$$

The metric induced on Σ_t is

$$\gamma_{\mu\nu} \equiv g_{\mu\nu} + n_\mu n_\nu.$$

The ADM form of the equations is obtained by systematic contraction with n^μ and $\gamma_{\mu\nu}$. This geometric construction is discussed in most numerical relativity textbooks [112–114]. The spacetime metric takes the form

$$g_{\mu\nu} = \begin{pmatrix} -\alpha^2 + \beta_k \beta^k & \beta_i \\ \beta_j & \gamma_{ij} \end{pmatrix},$$

where lowercase Latin indices denote spatial components. The inverse of $g_{\mu\nu}$ is

$$g^{\mu\nu} = \begin{pmatrix} -\alpha^{-2} & \alpha^{-2}\beta^i \\ \alpha^{-2}\beta^j & \gamma^{ij} - \alpha^{-2}\beta^i\beta^j \end{pmatrix}.$$

By comparing the 3+1 form of the metric and its inverse to the generalized Bondi version (3.1) we can interpret the Bondi-like gauges in terms of lapse and shift, and relate the characteristic variables to the ADM ones. Every Bondi-like vector basis gives (3.2), which in ADM coordinates reads

$$g^{uu} = \frac{\partial u}{\partial x^\mu} \frac{\partial u}{\partial x^\nu} g^{\mu\nu} = g^{tt} - 2f'g^{t\rho} + (f')^2g^{\rho\rho} = 0, \quad g^{uA} = \frac{\partial u}{\partial x^\mu} \frac{\partial x^A}{\partial x^\nu} g^{\mu\nu} = g^{tA} - f'g^{\rho A} = 0,$$

and leads to

$$\gamma^{\rho\rho} = \left(\frac{1 + f'\beta^\rho}{f'\alpha} \right)^2, \quad \gamma^{\rho A} = \beta^A \frac{1 + f'\beta^\rho}{f'\alpha^2}. \quad (3.6)$$

The Bondi-like metric ansatz (3.1) implies

$$g_{rr} = g_{rA} = 0,$$

which after using $\beta_i = \gamma_{ij}\beta^j$ yields

$$\gamma_{\rho\rho} = \frac{(f')^2(\alpha^2 + \beta^A\beta^B\gamma_{AB})}{(1 + f'\beta^\rho)^2}, \quad \gamma_{\rho A} = -\frac{f'}{1 + f'\beta^\rho}\beta^B\gamma_{AB}. \quad (3.7)$$

Using the latter and $g_{\mu'\nu'} = \frac{\partial x^\mu}{\partial x^{\mu'}} \frac{\partial x^\nu}{\partial x^{\nu'}} g_{\mu\nu}$ provides the following relations between the characteristic and ADM variables, for all Bondi-like gauges:

$$g_{uu} = \frac{\beta^A\beta_A - \alpha^2(1 + 2f'\beta^\rho)}{(1 + f'\beta^\rho)^2}, \quad g_{ur} = \frac{-f'\alpha^2}{1 + f'\beta^\rho}, \quad g_{uA} = -\gamma_{\rho A}/f', \quad g_{AB} = \gamma_{AB}. \quad (3.8)$$

The above combined with $\gamma^{AB} - \alpha^{-2}\beta^A\beta^B = g^{AB}$ further yield

$$\begin{aligned} \gamma^{\theta\theta} &= \left(\frac{\beta^\theta}{\alpha} \right)^2 + \frac{\gamma_{\phi\phi}}{\det(g_{AB})}, & \gamma^{\theta\phi} &= \frac{\beta^\theta\beta^\phi}{\alpha^2} - \frac{\gamma_{\theta\phi}}{\det(g_{AB})}, \\ \gamma^{\phi\phi} &= \left(\frac{\beta^\phi}{\alpha} \right)^2 + \frac{\gamma_{\theta\theta}}{\det(g_{AB})}. \end{aligned} \quad (3.9)$$

for all Bondi-like gauges.

To proceed with the mapping between characteristic and ADM formalism, we simply take the standard tensor transformation rule. The main system (3.3) written in the ADM coordinates

is then

$$\begin{aligned} R_{rr} &= (f')^2 R_{tt} + 2f' R_{t\rho} + R_{\rho\rho} = 0, \\ R_{rA} &= f' R_{tA} + R_{\rho A} = 0, \\ R_{AB} &= 0. \end{aligned} \quad (3.10)$$

The complete orthogonal projection onto Σ_t is given by

$$\gamma^\lambda{}_\mu \gamma^\sigma{}_\nu R_{\lambda\sigma} \equiv R_{\mu\nu}^\perp = -\mathcal{L}_n K_{\mu\nu} - \frac{1}{\alpha} D_\mu D_\nu \alpha + {}^{(3)}R_{\mu\nu} + K K_{\mu\nu} - 2K_{\mu\lambda} K^\lambda{}_\nu, \quad (3.11)$$

with $R_{\mu\nu}^\perp$ a purely spatial tensor, and

$$\gamma^\mu{}_\nu = \delta^\mu{}_\nu + n^\mu n_\nu, \quad K_{\mu\nu} = -(\nabla_\mu n_\nu + n_\mu n^\kappa \nabla_\kappa n_\nu), \quad (3.12)$$

the orthogonal projector and the extrinsic curvature of Σ_t when embedded in the full spacetime, respectively. The following purely spatial quantities have been used

$$\begin{aligned} D_\mu S_{\nu\lambda} &= \perp \nabla_\mu S_{\nu\lambda}, \quad {}^{(3)}\Gamma^\mu{}_{\nu\lambda} = \perp \Gamma^\mu{}_{\nu\lambda}, \\ {}^{(3)}R_{\mu\nu} &= \perp \left(\partial_\lambda {}^{(3)}\Gamma^\lambda{}_{\mu\nu} - \partial_\nu {}^{(3)}\Gamma^\lambda{}_{\mu\lambda} + {}^{(3)}\Gamma^\lambda{}_{\mu\nu} {}^{(3)}\Gamma^\sigma{}_{\lambda\sigma} - {}^{(3)}\Gamma^\lambda{}_{\mu\sigma} {}^{(3)}\Gamma^\sigma{}_{\nu\lambda} \right), \end{aligned}$$

where D_μ is the covariant derivative compatible with $\gamma_{\mu\nu}$, the symbol \perp denotes projection with $\gamma^\mu{}_\nu$ on every open index and $S_{\mu\nu}$ denotes an arbitrary spatial tensor. Imposing $R_{\mu\nu} = 0$ and focusing only on the spatial components of $R_{\mu\nu}^\perp$, one can obtain the evolution equations for the spatial components of the extrinsic curvature

$$\begin{aligned} \mathcal{K}_{ij} &\equiv -\partial_t K_{ij} - D_i D_j \alpha + \alpha \left({}^{(3)}R_{ij} + K K_{ij} - 2K_{im} K^m{}_j \right) \\ &+ \beta^m \partial_m K_{ij} + K_{im} \partial_j \beta^m + K_{mj} \partial_i \beta^m = 0, \end{aligned}$$

where $K = g^{\mu\nu} K_{\mu\nu}$. The full projection perpendicular to Σ_t is

$$n^\mu n^\nu R_{\mu\nu} \equiv R^\parallel = \mathcal{L}_n K + \frac{1}{\alpha} D^i D_i \alpha - K_{ij} K^{ij}.$$

Using

$$\mathcal{L}_n K = \gamma^{ij} \mathcal{L}_n K_{ij} + 2K_{ij} K^{ij},$$

Eq. (3.11) and imposing the EFE, R^\parallel provides the Hamiltonian constraint

$$H \equiv {}^{(3)}R + K^2 - K_{ij} K^{ij} = R^\parallel + \gamma^{ij} R_{ij}^\perp = 0.$$

Finally, the mixed projection is given by the contracted Codazzi relation

$$n^\mu \gamma^\lambda{}_\nu R_{\mu\lambda} \equiv R_\nu^\perp = D_\nu K - D_\mu K^\mu{}_\nu,$$

with $n^\mu R_\mu^\perp = 0$. After imposing the EFE it yields the momentum constraints

$$M_i \equiv D_j K^j_i - D_i K = 0.$$

From Eq. (3.12) and the previous projections we write

$$\delta^\alpha_\mu \delta^\beta_\nu R_{\alpha\beta} = R_{\mu\nu}^\perp + n_\mu n_\nu R^\parallel - n_\mu R_\nu^\perp - n_\nu R_\mu^\perp. \quad (3.13)$$

Using Eq. (3.13), with Eq. (3.10) and taking linear combinations of Eq. (3.3), we obtain the ADM system

$$\begin{aligned} \frac{((f')^2 - 1)(1 + f'\beta^\rho)^2}{(f')^2} \mathcal{K}_{\rho\rho} + \alpha^2 H - 2\alpha f'(1 + f'\beta^\rho) M_\rho - 2\alpha \beta^A M_A &= 0, \\ (1 + f'\beta^\rho) \mathcal{K}_{\rho A} - \alpha f' M_A &= 0, \\ \mathcal{K}_{AB} &= 0, \end{aligned} \quad (3.14)$$

that is equivalent to the main Bondi-like system (3.3), where we have also used Eq. (3.6), (3.7) and (3.9).

If the slope of Σ_t of the $3 + 1$ foliation in the u, r plane is $f' \neq 1$, then the main Bondi-like system (3.3) corresponds to evolution equations for all the components of K_{ij} with specific addition of the ADM Hamiltonian and momentum constraints. For $f' = 1$ though, the first equation of (3.14) involves only ADM constraints. In this foliation the evolution equation for $K_{\rho\rho}$ is provided by the trivial equation, which after imposing (3.14) reads

$$(1 + \beta^\rho) \mathcal{K}_{\rho\rho} - \alpha M_\rho + \frac{\alpha}{1 + \beta^\rho} \beta^A M_A = 0.$$

The lapse and shift are not determined by the Einstein equations, but in a $3 + 1$ formulation are arbitrarily specifiable. In the present setting, their choice is dictated by the explicit Bondi-like gauge imposed. Adopting the terminology of [115] we can classify between algebraic and differential gauge choices:

Affine null It is a complete algebraic gauge for the lapse and shift, which is apparent by combining (3.7) and

$$\beta^\rho = \alpha^2 - 1/f',$$

which results from $g^{ur} = -1 = 1/g_{ur}$. The determinant condition (3.4) does not act as a constraint among the three unknown metric components of the two-sphere, but merely relates them to the areal radius \hat{R} that is an unknown. The six equations of the main system (3.3) correspond to the six ADM equations for K_{ij} (if $f' \neq 1$) with a specific addition of Hamiltonian and momentum constraints, as well as the lapse and shift.

Bondi-Sachs proper This gauge choice is completed by the definition of the determinant (3.4).

As we show in Sec. 5.2 this definition can be viewed as providing a differential relation for the shift vector component β^ρ . In this sense, the Bondi-Sachs gauge proper is a mixed algebraic-differential gauge in terms of the lapse and shift.

Double null It is also a complete algebraic gauge. The complete gauge choice is implied by $g^{rr} = 0$, which combined with $g^{uu} = 0$ yields $\beta^\rho = 0$.

3.3 Coordinate light speeds

Bondi-like gauges are constructed using either incoming or outgoing null geodesics (or both). It is therefore natural to examine the coordinate light speeds in these gauges. It is helpful to employ a $2 + 1$ split of the spatial metric γ_{ij} for this purpose. We briefly review the key elements of this decomposition as necessary for our discussion. The interested reader can find a complete presentation in [116].

Level sets of constant ρ are two-spheres. The coordinate ρ defines an outward pointing normal vector on these spheres

$$s_{(\rho)}^i \equiv \gamma^{ij} L D_j \rho, \quad L^{-2} \equiv \gamma^{ij} (D_i \rho)(D_j \rho). \quad (3.15)$$

We call L the length scalar. The induced metric on two-spheres of constant ρ is

$$q_{(\rho)ij} \equiv \gamma_{ij} - s_{(\rho)i} s_{(\rho)j}, \quad (3.16)$$

where the indices of $s_{(\rho)}^i$ and $q_{(\rho)ij}$ are lowered and raised with γ_{ij} and its inverse. Let ρ^i be the vector tangent to the lines of constant angular coordinates x^A i.e. $\rho^i = (\partial_\rho)^i$. Then

$$\rho^i = L s_{(\rho)}^i + b^i, \quad (3.17)$$

where $b^i s_{(\rho)i} = 0$ and b^i is called the slip vector. The length scalar L and the slip vector b^i are analogous to the $3 + 1$ lapse and shift. They are not, however, freely specifiable but rather are pieces of the spatial metric γ_{ij} .

Let $\gamma(t)$ be a null curve parameterized by t and $L^\mu = \dot{x}^\mu = (1, \dot{x}^i(t))$ a null vector tangent to $\gamma(t)$. The coordinate light speeds are $C^i \equiv \dot{x}^i(t)$. Let us further assume that the chosen null vector obeys the relation

$$L^\mu \propto n^\mu \pm s_{(\rho)}^\mu. \quad (3.18)$$

From (3.15) we get

$$s_{(\rho)}^\mu = (0, L^{-1}, L\gamma^{\rho A}). \quad (3.19)$$

Using $\rho^\mu = (0, 1, 0, 0)$, solving (3.17) for $s_{(\rho)}^i$ and comparing with (3.19) we obtain

$$b^\rho = 0, \quad -b^A = L^2 \gamma^{\rho A}. \quad (3.20)$$

After multiplying (3.18) with α we have

$$L^\mu \propto (1, -\beta^\rho \pm \alpha L^{-1}, -\beta^A \mp \alpha L^{-1} b^A)$$

from which we read off the coordinate light speeds along null curves orthogonal to level sets of constant ρ . They are

$$c_\pm^\rho = -\beta^\rho \pm \alpha L^{-1}, \quad (3.21)$$

in the radial direction and

$$c_\pm^A = -\beta^A \mp b^A \alpha L^{-1}, \quad (3.22)$$

in the angular directions. The subscript \pm refers to outgoing/ingoing trajectories. See Fig. 3.1 for an illustration of the coordinate lightspeeds. For $f(\rho) = \rho$, using Eq. (3.20), the gauge conditions (3.6) yield

$$c_+^\rho = 1, \quad c_+^A = 0, \quad (3.23)$$

which just expresses the fact that transverse coordinates are Lie dragged along outgoing null geodesics. For an ingoing single-null Bondi-like characteristic formulation $c_+^i \rightarrow c_-^i$ and for double null $c_\pm^\rho = \pm 1$. Away from spherical symmetry it is not generally possible to have c_\pm^A both vanishing.

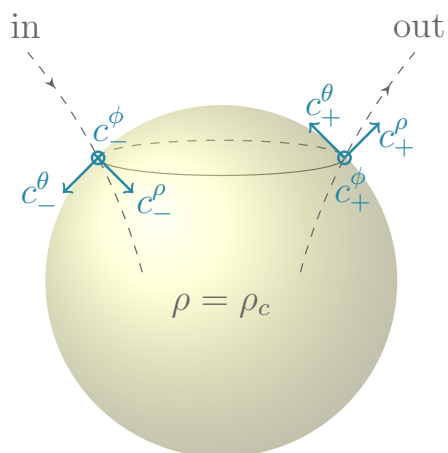


Figure 3.1: The coordinate light speeds for an ingoing and outgoing null ray that pass through a surface of constant radius ρ_c i.e. a two-sphere in this example. In an outgoing Bondi-like gauge $c_+^\theta = 0 = c_+^\phi$, i.e. the coordinates θ, ϕ are Lie dragged along the outgoing null ray. This ray is orthogonal to the depicted two-sphere, as illustrated by the vectors drawn. Notice that the coordinate light speeds are scalar quantities.

CHAPTER 4

Gauge fixing and the principal symbol

Contents

4.1	FT2S Systems and their principal part	33
4.2	Pure gauge and constraint subsystems	34
4.3	Projection operators	37
4.4	Discussion	39

Following closely [101, 115] we now discuss the structure of the principal symbol of the systems we analyze. See [117, 118] for interesting related work on systems with constraints. As shown in [101], working with the ADM formalism, in this context, one can distinguish between the gauge, constraint and physical variables of the system. This distinction is reflected in the structure of the principal symbol and allows us to understand which gauges can possibly result in SH systems.

4.1 FT2S Systems and their principal part

According to [119, 120] the general first order in time and second in space (FT2S) linear constant coefficient, system that admits a standard first order reduction is of the form

$$\begin{aligned}\partial_t \mathbf{v} &= \mathcal{A}_1^i \partial_i \mathbf{v} + \mathcal{A}_1 \mathbf{v} + \mathcal{A}_2 \mathbf{w} + \mathbf{S}_v, \\ \partial_t \mathbf{w} &= \mathcal{B}_1^{ij} \partial_i \partial_j \mathbf{v} + \mathcal{B}_1^i \partial_i \mathbf{v} + \mathcal{B}_1 \mathbf{v} + \mathcal{B}_2^i \partial_i \mathbf{w} + \mathcal{B}_2 \mathbf{w} + \mathbf{S}_w,\end{aligned}\tag{4.1}$$

where $\mathbf{S}_v, \mathbf{S}_w$ are forcing terms and $\mathcal{A}_1^i, \mathcal{A}_2, \mathcal{B}_1^{ij}, \mathcal{B}_2^i$ the principal matrices. In the linear constant coefficient approximation the ADM equations lie in this category. By *standard first order reduction* we mean one in which all first order derivatives (temporal and spatial) of variables that appear with second order derivatives are introduced as auxiliary variables. We call any first order reduction different than the aforementioned *non-standard*. In such a case only a subset of the first order derivatives of a variable that appears up to second order is introduced as auxiliary variables. Specific higher derivatives of certain variables could also be treated as auxiliary variables in a non-standard reduction, if necessary. Given an arbitrary unit spatial covector s_i (not to be confused with $s_{(\rho)}^i$ from Sec. 3.3), the principal

symbol of the system in the s_i direction is defined as

$$\mathbf{P}^s = \begin{pmatrix} \mathcal{A}_1^s & \mathcal{A}_2 \\ \mathcal{B}_1^{ss} & \mathcal{B}_2^s \end{pmatrix}, \quad (4.2)$$

where $\mathcal{A}_1^s \equiv \mathcal{A}_1^i s_i$ (and so forth). Writing $\mathbf{u} = (\partial_s \mathbf{v}, \mathbf{w})$, we have

$$\partial_t \mathbf{u} \simeq \mathbf{P}^s \partial_s \mathbf{u}, \quad (4.3)$$

where here we dropped non-principal terms and all derivatives transverse to s^i . The definitions of weak and strong hyperbolicity are identical to those discussed for first order systems in Sec. 2.2. Weak hyperbolicity is the requirement that the eigenvalues of \mathbf{P}^s are real for each s^i , while strong hyperbolicity is the requirement that it is also uniformly diagonalizable in s^i . The second order principal symbol (4.2) is inherited as a diagonal block of the principal symbol of any standard first order reduction, where the latter furthermore takes an upper block triangular form. Consequently only SH second order systems may admit a standard first order reduction that is SH. The importance of this is that (4.1) has a well-posed initial value problem in the norm

$$E_1 = \sum_i \|\partial_i \mathbf{v}\|_{L^2} + \|\mathbf{v}\|_{L^2} + \|\mathbf{w}\|_{L^2},$$

if and only if it is strongly hyperbolic, where here the norms are defined over spatial slices of constant t . For our analysis, observe that the original characteristic form of the equations of motion is not of the form (4.1), even after linearization. We overcome this issue by working instead with the ADM equivalent obtained in Sec. 3.2. Working with the equivalent ADM system not only provides an invertible time principal matrix, but has also the advantage that the theory discussed below was developed in this language, making application straightforward. Due to the freedom in choosing a time slicing, there is freedom in the construction of the equivalent ADM formulation. This was parameterized by $f'(\rho)$ in the previous section. For brevity we work assuming $f'(\rho) = 1$, but since the structural properties discussed above hold true in *any* alternative slicing this restriction does not affect the outcome of the analysis.

4.2 Pure gauge and constraint subsystems

The linearized ADM system allows us to identify specific variables that are associated with degrees of freedom related to pure gauge and constraint violation. The pure gauge and constraint subsystems are closed systems on their own, and their principal structure is inherited in the principal symbol of the linearized ADM system.

Pure gauge degrees of freedom: In many cases of physical interest FT2S systems arise with additional structure in their principal symbol. In GR for instance, structure arises as a consequence of gauge freedom. To see this, suppose that we are working in a coordinate basis with an arbitrary solution to the vacuum field equations. The field equations are of course invariant under changes of coordinates $x^\mu \rightarrow X^\mu$, so that both the metric and curvature transform in the same manner. This invariance has important consequences on the form of the field equations. Consider an infinitesimal change to the coordinates by $x^\mu \rightarrow x^\mu + \xi^\mu$. Such a change results in a perturbation to the metric of the form

$$\delta g_{\mu\nu} = -\nabla_\mu \xi_\nu - \nabla_\nu \xi_\mu = -\mathcal{L}_\xi g_{\mu\nu}.$$

This transformation, the linearization of the condition for covariance in a coordinate basis, simultaneously serves as the gauge freedom of linearized GR. Working now in the ADM language, and 3 + 1 decomposing ξ^a by

$$\Theta \equiv -n_\mu \xi^\mu, \quad \psi^i \equiv -\gamma^i_\mu \xi^\mu,$$

the pure gauge perturbations (Θ, ψ^i) satisfy (see [115])

$$\begin{aligned} \partial_t \Theta &= \delta\alpha - \psi^i D_i \alpha + \mathcal{L}_\beta \Theta, \\ \partial_t \psi^i &= \delta\beta^i + \alpha D^i \Theta - \Theta D^i \alpha + \mathcal{L}_\beta \psi^i, \end{aligned} \quad (4.4)$$

with $\delta\alpha$ and $\delta\beta^i$ the perturbation of the lapse and shift respectively. The resulting perturbations to the metric and extrinsic curvature can be explicitly computed [101], and are given by,

$$\delta\gamma_{ij} = -2\Theta K_{ij} + \mathcal{L}_\psi \gamma_{ij}, \quad (4.5a)$$

$$\delta K_{ij} = -D_i D_j \Theta + \Theta (R_{ij} - 2K^k_i K_{jk} + K_{ij} K) + \mathcal{L}_\psi K_{ij}, \quad (4.5b)$$

where γ_{ij} and K_{ij} are the metric and extrinsic curvature associated with the background metric. It is a remarkable fact that these equations are nothing more than the ADM evolution equations under the replacements $\alpha \rightarrow \Theta$ and $\beta^i \rightarrow \psi^i$, so that the ADM evolution equations can be interpreted as a local gauge transformation in a coordinate basis. Given a choice for either the lapse and shift, or an equation of motion for each, or a combination thereof, we may combine (4.4) and (4.5), to obtain a closed system for the pure gauge variables (Θ, ψ^i) and $(\delta\alpha, \delta\psi^i)$, on the background spacetime. We call this the *pure gauge subsystem*. Suppose for example that we employed a harmonic time coordinate ($\square t = 0$) with vanishing shift. In 3 + 1 language this gives

$$\partial_t \alpha = -\alpha^2 K.$$

The pure gauge subsystem (4.4) for (Θ, ψ^i) , is then completed by

$$\partial_t \delta \alpha \simeq \alpha^2 \partial^i \partial_i \Theta, \quad \delta \beta^i = 0,$$

where we have used (4.5) and discarded non-principal terms. The additional structure alluded to above is that for a given choice of gauge, the principal symbol of the pure gauge subsystem is inherited as a sub-block of the principal symbol of any formulation of GR that employs said gauge. This is demonstrated by using suitable projection operators which are stated explicitly in Sec. 4.3.

Constraint violating degrees of freedom: Yet more structure arises from the constraints. Assuming the ADM evolution equations hold, the Hamiltonian and Momentum constraints formally satisfy evolution equations,

$$\begin{aligned} \partial_t H &= -2\alpha D^i M_i - 4M^i D_i \alpha + 2\alpha K H + \mathcal{L}_\beta H, \\ \partial_t M_i &= -\frac{1}{2}\alpha D_i H + \alpha K M_i - D_i \alpha H + \mathcal{L}_\beta M_i, \end{aligned}$$

so given constraint satisfying initial data, the solution in their future domain of dependence satisfies these constraints as well. These equations follow from the contracted Bianchi identities. In free-evolution formulations of GR however, the ADM evolution equations need not hold, since combinations of the constraints can be freely added to the evolution equations. Doing so results in adjusted evolution equations for the constraints, which nevertheless remain a closed set of equations. Just as the principal symbol of the full equations of motion inherits the pure gauge principal symbol, the principal symbol of the constraint subsystem manifests as a sub-block. This is again seen using the projection operators stated in Sec. 4.3.

Linearized ADM: To apply straightforwardly the theory described at Sec. 4.1 we linearize about flat space in global inertial coordinates. The analysis can be carried out around a general background leading to the same conclusions. In this setting we obtain for the metric and extrinsic curvature perturbations the evolution equations,

$$\partial_t \delta \gamma_{ij} = -2\delta K_{ij} + \partial_{(i} \delta \beta_{j)}, \quad (4.6a)$$

$$\partial_t \delta K_{ij} = -\partial_i \partial_j \delta \alpha - \frac{1}{2} \partial^k \partial_k \delta \gamma_{ij} - \frac{1}{2} \partial_i \partial_j \delta \gamma + \partial^k \partial_{(i} \delta \gamma_{j)k}. \quad (4.6b)$$

The constraints become

$$\begin{aligned} \delta H &= \partial^i \partial^j \delta \gamma_{ij} - \partial^i \partial_i \delta \gamma, \\ \delta M_i &= \partial^j \delta K_{ij} - \partial_i \delta K, \end{aligned}$$

and evolve according to

$$\begin{aligned}\partial_t \delta H &= -2\partial^i \delta M_i, \\ \partial_t \delta M_i &= -\frac{1}{2}\partial_i \delta H.\end{aligned}\tag{4.7}$$

About this background the pure gauge equations (4.4) simplify to

$$\partial_t \Theta = \delta \alpha, \tag{4.8a}$$

$$\partial_t \psi_i = \delta \beta_i + \partial_i \Theta. \tag{4.8b}$$

4.3 Projection operators

To unravel the special structure of the principal symbol of the linearized ADM system we use projection operators. This structure distinguishes in the linear, constant coefficient approximation between the pure gauge, constraint violating and physical ADM variables, along an arbitrary spatial direction.

Pure gauge projection operators: Let s^i be an arbitrary constant spatial unit vector. To extract the gauge, constraint and physical degrees of freedom within the principal symbol in this direction we must decompose the state vector appropriately. The induced metric on the surface transverse to s^i is

$$q_{ij} \equiv \gamma_{ij} - s_i s_j.$$

Here we denote by \hat{A} , \hat{B} the spatial directions transverse to s^i , which—since in general $s^i \neq s^i_{(\rho)}$ —do not necessarily coincide with the angular directions from Sec. 3.3. Projections of the ADM variables that capture pure gauge equations of motion (4.8) are given by,

$$[\partial_s^2 \Theta] = -\delta K_{ss}, \quad [\partial_s^2 \psi_s] = \frac{1}{2}\partial_s \delta \gamma_{ss}, \quad [\partial_s^2 \psi_{\hat{A}}] = \partial_s \delta \gamma_{s\hat{A}}.\tag{4.9}$$

Here the notation $[\dots]$ is used to emphasize that the specific projection of the ADM variables on the right-hand-side shares, within the principal symbol, the structure of the pure gauge variable named on the left-hand-side. This is spelled out below. Thus, together with $\partial_s \delta \alpha$, $\partial_s \delta \beta_s$, $\partial_s \delta \beta_{\hat{A}}$ they encode the complete pure gauge variables of the system, with $\delta \alpha$, $\delta \beta^i$ the perturbation to the lapse and shift.

Constraint projection operators: Likewise, within the principal symbol the Hamiltonian and Momentum constraints are encoded by the projections,

$$[H] = -\partial_s \delta \gamma_{qq}, \quad [M_s] = -\delta K_{qq}, \quad [M_{\hat{A}}] = \delta K_{s\hat{A}}, \tag{4.10}$$

with the naming convention as above. Here and in the following indices qq denote that the trace was taken with q^{ij} .

Physical projection operators: Finally, the remaining variables to be taken account of are the trace free projections. Defining the projection operator familiar from textbook treatments of linear gravitational waves,

$$P_{ij}^{\perp kl} \equiv q^k_{(i} q^l_{j)} - \frac{1}{2} q_{ij} q^{kl}. \quad (4.11)$$

we define

$$\partial_s \delta \gamma_{\hat{A}\hat{B}}^{\text{TF}} = P_{\hat{A}\hat{B}}^{\perp ij} \partial_s \delta \gamma_{ij}, \quad \delta K_{\hat{A}\hat{B}}^{\text{TF}} = P_{\hat{A}\hat{B}}^{\perp ij} \delta K_{ij}.$$

The superscript TF denotes trace free. These variables are associated with the physical degrees of freedom.

The principal symbol: Employing the notation above we can now write out the principal symbol in the form (4.3). Starting with the pure gauge block, this gives

$$\begin{aligned} \partial_t[\partial_s^2 \Theta] &\simeq \partial_s(\partial_s \delta \alpha) + \frac{1}{2} \partial_s[H], \\ \partial_t[\partial_s^2 \psi_s] &\simeq \partial_s(\partial_s \delta \beta_s) + \partial_s[\partial_s^2 \Theta], \\ \partial_t[\partial_s^2 \psi_{\hat{A}}] &\simeq \partial_s(\partial_s \delta \beta_{\hat{A}}) - 2\partial_s[M_{\hat{A}}]. \end{aligned} \quad (4.12)$$

Comparing this with (4.8) it is clear that up to additions of the “constraint variables” there is agreement. Next, the constraint violating block gives

$$\begin{aligned} \partial_t[H] &\simeq -2\partial_s[M_s], \\ \partial_t[M_s] &\simeq -\frac{1}{2}\partial_s[H], \\ \partial_t[M_{\hat{A}}] &\simeq 0. \end{aligned} \quad (4.13)$$

Comparing this with (4.7) there is perfect agreement. Finally the physical block is

$$\begin{aligned} \partial_t \partial_s \delta \gamma_{\hat{A}\hat{B}}^{\text{TF}} &\simeq -2\partial_s \delta K_{\hat{A}\hat{B}}^{\text{TF}}, \\ \partial_t \delta K_{\hat{A}\hat{B}}^{\text{TF}} &\simeq -\frac{1}{2} \partial_s^2 \delta \gamma_{\hat{A}\hat{B}}^{\text{TF}}, \end{aligned} \quad (4.14)$$

which is decoupled from the rest of the equations. These equations are not yet complete, because we have not yet made a concrete choice of gauge. Several Bondi-like gauges are treated in detail in Chap. 5.

4.4 Discussion

The results of the foregoing discussion follow because GR is a constrained Hamiltonian system that satisfies the hypotheses of [101]. To make the presentation here somewhat more standalone however, let us consider a plane wave ansatz

$$\begin{aligned}
\delta\gamma_{ij} &= 2e^{\kappa_\mu^{(\psi_s)} x^\mu} s_i s_j [\partial_s \tilde{\psi}_s] - \frac{1}{2} q_{ij} e^{\kappa_\mu^{(H)} x^\mu} [\tilde{H}] \\
&\quad + 2e^{\kappa_\mu^{(\psi_A)} x^\mu} q^{\hat{A}}_{(i} s_{j)} [\partial_s \tilde{\psi}_{\hat{A}}] + e^{\kappa_\mu^{(P)} x^\mu} P_{\perp ij}^{\hat{A}\hat{B}} \delta\gamma_{\hat{A}\hat{B}}^{\text{TF}}, \\
\delta K_{ij} &= -e^{\kappa_\mu^{(\Theta)} x^\mu} s_i s_j [\partial_s^2 \tilde{\Theta}] - \frac{1}{2} q_{ij} e^{\kappa_\mu^{(M_s)} x^\mu} [\tilde{M}_s] \\
&\quad + 2e^{\kappa_\mu^{(M_A)} x^\mu} q^{\hat{A}}_{(i} s_{j)} [\tilde{M}_{\hat{A}}] + e^{\kappa_\mu^{(P)} x^\mu} P_{\perp ij}^{\hat{A}\hat{B}} \delta K_{\hat{A}\hat{B}}^{\text{TF}},
\end{aligned} \tag{4.15}$$

with each wave vector of the form $\kappa_\mu = (\kappa, i\omega s_i)$. These solutions travel in the $\pm s^i$ directions, although since the lapse and shift are as yet undetermined, the κ 's can not be solved for so far. Defining the projections exactly as above, the unknowns can be decomposed *explicitly* into their gauge, constraint violating and gravitational wave pieces as indicated by the naming, and equations (4.12), (4.13) and (4.14) become exact. In the nonlinear setting it is of course hopeless to try and decompose metric components into their constituent gauge, constraint violating and physical degrees of freedom. But even in the linear constant coefficient approximation, solutions consist in general of a sum over many such plane waves propagating in different directions, and so the decomposition (4.15) is not a sufficient description. What is important for our purposes however, is that the structure in the field equations that permits the decomposition (4.15) for plane wave solutions is present regardless of the direction s^i considered. The principal symbol sees only this structure and thus, with the equations (4.12), (4.13) and (4.14) above completed with a choice for the lapse and shift, can be written in the schematic form

$$\mathbf{P}^s = \begin{pmatrix} \mathbf{P}_G & \mathbf{P}_{GP} & \mathbf{P}_{GC} \\ 0 & \mathbf{P}_P & \mathbf{P}_{PC} \\ 0 & 0 & \mathbf{P}_C \end{pmatrix}, \tag{4.16}$$

even upon linearization about an arbitrary background. Here \mathbf{P}_G , \mathbf{P}_C , \mathbf{P}_P denote the gauge, constraint and physical sub-blocks and \mathbf{P}_{GC} , \mathbf{P}_{GP} , \mathbf{P}_{PC} parameterize the coupling between them. As seen in [101] there is a very large class of gauge conditions and natural constraint additions that result in $\mathbf{P}_{GP} = \mathbf{P}_{GC} = \mathbf{P}_{PC} = 0$. The affine null gauge analyzed in Sec. 5.1 is however an explicit example where both \mathbf{P}_{GP} and \mathbf{P}_{GC} are non-vanishing. Consequently, it follows from (4.16) that a necessary condition for strong hyperbolicity of the formulation is that the pure gauge and constraint subsystems are themselves strongly hyperbolic (see e.g. App. A of [119] for details). Following [115] we may therefore restrict our attention first to pure gauge systems of interest, which have the advantage of being smaller, and thus much easier to treat.

Bondi-like gauges: The gauges we are concerned with all require the condition (3.2), which in characteristic coordinates implies the same for the perturbation to the metric, that is,

$$\delta g^{uu} = \delta g^{uA} = 0.$$

There remains one gauge condition to be specified, namely the parameterization along outgoing null surfaces by a radial coordinate. In Chap. 5 we study specific instances of this condition.

CHAPTER 5

Hyperbolicity of Bondi-like PDE systems

Contents

5.1	The affine null gauge	44
5.1.1	Pure gauge subsystem	44
5.1.2	Pure gauge sub-block: radial direction	45
5.1.3	Pure gauge sub-block: angular direction θ	50
5.1.4	Asymptotically anti-de Sitter spacetimes	54
5.2	The Bondi-Sachs gauge proper	60
5.2.1	Pure gauge subsystem	61
5.2.2	Pure gauge sub-block: angular direction θ	62
5.2.3	Axisymmetry in characteristic variables	63
5.3	Double-null and more gauges	67
5.4	Frame independence	69
5.5	Conclusions	72

We perform hyperbolicity analyses for some popular Bondi-like free evolution PDE systems. For the affine null gauge we identify the pure gauge sub-block in the ADM equivalent system, as well as in the characteristic one for asymptotically flat spacetimes and show that the system is only WH due to the angular sector of the pure gauge subsystem. We also demonstrate weak hyperbolicity for a planar symmetric asymptotically AdS_5 setup based on the affine null gauge. The Bondi-Sachs pure gauge subsystem is also shown to be WH due to its angular structure and the inheritance of this is demonstrated for the ADM equivalent setup. An axisymmetric characteristic setup in Bondi-Sachs coordinates is shown to be only WH as well due to its angular structure. After identifying the same type of weak hyperbolicity for the double-null pure gauge subsystem as well, we argue in Sec. 5.3 that under certain conditions all Bondi-like free evolution PDE systems with up to second order metric derivatives are only WH.

The intrinsic equations of the systems in Subsecs. 5.1.4 and 5.2.3 possess a nested structure that makes them convenient for numerical studies, since they require less computational resources. It is not clear why this structure appears and it seems to be affected by the choice

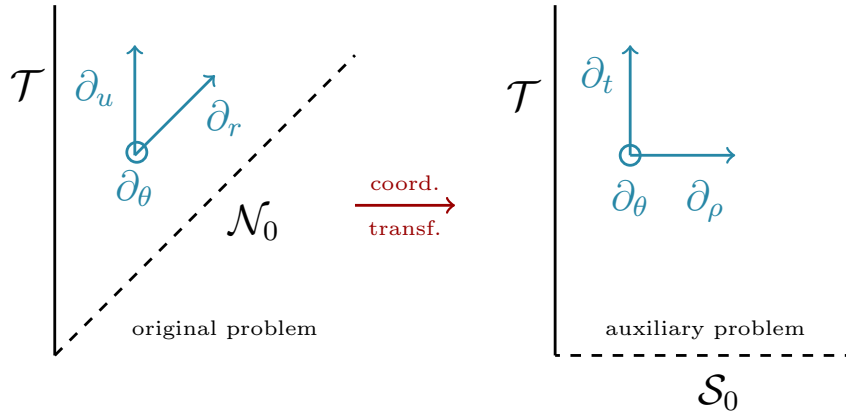


Figure 5.1: The original CIBVP is transformed into an auxiliary frame using the coordinate transformation (5.1) as shown. This allows us to employ the hyperbolicity definitions of Sec. 2.2 but does not affect the solution space.

of variables used [111]. This however is not a generic feature of characteristic PDEs but rather a special structure that can be found in Bondi-like systems.

The PDE systems under consideration are quasilinear, whereas the definitions for the degree of hyperbolicity provided in Sec. 2.2 refer to first order linear systems. To apply these definitions we perform a linearization about a fixed background and a first order reduction. We chose this background to be Minkowski except for Subsec. 5.1.4 where it is vacuum AdS_5 . In [121] and in the ancillary files of [2] the same calculations for arbitrary backgrounds can be found. It turns out that the hyperbolic character of the analyzed PDEs is unaffected by the choice of background for this analysis. To determine the degree of hyperbolicity of each system we work in the frozen coefficient approximation and demand that for a system to be WH or SH, the definitions of Sec. 2.2 are satisfied at each point in the domain of interest. In [122] and [123] the authors studied existence and uniqueness of the CIBVP for a free evolution system in Bondi-Sachs coordinates. They considered the linearized and quasilinear systems, but did not study continuous dependence on given data. The latter is the main focus here and in chapters 6 and 7 we provide more details at the continuum and numerical level, respectively.

The time principal part matrix of characteristic PDE systems is non-invertible. To construct the principal symbol (2.9) after linearization and first order reduction we employ a coordinate transformation to an auxiliary Cauchy-type setup. We wish to bring the characteristic system to the form (2.1), with an invertible principal part matrix \mathcal{A}^t . In the following sections we use the coordinate transformation (3.5) with $f(\rho) = \rho$, namely

$$u = t - \rho, \quad r = \rho, \quad (5.1)$$

with the angular coordinates unchanged, which yields the following relation between the old and new basis vectors,

$$\partial_u = \partial_t, \quad \partial_r = \partial_t + \partial_\rho,$$

with the remaining vectors unaltered. An illustration of the auxiliary setup is given in Fig. 5.1. Applying the transformation yields

$$\mathcal{A}^t \partial_t \mathbf{u} + \mathcal{A}^r \partial_\rho \mathbf{u} + \mathcal{A}^\theta \partial_\theta \mathbf{u} + \mathcal{S} = 0,$$

with $\mathcal{A}^t = \mathcal{A}^u + \mathcal{A}^r$ invertible. After multiplying from the left with $(\mathcal{A}^t)^{-1}$ we can bring the system in the form

$$\partial_t \mathbf{u} + \mathbf{B}^p \partial_p \mathbf{u} + \mathcal{S} = 0, \quad (5.2)$$

where the principal symbol is simply $\mathbf{P}^s = \mathbf{B}^p s_p$. In comparison to the form (2.10) notice the difference in the sign convention, namely $\mathbf{B}^p = -\mathcal{B}^p$ and $\mathcal{B}\mathbf{u} = -\mathcal{S}$. The solution space in this frame is equivalent to that of the original one, so in this sense the character of the PDE is invariant. In Sec. 5.4 we show that the hyperbolic character of the system is also independent of the auxiliary frame chosen for the analysis. An auxiliary Cauchy setup was also used in [124] to show well-posedness of the CIBVP for a symmetric hyperbolic characteristic system.

To treat the system in the original higher-order derivative form, we could follow [119, 120]. But for convenience in building the principal parts we instead perform an explicit first order reduction. Since this PDE is built as a reduction, there is the subtlety of the associated reduction constraints and the specific choice of reduction, which we discuss in detail making use of *generalized characteristic variables*. To understand this notion consider the principal symbol \mathbf{P}^s and the generalized eigenvalue problem,

$$\mathbf{l}_{\lambda_i} (\mathbf{P}^s - \lambda_i \mathbf{1})^m = 0,$$

with λ_i standing for the various eigenvalues, and \mathbf{l}_{λ_i} representing either a true eigenvector when $m = 1$ or else a generalized eigenvector when $m > 1$. Defining the invertible matrix \mathbf{T}_s^{-1} with the vectors \mathbf{l}_{λ_i} , as rows, we obtain the Jordan normal form of the principal symbol in the s direction by the similarity transformation

$$\mathbf{J}^s \equiv \mathbf{T}_s^{-1} \mathbf{P}^s \mathbf{T}_s.$$

The same matrix can be used to construct the generalized characteristic variables of the system in the s direction, namely the components of $\mathbf{v} \equiv \mathbf{T}_s^{-1} \mathbf{u}$. These are of course nothing more than the left generalized eigenvectors contracted with the state vector. Working in the frozen coefficient approximation, focusing on the t, s parts of (5.2) and multiplying on the

left with \mathbf{T}_s^{-1} one can get

$$\partial_t \mathbf{v} + \mathbf{J}_s \partial_s \mathbf{v} \simeq 0, \quad (5.3)$$

with \simeq denoting here equality up to non-principal terms and spatial derivatives transverse to ∂_s . In this form, weak hyperbolicity can be understood as the failure of a generalized characteristic variable to satisfy an advection equation along ∂_s with some characteristic speed λ_s which may also be vanishing.

5.1 The affine null gauge

In terms of lapse and shift specification, the complete affine null gauge fixing is given by

$$\alpha = L^{-1}, \quad \beta^\rho = L^{-2} - 1, \quad \beta^A = -b^A L^{-2}, \quad (5.4)$$

where Eqs. (3.21)-(3.23) and $g^{ur} = -1$ have been combined and $f(\rho) = \rho$ in Eq. (3.5) is assumed.

5.1.1 Pure gauge subsystem

Let us first consider pure gauge metric perturbations (4.5). To close the system (4.8) further input for $\delta\alpha$ and $\delta\beta^i$ is needed. For the affine null gauge this follows from (5.4), which after linearization about flat space reads

$$\begin{aligned} \delta\alpha &= -\frac{1}{2}\delta\gamma_{\rho\rho}, & \delta\beta^\theta &= -\rho^{-2}\delta\gamma_{\rho\theta}, \\ \delta\beta^\rho &= -\delta\gamma_{\rho\rho}, & \delta\beta^\phi &= -\rho^{-2}\sin^2\theta\delta\gamma_{\rho\phi}. \end{aligned} \quad (5.5)$$

Using $\delta\gamma_{ij} = \partial_i\psi_j + \partial_j\psi_i$ and $\psi^i = \gamma^{ij}\psi_j$ the latter reads

$$\begin{aligned} \delta\alpha &= -\partial_\rho\psi^\rho, & \delta\beta^\theta &= -\partial_\rho\psi^\theta - \rho^{-2}\partial_\theta\psi^\rho, \\ \delta\beta^\rho &= -2\partial_\rho\psi^\rho, & \delta\beta^\phi &= -\partial_\rho\psi^\phi - \rho^{-2}\sin^2\theta\partial_\phi\psi^\rho. \end{aligned} \quad (5.6)$$

The pure gauge subsystem (4.8) is then

$$(\partial_t + \partial_\rho)(\psi^\rho - \Theta) = 0, \quad (5.7a)$$

$$(\partial_t + \partial_\rho)\psi^\rho + \partial_\rho(\psi^\rho - \Theta) = 0, \quad (5.7b)$$

$$(\partial_t + \partial_\rho)\psi^\theta + \rho^{-2}\partial_\theta(\psi^\rho - \Theta) = 0, \quad (5.7c)$$

$$(\partial_t + \partial_\rho)\psi^\phi + (\rho\sin\theta)^{-2}\partial_\phi(\psi^\rho - \Theta) = 0, \quad (5.7d)$$

where $\partial_t + \partial_\rho = \partial_r$ is an outgoing null derivative and (5.7a) results from a linear combination of (4.8a) and (4.8b) with $i = \rho$. The principal symbol of the pure gauge subsystem (5.7) is clearly non-diagonalizable along the ρ, θ, ϕ directions, and in fact in any direction.

In (5.7b), (5.7c) and (5.7d) the terms $\partial_\rho(\psi^\rho - \Theta)$, $\partial_\theta(\psi^\rho - \Theta)$ and $\partial_\phi(\psi^\rho - \Theta)$ result in 2×2 Jordan blocks, along ρ , θ and ϕ respectively. The principal symbol of the full set of equations of motion for GR has the upper triangular form (4.16) when a standard first order reduction is considered. Thus it will possess non-trivial Jordan blocks along all ρ , θ , ϕ directions as well. In Subsecs. 5.1.2 and 5.1.3 we show this explicitly and demonstrate the connection to the PDE system in characteristic coordinates.

An intriguing observation is that the pure gauge variable $(\psi^\rho - \Theta)$ satisfies a transport equation along ∂_r . So, acting from the left on (5.7) with ∂_r and commuting the spatial and null derivatives on $(\psi^\rho - \Theta)$, one obtains

$$\partial_r^2(\Theta - \psi^\rho) = 0, \quad (5.8a)$$

$$\partial_r^2\psi^\rho = 0, \quad (5.8b)$$

$$\partial_r^2\psi^\theta = 0, \quad (5.8c)$$

$$\partial_r^2\psi^\phi = 0. \quad (5.8d)$$

This system admits a non-standard reduction to first order which is strongly hyperbolic. To see this, we introduce only outgoing null derivatives of the unknowns as auxiliary variables. All of the variables then satisfy transport equations in the outgoing null direction. In contrast to this, for a standard first order reduction both the time and space derivatives of the unknowns would be introduced as auxiliary variables.

The relevant question is whether or not there exists a formulation of GR that inherits the structure of the second version of the pure gauge subsystem (5.8), rather than the first (5.7). In view of the results of [101], if such a formulation exists it would necessarily admit a non-standard first order reduction. In Subsec. 5.1.2 we show that there is a convenient combination of ADM variables that allows one to remove the non-trivial Jordan block along the ρ direction that appears in a standard first order reduction. This is true due to the specific gauge choice and its construction upon outgoing null geodesics. Crucially however, this special combination is only possible along the ρ direction but not θ , ϕ . So, away from spherical symmetry the EFE in the affine null gauge are only WH.

5.1.2 Pure gauge sub-block: radial direction

We now demonstrate how the radial part of the pure gauge subsystem (5.7) is inherited by the linearized EFE. For brevity in this subsection we work in spherical symmetry, which is sufficient, since the coupled gauge variables in the radial Jordan block of (5.7) are present already under this assumption.

ADM setup

In spherical symmetry the principal part of the linearized ADM equations in outgoing affine null gauge is

$$\partial_t \delta \gamma_{\rho\rho} \simeq -2\delta K_{\rho\rho} - 2\partial_\rho \delta \gamma_{\rho\rho}, \quad (5.9a)$$

$$\partial_t \delta K_{\rho\rho} \simeq \frac{1}{2} \partial_\rho^2 \delta \gamma_{\rho\rho} - \rho^{-2} \partial_\rho^2 \delta \gamma_{\theta\theta}, \quad (5.9b)$$

$$\partial_t \delta \gamma_{\theta\theta} \simeq -2\delta K_{\theta\theta}, \quad (5.9c)$$

$$\partial_t \delta K_{\theta\theta} \simeq -\frac{1}{2} \partial_\rho^2 \delta \gamma_{\theta\theta}. \quad (5.9d)$$

From Eq. (4.9), the gauge variables along the ρ direction in spherical symmetry are

$$-\delta K_{\rho\rho} = [\partial_\rho^2 \Theta], \quad \frac{1}{2} \partial_\rho \delta \gamma_{\rho\rho} = [\partial_\rho^2 \psi^\rho]. \quad (5.10)$$

To recover the pure gauge structure it suffices to analyze the coupling between (5.9a) and (5.9b)

$$\partial_r (\frac{1}{2} \delta \gamma_{\rho\rho}) \simeq -\delta K_{\rho\rho} - \partial_\rho (\frac{1}{2} \delta \gamma_{\rho\rho}), \quad (5.11a)$$

$$\partial_r (\delta K_{\rho\rho} + \frac{1}{2} \partial_\rho \delta \gamma_{\rho\rho}) \simeq -\rho^{-2} \partial_\rho^2 \delta \gamma_{\theta\theta}, \quad (5.11b)$$

where $\partial_r = \partial_t + \partial_\rho$ is an outgoing null vector, and (5.11b) results from a linear combination of (5.9a) and (5.9b). The right-hand-side of (5.11b) involves the constraint variable

$$[H] = -\partial_\rho \delta \gamma_{\rho\rho} = -2\rho^{-2} \partial_\rho \delta \gamma_{\theta\theta}.$$

In a standard first order reduction, the term $(\partial_\rho \delta \gamma_{\rho\rho})$ would be introduced as an evolved variable satisfying

$$\partial_r (\frac{1}{2} \partial_\rho \delta \gamma_{\rho\rho}) \simeq -\partial_\rho \delta K_{\rho\rho} - \partial_\rho (\frac{1}{2} \partial_\rho \delta \gamma_{\rho\rho}). \quad (5.12)$$

The above and (5.11b) expressed in terms of gauge and constraint variables read

$$\partial_r [\partial_\rho^2 \psi^\rho] + \partial_\rho [\partial_\rho^2 (\psi^\rho - \Theta)] \simeq 0,$$

$$\partial_r [\partial_\rho^2 (\Theta - \psi^\rho)] \simeq \frac{1}{2} \partial_\rho [H].$$

As explained in Sec. 4.4, this system has a pure gauge part which consists of the coupling among the gauge variables Θ and ψ^ρ and a part that captures the coupling of the gauge to the constraint variables. The pure gauge part \mathbf{P}_G is obtained by neglecting the term $\partial_\rho [H]/2$. This part has the same principal structure as the pure gauge subsystem (5.7) in the radial direction, since it is just an overall ∂_ρ^2 derivative of the latter. This is in accordance with the result of [101], because for a standard first order reduction \mathbf{P}_G inherits the structure of the first order system formed by $(\Theta, \psi_i, \delta\alpha, \delta\beta_i)$. The term $\partial_\rho [H]/2$ is encoded in the \mathbf{P}_{GC}

sub-block of the full principal symbol \mathbf{P}^ρ .

Next, let us consider a reduction in which $(\partial_r \delta \gamma_{\rho\rho})$ is introduced as an auxiliary variable rather than $(\partial_\rho \delta \gamma_{\rho\rho})$. From (5.11a) and (5.10) we get

$$\partial_r(\tfrac{1}{2}\delta\gamma_{\rho\rho}) = [\partial_r\partial_\rho\psi^\rho] \simeq [\partial_\rho^2(\Theta - \psi^\rho)], \quad (5.13)$$

where in the first step we are just using our normal naming convention with [...], and likewise in the second Eq. (5.10). Similarly, from Eq. (5.10) we get

$$\tfrac{1}{2}\partial_\rho\delta\gamma_{\rho\rho} + \delta K_{\rho\rho} = [\partial_\rho^2(\psi^\rho - \Theta)] = [\partial_r\partial_\rho\psi^\rho] = -[\partial_r\partial_\rho\Theta], \quad (5.14)$$

where in the second step Eq. (5.7b) and in the third Eq. (5.7a) are used. The equation of motion for the auxiliary variable $(\partial_r \delta \gamma_{\rho\rho})$ results from (5.11a) after acting with ∂_r , namely

$$\partial_r(\tfrac{1}{2}\partial_r\delta\gamma_{\rho\rho}) \simeq -\partial_r(\delta K_{\rho\rho} + \tfrac{1}{2}\partial_\rho\delta\gamma_{\rho\rho}) \simeq \rho^{-2}\partial_\rho^2\delta\gamma_{\theta\theta}, \quad (5.15)$$

where in the second step Eq. (5.11b) is used. The above together with Eq. (5.11b) in terms of the gauge and constraint variables read

$$\partial_r[\partial_r\partial_\rho\psi^\rho] \simeq -\tfrac{1}{2}\partial_\rho[H], \quad (5.16a)$$

$$\partial_r[\partial_r\partial_\rho\Theta] \simeq \tfrac{1}{2}\partial_\rho[H], \quad (5.16b)$$

where the relations (5.13), (5.14) have been used. Thus, the system (5.11b), (5.15) inherits the principal structure of (5.8a)-(5.8b) in \mathbf{P}_G . Again the term $\partial_\rho[H]/2$ is in the \mathbf{P}_{GC} sub-block. This result does not contradict [101] due to the non-standard first order reduction considered. In the outgoing affine null gauge the outgoing null direction possesses a special role as the foundational piece of the construction. This construction provides the opportunity to group ADM variables in such a way that we can avoid the non-trivial Jordan block in the radial direction.

Characteristic setup

The ADM analysis above teaches us which variables inherit the principal structure of the pure gauge degrees of freedom. However, the original PDE problem is formulated in the characteristic domain. In [101] the pure gauge structure was identified for a spacelike foliation. Whether or not this is possible in the characteristic domain is closely related to the existence of the previous first order reductions in this domain as well. We show here that both previous first order reductions and their principal structure can be realized in the characteristic setup directly.

To demonstrate this consider the affine null gauge in an outgoing characteristic formulation. The complete calculation can be found in the ancillary files of [2]. We first employ the metric

ansatz

$$ds^2 = g_{uu}du^2 - 2dudr + g_{\theta\theta}d\theta^2 + g_{\phi\phi}d\phi^2,$$

which for flat space reads

$$g_{uu} = -1, \quad g_{\theta\theta} = r^2, \quad g_{\phi\phi} = r^2 \sin^2 \theta.$$

Analyzing the main equations $R_{rr} = R_{\theta\theta} = R_{\phi\phi} = 0$ linearized about flat space we see the following structure

$$\partial_r \delta g_{uu} - \frac{1}{2\rho} \partial_\rho \left(\partial_r \delta g_{\theta\theta} + \sin^{-2} \theta \partial_r \delta g_{\phi\phi} \right) = 0, \quad (5.17a)$$

$$\partial_r \left(\partial_r \delta g_{\theta\theta} + \sin^{-2} \theta \partial_r \delta g_{\phi\phi} \right) = 0. \quad (5.17b)$$

The variable $(\partial_r \delta g_{\theta\theta} + \sin^{-2} \theta \partial_r \delta g_{\phi\phi})$ in (5.17a) prevents δg_{uu} from satisfying just an advection equation along ∂_r and so provides a non-trivial Jordan block. The combination of $\delta g_{\theta\theta}$ and $\delta g_{\phi\phi}$ in the former hints that a different choice of variables may be more appropriate. This combination of variables furthermore appears in the trivial equation $R_{ur} = 0$ when linearized about flat space, and so it may be optimal to group them together. We thus next consider the equations as resulting from the metric ansatz

$$ds^2 = g_{uu}du^2 - 2dudr + \hat{R}(u, r)^2 \left(d\theta^2 + \sin^2 \theta d\phi^2 \right),$$

where \hat{R} is the radius of the two-sphere. This form of the metric ansatz is used in the spherically symmetric case of [111], employed by [86] in the study of gravitational collapse of a massless scalar field, as well as in [97] for cosmological considerations using past null cones. Upon linearization about flat space the characteristic PDE system takes the form

$$\partial_r^2 \delta \hat{R} = 0, \quad (5.18a)$$

$$2r \partial_u \partial_r \delta \hat{R} + 2\partial_u \delta \hat{R} - 2\partial_r \delta \hat{R} + r \partial_r \delta g_{uu} + \delta g_{uu} = 0, \quad (5.18b)$$

$$4\partial_u \partial_r \delta \hat{R} + r \partial_r^2 \delta g_{uu} + 2\partial_r \delta g_{uu} = 0. \quad (5.18c)$$

Eq. (5.18a) and (5.18b) correspond to the main equations $R_{rr} = 0$ and $R_{\theta\theta} = 0$ respectively, and Eq. (5.18c) to the trivial one $R_{ur} = 0$. The main equation $R_{\phi\phi}$ is dropped since it is proportional to $R_{\theta\theta}$ and the two-sphere is parameterized only by its radius.

Comparing once more with the ADM form of the problem, including the trivial equation (5.18c) in the system corresponds to including the linearized ADM equation for $\delta K_{\rho\rho}$ in the analysis. This is an essential component in identifying the pure gauge sub-block along

the radial direction. To achieve this we first make the following identification using Eq. (3.8)

$$g_{uu} = \alpha^{-2} - 2,$$

which after linearization about flat space yields

$$\delta g_{uu} = -2\delta\alpha = \delta\gamma_{\rho\rho}, \quad (5.19)$$

where the gauge condition $\delta\alpha = -\delta\gamma_{\rho\rho}/2$ is used. We consider now a first order reduction with

$$(\partial_r \delta \hat{R}), \quad (\partial_u \delta \hat{R}), \quad (\partial_r \delta g_{uu})$$

promoted to independent variables where, by (5.19), the latter is equivalent to $(\partial_r \delta \gamma_{\rho\rho})$ being treated as a reduction variable. This first order reduction provides a diagonalizable radial principal part for (5.18) with advection equations along ∂_r for all variables—original and auxiliary—and corresponds to the pure gauge subsystem (5.8). More precisely, the relation between the ADM gauge variables and the characteristic variables is

$$\frac{1}{2}\partial_\rho \delta \gamma_{\rho\rho} = \frac{1}{2}(\partial_r \delta g_{uu} - \partial_u \delta g_{uu}), \quad (5.20a)$$

$$-\delta K_{\rho\rho} = \partial_r \delta g_{uu} - \frac{1}{2}\partial_u \delta g_{uu}. \quad (5.20b)$$

Since all characteristic variables satisfy advection equations along ∂_r , combining (5.20) with (5.13), (5.14) one recovers (5.16).

If $(\partial_u \delta g_{uu})$ is also taken as an auxiliary variable, then the first order reduction is of the standard type, since

$$\partial_\rho \delta g_{uu} = \partial_r \delta g_{uu} - \partial_u \delta g_{uu}.$$

The equation of motion for $(\partial_u \delta g_{uu})$ can be obtained from

$$\partial_r(\partial_u \delta g_{uu}) = \partial_u(\partial_r \delta g_{uu}).$$

This first order reduction of (5.18) possesses the following non-trivial Jordan block

$$(\partial_t + \partial_\rho)(\partial_u \delta g_{uu}) + \partial_\rho(\partial_r \delta g_{uu}) = 0,$$

$$(\partial_t + \partial_\rho)(\partial_r \delta g_{uu}) = 0,$$

and a linear combination yields

$$(\partial_t + \partial_\rho)[(\partial_r \delta g_{uu}) - (\partial_u \delta g_{uu})] = \partial_\rho(\partial_r \delta g_{uu}).$$

Via the identification (5.20) the latter matches (5.12), modulo an overall factor of $1/2$. Hence, the Jordan block of the characteristic PDE with this characteristic standard first order reduction coincides precisely with the pure gauge principal part (5.7a), (5.7b). This is merely the characteristic version of the standard first order reduction in the Cauchy frame. The alternative choice where, instead of introducing both $(\partial_u \delta g_{uu})$ and $(\partial_r \delta g_{uu})$ as auxiliary variables, only the latter is introduced, renders the characteristic PDE system in spherical symmetry strongly hyperbolic. Consequently, the initial value problem of this system is not well-posed in a norm where both $(\partial_t \delta g_{uu})^2$ and $(\partial_\rho \delta g_{uu})^2$ are included in the integrand, but in one that involves only $(\partial_r \delta g_{uu})^2$. Based on this norm, one can study well-posedness of the CIBVP of the system by seeking energy estimates. In Chap. 6 we discuss this topic further. In [125] similar type of energy estimates for the wave and Maxwell equations in a single-null characteristic setup were provided. Energy estimates for the CIBVP of the wave equation were also provided in [54] for asymptotically flat and in [126] for asymptotically AdS spacetimes.

5.1.3 Pure gauge sub-block: angular direction θ

We next expand the previous analysis to a setup without symmetry, focusing purely on the angular direction θ . The pure gauge structure is identified in both the ADM and characteristic setups. In contrast, however, to the radial direction there is no combination of variables that allows us to avoid the non-trivial Jordan block of the pure gauge. We also discuss which choice of variables is most convenient for the analysis.

ADM setup

The partition into gauge, constraint and physical variables along the θ direction is still achieved using Eq. (4.9), (4.10) and (4.11), respectively. The gauge variables are

$$\begin{aligned} [\partial_\theta^2 \Theta] &= -\delta K_{\theta\theta}, & [\partial_\theta^2 \psi^\rho] &= \partial_\theta \delta \gamma_{\rho\theta}, \\ [\partial_\theta^2 \psi^\theta] &= \frac{1}{2\rho^2} \partial_\theta \delta \gamma_{\theta\theta}, & [\partial_\theta^2 \psi^\phi] &= \frac{1}{\rho^2 \sin^2 \theta} \partial_\theta \delta \gamma_{\theta\phi}. \end{aligned} \quad (5.21)$$

The constraint variables are

$$\begin{aligned} [H] &= -\partial_\theta \delta \gamma_{\rho\rho} - \frac{1}{\rho^2 \sin^2 \theta} \partial_\theta \delta \gamma_{\phi\phi}, & [M_\rho] &= \delta K_{\rho\theta}, \\ [M_\theta] &= -\delta K_{\rho\rho} - \frac{1}{\rho^2 \sin^2 \theta} \delta K_{\phi\phi}, & [M_\phi] &= \delta K_{\theta\phi}. \end{aligned} \quad (5.22)$$

The physical variables are obtained with the action of P_\perp on $\delta \gamma_{ij}$ and δK_{ij} . As seen from the physical subsystem (4.14), the latter is essentially a time derivative of the former. We

work with the physical variables

$$[h_+] \equiv \frac{1}{2}\delta\gamma_{\rho\rho} - \frac{1}{2\rho^2\sin^2\theta}\delta\gamma_{\phi\phi}, \quad [h_\times] \equiv \delta\gamma_{\rho\phi}, \quad (5.23a)$$

$$[\dot{h}_+] \equiv \frac{1}{\rho^2\sin^2\theta}\delta K_{\phi\phi} - \delta K_{\rho\rho}, \quad [\dot{h}_\times] \equiv -2\delta K_{\rho\phi}, \quad (5.23b)$$

which correspond to the two polarizations of the gravitational waves in GR. In Eq. (5.23b) we have multiplied with an overall factor of -2 for the definitions to be compatible with the physical subsystem (4.14) when $[\dot{h}_+] = \partial_t h_+$, and similarly for $[h_\times]$. As expected for a gravitational wave that travels along the θ direction, the physical variables involve only spatial metric components that are transverse to this direction. The principal symbol in the form (4.3) in the θ direction for the linearized ADM formulation is

$$\partial_t \delta\gamma_{\rho\rho} \simeq -2\delta K_{\rho\rho}, \quad (5.24a)$$

$$\partial_t \delta\gamma_{\rho\theta} \simeq -2\delta K_{\rho\theta} - \partial_\theta \delta\gamma_{\rho\rho}, \quad (5.24b)$$

$$\partial_t \delta\gamma_{\rho\phi} \simeq -2\delta K_{\rho\phi}, \quad (5.24c)$$

$$\partial_t \delta\gamma_{\theta\theta} \simeq -2\delta K_{\theta\theta} - 2\partial_\theta \delta\gamma_{\rho\theta}, \quad (5.24d)$$

$$\partial_t \delta\gamma_{\theta\phi} \simeq -2\delta K_{\theta\phi} - \partial_\theta \delta\gamma_{\rho\phi}, \quad (5.24e)$$

$$\partial_t \delta\gamma_{\phi\phi} \simeq -2\delta K_{\phi\phi}, \quad (5.24f)$$

and

$$\partial_t \delta K_{\rho\rho} \simeq -\frac{1}{2\rho^2}\partial_\theta^2 \delta\gamma_{\rho\rho}, \quad (5.25a)$$

$$\partial_t \delta K_{\rho\theta} \simeq 0, \quad (5.25b)$$

$$\partial_t \delta K_{\rho\phi} \simeq -\frac{1}{2\rho^2}\partial_\theta^2 \delta\gamma_{\rho\phi}, \quad (5.25c)$$

$$\partial_t \delta K_{\theta\theta} \simeq -\frac{1}{2\rho^2\sin^2\theta}\partial_\theta^2 \delta\gamma_{\phi\phi}, \quad (5.25d)$$

$$\partial_t \delta K_{\theta\phi} \simeq 0, \quad (5.25e)$$

$$\partial_t \delta K_{\phi\phi} \simeq -\frac{1}{2\rho^2}\partial_\theta^2 \delta\gamma_{\phi\phi}. \quad (5.25f)$$

For a standard first order reduction the pure gauge principal structure along the θ direction is inherited by

$$\partial_t \left(\frac{1}{2\rho^2} \partial_\theta \delta\gamma_{\theta\theta} \right) \simeq -\rho^{-2} \partial_\theta (\partial_\theta \delta\gamma_{\rho\theta} + \delta K_{\theta\theta}), \quad (5.26a)$$

$$\partial_t (\partial_\theta \delta\gamma_{\rho\theta} + \delta K_{\theta\theta}) \simeq -\partial_\theta^2 \delta\gamma_{\rho\rho} - \frac{1}{2\rho^2\sin^2\theta} \partial_\theta^2 \delta\gamma_{\phi\phi} - 2\partial_\theta \delta K_{\rho\theta}. \quad (5.26b)$$

After using Eq.(5.21), (5.22), (5.23) the system (5.26) yields

$$\begin{aligned} \partial_t[\partial_\theta^2 \psi^\theta] + \rho^{-2} \partial_\theta[\partial_\theta^2 (\psi^\rho - \Theta)] &\simeq 0, \\ \partial_t[\partial_\theta^2 (\psi^\rho - \Theta)] &\simeq \frac{3}{4} \partial_\theta[H] - 2\partial_\theta[M_\theta] - \frac{1}{2} \partial_\theta^2[h_+], \end{aligned} \quad (5.27)$$

so that, comparing with (5.7), the pure gauge structure of \mathbf{P}_G is manifest within the full principal symbol, as too is the coupling between gauge, constraint and physical variables encoded in \mathbf{P}_{GC} and \mathbf{P}_{GP} . Here we have worked with the plain ADM evolution equations. Working with the ADM equivalent discussed in Sec. 3.2 changes only the coupling to the constraints. To obtain this result the necessary conditions were:

1. Introduction of the quantities $(\partial_\theta \delta \gamma_{\theta\theta})$ and $(\partial_\theta \delta \gamma_{\rho\theta})$ as auxiliary variables.
2. Inclusion of the equation of motion for $\delta K_{\theta\theta}$ in the analyzed system.

Interestingly, the affine null gauge provides an explicit example where the sub-block \mathbf{P}_{GP} of the full principal symbol \mathbf{P}^s is non-vanishing, so there is non-trivial coupling between gauge and physical variables in the principal symbol.

Characteristic setup

We repeat now the previous analysis directly in the characteristic coordinates and variables to demonstrate how the pure gauge structure is inherited in \mathbf{P}^θ for the characteristic setup. The ADM analysis is again used as guidance in this. More specifically, from the equivalent ADM system (3.14) we know that the characteristic system involves the equation of motion for $\delta K_{\theta\theta}$, which is one of the two necessary conditions in order to recover the structure we are looking for. We parameterize the metric functions simply by $g_{uu}, g_{u\theta}, g_{u\phi}, g_{\theta\theta}, g_{\phi\theta}, g_{\phi\phi}$. For the present calculations this choice, as opposed to that of [111], is preferred due to its cleaner connection to the ADM variables, and allows us to uncover the pure gauge structure more easily.

With this parameterization the PDE system consisting of the main equations (3.3) does not involve terms of the form $\partial_\theta^2 \delta g_{u\theta}$ and $\partial_\theta^2 \delta g_{\theta\theta}$, which in the ADM language correspond to $\partial_\theta^2 \delta \gamma_{\rho\theta}$ and $\partial_\theta^2 \delta \gamma_{\theta\theta}$. A minimal first order reduction of the characteristic system, the details of which can be found in the ancillary files of [2], exhibits the following Jordan block in the θ direction

$$\begin{aligned} \partial_t \delta g_{uu} + \frac{1}{2\rho \sin^2 \theta} \partial_t (\partial_r \delta g_{\theta\theta}) - \frac{1}{\rho^2} \partial_\theta \delta g_{u\theta} + \frac{\cot \theta}{2\rho^3} \partial_\theta \delta g_{\theta\theta} &\simeq 0, \\ \frac{1}{\rho^2} \partial_t \delta g_{u\theta} - \frac{\cot \theta}{2\rho^3} \partial_t \delta g_{\theta\theta} &\simeq 0. \end{aligned}$$

This reduction is minimal in the sense that the minimum number of auxiliary variables needed to form a complete first order system were introduced. The above structure motivates the introduction of $(\partial_\theta \delta g_{u\theta})$ and $(\partial_\theta \delta g_{\theta\theta})$ as auxiliary variables in addition to the minimum,

since they form the non-trivial Jordan block. But, as we saw earlier, this is the other necessary condition to recover the pure gauge structure in the full system. Thus in the new first order reduction the 2×2 Jordan block along the θ direction persists, namely

$$\partial_t(\partial_\theta \delta g_{\theta\theta}) - \rho^2 \partial_t(\partial_r \delta g_{u\theta}) - \partial_\theta(\partial_r \delta g_{\theta\theta}) - \frac{1}{\sin^2 \theta} \partial_\theta(\partial_r \delta g_{\phi\phi}) \simeq 0, \quad (5.28a)$$

$$\partial_t(\partial_r \delta g_{\theta\theta}) + \frac{1}{\sin^2 \theta} \partial_t(\partial_r \delta g_{\phi\phi}) \simeq 0. \quad (5.28b)$$

The latter is indeed the pure gauge sub-block expected from the ADM analysis. To realize this explicitly we first express the characteristic auxiliary variables in terms of the ADM ones

$$\begin{aligned} \partial_\theta \delta g_{\theta\theta} &= \partial_\theta \delta \gamma_{\theta\theta}, \\ \partial_r \delta g_{\theta\theta} &= (\partial_t + \partial_\rho) \delta \gamma_{\theta\theta} \simeq -2\delta K_{\theta\theta} - 2\partial_\theta \delta \gamma_{\rho\theta}, \\ \partial_r \delta g_{u\theta} &= (\partial_t + \partial_\rho) \delta \gamma_{\rho\theta} \simeq -2\delta K_{\rho\theta} - \partial_\theta \delta \gamma_{\rho\rho}, \\ \partial_r \delta g_{\phi\phi} &= (\partial_t + \partial_\rho) \delta \gamma_{\phi\phi} \simeq -2\delta K_{\phi\phi}, \end{aligned}$$

where we have dropped derivatives transverse to ∂_θ . Then, (5.28) reads

$$\begin{aligned} \partial_t \partial_\theta \delta \gamma_{\theta\theta} + 2\rho^2 \partial_t \delta K_{\rho\theta} + \rho^2 \partial_\theta \partial_t \delta \gamma_{\rho\rho} + 2\partial_\theta \delta K_{\theta\theta} + 2\partial_\theta^2 \delta \gamma_{\rho\theta} + \frac{2}{\sin^2 \theta} \partial_\theta \delta K_{\phi\phi} &\simeq 0, \\ \partial_t \delta K_{\theta\theta} + \partial_t \partial_\theta \delta \gamma_{\rho\theta} + \frac{1}{\sin^2 \theta} \partial_t \delta K_{\phi\phi} &\simeq 0 \end{aligned}$$

which after replacing $\partial_t \delta \gamma_{\rho\rho}$, $\partial_t \delta K_{\rho\theta}$, $\partial_t \delta K_{\phi\phi}$ with the right-hand-side of (5.24a), (5.25b), (5.25f) respectively yields

$$\partial_t \left(\frac{1}{2\rho^2} \partial_\theta \delta \gamma_{\theta\theta} \right) + \rho^{-2} \partial_\theta (\delta K_{\theta\theta} + \partial_\theta \delta \gamma_{\rho\theta}) \simeq \partial_\theta \delta K_{\rho\rho} - \frac{1}{\rho^2 \sin^2 \theta} \partial_\theta \delta K_{\phi\phi}, \quad (5.29a)$$

$$\partial_t (\delta K_{\theta\theta} + \partial_\theta \delta \gamma_{\rho\theta}) \simeq \frac{1}{2\rho^2 \sin^2 \theta} \partial_\theta^2 \delta \gamma_{\phi\phi}, \quad (5.29b)$$

where in (5.29a) we have multiplied overall with a factor of $1/2\rho^2$. The right-hand-side of (5.29) involves only constraint and physical variables along the θ direction, while the left-hand-side shows the coupling only between gauge variables. Using the relations (5.21), (5.22) and (5.23) the system (5.29) reads

$$\partial_t [\partial_\theta^2 \psi^\theta] + \rho^{-2} \partial_\theta [\partial_\theta^2 (\psi^\rho - \Theta)] \simeq -\partial_\theta [\dot{h}_+], \quad (5.30a)$$

$$\partial_t [\partial_\theta^2 (\psi^\rho - \Theta)] \simeq -\frac{1}{4} \partial_\theta [H] + \frac{1}{2} \partial_\theta^2 [h_+], \quad (5.30b)$$

which again inherits the structure of the pure gauge subsystem, namely the Jordan block (5.7a), (5.7c), and provides non-trivial coupling of gauge to constraint and physical variables. Hence, the non-trivial Jordan block of \mathbf{P}^θ in the characteristic affine null system corresponds precisely to the non-trivial Jordan block of the pure gauge subsystem (5.7) along the same direction. Comparing the form (5.30) to the form (5.27) in the ADM setup, the only difference is in

the coupling of gauge variables to constraint and physical ones.

A different choice of variables that makes use of the definition (3.4) is common in affine null formulations. Such a choice can however make less clear the distinction between gauge, constraint and physical variables. In the ancillary files of [2] we include analyses where we explore such parameterizations. Crucially, the principal symbol of the characteristic system is still non-diagonalizable along θ, ϕ , but the choice of variables is inconvenient in identifying the different sub-blocks.

5.1.4 Asymptotically anti-de Sitter spacetimes

The affine-null gauge is particularly popular for evolutions in AAdS spacetimes within the context of holography. Part II of the thesis is devoted to this research direction. Here, we treat the specific system that occurs in the case of five-dimensional AAdS spacetimes with planar symmetry in the affine null gauge choice, but we expect similar results in setups with less symmetry. The metric is written as

$$ds^2 = -Adv^2 + \Sigma^2 \left[e^B dx_\perp^2 + e^{-2B} dz^2 \right] + 2dR dv + 2Fdv dz. \quad (5.31)$$

Here v denotes the advanced time, R is called the holographic coordinate, and increases from the bulk of the spacetime towards the boundary. All metric components are functions of (v, R, z) . We also denote by dx_\perp^2 the flat metric in the plane spanned by x_\perp , the two coordinates associated with the symmetry. Using the convenient definitions

$$d_z \equiv \partial_z - F \partial_R, \quad d_+ \equiv \partial_v + \frac{A}{2} \partial_R, \quad (5.32)$$

the field equations can be succinctly stated, and are

$$\begin{aligned} \partial_R^2 \Sigma &= -\frac{1}{2} (\partial_R B)^2 \Sigma, \\ \Sigma^2 \partial_R^2 F &= \Sigma (6 d_z \Sigma \partial_R B + 4 \partial_R d_z \Sigma + 3 \partial_R F \partial_R \Sigma) + \Sigma^2 (3 d_z B \partial_R B + 2 \partial_R d_z B) - 4 d_z \Sigma \partial_R \Sigma, \\ 12 \Sigma^3 \partial_R d_+ \Sigma &= -8 \Sigma^2 \left(-3 \Sigma^2 + 3 d_+ \Sigma \partial_R \Sigma \right) + e^{2B} \left\{ \Sigma^2 \left[4 d_z B \partial_R F - 4 d_z^2 B - 7 (d_z B)^2 \right. \right. \\ &\quad \left. \left. + 2 \partial_R d_z F + (\partial_R F)^2 \right] + 4 (d_z \Sigma)^2 + 2 \Sigma \left[d_z \Sigma (\partial_R F - 8 d_z B) - 4 d_z^2 \Sigma \right] \right\}, \\ 6 \Sigma^4 \partial_R d_+ B &= -9 \Sigma^3 (\partial_R \Sigma d_+ B + \partial_R B d_+ \Sigma) + e^{2B} \left\{ \Sigma^2 \left[(d_z B)^2 - d_z B \partial_R F + d_z^2 B \right. \right. \\ &\quad \left. \left. - 2 \partial_R d_z F - (\partial_R F)^2 \right] - 4 (d_z \Sigma)^2 + \Sigma \left[d_z \Sigma (d_z B + 4 \partial_R F) + 2 d_z^2 \Sigma \right] \right\}, \\ 6 \Sigma^4 \partial_R^2 A &= 72 \Sigma^2 d_+ \Sigma \partial_R \Sigma - 2 \Sigma^4 (9 \partial_R B d_+ B + 12) + 3 e^{2B} \left\{ \Sigma^2 \left[4 d_z^2 B + 7 (d_z B)^2 - (\partial_R F)^2 \right] \right. \\ &\quad \left. + 8 \Sigma \left(2 d_z B d_z \Sigma + d_z^2 \Sigma \right) - 4 (d_z \Sigma)^2 \right\}, \end{aligned} \quad (5.33)$$

and finally

$$\partial_v B = d_+ B - \frac{A}{2} \partial_R B. \quad (5.34)$$

We still analyze only the free evolution system in vacuum, but with a non-vanishing cosmological constant. The vector d_+ points to the direction of the outgoing null rays and hence equations (5.33) do involve derivatives extrinsic to the hypersurfaces of constant time. However, if one considers $d_+ B$ and $d_+ \Sigma$ as independent variables of the system, then equations (5.33) are intrinsic to the ingoing null hypersurfaces. Furthermore, this choice of variables provides intrinsic equations with a nested structure. The only equation that involves derivatives extrinsic to the hypersurfaces of constant retarded time is (5.34). To analyze the hyperbolicity of the resulting PDE system we follow the steps described in the beginning of the chapter, namely first order reduction, linearization and coordinate transformation to an auxiliary Cauchy-type setup.

First order reduction and Linearization

The definition (5.32) was used earlier to write the field equations in a more compact form, but for the rest of the analysis we expand out the definition of d_z . Before performing the first order reduction, we apply the coordinate transformation $r = 1/R$, drawing the boundary to $r = 0$. The metric components however still exhibit singular behavior there, so as elsewhere in the literature, [127], we apply appropriate field redefinitions to obtain regular fields on the boundary, namely

$$\begin{aligned} A(v, r, z) &\rightarrow \frac{1}{r^2} + r^2 A(v, r, z), & B(v, r, z) &\rightarrow r^4 B(v, r, z), \\ \Sigma(v, r, z) &\rightarrow \frac{1}{r} + r^3 \Sigma(v, r, z), & F(v, r, z) &\rightarrow r^2 F(v, r, z), \end{aligned}$$

and similarly for derivatives of the above fields. To simplify the presentation we linearize here about vacuum AdS. Our conclusions are however unaltered if we work about an arbitrary background. Full expressions in the general case can be found in [121]. We define reduction variables according to

$$\begin{aligned} A_r &= \partial_r A, & B_r &= \partial_r B, & F_r &= \partial_r F, & \Sigma_r &= \partial_r \Sigma, \\ A_z &= \partial_z A, & B_z &= \partial_z B, & F_z &= \partial_z F, & \Sigma_z &= \partial_z \Sigma, \\ B_+ &= d_+ B, & \Sigma_+ &= d_+ \Sigma. \end{aligned}$$

The complete first order system is then

$$\begin{aligned}
r^4 \partial_v B &= -S_1, \\
r^4 \partial_v B_r &= \frac{r^4}{2} \partial_r B_r + r^3 \partial_r B_+ - S_2, \\
-6r \partial_r B_+ &= 2r^2 \partial_r F_z + r^2 \partial_z B_z + 2r^2 \partial_z \Sigma_z - S_3, \\
\partial_r B_z &= \partial_z B_r, \\
\partial_r \Sigma &= -S_5, \\
r^7 \partial_r \Sigma_r &= -S_6, \\
12r \partial_r \Sigma_+ &= 2r^2 \partial_r F_z + 4r^2 \partial_z B_z + 8r^2 \partial_z \Sigma_z - S_7, \\
\partial_r \Sigma_z &= \partial_z \Sigma_r, \\
\partial_r F &= -S_9, \\
r^4 \partial_r F_r &= -4r^4 \partial_r \Sigma_z - 2r^4 \partial_r B_z - S_{10}, \\
\partial_r F_z &= \partial_z F_r, \\
\partial_r A &= -S_{12}, \\
6r^2 \partial_r A_r &= 12r^2 \partial_z B_z + 24r^2 \partial_z \Sigma_z - S_{13}, \\
\partial_r A_z &= \partial_z A_r,
\end{aligned} \tag{5.35}$$

which can be written as

$$\mathcal{A}^v \partial_v \mathbf{u} + \mathcal{A}^r \partial_r \mathbf{u} + \mathcal{A}^z \partial_z \mathbf{u} + \mathcal{S} = 0, \tag{5.36}$$

with state vector

$$\mathbf{u} = (A_r, B_+, \Sigma_+, \Sigma_r, F_r, B_z, \Sigma_z, B_r, A_z, F_z, A, F, B, \Sigma)^T.$$

The principal part matrix associated with the retarded time \mathcal{A}^v is not invertible as expected for a characteristic setup and hence we proceed with a transformation to an appropriate auxiliary frame.

Coordinate transformation

To obtain a suitable coordinate frame we transform from (v, r, z) to (t, ρ, z) with

$$v = t - \rho, \quad r = \rho,$$

and the remaining coordinates unaltered, which gives

$$\partial_v = \partial_t, \quad \partial_r = \partial_t + \partial_\rho,$$

with ∂_z unaffected. Applying the transformation yields

$$\mathcal{A}^t \partial_t \mathbf{u} + \mathcal{A}^r \partial_\rho \mathbf{u} + \mathcal{A}^z \partial_z \mathbf{u} + \mathcal{S} = 0,$$

where now $\mathcal{A}^t = \mathcal{A}^v + \mathcal{A}^r$ is invertible. After multiplying from the left with the inverse of \mathcal{A}^t we again bring the system to the form

$$\partial_t \mathbf{u} + \mathbf{B}^\rho \partial_\rho \mathbf{u} + \mathbf{B}^z \partial_z \mathbf{u} + \mathbf{S} = 0, \quad (5.37)$$

where $\mathbf{B}^\rho = (\mathcal{A}^t)^{-1} \mathcal{A}^r$ and $\mathbf{B}^z = (\mathcal{A}^t)^{-1} \mathcal{A}^z$. The principal part \mathbf{B}^ρ is diagonalizable with real eigenvalues 0 and ± 1 . The principal part \mathbf{B}^z has the same real eigenvalues but it does not have a complete set of eigenvectors, so it is not diagonalizable. The system resulting from this specific first order reduction is thus only WH. Next, by constructing generalized characteristic variables in the z direction we will examine whether or not an appropriate addition of the reduction constraints can render the reduction strongly hyperbolic. The reduction constraints are

$$\begin{aligned} \partial_z A - A_z &= 0, & \partial_z B - B_z &= 0, \\ \partial_z \Sigma - \Sigma_z &= 0, & \partial_z F - F_z &= 0, \\ \partial_z B_\rho - \partial_\rho B_z &= \frac{1}{2} \partial_z B_r - \partial_z B_+ - \partial_\rho B_z = 0, \\ \partial_z \Sigma_\rho - \partial_\rho \Sigma_z &= \frac{1}{2} \partial_z \Sigma_r - \partial_z \Sigma_+ - \partial_\rho \Sigma_z = 0. \end{aligned} \quad (5.38)$$

Generalized characteristic variables

The eigenvalues of \mathbf{B}^z are $\lambda = \pm 1$ with algebraic multiplicity one and $\lambda = 0$ with algebraic multiplicity twelve. There is one eigenvector for $\lambda = 1$, one for $\lambda = -1$ and nine for $\lambda = 0$. Since the algebraic and geometric multiplicity of $\lambda = 0$ differ by three, the Jordan normal form

$$\mathbf{J}^z \equiv \mathbf{T}_z^{-1} \mathbf{B}^z \mathbf{T}_z,$$

must have some non-trivial block. Let us consider the t, z part of (5.37) and, use \mathbf{T}_z^{-1} to construct the generalized characteristic variables in the z direction,

$$\mathbf{v} = \mathbf{T}_z^{-1} \mathbf{u} \quad (5.39)$$

satisfying

$$\partial_t \mathbf{v} + \mathbf{J}_z \partial_z \mathbf{v} \simeq 0, \quad (5.40)$$

with \simeq here denoting equality up to transverse derivatives and non-principal terms. The components of \mathbf{v} begin,

$$\begin{aligned} & -B_r - \frac{1}{3}B_z - \frac{2}{3}F_r - 2\Sigma_r - \frac{2}{3}\Sigma_z, \\ & -B_r + \frac{1}{3}B_z + \frac{2}{3}F_r - 2\Sigma_r + \frac{2}{3}\Sigma_z, \end{aligned}$$

with speeds ∓ 1 respectively. Next we have those with vanishing speeds, which are most naturally presented in three blocks. The first of these consists of the set of *true* characteristic variables,

$$\begin{aligned} & B_+ - \frac{\rho}{2}B_r - \rho\Sigma_r, \quad \Sigma_+ - \frac{\rho}{8}A_r + \frac{\rho}{4}B_r + \frac{\rho}{2}\Sigma_r, \\ & \frac{1}{4}A_r + \frac{3}{2}B_r + F_z + 3\Sigma_r, \quad A, \quad F, \quad B, \quad \Sigma, \end{aligned}$$

a coupled pair consisting of one generalized and one characteristic variable, respectively,

$$-\frac{4}{3}B_z - \frac{2}{3}F_r - \frac{2}{3}\Sigma_z, \quad -2\Sigma_r, \quad (5.41)$$

and finally a coupled triplet of two generalized characteristic variables and one characteristic variable, respectively,

$$\begin{aligned} & \frac{1}{4}A_z + \frac{1}{6}B_z + \frac{1}{3}F_r + \frac{1}{3}\Sigma_z, \quad -\frac{1}{4}A_r + \frac{1}{2}B_r + \Sigma_r, \\ & \frac{2}{3}B_z + \frac{1}{3}F_r + \frac{4}{3}\Sigma_z. \end{aligned} \quad (5.42)$$

In other words, from the structure of the Jordan blocks of \mathbf{J}^z , reading off the components of (5.40) the first member of the pair (5.41) and the first two members of the triple (5.42) we have the schematic form,

$$\partial_t v_i + \partial_z v_{i+1} \simeq 0, \quad (5.43)$$

with v_i referring to the field and v_{i+1} the next element of the pair or triple. The question is whether or not there exists an appropriate addition of the reduction constraints (5.38) such that equations of the form (5.43) are turned into equations of the form

$$\partial_t v_i + \lambda_i \partial_z v_i \simeq 0, \quad (5.44)$$

where we are allowing different first order reductions to adjust also characteristic speeds. This is a necessary condition for building an alternative reduction that is SH. This would mean that the generalized characteristic variable v_i that is originally coupled with v_{i+1} could be decoupled, and the respective generalized eigenvector replaced by a simple eigenvector. We examine this for the second two elements of the triplet (5.42) and show by contradiction that this necessary condition can not be fulfilled. With our original, specific reduction we

have

$$\begin{aligned} \partial_t \left(\frac{2}{3}B_z + \frac{1}{3}F_r + \frac{4}{3}\Sigma_z \right) &\simeq 0, \\ \partial_t \left(-\frac{1}{4}A_r + \frac{1}{2}B_r + \Sigma_r \right) + \partial_z \left(\frac{2}{3}B_z + \frac{1}{3}F_r + \frac{4}{3}\Sigma_z \right) &\simeq 0. \end{aligned} \quad (5.45)$$

Observe, first of all, that neither of these two equations, nor the two large terms grouped separately in the second, can be written as a linear combination (equality taken here in the sense of \simeq) of the reduction constraints (5.38). The choice of reduction lies in the freedom to add multiples of the six reduction constraints (5.38) to the evolution equations. Suppose that some choice of addition of these constraints did result in a SH first order reduction. Starting with the first equation of (5.45), for our alternative reduction we have

$$\partial_t \left(\frac{2}{3}B_z + \frac{1}{3}F_r + \frac{4}{3}\Sigma_z \right) \simeq \sum_{\alpha} c_{\alpha} C_{\alpha}, \quad (5.46)$$

with the terms on the right-hand-side a linear combination of the reduction constraints C_{α} . Since this alternative reduction is SH we have,

$$\sum_{\alpha} c_{\alpha} C_{\alpha} \simeq \sum_{\alpha} a_{\alpha}^0 \partial_z v_{\alpha}^0 + \sum_{\alpha} a_{\alpha}^{\pm} \partial_z v_{\alpha}^{\pm},$$

with v_{α}^0 denoting the set of 0-speed characteristic variables and v_{α}^{\pm} denoting the remaining characteristic variables. Using $\partial_t v_{\alpha}^{\pm} \simeq \lambda_{\alpha} \partial_z v_{\alpha}^{\pm}$ we may therefore rewrite (5.46) as

$$\partial_t \left(\frac{2}{3}B_z + \frac{1}{3}F_r + \frac{4}{3}\Sigma_z - \sum_{\alpha} a_{\alpha}^{\pm} \lambda_{\alpha}^{-1} v_{\alpha}^{\pm} \right) \simeq \sum_{\alpha} a_{\alpha}^0 \partial_z v_{\alpha}^0.$$

Now, by our observation directly after (5.45), the term inside the large bracket can not vanish identically. Therefore we must have $a_{\alpha}^0 = 0$ or we have found, on the left-hand-side, a non-trivial generalized characteristic variable, in contradiction to the assumption that our reduction is SH. Moving on to the second equation of (5.45), we can write the equivalent expression for the alternative first order reduction as,

$$\partial_t \left(-\frac{1}{4}A_r + \frac{1}{2}B_r + \Sigma_r \right) + \partial_z \left(\frac{2}{3}B_z + \frac{1}{3}F_r + \frac{4}{3}\Sigma_z \right) \simeq \sum_{\alpha} c'_{\alpha} C_{\alpha},$$

again with the right-hand-side a linear combination of the reduction constraints. From here a simple calculation shows that

$$-\frac{1}{4}A_r + \frac{1}{2}B_r + \Sigma_r + \sum_{\alpha} a'_{\alpha} \lambda_{\alpha}^{-1} v_{\alpha}^{\pm},$$

is nevertheless *still* a non-trivial generalized characteristic variable for a suitable choice of a'_{α} . By contradiction we have therefore shown that there is no first order reduction that gives a SH first order PDE system in the (t, ρ, z) frame used here.

5.2 The Bondi-Sachs gauge proper

In the outgoing Bondi-Sachs proper gauge the coordinate light speed conditions $c_+^\rho = 1$, $c_+^A = 0$ are imposed—as in all outgoing Bondi-like gauges—and lead to

$$\alpha L^{-1} - \beta^\rho = 1, \quad \beta^A = -b^A \alpha L^{-1},$$

in terms of lapse and shift. The gauge is closed by setting

$$\rho = \hat{R}. \quad (5.47)$$

In this form the gauge fixing is not so easily expressed in an ADM setup, since we do not have a complete specification of the lapse and shift. We can however achieve this by combining the ADM equations (4.6), the 2 + 1 split (3.16) of the spatial metric γ_{ij} and the determinant condition (5.47). We basically want to specify a β^ρ for which the determinant condition (5.47) is satisfied at later times. Starting from the standard ADM equations on the two-sphere we get

$$\mathcal{L}_t q_{AB} = -2\alpha \overset{(q)}{\perp} K_{AB} + \mathcal{L}_{[\beta^\rho \partial_\rho]} q_{AB} - \mathcal{L}_{[(1+\beta^\rho)b]} q_{AB}, \quad (5.48)$$

where $\overset{(q)}{\perp}$ denotes the projection with respect to q_{AB} on every open index and b^a denotes the slip vector. The general relation between the derivative of a matrix and the derivative of its determinant applied to q_{AB} yields

$$q^{ab} \mathcal{L}_t q_{ab} = q^{ab} \partial_t q_{ab} = \partial_t \ln(q),$$

where $q \equiv \det(q)$. Imposing the determinant condition (5.47) the latter yields $q^{ab} \mathcal{L}_t q_{ab} = 0$. Then, Eq. (5.48) after tracing with q^{AB} returns

$$0 = -2\alpha K_{qq} + \beta^\rho \left[\partial_\rho \ln(q) - 2\mathcal{D}_A b^A \right] - 2\mathcal{D}_A b^A,$$

where \mathcal{D}_A is the covariant derivative compatible with q_{AB} . Using $c_+^\rho = 1 = -\beta^\rho + \alpha/L$ we finally obtain $\beta^\rho = \rho X / (4 - \rho X)$ with

$$X = 2LK_{qq} + 2\mathcal{D}_a b^a$$

and $\partial_\rho \ln(q) = 4/\rho$. In terms of the lapse and shift the Bondi-Sachs proper gauge can thus be imposed by

$$\alpha = L(1 + \beta^\rho), \quad \beta^\rho = \frac{X \rho / 4}{1 - X \rho / 4}, \quad \beta^\theta = -b^\theta \alpha L^{-1}, \quad \beta^\phi = -b^\phi \alpha L^{-1}, \quad (5.49)$$

which is a mixed algebraic-differential gauge.

5.2.1 Pure gauge subsystem

To proceed with our analysis we first need to obtain the pure gauge subsystem (4.8) for the Bondi-Sachs gauge. We continue in the linear constant coefficient approximation. Under this assumption the Bondi-Sachs proper gauge (5.49) reads

$$\begin{aligned}
\delta\alpha &= \delta\beta^\rho + \frac{1}{2}\delta\gamma_{\rho\rho}, \\
\delta\beta^\rho &= \frac{\delta K_{\theta\theta}}{2\rho} + \frac{\delta K_{\phi\phi}}{2\rho\sin^2\theta} + \frac{\partial_\theta\delta\gamma_{\rho\theta}}{2\rho} + \frac{\partial_\phi\delta\gamma_{\rho\phi}}{2\rho\sin^2\theta} + \frac{\cot\theta\delta\gamma_{\rho\theta}}{2\rho}, \\
\delta\beta^\theta &= -\rho^{-2}\delta\gamma_{\rho\theta}, \\
\delta\beta^\phi &= -(\rho\sin\theta)^{-2}\delta\gamma_{\rho\phi}.
\end{aligned} \tag{5.50}$$

Replacing these in Eq. (4.8) and using the relations (5.21) to translate to the gauge variables, the pure gauge subsystem of the Bondi-Sachs proper gauge reads

$$\begin{aligned}
&\partial_t\Theta + \frac{1}{2\rho}\partial_\theta^2\Theta + \frac{1}{2\rho\sin^2\theta}\partial_\phi^2\Theta - \frac{1}{2\rho}\partial_\theta^2\psi^\rho - \frac{1}{2\rho\sin^2\theta}\partial_\phi^2\psi^\rho \\
&\quad - \frac{\rho}{2}\partial_\rho\partial_\theta\psi^\theta - \frac{\rho}{2}\partial_\rho\partial_\phi\psi^\phi - \partial_\rho\psi^\rho - \frac{\cot\theta}{2\rho}\partial_\theta\psi^\rho - \frac{\rho\cot\theta}{2}\partial_\rho\psi^\theta = 0, \\
&\partial_t\psi^\rho + \frac{1}{2\rho}\partial_\theta^2\Theta + \frac{1}{2\rho\sin^2\theta}\partial_\phi^2\Theta - \frac{1}{2\rho}\partial_\theta^2\psi^\rho - \frac{1}{2\rho\sin^2\theta}\partial_\phi^2\psi^\rho \\
&\quad - \frac{\rho}{2}\partial_\rho\partial_\theta\psi^\theta - \frac{\rho}{2}\partial_\rho\partial_\phi\psi^\phi - \partial_\rho\Theta - \frac{\cot\theta}{2\rho}\partial_\theta\psi^\rho - \frac{\rho\cot\theta}{2}\psi_\rho\psi^\theta = 0, \\
&\partial_t\psi^\theta + \partial_\rho\psi^\theta + \rho^{-2}\partial_\theta(\psi^\rho - \Theta) = 0, \\
&\partial_t\psi^\phi + \partial_\rho\psi^\phi + (\rho\sin\theta)^{-2}\partial_\phi(\psi^\rho - \Theta) = 0.
\end{aligned} \tag{5.51}$$

To analyze the hyperbolicity of this second order in space system we consider a first order reduction with variables

$$\Theta - \psi^\rho, \quad \partial_\theta(\Theta - \psi^\rho), \quad \partial_\phi(\Theta - \psi^\rho), \quad \Theta + \psi^\rho, \quad \psi^\theta, \quad \partial_\theta\psi^\theta, \quad \psi^\phi, \quad \partial_\phi\psi^\phi.$$

The minimal first order reduction of this system reads

$$\partial_t(\Theta - \psi^\rho) + \partial_\rho(\Theta - \psi^\rho) = 0, \tag{5.52a}$$

$$\partial_t[\partial_\theta(\Theta - \psi^\rho)] + \partial_\rho[\partial_\theta(\Theta - \psi^\rho)] = 0, \tag{5.52b}$$

$$\partial_t[\partial_\phi(\Theta - \psi^\rho)] + \partial_\rho[\partial_\phi(\Theta - \psi^\rho)] = 0, \tag{5.52c}$$

$$\begin{aligned}
&\partial_t(\Theta + \psi^\rho) - \partial_\rho(\Theta + \psi^\rho) - \frac{\cot\theta}{2\rho}\partial_\theta(\Theta + \psi^\rho) \\
&\quad + \rho^{-1}\partial_\theta[\partial_\theta(\Theta - \psi^\rho)] + \rho^{-1}\sin^{-2}\theta\partial_\phi[\partial_\phi(\Theta - \psi^\rho)] + \frac{\cot\theta}{2\rho}\partial_\theta(\Theta - \psi^\rho) \\
&\quad + \rho\cot\theta\partial_\rho\psi^\theta - \rho\partial_\rho(\partial_\theta\psi^\theta) - \rho\partial_\rho(\partial_\phi\psi^\phi) = 0,
\end{aligned} \tag{5.52d}$$

$$\partial_t\psi^\theta + \partial_\rho\psi^\theta - \rho^{-2}[\partial_\theta(\Theta - \psi^\rho)] = 0, \tag{5.52e}$$

$$\partial_t(\partial_\theta\psi^\theta) + \partial_\rho(\partial_\theta\psi^\theta) - \rho^{-2}\partial_\theta[\partial_\theta(\Theta - \psi^\rho)] = 0, \quad (5.52f)$$

$$\partial_t\psi^\phi + \partial_\rho\psi^\phi - \rho^{-2}\sin^{-2}\theta[\partial_\phi(\Theta - \psi^\phi)] = 0, \quad (5.52g)$$

$$\partial_t(\partial_\phi\psi^\phi) + \partial_\rho(\partial_\phi\psi^\phi) - (\rho\sin\theta)^{-2}\partial_\phi[\partial_\phi(\Theta - \psi^\rho)] = 0. \quad (5.52h)$$

All principal matrices of this system possess real eigenvalues, but the angular principal matrices are non-diagonalizable. The non-trivial Jordan block along the θ direction is given by (see ancillary files of [2])

$$\begin{aligned} \partial_t[\partial_\theta(\Theta - \psi^\rho)] &\simeq 0, \\ \partial_t(\partial_\theta\psi^\theta) - \rho^{-2}\partial_\theta[\partial_\theta(\Theta - \psi^\rho)] &\simeq 0, \end{aligned}$$

and similarly along ϕ by

$$\begin{aligned} \partial_t(\partial_\phi\psi^\phi) - \rho^{-2}\sin^{-2}\theta\partial_\phi[\partial_\phi(\Theta - \psi^\rho)] &\simeq 0, \\ \partial_t[\partial_\phi(\Theta - \psi^\rho)] &\simeq 0. \end{aligned}$$

The coupled generalized characteristic variables obtained here effectively involve second order angular derivatives. Hence, they cannot be removed with a different first order reduction of the second order system (5.51). Thus, the analysis based on the minimal reduction just performed suffices to show that the pure gauge subsystem of the Bondi-Sachs proper gauge (5.51) is only WH.

5.2.2 Pure gauge sub-block: angular direction θ

Similarly to Subsec. 5.1.3 we present here the set of evolution equations that inherit the structure of the pure gauge subsystem in the ADM setup, for the Bondi-Sachs gauge proper. The necessary conditions to uncover this structure remain the same. The system that captures the structure of the pure gauge subsystem along the θ direction is

$$-\partial_t(\delta K_{\theta\theta} + \partial_\theta\delta\gamma_{\rho\theta}) \simeq \frac{1}{2}\partial_\theta^2\delta\gamma_{\rho\rho} + 2\partial_\theta\delta K_{\rho\theta} + \frac{1}{2}\partial_\theta^2\delta\gamma_{\rho\rho} + \frac{1}{2\rho^2\sin^2\theta}\partial_\theta^2\delta\gamma_{\phi\phi}, \quad (5.53a)$$

$$-\partial_t(\delta K_{\theta\theta} - \partial_\theta\delta\gamma_{\rho\theta}) \simeq \frac{1}{2}\partial_\theta^2\delta\gamma_{\rho\rho} - 2\partial_\theta\delta K_{\rho\theta} + \frac{1}{2}\partial_\theta^2\delta\gamma_{\rho\rho} + \frac{\partial_\theta^2\delta\gamma_{\phi\phi}}{2\rho^2\sin^2\theta} + \partial_\theta^2\delta\beta_\rho, \quad (5.53b)$$

$$\frac{1}{2\rho^2}\partial_t(\partial_\theta\delta\gamma_{\theta\theta}) \simeq -\frac{1}{\rho^2}\partial_\theta\delta K_{\theta\theta} + \frac{1}{\rho^2}\partial_\theta^2\delta\beta_\theta, \quad (5.53c)$$

$$\frac{1}{\rho^2\sin^2\theta}\partial_t(\partial_\theta\delta\gamma_{\theta\phi}) \simeq \frac{-2}{\rho^2\sin^2\theta}\partial_\theta\delta K_{\theta\phi} + \frac{1}{\rho^2\sin^2\theta}\partial_\theta^2\delta\beta_\phi, \quad (5.53d)$$

where spatial derivatives transverse to θ are dropped. This system results from linear combinations of the linearized about flat space ADM equations and does not include equations outside the main system (3.3). Combining Eqs. (5.50), (5.21), (5.22), (5.23) and (4.7), the

system (5.53) yields

$$\partial_t[\partial_\theta^2(\Theta - \psi^\rho)] \simeq -\frac{3}{4}\partial_\theta[H] + 2\partial_\theta[M_\rho] + \frac{1}{2}\partial_\theta^2[h_+], \quad (5.54a)$$

$$\begin{aligned} \partial_t[\partial_\theta^2(\Theta + \psi^\rho)] &\simeq -\rho^{-1}\partial_\theta^2[\partial_\theta^2(\Theta - \psi^\rho)] - \frac{\cot\theta}{\rho}\partial_\theta[\partial_\theta^2\psi^\rho] \\ &\quad - \frac{3}{4}\partial_\theta[H] - 2\partial_\theta[M_\rho] - \frac{3}{2}\partial_\theta^2[M_\theta] + \frac{1}{2}\partial_\theta^2[h_+] + \frac{1}{2}\partial_\theta^2[\dot{h}_+], \end{aligned} \quad (5.54b)$$

$$\partial_t[\partial_\theta^2\psi^\theta] \simeq \rho^{-2}\partial_\theta[\partial_\theta^2(\Theta - \psi^\rho)], \quad (5.54c)$$

$$\partial_t[\partial_\theta^2\psi^\phi] \simeq \frac{-2}{\rho^2\sin^2\theta}\partial_\theta[M_\theta] + \frac{1}{\rho^2\sin^2\theta}\partial_\theta^2[h_\times]. \quad (5.54d)$$

To see how this system inherits the structure of the pure gauge subsystem (5.52), let us neglect all non-gauge variables. Let us furthermore consider adding to the system the following equations: ∂_θ of (5.53a), ∂_ϕ of (5.53a), ∂_θ of (5.53c) and ∂_ϕ of (5.53d). As seen from the form (5.54) these additional equations provide the identification to Eq. (5.52b), (5.52c), (5.52f) and (5.52h), respectively i.e. the equations of the auxiliary variables introduced by the minimal first order reduction. The resulting system is an overall ∂_θ^2 derivative of the first order reduced pure gauge subsystem (5.52). Thus, the hyperbolic character of the sub-block \mathbf{P}_G is that of the pure gauge subsystem, which is WH. Furthermore, from the form (5.54) we see another explicit example of a Bondi-like gauge where $\mathbf{P}_{GP} \neq 0$. Identification of the pure gauge structure directly in the characteristic setup is messy with this radial coordinate, so we do not discuss it in detail. However, in Subsec. 5.2.3 we do show weak hyperbolicity for the original characteristic system in axisymmetry.

5.2.3 Axisymmetry in characteristic variables

In Bondi-Sachs gauge [110, 128] a generic 4-dimensional axially symmetric metric can be written as

$$\begin{aligned} ds^2 &= \left(\frac{V}{r}e^{2\beta} - U^2r^2e^{2\gamma} \right) du^2 + 2e^{2\beta} du dr \\ &\quad + 2Ur^2e^{2\gamma} du d\theta - r^2 \left(e^{2\gamma} d\theta^2 + e^{-2\gamma} \sin^2\theta d\phi^2 \right). \end{aligned} \quad (5.55)$$

Here u denotes the retarded time, r is the areal radius, and θ, ϕ give coordinates on the two-sphere in the standard way. All metric functions are functions of (u, r, θ) . The signature convention chosen here is $(+, -, -, -)$, which is the same as in [53]. This convention does not affect the degree of hyperbolicity of the free evolution PDE system. For axially symmetric spacetimes the PDE system consists of three equations intrinsic to the hypersurfaces of

constant retarded time,

$$\begin{aligned}
\beta_{,r} &= \frac{1}{2}r(\gamma_{,r})^2, \\
\left[r^4 e^{2(\gamma-\beta)} U_{,r} \right]_{,r} &= 2r^2 \left[r^2 \left(\frac{\beta}{r^2} \right)_{,r\theta} - \frac{(\sin^2 \theta \gamma)_{,r\theta}}{\sin^2 \theta} + 2\gamma_{,r} \gamma_{,\theta} \right], \\
V_{,r} &= -\frac{1}{4}r^4 e^{2(\gamma-\beta)} (U_{,r})^2 + \frac{(r^4 \sin \theta U)_{,r\theta}}{2r^2 \sin \theta} \\
&\quad + e^{2(\beta-\gamma)} \left[1 - \frac{(\sin \theta \beta_{,\theta})_{,\theta}}{\sin \theta} + \gamma_{,\theta\theta} + 3 \cot \theta \gamma_{,\theta} - (\beta_{,\theta})^2 - 2\gamma_{,\theta} (\gamma_{,\theta} - \beta_{,\theta}) \right],
\end{aligned} \tag{5.56}$$

and one equation that involves extrinsic derivatives,

$$\begin{aligned}
4r(r\gamma)_{,ur} &= \left\{ 2r\gamma_{,r} V - r^2 \left[2\gamma_{,\theta} U + \sin \theta \left(\frac{U}{\sin \theta} \right)_{,\theta} \right] \right\}_{,r} \\
&\quad - 2r^2 \frac{(\gamma_{,r} U \sin \theta)_{,\theta}}{\sin \theta} + \frac{1}{2}r^4 e^{2(\gamma-\beta)} (U_{,r})^2 + 2e^{2(\beta-\gamma)} \left[(\beta_{,\theta})^2 + \sin \theta \left(\frac{\beta_{,\theta}}{\sin \theta} \right)_{,\theta} \right].
\end{aligned} \tag{5.57}$$

The intrinsic equations possess a nested structure. The above free evolution scheme is formed by the main equations (3.3) in axisymmetry and the supplementary equations are ignored. To determine the degree of hyperbolicity we again follow a first order reduction, a linearization about Minkowski, and a coordinate transformation to an auxiliary Cauchy-type frame. In [121] the same analysis for an arbitrary background can be found. The degree of hyperbolicity is the same for both cases.

First order reduction and Linearization

The minimal set of reduction variables are given by

$$U_r = \partial_r U, \gamma_r = \partial_r \gamma, \gamma_\theta = \partial_\theta \gamma, \beta_\theta = \partial_\theta \beta.$$

The linearized about flat space first order reduced system reads

$$\begin{aligned}
\partial_r \beta &= 0, \\
\partial_r U_r - \frac{2}{r^2} \partial_r \beta_\theta + \frac{2}{r^2} \partial_r \gamma_\theta + S_2 &= 0, \\
\partial_r V + \partial_\theta \beta_\theta - \partial_\theta \gamma_\theta - 2r \partial_\theta U - \frac{r^2}{2} \partial_\theta U_r + S_3 &= 0, \\
4r^2 \partial_u \gamma_r + 4r \partial_u \gamma - 2r^2 \partial_r \gamma_r + 2r \partial_\theta U + r^2 \partial_\theta U_r - 2\partial_\theta \beta_\theta + S_4 &= 0, \\
\partial_r U + S_5 &= 0, \\
\partial_r \gamma + S_6 &= 0, \\
\partial_r \gamma_\theta - \partial_\theta \gamma_r &= 0, \\
\partial_r \beta_\theta &= 0,
\end{aligned} \tag{5.58}$$

where S_i denotes the various source terms and as earlier we work in the frozen coefficient approximation, so that r and so forth must be treated as constants. The variables can be collected in the state vector

$$\mathbf{u} = (\beta, \gamma, U, V, \gamma_r, U_r, \beta_\theta, \gamma_\theta)^T,$$

and the system can be written in the form (2.1) with

$$\mathcal{A}^u \partial_u \mathbf{u} + \mathcal{A}^r \partial_r \mathbf{u} + \mathcal{A}^\theta \partial_\theta \mathbf{u} + \mathcal{S} = 0 \quad (5.59)$$

where the principal part matrix \mathcal{A}^u associated with retarded time u is not invertible.

Coordinate transformation

After applying the coordinate transformation (5.1) and multiplying on the left with the inverse of \mathcal{A}^t we bring the system to the form,

$$\partial_t \mathbf{u} + \mathbf{B}^\rho \partial_\rho \mathbf{u} + \mathbf{B}^{\hat{\theta}} \partial_{\hat{\theta}} \mathbf{u} + \mathbf{S} = 0, \quad (5.60)$$

where $\mathbf{B}^\rho = (\mathcal{A}^t)^{-1} \mathcal{A}^r$ and $\mathbf{B}^{\hat{\theta}} = \rho (\mathcal{A}^t)^{-1} \mathcal{A}^\theta$ with $\partial_{\hat{\theta}} \equiv 1/\rho \partial_\theta$, and \mathbf{S} was redefined in the obvious manner. For our system, the principal part matrix \mathbf{B}^ρ is diagonalizable with real eigenvalues. Although $\mathbf{B}^{\hat{\theta}}$ has real eigenvalues, it does not have a complete set of eigenvectors, and hence is not diagonalizable. Therefore the system resulting from the specific first order reduction we made is only WH. In [129] a subsystem of a similar first-order reduction was shown to be symmetric hyperbolic. Here, however, we are concerned with the best estimates that can be made for the full system. In Sec. 6.2 we elaborate further on this using toy models.

So far we have not ruled out the existence of an alternative first order reduction that *is* SH however. To examine this possibility we have to understand if any potential addition of reduction constraints can make the system SH. The reduction constraints are

$$\partial_\theta \beta - \beta_\theta = 0, \quad \partial_\theta \gamma - \gamma_\theta = 0, \quad (5.61)$$

The definitions of the variables γ_r and U_r are solved explicitly as time evolution equations within the system (6.16) and therefore do not have an associated constraint. Using the generalized characteristic variables of the system we examine next this subtlety, along with the form of the degeneracy.

Generalized characteristic variables

The generalized characteristic variables $\mathbf{v} \equiv \mathbf{T}_{\hat{\theta}}^{-1} \mathbf{u}$ with speed (eigenvalue) zero are

$$\rho U + \frac{\rho^2}{2} U_r - \beta_\theta + \gamma_\theta, \quad \beta_\theta, \quad V, \quad \rho \left(-2\rho U - \frac{\rho^2}{2} U_r + \beta_\theta - \gamma_\theta \right), \quad \gamma, \quad \beta,$$

of which the third and fourth are associated with the non-trivial 2×2 Jordan block within

$$\mathbf{J}^{\hat{\theta}} \equiv \mathbf{T}_{\hat{\theta}}^{-1} \mathbf{B}^{\hat{\theta}} \mathbf{T}_{\hat{\theta}}.$$

Likewise we have

$$-\frac{\rho}{2} U + \frac{\rho}{2} \gamma_r - \frac{\rho^2}{4} U_r + \frac{1}{2} \beta_\theta, \quad -\frac{\rho}{2} U - \frac{\rho}{2} \gamma_r - \frac{\rho^2}{4} U_r + \frac{1}{2} \beta_\theta,$$

with speeds ± 1 respectively. The structure of $\mathbf{J}_{\hat{\theta}}$ and the relation

$$\partial_t \mathbf{v} + \mathbf{J}_{\hat{\theta}} \partial_{\hat{\theta}} \mathbf{v} \simeq 0, \tag{5.62}$$

obtained in the frozen coefficient approximation and focusing on the t, θ directions yield

$$\begin{aligned} -\partial_t \left(2\rho U + \frac{\rho^2}{2} U_r - \beta_\theta + \gamma_\theta \right) &\simeq 0, \\ \partial_t V - \rho \partial_{\hat{\theta}} \left(2\rho U + \frac{\rho^2}{2} U_r - \beta_\theta + \gamma_\theta \right) &\simeq 0. \end{aligned} \tag{5.63}$$

Strongly hyperbolic systems admit a complete set of characteristic variables in each direction. In other words, if our system were strongly hyperbolic then up to non-principal and transverse derivative terms each component of \mathbf{v} would satisfy an advection equation. Presently the best we can achieve for V however is (5.63). Physically we may therefore understand weak hyperbolicity as the failure of V , a *generalized* characteristic variable, to satisfy such an advection equation. As mentioned earlier, we could try and cure the equations by using a different first order reduction. Observe that the choice of different reductions corresponds to the freedom to add (derivatives of) the reduction constraints to (5.63) without introducing second derivatives. As V appears at most once differentiated in the original equations there is no associated constraint, so we must hope to eradicate the ∂_θ term from (5.63) using (5.61) without introducing second derivatives. Even if the variable $U_\theta = \partial_\theta U$ were introduced in the reduction however, the $\partial_\theta \beta_\theta$ and $\partial_\theta \gamma_\theta$ terms would obviously persist. Thus one non-trivial *generalized* characteristic variable always survives and prevents the existence of a complete set of characteristic variables. Hence within the coordinate basis built from (t, ρ, θ) , the field equations are at best only weakly hyperbolic regardless of the specific reduction. In Sec. 5.4 we show that this result carries over to other auxiliary frames as well. Notice that the structure that renders the system of this section only WH is essentially the same as that

of the WH pure gauge subsystem in Bondi-Sachs coordinates, namely the angular sector.

5.3 Double-null and more gauges

Another common choice is to use double null coordinates. This was used in [109, 124, 130] to construct initial data on intersecting ingoing and outgoing null hypersurfaces. [124] provided a first well-posedness result for the CIVP in the region near the intersection, using the harmonic gauge though for the evolution system, which is symmetric hyperbolic. [130] improved this result including in the analysis metric derivatives higher than second order. A similar approach was used in [109] as well to analyze the mathematical conditions for black hole formation. Norm-type estimates are of course central in these studies, but they are obtained using PDE systems that are not of the free evolution type and for which the hyperbolic character is not manifest. If instead one is interested in analyzing a free evolution system—which is the topic of the current study—then a certain subset of the systems used in [109, 130] has to be extracted. There are different choices on how to construct this subsystem, and in [131] a specific one was shown to provide a symmetric hyperbolic free evolution scheme in double-null coordinates. To the best of our knowledge, an evolution scheme with up to second order metric derivatives using the double null gauge choice has been used numerically only in spherical symmetry [85, 87].

Working with $f(\rho) = \rho$ in the coordinate transformation (3.5), the conditions $g^{uu} = 0$ and $g^{rr} = 0$ yield

$$(\beta^\rho + 1)^2 = \alpha^2 \gamma^{\rho\rho}, \quad (\beta^\rho - 1)^2 = \alpha^2 \gamma^{\rho\rho}, \quad (5.64)$$

where the first is the former of the conditions (3.6) with $f' = 1$. The conditions $g^{uA} = 0$ are still imposed in the double null gauge, which provide the latter of conditions (3.6) with $f' = 1$. From the coordinate light speed expressions (3.21) the conditions (5.64) yield

$$c_+^\rho = \pm 1, \quad c_-^\rho = \mp 1.$$

We choose to set $c_+^\rho = 1$ and $c_-^\rho = -1$. Then, $c_+^\rho + c_-^\rho = 0 = -2\beta^\rho$ implies $\beta^\rho = 0$, which from (5.64) leads to $\alpha = L$. Replacing these in the second of conditions (5.64) with $f' = 1$ and using (3.20) provides $\beta^A = -b^A \alpha L^{-1}$. Then, the whole set of the coordinate light speeds (3.21), (3.22) in the double null gauge reads

$$c_+^\rho = 1, \quad c_-^\rho = -1, \quad c_+^A = 0.$$

After linearization about Minkowski, the lapse and shift perturbations read

$$\delta\alpha = -\frac{1}{2}\delta\gamma_{\rho\rho}, \quad \delta\beta^\rho = 0, \quad \delta\beta^\theta = -\rho^{-2}\delta\gamma_{\rho\theta}, \quad \delta\beta^\phi = -\rho^{-2}\sin^2\theta\delta\gamma_{\rho\phi}.$$

In terms of Θ and ψ^i the above is similar to (5.5) with the only difference that here $\delta\beta^\rho = 0$. Then, the pure gauge subsystem (4.8) for the double null gauge choice reads

$$\begin{aligned}\partial_t\Theta - \partial_\rho\psi^\rho &= 0, \\ \partial_t\psi^\rho - \partial_\rho\Theta &= 0, \\ \partial_t\psi^\theta + \partial_\rho\psi^\theta + \rho^{-2}\partial_\theta(\psi^\rho - \Theta) &= 0, \\ \partial_t\psi^\phi + \partial_\rho\psi^\phi + (\rho\sin\theta)^{-2}\partial_\phi(\psi^\rho - \Theta) &= 0,\end{aligned}$$

which again possesses non-trivial Jordan blocks along the θ and ϕ directions and so is only WH. This was expected since the difference among the affine null, Bondi-Sachs proper and double null cases with respect to the lapse and shift is only in the specification of the radial coordinate.

This structure in the pure gauge subsystem of the double null gauge was already discovered in [116]. We review it here in order to stress its differences and similarities with other Bondi-like gauges. We observe that in all three examples that are presented, the gauge choice $\beta^A = -b^A\alpha L^{-1}$ renders the pure gauge subsystem only WH. This choice implies the condition $c_+^A = 0$. Thus the pure gauge subsystem will also be WH if $c_-^A = 0$ is instead imposed. In such a case the difference would be a sign change in the non-trivial Jordan block along the angular directions. Furthermore, since the specific nature of the angular coordinates (i.e. coordinates on a two-sphere) is not essential to the WH, we expect that the pure gauge subsystem would retain this structure if these coordinates parameterize level sets of a different topology. Our expectation is the same for higher dimensional spacetimes. The value of the cosmological constant does not affect the principal part of the EFEs and so neither their hyperbolic character. An explicit example that verifies this expectation is the one of Subsec. 5.1.4.

In summary, we expect that formulations that result from the EFE, including up to second order metric derivatives will be at best WH if they are formulated in a Bondi-like gauge. The claim is based on the following:

1. The system admits an equivalent ADM setup.
2. The principal symbol \mathbf{P}^s has the upper triangular form (4.16).
3. The pure gauge sub-block \mathbf{P}_G inherits the structure of the pure gauge subsystem.
4. The pure gauge subsystem is WH.

Notice however the symmetric hyperbolic free evolution systems of [132] in affine null and [131] double null gauge. These systems include equations with higher than second order metric derivatives and so do not fall into the category analyzed here. Since these systems are symmetric hyperbolic, their CI(B)VP is well-posed in the L^2 -norm. However, this is not the L^2 -norm of the systems we analyzed here in those gauges. It is interesting to understand

the possible relation between the second and higher order metric formulations in the same Bondi-like gauge, as well as the implication on well-posedness.

5.4 Frame independence

Earlier we presented hyperbolicity analyses of widely used Bondi-like formulations of GR. We worked with a particular auxiliary Cauchy-type frame with one timelike element and the remainder spacelike. The auxiliary basis was used to express the original PDEs in a form that allowed us to utilize the definitions of Sec. 2.2 and show weak hyperbolicity. In this section we argue that this result persists for other auxiliary frames. Our argument is based on the dual foliation (DF) approach of [116] and follows closely Sec. II.D of [133]. Here, Latin letters $a \dots e$ are used as abstract indices, Greek letters run from 0 to $d + 1$ for a $d + 1$ -dimensional spacetime and a given basis and Latin indices i, j, k denote only the spatial components of this basis. We also use p as an abstract index for the spatial derivatives appearing on the right-hand-side of a first order PDE. The symbol ∂_α stands for the flat covariant derivative naturally defined by x^μ .

The idea of the DF approach is to express a region of spacetime in terms of two different frames, which we call uppercase and lowercase. Considering a $d + 1$ split of the spacetime, let us denote as n^a and N^a the normal vectors on the hypersurfaces of constant time for the lower and uppercase frames, respectively. We call v^a and V^a the boost vectors for each frame, which are spatial with respect to the corresponding normal vector. The Lorentz factor is $W = (1 - v^a v_a)^{-1/2} = (1 - V^a V_a)^{-1/2}$ and we denote as γ_{ab} and ${}^{(N)}\gamma_{ab}$ the lower and uppercase spatial metrics. The following useful relations hold

$$\delta^a_b = \gamma^a_b - n^a n_b = {}^{(N)}\gamma^a_b - N^a N_b, \quad n^a = W (N^a + V^a), \quad N^a = W (n^a + v^a). \quad (5.65)$$

Let us consider a first order PDE in the compact form

$$\mathcal{A}^b \delta^a_b \partial_a \mathbf{u} + \mathcal{S} = 0,$$

and $d + 1$ split using the lower and uppercase frames, replacing δ^a_b by means of (5.65), giving

$$\mathcal{A}^n \partial_n \mathbf{u} \simeq \mathcal{A}^b \gamma^a_b \partial_a \mathbf{u}, \quad \mathcal{A}^N \partial_N \mathbf{u} \simeq \mathcal{A}^b {}^{(N)}\gamma^a_b \partial_a \mathbf{u}. \quad (5.66)$$

We obtain two evolution systems for the variables of \mathbf{u} , with

$$\mathcal{A}^a n_a \equiv \mathcal{A}^n, \quad n^a \partial_a \equiv \partial_n, \quad \mathcal{A}^a N_a \equiv \mathcal{A}^N, \quad N^a \partial_a \equiv \partial_N. \quad (5.67)$$

Without loss of generality we choose to identify the uppercase frame with the auxiliary

frames used in Subsec. 5.1.4 and 5.2.3. The definitions

$$\mathcal{A}^n \equiv \mathbf{A}^n, \quad \mathcal{A}^a \gamma_a^b \equiv \mathbf{A}^b, \quad \mathcal{A}^N \equiv \mathbf{B}^N, \quad \mathcal{A}^{a(N)} \gamma_a^b \equiv \mathbf{B}^b,$$

imply $\mathbf{B}^b N_b = 0$, $\mathbf{A}^b n_b = 0$ and lead to the following upper and lowercase first order PDE forms

$$\partial_N \mathbf{u} = \mathbf{B}^p \partial_p \mathbf{u} - \mathbf{S}, \quad \mathbf{A}^n \partial_n \mathbf{u} = \mathbf{A}^p \partial_p \mathbf{u} - \mathbf{S}, \quad (5.68)$$

where $\mathbf{B}^N = \mathbb{1}$ by assumption. The former is the same form as in equations (5.60) and (5.37). In this form we found the PDE systems only WH due the 2×2 Jordan blocks of the angular principal parts. This can be represented in a generalized eigenvalue problem of the form

$$\mathbf{I}_{\lambda_N}^N \left(\mathbf{P}^S - \mathbb{1} \lambda_N \right)^M = 0, \quad (5.69)$$

where S^a is a unit spatial vector, $\mathbf{P}^S \equiv \mathbf{B}^a S_a$ the principal symbol and M is the rank of the generalized left eigenvector $\mathbf{I}_{\lambda_N}^N$ with eigenvalue λ_N , with $M = 2$ for the generalized eigenvectors that correspond to the aforementioned Jordan blocks. We wish to examine if generalized eigenvalue problems of this form exist also in the lowercase frame. Hence we need to relate the two equations of (5.68), obtaining

$$\mathbf{A}^n = W(\mathbb{1} + \mathbf{B}^V), \quad \mathbf{A}^p = \mathbf{B}^a (\gamma_a^p + W V_a v^p) - W(\mathbb{1} + \mathbf{B}^V) v^p, \quad (5.70)$$

and

$$\mathbf{B}^N = \mathbb{1} = W(\mathbf{A}^n + \mathbf{A}^v), \quad \mathbf{B}^p = \mathbf{A}^{a(N)} \gamma_a^p - W \mathbf{A}^n V^p, \quad (5.71)$$

where we write $\mathbf{B}^a V_a \equiv \mathbf{B}^V$. Let us examine $\mathbb{1} + \mathbf{B}^V$. In [133] invertibility of this matrix was guaranteed by strong hyperbolicity. Here we want to analyze PDEs that are only WH and so may not assume that \mathbf{B}^V is diagonalizable. Hence, let us denote as

$$\mathbf{J}^{S_V} = \mathbf{T}_{S_V}^{-1} \mathbf{B}^{S_V} \mathbf{T}_{S_V},$$

the Jordan normal form of $\mathbf{B}^{S_V} = \mathbf{B}^a (S_V)_a$, where $V^a = |V| S_V^a$ is the uppercase boost vector with norm $|V|$ pointing in the direction of S_V^a . One can write each block \mathbf{j} of the Jordan form \mathbf{J} with only the eigenvalue λ_i on the diagonal as

$$\mathbf{j} = \lambda_i \mathbb{1} + \mathbf{N},$$

where \mathbf{N} is a nilpotent matrix of the size of \mathbf{j} with $\mathbf{N}^q = 0$. Consequently

$$\mathbf{T}_{S_V}^{-1} \left(\mathbb{1} + \mathbf{B}^V \right) \mathbf{T}_{S_V} = \mathbb{1} + \mathbf{J}^{S_V} |V|,$$

and for each block \mathbf{j}^{S_V} ,

$$\mathbb{1} + \mathbf{j}^{S_V} = \tilde{\lambda}_i^{S_V} \left(\mathbb{1} + \frac{|V|}{\tilde{\lambda}_i^{S_V}} \mathbf{N}^{S_V} \right),$$

assuming that

$$\tilde{\lambda}_i^{S_V} = 1 + |V|\lambda_i^{S_V} \neq 0. \quad (5.72)$$

The inverse of this block is then

$$\frac{1}{\tilde{\lambda}_i^{S_V}} \left[\mathbb{1} + \sum_{j=1}^{q-1} \left(-\frac{|V|}{\tilde{\lambda}_i^{S_V}} \right)^j (\mathbf{N}^{S_V})^j \right],$$

and hence $\mathbb{1} + \mathbf{B}^V$ is invertible as long as condition (5.72) is satisfied for each λ_i . Note that in our normalization light-speed corresponds to $\lambda = 1$. Since $|V| < 1$, inequality (5.72) is always satisfied for physical propagation speeds, although could be violated when superluminal gauge speeds are present. If one considers for instance the analysis of subsections 5.1.4 and 5.2.3 on top of vacuum AdS and Minkowski background respectively, then this condition is satisfied. We wish to find the equivalent of the uppercase generalized eigenvalue problem (5.69) in the lowercase frame. Thus, using the second equation of (5.71) and $S_a = \mathbf{s}_a - WV^S n_a$ [133, 134] we express the principal symbol in the lowercase frame, namely

$$\mathbf{P}^S \equiv \mathbf{B}^a S_a = \mathbf{A}^a \mathbf{s}_a - \mathbf{A}^n WV^S.$$

Hence, the equivalent of (5.69) in the lowercase frame is

$$\mathbf{I}_{\lambda_N}^N \left[\mathbf{A}^{(\mathbf{s} - \lambda_N W v)} - W(\lambda_N + V^S) \mathbf{A}^n \right]^M = 0. \quad (5.73)$$

Thus if in the uppercase frame the eigenproblem (5.69) with $M = 1$ fails to admit a complete set of left eigenvectors then so does the lowercase frame, and so both setups would be at best weakly hyperbolic. To see this we need only set $M = 1$ in (5.73) and note that the lowercase principal symbol in the $\mathbf{s}_a - \lambda_N W v_a$ direction is proportional to

$$(\mathbf{A}^n)^{-1} \mathbf{A}^{(\mathbf{s} - \lambda_N W v)},$$

and so deficiency of the lower case principal symbol in this direction is equivalent to that of the upper case principal symbol stated before. Unfortunately the relationship between the upper and lowercase generalized left eigenvectors is more subtle. Returning to our specific systems and identifying the uppercase unit spatial vector S^a with the unit spatial vectors in the ∂_z and ∂_θ directions of Subsec. 5.1.4 and 5.2.3 respectively, we conclude that weak hyperbolicity of those PDEs persists in other frames.

5.5 Conclusions

In this chapter we analyzed the hyperbolic character of some popular Bondi-like free evolution systems and their pure gauge subsystems. We found that all of them are weakly hyperbolic due to their structure in the angular directions. In some examples we were able to explicitly identify the pure gauge sub-block as the source of the weakly hyperbolic structure for the principal symbol of the full system. To show this we had to jump through a number of technical hoops. We mapped the characteristic free evolution system to an ADM setup so that the results of [101, 115] could be easily used. This allowed us to distinguish between the gauge, constraint and physical degrees in the linear, constant coefficient approximation. Crucially it is known that weakly hyperbolic pure gauges give rise to weakly hyperbolic formulations. We were able to show the former in the affine null, the Bondi-Sachs proper and the double null gauges. All three have the same degenerate structure rendering the pure gauge subsystem weakly hyperbolic, which is caused by the gauge condition $g^{uA} = 0$. We have thus argued that when the EFE are written in a Bondi-like gauge with at most second derivatives of the metric and there are non-trivial dynamics in at least two spatial directions, then, due to the weak hyperbolicity of the pure gauge subsystem, the resulting PDE system is only WH.

Given the above, the obvious approach to circumvent weak hyperbolicity is to adopt a different gauge. Yet, symmetric hyperbolic formulations of GR employing Bondi-like gauges are known [131, 132, 135, 136]. At first sight this seems to contradict the claim that any formulation of GR inherits the pure gauge principal symbol within its own. But these formulations all promote the curvature to be an evolved variable, so the results of [101] do not apply. As we have seen in Subsec. 5.1.1, taking an outgoing null derivative of the affine null pure gauge subsystem, we obtain a strongly hyperbolic PDE. It is thus tempting to revisit the model of [101] to investigate the conjecture that formulations of GR with evolved curvature can be built that inherit specific derivatives of the pure gauge subsystem. A deeper understanding of this would shed more light into the reason that these formulations avoid weak hyperbolicity. As mentioned in Chap. 2, the hyperbolic character of a PDE system dictates the existence and the form of the norms in which the respective PDE problems are well-posed. This is the topic of the following chapter, as well as the implications for applications of characteristic formulations in precision gravitational wave astronomy.

CHAPTER 6

Well-posedness of Bondi-like PDE problems

Contents

6.1	Toy model PDEs	74
6.2	Algebraic determination of well-posedness	75
6.2.1	Homogeneous WH model	76
6.2.2	Inhomogeneous WH model	77
6.3	Toy CCE and CCM energy estimates	78
6.4	Energy estimates for the axisymmetric Bondi-Sachs system	82
6.5	CIBVP energy estimates for symmetric hyperbolic PDEs	86
6.5.1	Domain \mathcal{D}_1	87
6.5.2	Domain \mathcal{D}_2	90
6.6	Conclusions	93

The hyperbolic character of a PDE relates to the well-posedness of its CIBVP. Here we examine this relation in detail. We first do so by using toy models that we introduce in Sec. 6.1 and which mimic the structure of Bondi-like characteristic systems. We analyze their algebraic character for well-posedness as described in Sec. 2.3. This determines the well-posedness of their IVP [102, 103], which we later adjust to the CIBVP. Specifically, we wish to understand what inequalities, with what norms, can be used to bound solutions in terms of their given data, and how lower order perturbations affect such estimates. In Sec. 6.3 we examine energy estimates for model CCE and CCM setups based on the toy PDE systems introduced. In Sec. 6.4 we repeat the algebraic characterization for the Bondi-Sachs axisymmetric system of Subsec. 5.2.3 and comment on energy estimates. In Sec. 6.5 we provide an energy estimate for the CIBVP of a model symmetric hyperbolic PDE system. All the calculations are performed in the linear constant coefficient approximation. The material of Secs. 6.4 and 6.5 is not part of any publication or preprint and may be included in future ones.

6.1 Toy model PDEs

A simple WH PDE model that captures the structure of Bondi-like systems is the following

$$\begin{aligned} \partial_x \phi &= -S_\phi, \\ \partial_x \psi_v - \partial_z \phi &= -S_{\psi_v}, \\ \partial_u \psi - \frac{(1-x^2)^{3/2}}{2c_x} \partial_x \psi - \partial_z \psi &= -S_\psi, \end{aligned} \tag{6.1}$$

where $x \in [0, 1]$, $z \in [0, 2\pi)$ with periodic boundary conditions, $u \geq u_0$ for some initial time u_0 and c_x a constant. This PDE can be written in the form

$$\mathcal{A}^u \partial_u \mathbf{u} + \mathcal{A}^x \partial_x \mathbf{u} + \mathcal{A}^z \partial_z \mathbf{u} + \mathcal{S} = 0, \tag{6.2}$$

where $\mathbf{u} = (\phi, \psi_v, \psi)^T$ is the state vector, and the principal matrices are given by

$$\mathcal{A}^u = \text{diag}(0, 0, 1), \quad \mathcal{A}^x = \text{diag}(1, 1, \frac{-1}{2c_x}(1-x^2)^{3/2}),$$

and

$$\mathcal{A}^z = \begin{pmatrix} 0 & 0 & 0 \\ -1 & 0 & 0 \\ 0 & 0 & -1 \end{pmatrix}.$$

The source terms are denoted by S_ϕ , S_{ψ_v} and S_ψ . The first two Eqs. of (6.1) are intrinsic to a hypersurface of constant u , whereas the last is the “evolution equation” of the system i.e. involves also directional derivatives pointing outside a null hypersurface. The angular principal part \mathcal{A}^z is not diagonalizable since it has a 2×2 Jordan block for the intrinsic equations, mimicking the core structure of the previously analyzed Bondi-like PDEs. One may think of this model as a simplified analog of these systems with a compactified radial coordinate, similar to the way that Bondi-like formulations are used for characteristic extraction. This role can be played by the coordinate x with c_x a constant involved in the compactification. More specifically

$$x = \frac{r - r_{\min}}{\sqrt{c_x^2 + (r - r_{\min})^2}},$$

where r_{\min} is the minimum physical radius that we consider and the factor c_x controls the density of points towards $r \rightarrow \infty$, if we were to map the compactified grid x to the physical radius grid r .

By removing the angular derivative from the second intrinsic equation (6.1) we obtain our

SH toy model

$$\begin{aligned}\partial_x \phi &= -S_\phi, \\ \partial_x \psi_v &= -S_{\psi_v}, \\ \partial_u \psi - \frac{(1-x^2)^{3/2}}{2c_x} \partial_x \psi - \partial_z \psi &= -S_\psi,\end{aligned}\tag{6.3}$$

which has the same principal part matrices \mathcal{A}^u and \mathcal{A}^x as before, but has diagonal \mathcal{A}^z . We employ this model for comparison between numerical results with SH and WH systems. The PDE problem for both systems (6.1) and (6.3) has as domain

$$x \in [0, 1], \quad z \in [0, 2\pi), \quad u \in [u_0, u_f],$$

for some initial and final times u_0 and u_f respectively. We apply periodic boundary conditions in the z direction for simplicity. The initial and boundary data are

$$\psi_* \equiv \psi(u_0, x, z)\tag{6.4}$$

and

$$\hat{\phi} \equiv \phi(u, 0, z), \quad \hat{\psi}_v \equiv \psi_v(u, 0, z),\tag{6.5}$$

respectively and are freely specifiable.

6.2 Algebraic determination of well-posedness

We wish to apply the tools of Sec. 2.3 to the toy models. For this we want to write the system in the form (2.10) where the time principal part is the identity matrix. We achieve the latter via a coordinate transformation similar to (3.5), namely

$$u = t - \rho, \quad x = \rho, \quad z = z.$$

Starting from Eqs. (6.1), we bring the system to the form

$$\begin{aligned}\partial_t \phi &= -\partial_\rho \phi - S_\phi, \\ \partial_t \psi_v &= -\partial_\rho \psi_v + \partial_z \phi - S_{\psi_v}, \\ \partial_t \psi &= F \partial_\rho \psi + G \partial_z \psi - G S_\psi,\end{aligned}$$

where

$$F = \frac{(1-\rho^2)^{3/2}}{2c_x - (1-\rho^2)^{3/2}}, \quad G = \frac{2c_x}{2c_x - (1-\rho^2)^{3/2}}$$

are fixed real constants for fixed ρ and c_x , with non-zero denominator for our ρ domain and an appropriately chosen c_x . In this frame the principal parts are $\mathcal{B}^t = \mathbb{1}$ and

$$\mathcal{B}^\rho = \begin{pmatrix} -1 & 0 & 0 \\ 0 & -1 & 0 \\ 0 & 0 & F \end{pmatrix}, \quad \mathcal{B}^z = \begin{pmatrix} 0 & 0 & 0 \\ 1 & 0 & 0 \\ 0 & 0 & G \end{pmatrix}.$$

This is the auxiliary Cauchy-type setup for the WH model, similarly to the earlier Bondi-like PDEs in Chap. 5. After applying a Fourier transformation, the principal symbol for the WH model is

$$i\omega_p \mathcal{B}^p = i\omega_\rho \mathcal{B}^\rho + i\omega_z \mathcal{B}^z.$$

By algebraic characterization of well-posedness we mean the study of the inequalities the symbol $\mathbf{P}(i\omega)$ as defined in Eq. (2.13) satisfies. These inequalities inform us on the existence and the form of the norms that can be used to control the solution for the IVP of a given PDE system.

6.2.1 Homogeneous WH model

Focusing first on the homogeneous WH model where $S_\phi = S_{\psi_v} = S_\psi = 0$, we obtain

$$e^{(i\hat{\omega}_p \mathcal{B}^p)|\omega|t} = \begin{pmatrix} e^{-i|\omega|\hat{\omega}_\rho t} & 0 & 0 \\ i|\omega|\hat{\omega}_z t e^{-i|\omega|\hat{\omega}_\rho t} & e^{-i|\omega|\hat{\omega}_\rho t} & 0 \\ 0 & 0 & e^{i|\omega|(F\hat{\omega}_\rho + G\hat{\omega}_z)t} \end{pmatrix}, \quad (6.6)$$

where we express the wavevector as

$$\omega_p = |\omega|\hat{\omega}_p,$$

with $|\omega|$ its magnitude so that $\hat{\omega}_\rho^2 + \hat{\omega}_z^2 = 1$. The norm of (6.6) is (see chapter 2 of [106] for useful definitions)

$$\left| e^{(i\hat{\omega}_p \mathcal{B}^p)|\omega|t} \right|^2 = 1 + \frac{|\omega|^2 \hat{\omega}_z^2 t^2}{2} + \left[\left(1 + \frac{|\omega|^2 \hat{\omega}_z^2 t^2}{2} \right)^2 - 1 \right]^{1/2}. \quad (6.7)$$

This norm behaves as $|\omega|t$ for large $|\omega|$ and so the homogeneous WH model obeys an inequality of the form (2.14), with $q = 1$. Hence, this PDE is only weakly well-posed, and so satisfies an estimate in some $\|\cdot\|_q$ -norm, which we call *lopsided*. This norm is specified for our system in Sec. 6.3. If one would discard from the previous analysis the equation for ψ_v of the homogeneous WH model (6.1) since it is decoupled, the remaining subsystem would be symmetric hyperbolic and one might expect well-posedness of the full PDE problem in

the L^2 -norm. However, it is important to keep in mind that well-posedness is a property of the full PDE problem, which means that the PDE system should be treated as whole when studying its hyperbolic character. As a matter of fact, in Chap. 7 we present numerical experiments that demonstrate this point.

6.2.2 Inhomogeneous WH model

For the homogeneous WH model we computed the norm of $e^{(i\hat{\omega}_p \mathcal{B}^p)|\omega|t}$ to estimate the behavior of solutions. However, we could also examine the form of the eigenvalues of the full symbol $\mathbf{P}(i\omega)$ for large $|\omega|$ to understand if the solutions exhibit exponential growth in ω_p (see lemma 2.3.1 of [102]). If there is any eigenvalue λ of $\mathbf{P}(i\omega)$ such that

$$\Re[\lambda] \sim |\omega|^s > 0 \text{ with } s > 0,$$

for large $|\omega|$, then solutions of the PDE may exhibit frequency dependent exponential growth, and the PDE problem is ill-posed in any sense. For the inhomogeneous WH model we consider the following possible lower order source terms

$$\mathcal{B}_1 = \begin{pmatrix} 0 & 0 & 1 \\ 1 & 0 & 1 \\ 1 & 0 & 0 \end{pmatrix}, \quad \mathcal{B}_2 = \begin{pmatrix} 1 & 0 & 1 \\ 1 & 1 & 1 \\ 1 & 1 & 1 \end{pmatrix}, \quad \mathcal{B}_3 = \begin{pmatrix} 0 & 1 & 0 \\ 0 & 0 & 0 \\ 0 & 0 & 0 \end{pmatrix},$$

where $-\mathcal{S} = \mathcal{B}\mathbf{u}$. The choice \mathcal{B}_1 is motivated by analogy with the linearized Bondi-Sachs system with $\phi \sim \beta$, $\psi_v \sim V$ and $\psi \sim \gamma_r$. In \mathcal{B}_2 we include all possible source terms that do not break the nested structure of the intrinsic equations and finally in the choice \mathcal{B}_3 we introduce source terms that violate the nested structure, thus rendering the intrinsic subsystem a coupled PDE. For both \mathcal{B}_1 and \mathcal{B}_2 the eigenvalues of $\mathbf{P}(i\omega)$ are

$$\lambda_1 = \lambda_2 = -i|\omega|\hat{\omega}_\rho, \quad \lambda_3 = i|\omega|(F\hat{\omega}_\rho + G\hat{\omega}_z),$$

as $|\omega| \rightarrow \infty$, with the next terms appearing at order $|\omega|^0$. For these choices of lower order source terms the inhomogeneous WH model remains well-posed in the lopsided norm. On the other hand if $\mathcal{B} = \mathcal{B}_3$ the eigenvalues of the symbol are

$$\begin{aligned} \lambda_1 &= -i|\omega|\hat{\omega}_\rho - (-1)^{1/4}\sqrt{|\omega|\hat{\omega}_z} + O(|\omega|^0), \\ \lambda_2 &= -i|\omega|\hat{\omega}_\rho + (-1)^{1/4}\sqrt{|\omega|\hat{\omega}_z} + O(|\omega|^0), \\ \lambda_3 &= i|\omega|(F\hat{\omega}_\rho + G\hat{\omega}_z) + O(|\omega|^0), \end{aligned}$$

for large $|\omega|$. Since $\Re[\lambda] \sim |\omega|^{1/2}$, we conclude that when the nested structure of the intrinsic equations is broken, the solution of the inhomogeneous WH exhibits frequency dependent exponential growth. Consequently, the IVP with this system is no longer weakly well-posed

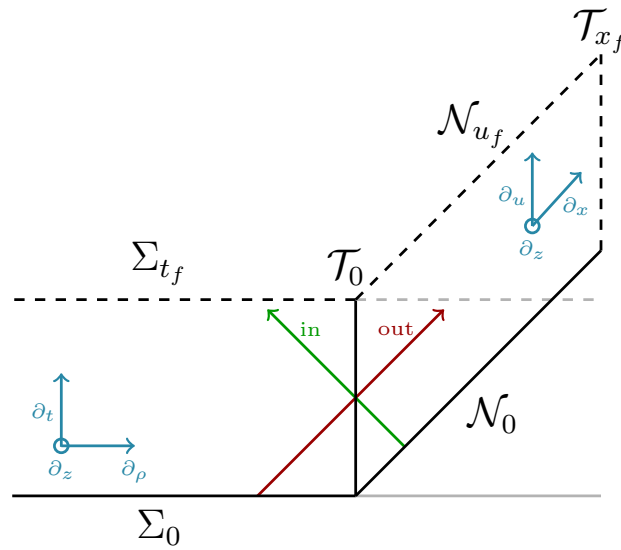


Figure 6.1: The IBVP (left) and the CIBVP (right) setups. For CCE outgoing data from the IBVP serve as boundary data on \mathcal{T}_0 for the CIBVP, which can be viewed as an independent PDE problem. In this case the IBVP's spatial domain is more extended such that data on \mathcal{T}_0 are unaffected by the boundary conditions chosen for the problem. For CCM the IBVP and CIBVP are solved simultaneously and out/ingoing data are communicated from one to the other via \mathcal{T}_0 . Effectively, the two problems are viewed as one.

but ill-posed. Note, in contrast, that for the homogeneous SH model we have

$$|e^{\mathbf{P}(i\omega)t}| = 1.$$

Hence for this model, the IVP is well-posed already in the L^2 -norm. Unlike the WH model, well-posedness for this model is not affected by source terms. The detailed calculations for both models can be found in [121].

6.3 Toy CCE and CCM energy estimates

The previous analysis was performed in Fourier space and yielded that an IVP based on the homogeneous WH model may be well-posed in an appropriate lopsided norm, whereas one on the SH model is (strongly) well-posed in the L^2 -norm. We now present our energy estimates for solutions to the IBVP and CIBVP by working in position space. For concreteness and simplicity the PDE system for the IBVP is a homogeneous SH model (which is furthermore

symmetric hyperbolic)

$$\begin{aligned}\partial_t \bar{\phi} + \partial_\rho \bar{\phi} + \partial_z \bar{\psi}_v &= 0, \\ \partial_t \bar{\psi}_v + \partial_\rho \bar{\psi}_v + \partial_z \bar{\phi} &= 0, \\ \partial_t \bar{\psi} - \frac{1}{2} \partial_\rho \bar{\psi} - \partial_z \bar{\psi} &= 0,\end{aligned}\tag{6.8}$$

with initial data $\bar{\phi}_*$, $\bar{\psi}_{v*}$, $\bar{\psi}_*$ on Σ_0 , boundary data $\hat{\psi}$ on \mathcal{T}_0 and domain $t \in [0, t_f]$, $\rho \in (-\infty, 0]$ and the compact $z \in [0, 2\pi)$, and for the CIBVP the homogeneous WH model

$$\partial_x \phi = 0,\tag{6.9a}$$

$$\partial_x \psi_v - \partial_z \phi = 0,\tag{6.9b}$$

$$\partial_u \psi - \frac{1}{2} \partial_x \psi - \partial_z \psi = 0,\tag{6.9c}$$

with initial data ψ_* on \mathcal{N}_0 , boundary data $\hat{\phi}$ and $\hat{\psi}_v$ on \mathcal{T}_0 and domain $u \in [0, u_f]$, $x \in [0, x_f]$ and the aforementioned z . The domains of the two problems are illustrated in Fig. 6.1. We view the IBVP as a simplified analog of GR in strongly (here even symmetric) hyperbolic formulations widely used in Cauchy-type problems, with the CIBVP formulated in the Bondi-like gauges used in characteristic evolutions. We wish to understand whether or not problems with these features can be successfully used for CCE or CCM in principle.

For the IBVP estimate our starting point is

$$\partial_t \|\bar{\mathbf{u}}\|_{L^2(\Sigma_t)}^2 = \partial_t \int_{\Sigma_t} \bar{\mathbf{u}}^T \bar{\mathbf{u}} = \partial_t \int_{\Sigma_t} (\bar{\phi}^2 + \bar{\psi}_v^2 + \bar{\psi}^2),$$

which after using (6.8) reads

$$\partial_t \|\bar{\mathbf{u}}\|_{L^2(\Sigma_t)}^2 = 2 \int_{\Sigma_t} \left(-\bar{\phi} \partial_\rho \bar{\phi} - \bar{\phi} \partial_z \bar{\psi}_v - \bar{\psi}_v \partial_\rho \bar{\psi}_v - \bar{\psi}_v \partial_z \bar{\phi} + \frac{1}{2} \bar{\psi} \partial_\rho \bar{\psi} + \bar{\psi} \partial_z \bar{\psi} \right).$$

Applying here the divergence theorem (see App. A.1 for more details) assuming $\bar{\mathbf{u}} \rightarrow \mathbf{0}$ as $\rho \rightarrow -\infty$ yields

$$\partial_t \|\bar{\mathbf{u}}\|_{L^2(\Sigma_t)}^2 = \int \left(-\bar{\phi}^2|_{\rho=0} - \bar{\psi}_v^2|_{\rho=0} + \frac{1}{2} \bar{\psi}^2|_{\rho=0} \right) dz,$$

where the terms $\bar{\phi} \bar{\psi}_v|_{z=0} - \bar{\phi} \bar{\psi}_v|_{z=2\pi}$ and $\bar{\psi}^2|_{z=2\pi} - \bar{\psi}^2|_{z=0}$ vanish due to periodicity in z . Finally, and integrating in the t domain returns

$$\|\bar{\mathbf{u}}\|_{L^2(\Sigma_{t_f})}^2 + \|\bar{\mathbf{u}}\|_{L^2_{\text{out}}(\mathcal{T}_0)}^2 = \|\bar{\mathbf{u}}\|_{L^2(\Sigma_0)}^2 + \frac{1}{2} \|\bar{\mathbf{u}}\|_{L^2_{\text{in}}(\mathcal{T}_0)}^2,\tag{6.10}$$

where $\|\bar{\mathbf{u}}\|_{L^2_{\text{out}}(\mathcal{T}_0)}^2$ denotes integral over \mathcal{T}_0 that contains only the outgoing fields $\bar{\phi}$, $\bar{\psi}_v$, and similarly for the ingoing $\bar{\psi}$. The estimate (6.10) states that the energy of the solution equals the energy of its given data, so that the solution is controlled by the given data.

In a Cauchy-type setup we specify all fields on the initial spacelike hypersurface and, by solving the system we obtain all of them on spacelike hypersurfaces to the future. On the contrary, in a single-null characteristic setup, fields with “evolution” equations are chosen on the initial null hypersurface and those that satisfy equations intrinsic to the null hypersurfaces are specified as boundary data. As we will see in the following, this has a natural consequence on the type of estimates that we can hope to demonstrate, both in terms of the domain on which we integrate and the particular fields that appear. This is due to the geometry of the setup.

Motivated from the IVP estimates in Fourier space of Subsec. 6.2.1 and 6.2.2 we might naively first consider for the CIBVP the lopsided norm

$$\|\mathbf{u}\|_{q(\mathcal{D})}^2 = \int_{\mathcal{D}} \left(\phi^2 + \psi_v^2 + \psi^2 + (\partial_z \phi)^2 \right),$$

in some domain \mathcal{D} , where only $\partial_z \phi$ is added to the integrand of the L^2 -norm, because precisely this term causes the pathological structure in the angular principal part of the WH model. Following our previous discussion however, it is more appropriate to split the integrand into separate pieces for the ingoing and outgoing variables. The domain \mathcal{D} becomes \mathcal{N}_u and \mathcal{T}_x respectively for each. For the ingoing variables we start from

$$\partial_u \|\mathbf{u}\|_{q_{\text{in}}(\mathcal{N}_u)}^2 = \partial_u \int_{\mathcal{N}_u} \psi^2,$$

since there are no ∂_u equations for the outgoing ones. We assume that $\psi \rightarrow 0$ as $x \rightarrow x_f$ in the given data, which is the analog in our model to requiring no incoming gravitational waves from future null infinity, working on a compactified radial domain. After using (6.9c), the divergence theorem and integrating in the u domain we obtain

$$2\|\mathbf{u}\|_{q_{\text{in}}(\mathcal{N}_{u_f})}^2 + \|\mathbf{u}\|_{q_{\text{in}}(\mathcal{T}_0)}^2 = 2\|\mathbf{u}\|_{q_{\text{in}}(\mathcal{N}_0)}^2. \quad (6.11)$$

For the outgoing variables the starting point is

$$\partial_x \|\mathbf{u}\|_{q_{\text{out}}(\mathcal{T}_x)}^2 = \partial_x \int_{\mathcal{T}_x} \left(\phi^2 + \psi_v^2 + (\partial_z \phi)^2 \right),$$

and by using (6.9a) and (6.9b), the divergence theorem and integrating in the x domain up to some arbitrary x' we obtain

$$\|\mathbf{u}\|_{q_{\text{out}}(\mathcal{T}_{x'})}^2 = \|\mathbf{u}\|_{q_{\text{out}}(\mathcal{T}_0)}^2 + \int_0^{x'} \left(\int_{\mathcal{T}_x} 2\psi_v \partial_z \phi \right) dx, \quad (6.12)$$

where the last term is due to the hyperbolicity of the system and would not appear for our

SH example. Using $2\psi_v\partial_z\phi \leq \phi^2 + \psi_v^2 + (\partial_z\phi)^2$ the latter reads

$$\|\mathbf{u}\|_{q_{\text{out}}(\mathcal{T}_{x'})}^2 \leq \|\mathbf{u}\|_{q_{\text{out}}(\mathcal{T}_0)}^2 + \int_0^{x'} \|\mathbf{u}\|_{q_{\text{out}}(\mathcal{T}_x)}^2 dx,$$

and by applying Grönwall's inequality (see App. A.2 for more details) we obtain

$$\|\mathbf{u}\|_{q_{\text{out}}(\mathcal{T}_{x'})}^2 \leq e^{x'} \|\mathbf{u}\|_{q_{\text{out}}(\mathcal{T}_0)}^2. \quad (6.13)$$

Hence, the energy of the outgoing fields at each arbitrary timelike hypersurface $\mathcal{T}_{x'}$ in the characteristic domain is bounded. The sum of 6.11 and 6.13 is the complete energy estimate for the CIBVP and yields

$$2\|\mathbf{u}\|_{q_{\text{in}}(\mathcal{N}_{u_f})}^2 + \|\mathbf{u}\|_{q_{\text{in}}(\mathcal{T}_0)}^2 + \sup_{x'} \|\mathbf{u}\|_{q_{\text{out}}(\mathcal{T}_{x'})}^2 \leq 2\|\mathbf{u}\|_{q_{\text{in}}(\mathcal{N}_0)}^2 + e^{x_f} \|\mathbf{u}\|_{q_{\text{out}}(\mathcal{T}_0)}^2, \quad (6.14)$$

where we used that $e^{x'} \leq e^{x_f}$ for $x' \in [0, x_f]$ and chose the supremum of $\|\mathbf{u}\|_{q_{\text{out}}(\mathcal{T}_{x'})}^2$ to obtain the largest possible bounded left-hand-side, since the outgoing lopsided norm is not necessarily monotonically increasing with x . Thus, the energy of the solution to the CIBVP is controlled by the given data on \mathcal{N}_0 and \mathcal{T}_0 .

We first interpret these estimates in the framework of CCE. Choosing suitable data, our estimate for the IBVP shows that one obtains a smooth solution in the domain of the Cauchy-type setup. One can then use this solution to provide boundary data on \mathcal{T}_0 for the CIBVP that are finite also in the lopsided norm, and the solution to this characteristic problem has a good energy estimate as shown earlier too. Hence the CCE process is perfectly valid for our model, and provided analogous estimates for GR in the Bondi-like gauges used, would be in that context too. One question that arises for GR is whether or not this procedure excludes any data of interest. Effort in this direction is currently ongoing, but there is no clear answer at the time of writing of this thesis. In Sec. 6.4, 6.5 we collect the current status of this work.

For CCM the discussion is rather different, since IBVP and CIBVP are solved simultaneously and data are communicated between domains. Effectively, one joins the PDE problems and they may be viewed as one. Hence, let us try to obtain an energy estimate for the joint PDE problem, by adding (6.10)¹ and (6.14):

$$\begin{aligned} & \|\mathbf{u}\|_{L^2(\Sigma_{t_f})}^2 + \|\mathbf{u}\|_{L^2_{\text{out}}(\mathcal{T}_0)}^2 + 2\|\mathbf{u}\|_{q_{\text{in}}(\mathcal{N}_{u_f})}^2 + \|\mathbf{u}\|_{q_{\text{in}}(\mathcal{T}_0)}^2 + \sup_{x'} \|\mathbf{u}\|_{q_{\text{out}}(\mathcal{T}_{x'})}^2 \\ & \leq \|\mathbf{u}\|_{L^2(\Sigma_0)}^2 + \|\mathbf{u}\|_{L^2_{\text{in}}(\mathcal{T}_0)}^2 + 2\|\mathbf{u}\|_{q_{\text{in}}(\mathcal{N}_0)}^2 + e^{x_f} \|\mathbf{u}\|_{q_{\text{out}}(\mathcal{T}_0)}^2, \end{aligned} \quad (6.15)$$

where now $\bar{\mathbf{u}} = \mathbf{u}$. For the joint problem there is “effectively” no boundary \mathcal{T}_0 at which

¹A way to get the exact coefficients that appear in (6.15) is to add $\frac{1}{2}\|\mathbf{u}\|_{L^2_{\text{in}}(\mathcal{T}_0)}^2$ on the right-hand-side of (6.10) and change $=$ to \leq .

we are free to choose data, and hence any estimate should not involve integrals over this domain. The relevant terms can however cancel each other only if the two norms that appear coincide. This requires either that the CIBVP relies on a symmetric hyperbolic PDE system and hence is well-posed in the L^2 -norm (see for instance [137–139]), or that the IBVP relies on a system that is well-posed in the same lopsided norm as the CIBVP. But this requires special structure, above and beyond symmetric hyperbolicity, on the equations used in the IBVP. Regarding GR, the first option would translate into developing a SH (hopefully also symmetric hyperbolic) single-null formulation and the second to building a formulation that is well-posed in the same lopsided norm that Bondi-like gauges (perhaps) are. Given the long search for formulations that *work* for practical evolution however, such an artisanal construction seems poorly motivated. In summary; unless special structure is present in the field equations solved for the IBVP, the solution to the weakly hyperbolic CIBVP cannot be combined with that of an IBVP of a symmetric hyperbolic system in such a way as to provide a solution to the whole problem which has an energy bounded by that of the given data.

6.4 Energy estimates for the axisymmetric Bondi-Sachs system

Working again with the linearized about flat space equations and within the constant coefficient approximation, we explore energy estimates for the Bondi-Sachs setup in axisymmetry. All the calculations can be found in [140]. We work with the minimal first order reduction of Subsec. 5.2.3 and the PDE system reads

$$\begin{aligned}
\partial_r \beta &= 0, \\
\partial_r U_r - \frac{2}{r^2} \partial_r \beta_\theta + \frac{2}{r^2} \partial_r \gamma_\theta + S_2 &= 0, \\
\partial_r V + \partial_\theta \beta_\theta - \partial_\theta \gamma_\theta - 2r \partial_\theta U - \frac{r^2}{2} \partial_\theta U_r + S_3 &= 0, \\
4r^2 \partial_u \gamma_r + 4r \partial_u \gamma - 2r^2 \partial_r \gamma_r + 2r \partial_\theta U + r^2 \partial_\theta U_r - 2\partial_\theta \beta_\theta + S_4 &= 0, \\
\partial_r U + S_5 &= 0, \\
\partial_r \gamma + S_6 &= 0, \\
\partial_r \gamma_\theta - \partial_\theta \gamma_r &= 0, \\
\partial_r \beta_\theta &= 0,
\end{aligned} \tag{6.16}$$

We focus on the IVP in the auxiliary Cauchy-type frame, in order to understand whether the WH system (6.16) has any chance to be weakly well-posed in some lopsided norm. This approach may be viewed as a preliminary exercise prior to that of an energy estimate attempt in the characteristic setup. We expect it to be informative of possible shortcomings due to the weak hyperbolicity of the specific system. A similar approach was effectively used

in Sec. 6.3 where the lopsided norm was inspired by the algebraic characterization of the WH toy model performed in Sec. 6.2. The algebraic characterization of the homogeneous version of Eq. (6.16) suggests that there exists a lopsided norm for a weakly well-posed IVP. Unfortunately, we do not have such a result for the inhomogenous version of Eq. (6.16).

The auxiliary Cauchy frame

We consider the Cauchy-type version of the system (6.16) written in the form

$$\partial_t \mathbf{u} + \mathbf{B}^p \partial_p \mathbf{u} \simeq 0, \quad (6.17)$$

with the index p denoting an arbitrary spatial coordinate and \simeq equality up to principal terms. Driven by the structure of the Bondi-Sachs system and its pathology along the angular direction θ , we employ its generalized characteristic variables $\mathbf{v} \equiv \mathbf{T}_{\hat{\theta}}^{-1} \mathbf{u}$ to define an energy density. For convenience let us first repeat the angular generalized characteristic variables as given in Subsec. 5.2.3. The ones with speed zero are

$$\rho U + \frac{\rho^2}{2} U_r - \beta_\theta + \gamma_\theta, \quad \beta_\theta, \quad V, \quad \rho \left(-2\rho U - \frac{\rho^2}{2} U_r + \beta_\theta - \gamma_\theta \right), \quad \gamma, \quad \beta,$$

of which the third and fourth are associated with the non-trivial 2×2 Jordan block within $\mathbf{J}^{\hat{\theta}}$. Likewise we have

$$-\frac{\rho}{2} U + \frac{\rho}{2} \gamma_r - \frac{\rho^2}{4} U_r + \frac{1}{2} \beta_\theta, \quad -\frac{\rho}{2} U - \frac{\rho}{2} \gamma_r - \frac{\rho^2}{4} U_r + \frac{1}{2} \beta_\theta,$$

with speeds ± 1 respectively. The structure of $\mathbf{J}_{\hat{\theta}}$ yields

$$\begin{aligned} -\partial_t \left(2\rho U + \frac{\rho^2}{2} U_r - \beta_\theta + \gamma_\theta \right) &\simeq 0, \\ \partial_t V - \rho \partial_{\hat{\theta}} \left(2\rho U + \frac{\rho^2}{2} U_r - \beta_\theta + \gamma_\theta \right) &\simeq 0, \end{aligned} \quad (6.18)$$

where $\partial_{\hat{\theta}} = 1/\rho \partial_\theta$, with $\partial_{\hat{\theta}}$ unit spatial vector. We define the energy E_{Σ_t} contained within a spacelike hypersurface Σ_t as

$$\begin{aligned}
E_{\Sigma_t}^2 &= \int_{\Sigma_t} \epsilon^2 \\
&= \int_{\Sigma_t} \left(\rho U + \frac{\rho^2}{2} U_r - \beta_\theta + \gamma_\theta \right)^2 + \beta_\theta^2 + V^2 + \rho^2 \left(-2\rho U - \frac{\rho^2}{2} U_r + \beta_\theta - \gamma_\theta \right)^2 + \gamma^2 + \beta^2 \\
&\quad + \left(-\frac{\rho}{2} U + \frac{\rho}{2} \gamma_r - \frac{\rho^2}{4} U_r + \frac{1}{2} \beta_\theta \right)^2 + \left(-\frac{\rho}{2} U - \frac{\rho}{2} \gamma_r - \frac{\rho^2}{4} U_r + \frac{1}{2} \beta_\theta \right)^2 \\
&\quad + \rho^2 \left(-2\rho \partial_{\hat{\theta}} U - \frac{\rho^2}{2} \partial_{\hat{\theta}} U_r + \partial_{\hat{\theta}} \beta_\theta - \partial_{\hat{\theta}} \gamma_\theta \right)^2 \\
&\quad + (\partial_\rho \gamma)^2, \tag{6.19}
\end{aligned}$$

where the second to last term is motivated by the non-trivial Jordan block structure (6.18) and the last term by the homogeneous analysis. To simplify the analysis we focus on the IVP and neglect any boundaries i.e. integrals over worldtubes of constant radius ρ are assumed to vanish. The main goal here is to understand if the specific form of weak hyperbolicity leads to any bulk integrals in the energy estimate calculation that prevents us from bounding the solution at future times from the initial data.

The homogeneous setup

We take a ∂_t derivative of Eq (6.19) and replace with the right-hand-side of the Eq. (6.16). The total ∂_ρ terms are neglected and the ∂_θ ones, namely

$$\rho_c \partial_{\hat{\theta}} (\beta_\theta \gamma_r), \quad -\rho_c^2 \partial_{\hat{\theta}} \gamma_r U \quad - \frac{\rho_c^3}{2} \partial_{\hat{\theta}} (\gamma_r U_r), \tag{6.20}$$

vanish due to the periodicity in the angular direction. After integrating in $t \in [t_0, t_f]$ we obtain

$$E_{\Sigma_{t_f}}^2 = E_{\Sigma_{t_0}}^2 + \int_{t_0}^{t_f} \int_{\Sigma_t} \Xi_0, \tag{6.21}$$

where the bulk integrands is

$$\Xi_0 = 2\rho_c V (\partial_{\hat{\theta}} \gamma_\theta - \partial_{\hat{\theta}} \beta_\theta) + \boxed{2\rho_c \gamma_r \partial_\rho \gamma} + 4\rho_c^2 V \partial_{\hat{\theta}} U + \rho_c^3 (V - \gamma_r) \partial_{\hat{\theta}} U_r. \tag{6.22}$$

The boxed term in the above expression is the reason we introduced the last term in the energy definition (6.19). More specifically, if the energy density did not include $(\partial_\rho \gamma)^2$, then the quantity Ξ_0 could not be bounded by the energy density exactly because of the boxed term. The rest of the bulk terms already appear in the energy density due to the generalized characteristic variables. The next step is to prove that energy of the solution can be bounded

by the energy of the initial data. By using that $\Xi_0 \lesssim \epsilon^2$ we arrive at

$$E_{\Sigma_{t_f}}^2 \lesssim E_{\Sigma_{t_0}}^2 + \int_{t_0}^{t_f} E_{\Sigma_t}^2,$$

where \lesssim denotes smaller or equal up to an overall constant. Notice that $E_{\Sigma_{t_0}}^2, E_{\mathcal{T}_{\rho_0}}^2$ is initial data. We apply here the integral version of Grönwall's inequality to arrive at

$$E_{\Sigma_{t_f}}^2 \lesssim e^{t_f} E_{\Sigma_{t_0}}^2,$$

which states that the energy of the solution is bounded by the energy of the initial data. So the homogeneous linearized axisymmetric Bondi-Sachs system (6.16) has a weakly well-posed IVP in the lopsided norm (6.19). This result is compatible with the algebraic characterization of this system, which is not shown here but follows the same method as in Sec. (6.2) and can be found in [140].

The inhomogeneous setup

However, this result is only valid for the homogeneous case. The same energy density definition fails if one considers the inhomogeneous system of the auxiliary Cauchy frame. The equivalent energy estimate in this case reads

$$E_{\Sigma_{t_f}}^2 = E_{\Sigma_{t_0}}^2 + \int_{t_0}^{t_f} \int_{\Sigma_t} \Xi_0 + \Xi_1 + \Xi_2, \quad (6.23)$$

where

$$\begin{aligned} \Xi_1 = & 4V\beta - 6U\beta_\theta - 4V\gamma + 2\gamma\gamma_r + \frac{6\beta_\theta^2}{\rho_c} - \frac{4\beta_\theta\gamma_\theta}{\rho_c} + 4\rho_c\beta_\theta^2 - 2\rho_c U_r\gamma_\theta - 4\rho_c\beta_\theta\gamma_\theta - 3\rho_c^2 U U_r \\ & - 8\rho_c^2 U\beta_\theta - \frac{3\rho_c^3 U_r^2}{2} - 2\rho_c^3 U_r\beta_\theta - 2\cot(\theta_c)V\beta_\theta + 5\cot(\theta_c)\beta_\theta\gamma_r + 6\cot(\theta_c)V\gamma_\theta \\ & - 4\cot(\theta_c)\gamma_r\gamma_\theta + 4\rho_c\cot(\theta_c)UV - 5\rho_c\cot(\theta_c)U\gamma_r + \rho_c^2\cot(\theta_c)U_rV - \frac{5\rho_c^2\cot(\theta_c)U_r\gamma_r}{2} \\ & + 4\rho_c^2\cot(\theta_c)\beta_\theta\gamma_r - 4\rho_c^2\cot(\theta_c)\gamma_r\gamma_\theta - 8\rho_c^3\cot(\theta_c)U\gamma_r - 2\rho_c^4\cot(\theta_c)U_r\gamma_r, \end{aligned} \quad (6.24)$$

$$\begin{aligned} \Xi_2 = & 2(\partial_\rho\gamma)(\partial_\rho\gamma_r) + 4\rho_c(\partial_\theta\beta_\theta)^2 - 4\rho_c(\partial_\theta\beta_\theta)(\partial_\theta\gamma_\theta) - 8\rho_c^2(\partial_\theta U)(\partial_\theta\beta_\theta) \\ & - 2\rho_c^3(\partial_\theta U_r)(\partial_\theta\beta_\theta) + 4\rho_c^2\cot(\theta_c)(\partial_\theta\beta_\theta)(\partial_\theta\gamma_r) - 4\rho_c^2\cot(\theta_c)(\partial_\theta\gamma_r)(\partial_\theta\gamma_\theta) \\ & - 8\rho_c^3\cot(\theta_c)(\partial_\theta U)(\partial_\theta\gamma_r) - 2\rho_c^4\cot(\theta_c)(\partial_\theta U_r)(\partial_\theta\gamma_r). \end{aligned} \quad (6.25)$$

The terms Ξ_1 and Ξ_2 appear due to the source terms of the linearized system (6.16). More specifically, the terms Ξ_2 are a result of acting with ∂_t on

$$\rho^2 \left(-2\rho\partial_\theta U - \frac{\rho^2}{2}\partial_\theta U_r + \partial_\theta\beta_\theta - \partial_\theta\gamma_\theta \right)^2$$

and replacing the right-hand-side of the appropriate inhomogeneous equations of motion. Note that the above combination of variables together with $\partial_\rho\gamma$ in Eq. (6.19) control the terms of Ξ_0 . In Ξ_2 however there are terms of the form

$$\partial_\rho\gamma_r, \quad \partial_\theta\gamma_r,$$

that cannot be controlled by the energy (6.19). This is an explicit example where weak well-posedness in a specific lopsided norm is broken by lower order (source) terms. One first attempt to modify the previous energy definition to accommodate for the additional terms is to add in it terms of the form

$$(\partial_\rho\gamma_r)^2, \quad (\partial_\theta\gamma_r)^2.$$

It turns out though that such a change is not sufficient. Including these terms in the integrand results in terms that do not form total derivatives and are not controlled by the initial data in this norm. It becomes clear that finding an appropriate norm (if it exists) that provides an energy estimate for the IVP of a weakly hyperbolic PDE system is far from trivial. The fact that we have not found such a norm yet for the specific system analyzed here does not necessarily mean that it does not exist. Completing the algebraic characterization of this inhomogeneous system can answer whether such a norm exists. However, this analysis has its own challenges. Even if such a norm is found, this weak well-posedness may break by lower order perturbations due to non-linearities, when considering the original non-linear Bondi-Sachs system.

6.5 CIBVP energy estimates for symmetric hyperbolic PDEs

A symmetric hyperbolic PDE system has a well-posed IVP in the L^2 -norm (see [105] for a brief discussion and references therein for more details). We assume that there exists a unique solution to the CIBVP of a symmetric hyperbolic PDE and examine continuous dependence on the given data by means of energy estimates. More specifically, we study how the geometric setup of the CIBVP affects the specific form of the norm that is appropriate for the problem. We use standard methods of PDE analysis. More sophisticated mathematical tools that take full advantage of the geometric setup may be more appropriate, but are beyond the scope of this thesis. See [141] for an overview and references therein for more details.

The PDE system under consideration can be written as

$$\mathcal{A}^\mu\partial_\mu\mathbf{u} + \mathcal{A}\mathbf{u} = 0,$$

with \mathcal{A}^μ , \mathcal{A} , \mathbf{u} complex valued, $\mathcal{A}^\mu\xi_\mu = (\mathcal{A}^\mu\xi_\mu)^\dagger$ for all spacetime vectors ξ^μ and the hypersurface of constant time being an outgoing null hypersurface. Furthermore, there exists

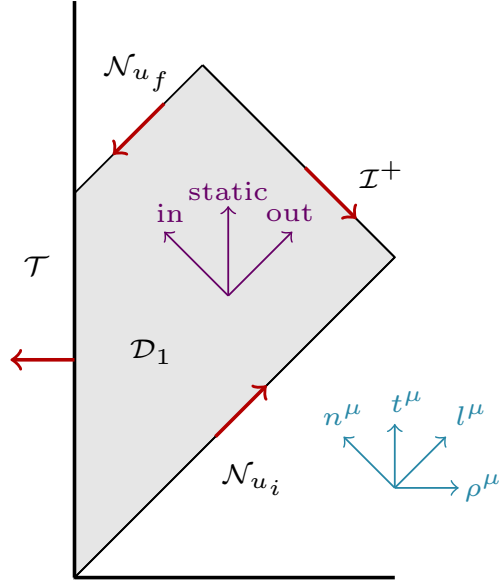


Figure 6.2: The geometry of the domain \mathcal{D}_1 of the CIBVP is illustrated, as well as its boundaries \mathcal{T} , \mathcal{N}_{u_i} , \mathcal{N}_{u_f} and \mathcal{I}^+ . The following vectors are shown: outgoing null l^μ , ingoing null n^μ , future pointing timelike t^μ , spacelike ρ^μ pointing towards increasing radius. The vectors normal to the boundary segments of \mathcal{D}_1 are also shown, see App. A.1 for details.

a timelike vector t^μ such that $\mathcal{A}^t \equiv \mathcal{A}^\mu t_\mu$ is positive definite. The system of [132] after linearization is such an example, which is based on the Newman-Penrose formalism and uses the affine-null gauge. In App. A.3 we review its basic features. This system avoids the pure gauge structure we identified earlier due to the promotion of the curvature into an independent variable. This system effectively includes third order metric derivatives and does not fall into the class of systems investigated earlier. The following analysis is quite generic and the specific system is used mainly as a motivation. We highlight the difference between the homogeneous and inhomogeneous setup.

6.5.1 Domain \mathcal{D}_1

Our main goal is to provide an energy estimate for a geometric setup related to Cauchy-Characteristic extraction. The domain \mathcal{D}_1 for which the CIBVP typically provides a solution is shown in Fig. 6.2. We assume that the PDE system has variables that are ingoing, outgoing and static (with zero speed) as illustrated in Fig. 6.2. The boundary $\partial\mathcal{D}_1$ of this domain can be split into the following segments:

Lower boundary \mathcal{N}_{u_i} is the outgoing null hypersurface of initial time u_i , with l^μ its normal vector. The ingoing and static variables are provided here as initial data.

Inner boundary \mathcal{T} is a worldtube of constant affine parameter. The vector normal to \mathcal{T} is ρ^μ . The outgoing variables are given here as boundary data, whereas the ingoing ones are

obtained as part of the solution. The static variables are known on \mathcal{T} provided that they are given on $\mathcal{N}_{u_i} \cap \mathcal{T}$ i.e. are provided by the initial data.

Outer boundary \mathcal{I}^+ is a part of future null infinity and is an ingoing null hypersurface with n^μ its normal vector. The outgoing and static variables are obtained as part of the solution on \mathcal{I}^+ , whereas the ingoing are known on \mathcal{I}^+ provided that they are given on $\mathcal{N}_{u_i} \cap \mathcal{I}^+$ i.e. are provided by the initial data.

Upper boundary \mathcal{N}_{u_f} is the outgoing null hypersurface at final time u_f , with normal vector l^μ . The ingoing and static variables are provided here as part of the solution.

Since the system under consideration is symmetric hyperbolic, it is convenient to define the flux ²

$$f \equiv \mathbf{u}^\dagger \mathcal{A}^\mu \partial_\mu \mathbf{u}. \quad (6.26)$$

Considering the integral of f in \mathcal{D}_1 and applying the divergence theorem yields

$$\begin{aligned} \int_{\mathcal{D}_1} f &= \int_{\partial \mathcal{D}_1} (\mathbf{u}^\dagger \mathcal{A}^\mu \mathbf{u})(g_{\mu\nu} \mathbf{N}^\nu) \\ &= \int_{\mathcal{N}_{u_i}} \mathbf{u}^\dagger \mathcal{A}^l \mathbf{u} - \int_{\mathcal{T}} \mathbf{u}^\dagger \mathcal{A}^\rho \mathbf{u} - \int_{\mathcal{N}_{u_f}} \mathbf{u}^\dagger \mathcal{A}^l \mathbf{u} - \int_{\mathcal{I}^+} \mathbf{u}^\dagger \mathcal{A}^n \mathbf{u}, \end{aligned} \quad (6.27)$$

where \mathbf{N}^μ is the vector normal to $\partial \mathcal{D}_1$ shown for the different segments in Fig. 6.2 and

$$\mathcal{A}^l \equiv \mathcal{A}^\mu l_\mu, \quad \mathcal{A}^\rho \equiv \mathcal{A}^\mu \rho_\mu, \quad \mathcal{A}^n \equiv \mathcal{A}^\mu n_\mu.$$

The homogeneous setup

We first consider the homogeneous setup

$$\mathcal{A}^\mu \partial_\mu \mathbf{u} = 0,$$

to obtain some insight of the problem. In this case the relation (6.27) yields

$$\int_{\mathcal{N}_{u_i}} \mathbf{u}^\dagger \mathcal{A}^l \mathbf{u} - \int_{\mathcal{T}} \mathbf{u}^\dagger \mathcal{A}^\rho \mathbf{u} = \int_{\mathcal{N}_{u_f}} \mathbf{u}^\dagger \mathcal{A}^l \mathbf{u} + \int_{\mathcal{I}^+} \mathbf{u}^\dagger \mathcal{A}^n \mathbf{u}, \quad (6.28)$$

which already provides the desired energy estimate. To make this more apparent, let us split $\mathbf{u}^\dagger \mathcal{A}^\rho \mathbf{u}$ into the ingoing and outgoing parts $\mathcal{A}^\rho = \mathcal{A}_{\text{in}}^\rho - \mathcal{A}_{\text{out}}^\rho$, which for the symmetric

²The flux defined in Eq. (6.26) trivially provides a total derivative for a symmetric hyperbolic system, so that we can conveniently apply the divergence theorem. For the SH and WH systems of Sec. 6.3, 6.4 additional care was needed to form total derivatives.

affine null system of [132] reads

$$d_n \equiv \mathbb{1}_{n \times n}, \quad \mathcal{A}_{\text{in}}^\rho \equiv \text{diag}(1, 0 \times d_{19}), \quad \mathcal{A}_{\text{out}}^\rho \equiv \text{diag}(0 \times d_4, d_{16}),$$

Considering this partition Eq. (6.28) reads

$$\int_{\mathcal{N}_{u_i}} \mathbf{u}^\dagger \mathcal{A}^l \mathbf{u} + \int_{\mathcal{T}} \mathbf{u}^\dagger \mathcal{A}_{\text{out}}^\rho \mathbf{u} = \int_{\mathcal{N}_{u_f}} \mathbf{u}^\dagger \mathcal{A}^l \mathbf{u} + \int_{\mathcal{T}} \mathbf{u}^\dagger \mathcal{A}_{\text{in}}^\rho \mathbf{u} + \int_{\mathcal{I}^+} \mathbf{u}^\dagger \mathcal{A}^n \mathbf{u}, \quad (6.29)$$

where the left-hand-side includes only given data and the right-hand-side only the solution. This manifests that the solution is completely controlled by the given data in this setup.

The inhomogeneous setup

For the inhomogenous case

$$\mathcal{A}^\mu \partial_\mu \mathbf{u} + \mathcal{A} \mathbf{u} = 0,$$

the relation (6.27) yields

$$\int_{\mathcal{N}_{u_i}} \mathbf{u}^\dagger \mathcal{A}^l \mathbf{u} + \int_{\mathcal{T}} \mathbf{u}^\dagger \mathcal{A}_{\text{out}}^\rho \mathbf{u} + \int_{\mathcal{D}_1} \mathbf{u}^\dagger \mathcal{A} \mathbf{u} = \int_{\mathcal{N}_{u_f}} \mathbf{u}^\dagger \mathcal{A}^l \mathbf{u} + \int_{\mathcal{T}} \mathbf{u}^\dagger \mathcal{A}_{\text{in}}^\rho \mathbf{u} + \int_{\mathcal{I}^+} \mathbf{u}^\dagger \mathcal{A}^n \mathbf{u}.$$

The difference in comparison to the homogenous case is the bulk term $\int_{\mathcal{D}_1} \mathbf{u}^\dagger \mathcal{A} \mathbf{u}$. The goal is to show that the solution on $\mathcal{N}_{u_f}, \mathcal{T}, \mathcal{I}^+$ is controlled by the given data on $\mathcal{N}_{u_i}, \mathcal{T}$. The idea is to use the Grönwall inequality. To make use of it we want to express the bulk term as a double integral over a hypersurface and an appropriate parameter such that the whole domain \mathcal{D}_1 is covered. The specific structure of the matrices $\mathcal{A}^l, \mathcal{A}^n, \mathcal{A}_{\text{in}}^\rho, \mathcal{A}_{\text{out}}^\rho$ and \mathcal{A} is crucial here. In characteristic setups it is common that the matrices $\mathcal{A}^l, \mathcal{A}^n, \mathcal{A}_{\text{in}}^\rho, \mathcal{A}_{\text{out}}^\rho$ are degenerate, meaning that some variables do not appear at all in the respective integrands. On the contrary, a generic assumption is that the integrand $\mathbf{u}^\dagger \mathcal{A} \mathbf{u}$ provides coupling between all of the variables, or at least it does not provide coupling solely between variables of one of the ingoing, outgoing and static classes. With this assumption, we can write

$$\begin{aligned} \int_{\mathcal{N}_{u_f}} \mathbf{u}^\dagger \mathcal{A}^l \mathbf{u} + \int_{\mathcal{T}} \mathbf{u}^\dagger \mathcal{A}_{\text{in}}^\rho \mathbf{u} + \int_{\mathcal{I}^+} \mathbf{u}^\dagger \mathcal{A}^n \mathbf{u} &\leq \\ \int_{\mathcal{N}_{u_i}} \mathbf{u}^\dagger \mathcal{A}^l \mathbf{u} + \int_{\mathcal{T}} \mathbf{u}^\dagger \mathcal{A}_{\text{out}}^\rho \mathbf{u} + C \int_{\mathcal{D}_1} \mathbf{u}^\dagger d_{\text{length}(\mathbf{u})} \mathbf{u}, &\end{aligned} \quad (6.30)$$

for some constant $C > 0$. To see this, let us focus on the bulk term. The integrand of the bulk term $\int_{\mathcal{D}_1} \mathbf{u}^\dagger \mathcal{A} \mathbf{u}$ is real valued and involves a sum of terms of the form

$$\pm(c_{ij} v_i \bar{v}_j + \bar{c}_{ij} \bar{v}_i v_j) = \pm \Re(c_{ij} v_i \bar{v}_j),$$

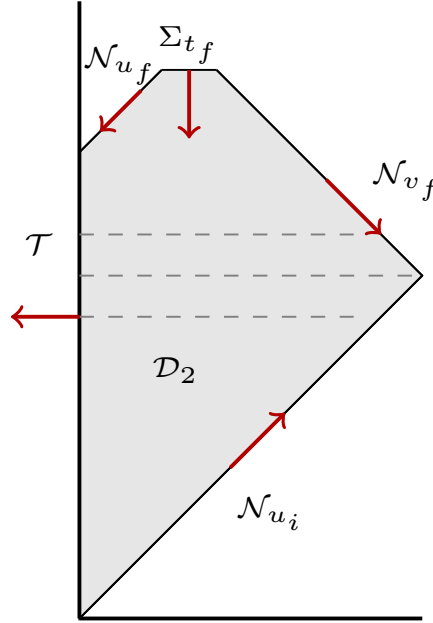


Figure 6.3: The geometry of the domain \mathcal{D}_2 . The upper boundary \mathcal{N}_{u_f} of domain \mathcal{D}_1 , which is an outgoing null hypersurface, is interrupted by the spacelike hypersurface Σ_{t_f} . Furthermore, for simplicity this domain does not extend all the way to infinity, but is truncated to some finite radius r_{out} .

where $v_i, \bar{v}_i \in \mathbf{u}$ and c_{ij} complex valued. For each such term the following holds:

$$|c_{ij}|^2 |v_i|^2 + |v_j|^2 \geq \mp \Re(c_{ij} v_i \bar{v}_j).$$

Choosing a big enough real constant $C \geq \max |c_{ij}|^2$ leads to (6.30).

In [132] the integrand $\mathbf{u}^\dagger \mathcal{A} \mathbf{u}$ provides coupling between ingoing and outgoing variables, which does not appear in any of the other integrands. This is why we cannot use the Grönwall inequality like we described earlier for this setup approach and we fail to obtain an energy estimate for the inhomogeneous case for the domain \mathcal{D}_1 . However, from the relation (6.30) we see that if there was a hypersurface integral with integrand of the form $\sim \mathbf{u}^\dagger d_{\text{length}(\mathbf{u})} \mathbf{u}$ i.e. without a degeneracy, then we could indeed apply the method previously explained.

6.5.2 Domain \mathcal{D}_2

We repeat the analysis for an inhomogeneous symmetric hyperbolic characteristic PDE system, but in a different domain, which we call \mathcal{D}_2 . The domain extends between the radii r_{in} and $r_{out} < r_\infty$. The upper boundary is the previous outgoing null hypersurface \mathcal{N}_{u_f} together with the spacelike hypersurface Σ_{t_f} . The outer boundary is a null hypersurface of constant retarded time \mathcal{N}_{v_f} . If we wish to extend the domain to infinity, then \mathcal{N}_{v_f} becomes \mathcal{I}^+ and Σ_{t_f} a hyperboloid i.e. a hypersurface that is everywhere spacelike but becomes null at

infinity.

The divergence theorem in \mathcal{D}_2 returns

$$\begin{aligned} & \int_{\mathcal{N}_{u_i}} \mathbf{u}^\dagger \mathcal{A}^l \mathbf{u} + \int_{\mathcal{T}} \mathbf{u}^\dagger \mathcal{A}_{\text{out}}^\rho \mathbf{u} + \int_{\mathcal{D}_2} \mathbf{u}^\dagger \mathcal{A} \mathbf{u} = \\ & \int_{\Sigma_{t_f}} \mathbf{u}^\dagger \mathcal{A}^t \mathbf{u} + \int_{\mathcal{N}_{u_f}} \mathbf{u}^\dagger \mathcal{A}^l \mathbf{u} + \int_{\mathcal{T}} \mathbf{u}^\dagger \mathcal{A}_{\text{in}}^\rho \mathbf{u} + \int_{\mathcal{N}_{v_f}} \mathbf{u}^\dagger \mathcal{A}^n \mathbf{u}, \end{aligned} \quad (6.31)$$

where $\mathcal{A}^t = d_{20} + \text{diag}(0, 1, 1, 1, 0 \times d_{16})$ in [132]. Like earlier the above yields

$$\begin{aligned} & \int_{\Sigma_{t_f}} \mathbf{u}^\dagger \mathcal{A}^t \mathbf{u} + \int_{\mathcal{N}_{u_f}} \mathbf{u}^\dagger \mathcal{A}^l \mathbf{u} + \int_{\mathcal{T}} \mathbf{u}^\dagger \mathcal{A}_{\text{in}}^\rho \mathbf{u} + \int_{\mathcal{N}_{v_f}} \mathbf{u}^\dagger \mathcal{A}^n \mathbf{u} \leq \\ & \int_{\mathcal{N}_{u_i}} \mathbf{u}^\dagger \mathcal{A}^l \mathbf{u} + \int_{\mathcal{T}} \mathbf{u}^\dagger \mathcal{A}_{\text{out}}^\rho \mathbf{u} + C \int_{\mathcal{D}_2} \mathbf{u}^\dagger d_{20} \mathbf{u} \leq \\ & \int_{\mathcal{N}_{u_i}} \mathbf{u}^\dagger \mathcal{A}^l \mathbf{u} + \int_{\mathcal{T}} \mathbf{u}^\dagger \mathcal{A}_{\text{out}}^\rho \mathbf{u} + C \int_{\mathcal{D}_2} \mathbf{u}^\dagger \mathcal{A}^t \mathbf{u}, \end{aligned} \quad (6.32)$$

Next, consider foliating \mathcal{D}_2 with spacelike hypersurfaces Σ_t (gray dashed lines in Fig. 6.3) i.e.

$$\int_{\mathcal{D}_2} \mathbf{u}^\dagger \mathcal{A}^t \mathbf{u} = \int_{t_i}^{t_f} \left(\int_{\Sigma_t} \mathbf{u}^\dagger \mathcal{A}^t \mathbf{u} \right) dt.$$

Then, (6.32) can be rearranged into

$$\int_{\Sigma_{t_f}} \mathbf{u}^\dagger \mathcal{A}^t \mathbf{u} \leq F + C \int_{t_i}^{t_f} \left(\int_{\Sigma_t} \mathbf{u}^\dagger \mathcal{A}^t \mathbf{u} \right) dt, \quad (6.33)$$

with

$$F \equiv \int_{\mathcal{N}_{u_i}} \mathbf{u}^\dagger \mathcal{A}^l \mathbf{u} - \int_{\mathcal{N}_{u_f}} \mathbf{u}^\dagger \mathcal{A}^l \mathbf{u} + \int_{\mathcal{T}} \mathbf{u}^\dagger (\mathcal{A}_{\text{out}}^\rho - \mathcal{A}_{\text{in}}^\rho) \mathbf{u} - \int_{\mathcal{N}_{v_f}} \mathbf{u}^\dagger \mathcal{A}^n \mathbf{u}.$$

Without any assumption on the monotonicity of $F = F(t)$, we can apply the first version of the Grönwall inequality as given in App. A.2 on (6.33) to obtain

$$\int_{\Sigma_{t_f}} \mathbf{u}^\dagger \mathcal{A}^t \mathbf{u} \leq F + \int_{t_i}^{t_f} F(t) C \exp \left(\int_t^{t_f} C ds \right) dt = F + C \int_{t_i}^{t_f} F(t) e^{C(t_f-t)} dt,$$

which after expanding out F yields

$$\begin{aligned}
& \int_{\Sigma_{t_f}} \mathbf{u}^\dagger \mathcal{A}^t \mathbf{u} + \\
& \int_{\mathcal{N}_{u_f}} \mathbf{u}^\dagger \mathcal{A}^l \mathbf{u} + C \int_{t_i}^{t_f} e^{C(t_f-t)} \left(\int_{\mathcal{N}_{u_f}} \mathbf{u}^\dagger \mathcal{A}^l \mathbf{u} \right) dt + \\
& \int_{\mathcal{T}} \mathbf{u}^\dagger \mathcal{A}_{\text{in}}^\rho \mathbf{u} + C \int_{t_i}^{t_f} e^{C(t_f-t)} \left(\int_{\mathcal{T}} \mathbf{u}^\dagger \mathcal{A}_{\text{in}}^\rho \mathbf{u} \right) dt + \\
& \int_{\mathcal{N}_{v_f}} \mathbf{u}^\dagger \mathcal{A}^n \mathbf{u} + C \int_{t_i}^{t_f} e^{C(t_f-t)} \left(\int_{\mathcal{N}_{v_f}} \mathbf{u}^\dagger \mathcal{A}^n \mathbf{u} \right) dt \leq \\
& \int_{\mathcal{N}_{u_i}} \mathbf{u}^\dagger \mathcal{A}^l \mathbf{u} + C \int_{t_i}^{t_f} e^{C(t_f-t)} \left(\int_{\mathcal{N}_{u_i}} \mathbf{u}^\dagger \mathcal{A}^l \mathbf{u} \right) dt + \\
& \int_{\mathcal{T}} \mathbf{u}^\dagger \mathcal{A}_{\text{out}}^\rho \mathbf{u} + C \int_{t_i}^{t_f} e^{C(t_f-t)} \left(\int_{\mathcal{T}} \mathbf{u}^\dagger \mathcal{A}_{\text{out}}^\rho \mathbf{u} \right) dt, \tag{6.34}
\end{aligned}$$

where terms have been rearranged such that all the solution parts appear on the left-hand-side of the inequality. Since $C > 0$ and $t_f \geq t$ the following holds for the terms of the left-hand-side of (6.34)

$$\begin{aligned}
& \int_{\Sigma_{t_f}} \mathbf{u}^\dagger \mathcal{A}^t \mathbf{u} + \int_{\mathcal{N}_{u_f}} \mathbf{u}^\dagger \mathcal{A}^l \mathbf{u} + \int_{\mathcal{T}} \mathbf{u}^\dagger \mathcal{A}_{\text{in}}^\rho \mathbf{u} + \int_{\mathcal{N}_{v_f}} \mathbf{u}^\dagger \mathcal{A}^n \mathbf{u} \leq \\
& \int_{\Sigma_{t_f}} \mathbf{u}^\dagger \mathcal{A}^t \mathbf{u} + \\
& \int_{\mathcal{N}_{u_f}} \mathbf{u}^\dagger \mathcal{A}^l \mathbf{u} + C \int_{t_i}^{t_f} e^{C(t_f-t)} \left(\int_{\mathcal{N}_{u_f}} \mathbf{u}^\dagger \mathcal{A}^l \mathbf{u} \right) dt + \\
& \int_{\mathcal{T}} \mathbf{u}^\dagger \mathcal{A}_{\text{in}}^\rho \mathbf{u} + C \int_{t_i}^{t_f} e^{C(t_f-t)} \left(\int_{\mathcal{T}} \mathbf{u}^\dagger \mathcal{A}_{\text{in}}^\rho \mathbf{u} \right) dt + \\
& \int_{\mathcal{N}_{v_f}} \mathbf{u}^\dagger \mathcal{A}^n \mathbf{u} + C \int_{t_i}^{t_f} e^{C(t_f-t)} \left(\int_{\mathcal{N}_{v_f}} \mathbf{u}^\dagger \mathcal{A}^n \mathbf{u} \right) dt,
\end{aligned}$$

which when combined with (6.34) yields

$$\begin{aligned}
& \int_{\Sigma_{t_f}} \mathbf{u}^\dagger \mathcal{A}^t \mathbf{u} + \int_{\mathcal{N}_{u_f}} \mathbf{u}^\dagger \mathcal{A}^l \mathbf{u} + \int_{\mathcal{T}} \mathbf{u}^\dagger \mathcal{A}_{\text{in}}^\rho \mathbf{u} + \int_{\mathcal{N}_{v_f}} \mathbf{u}^\dagger \mathcal{A}^n \mathbf{u} \leq \\
& \int_{\mathcal{N}_{u_i}} \mathbf{u}^\dagger \mathcal{A}^l \mathbf{u} + C \int_{t_i}^{t_f} e^{C(t_f-t)} \left(\int_{\mathcal{N}_{u_i}} \mathbf{u}^\dagger \mathcal{A}^l \mathbf{u} \right) dt + \\
& \int_{\mathcal{T}} \mathbf{u}^\dagger \mathcal{A}_{\text{out}}^\rho \mathbf{u} + C \int_{t_i}^{t_f} e^{C(t_f-t)} \left(\int_{\mathcal{T}} \mathbf{u}^\dagger \mathcal{A}_{\text{out}}^\rho \mathbf{u} \right) dt. \tag{6.35}
\end{aligned}$$

Hence, the solution to the CIBVP (the left-hand-side of (6.35)) is controlled by the given data (the right-hand-side of (6.35)).

6.6 Conclusions

Popular Bondi-like systems are weakly hyperbolic and textbook results on these systems then show that they are ill-posed in the L^2 -norm or its obvious derivatives. Considering model problems of a similar structure we saw that the same result naturally carries over to the CIBVP. In the latter case care is needed not to confuse the usual degeneracy of the norms that appear naturally in characteristic problems with high-frequency blow-up of solutions. This degeneracy is apparent in the calculations of Sec. 6.5 and leads to the change of domain for the energy estimate as shown in Figs. 6.2 and 6.3.

Although our weakly hyperbolic toy model is ill-posed in L^2 , it may be well-posed in a lopsided norm in which the angular derivative of some specific components of the state vector are included. Thus in such a case one must be able to control the size of not only the elements of the state vector in the given data, but also some of their derivatives. This weaker notion of well-posedness is sensitive to the presence of lower order source terms. For example, our weakly hyperbolic model is well-posed in a (specific) lopsided norm if it is homogeneous, or inhomogeneous with sources that respect the nested structure of the equations intrinsic to the characteristic hypersurfaces. If this nested structure is broken by the source terms, it becomes ill-posed in any sense.

Bringing our attention back to the characteristic initial boundary value problem for GR, which covers both CCE and applications in numerical holography, it is clear that the Bondi-like formulations we considered are ill-posed in L^2 -norm. It is not clear however, in general, if they will admit estimates in suitable lopsided norms. But since the field equations *do* have a nested structure, and our weakly hyperbolic model problem turned out to admit estimates in lopsided norms whenever this structure was present, there is reason to be hopeful. More importantly, Bondi-like formulations where the curvature is an evolved variable provide symmetric hyperbolic setups [131, 132, 136, 142]. Promoting the curvature to an evolved variable effectively translates into including specific combinations of second order metric derivatives as independent variables. In addition, in these setups, the Bianchi identities provide equations of motion for some variables. In Sec. 6.5 we present work towards obtaining energy estimates with model symmetric hyperbolic systems for the CIBVP. If this system is one of the latter, then it could assist us in finding a lopsided norm for the weakly hyperbolic Bondi-like systems analyzed earlier. Comparing with the results of Sec. 6.4 it seems that constructing an appropriate lopsided norm directly within the weakly hyperbolic formulations could be cumbersome. The hope is that by performing an explicit mapping between the variables of the different formalisms, we can construct an appropriate lopsided norm for the weakly hyperbolic one guided by the L^2 -norm of the symmetric hyperbolic system. Work in this direction is undergoing.

A true *principle* solution to wave-extraction would be one where the PDE problem solved is manifestly well-posed and the GW signal is computed at null infinity. A robust scheme for

CCM could be such a solution, meaning a CCM setup where the composite PDE problem is well-posed. An alternative to CCM is the use of compactified hyperboloidal slices, which is also an active research topic for full GR [58–61, 63, 66, 143–146]. Clearly, a well-posed PDE problem is essential for the hyperboloidal approach as well. To understand the consequences of our findings for CCM, in Sec. 6.3 we considered a model in which the IBVP is solved for a symmetric hyperbolic system, and the solutions are then glued through boundary conditions to those of a weakly hyperbolic system accepting estimates in lopsided norms. The former of these two sets of equations is viewed as a model for the formulation used in the strong-field region, the latter for a WH Bondi-like formulation used on the outer characteristic domain. With this setup, we found that the fundamental incompatibility of the norms naturally associated with the two domains prohibits their combined use in building estimates. But if the weakly hyperbolic system were made symmetric hyperbolic progress could be made. A less appealing possibility would be to demonstrate that the formulation in the Cauchy domain, or some suitable replacement, admits estimates in a lopsided norm compatible with that of the characteristic region. Since this relies on very special structure in the field equations, the outlook for a complete proof of well-posedness of CCM using existing Bondi-like gauges is, unfortunately, not rosy. Furthermore, the fact that numerical approximation to weakly hyperbolic systems (using lopsided norms) is poorly understood, it is desirable to obtain and adopt strongly or ideally symmetric hyperbolic alternatives.

CHAPTER 7

Numerical Experiments

Contents

7.1	Toy models	95
7.1.1	Implementation	95
7.1.2	Convergence tests	96
7.2	GR in the Bondi-Sachs proper gauge	104
7.2.1	The setup	104
7.2.2	Convergence tests	108
7.3	Conclusions	111

When a PDE problem is well-posed, then its numerical approximation converges to the true solution of the problem with increasing resolution. In this convergence process, it is necessary to specify the norm in which the problem is well-posed. Following the analysis of the previous chapter, we put to the test some of the norms presented there. The tests are performed both for the toy models, and in full GR.

7.1 Toy models

First, we use the toy models introduced in Sec. 6.1 to diagnose the effects of weak hyperbolicity at the numerical level. We perform convergence tests in the single-null setup for both the WH and SH models in a discrete approximation to the L^2 -norm, for smooth and noisy given data. We also perform convergence tests with noisy given data in the lopsided norm, for the different versions of the WH model analyzed in the previous section.

7.1.1 Implementation

As in other schemes to solve the CIBVP, several different ingredients are needed in the algorithm. These can be summarized for our models (6.1) and (6.3) as follows:

1. The domain of the PDE problem is $x \in [0, 1]$, $z \in [0, 2\pi)$ with periodic boundary conditions and $u \in [u_0, u_f]$, with u_0 and u_f the initial and final times respectively. We always include the point $x = 1$ in the computational domain so that we do not need

to impose boundary conditions at the outer boundary, since there are no incoming characteristic variables there.

2. For the initial time u_0 provide initial data $\psi(u_0, x, z)$ on the surface $u = u_0$ and boundary data $\phi(u_0, 0, z)$ and $\psi_v(u_0, 0, z)$.
3. Integrate the intrinsic equations of each model to obtain $\phi(u_0, x, z)$ and $\psi_v(u_0, x, z)$. We perform this integration using the two-stage, second order strong stability preserving method of Shu and Osher (SSPRK22) [147].
4. Integrate the evolution equation of each model to obtain $\psi(u_1, x, z)$ at the surface $u = u_1 = u_0 + \Delta u$. We choose $\Delta u = 0.25\Delta x$ to satisfy the Courant-Friedrichs-Lewy (CFL) condition and the numerical integration is performed using the fourth order Runge-Kutta (RK4) method.
5. Any derivative appearing in the right-hand-sides of these integrations is approximated using second order accurate centered finite difference operators, except at the boundaries, where second order accurate forward and backward difference operators are used respectively.
6. Providing boundary data $\phi(u, 0, z)$ and $\psi_v(u, 0, z)$ as in the PDE specification (6.5), we repeat steps 2 and 3 to obtain $\phi(u, x, z)$, $\psi_v(u, x, z)$ and $\psi(u, x, z)$ until the final time u_f . This is the solution of the PDE.

No artificial dissipation is introduced. The implementation was made using the Julia language [148] with the DifferentialEquations.jl package [149] to integrate the equations. Our code is freely available [121]. We apply convergence tests to our numerical scheme for both toy models. The tests are performed for smooth, as well as for noisy given data. The latter are often called robust stability tests. They form part of the Mexico-city testbed for numerical relativity [150]. These tests have been performed widely in the literature [151–156], often, as in our case, with adaptations for the setup under consideration.

7.1.2 Convergence tests

By *convergence* we mean the requirement that the difference between the numerical approximation provided by a finite difference scheme and the exact solution of the continuum PDE system tends to zero as the grid spacing is increased. The finite difference scheme is called *consistent* when it approximates the correct PDE system and the degree to which this is achieved is its *accuracy*. The scheme is called *stable* if it satisfies a discretized version of (2.12) or (2.14). In this context versions of each continuum norm are replaced by a suitable discrete analog. Here we replace the L^2 -norm for the characteristic setup with

$$\|\mathbf{u}\|_{h_u, h_x, h_z}^2 = \sum_{x,z} \psi^2 h_x h_z + \max_x \sum_{u,z} (\phi^2 + \psi_v^2) h_u h_z, \quad (7.1)$$

with the first sum taken over all points on the grid, with h_x and h_z the grid-spacing in the x and z directions respectively, and the second sum over all points in the z and u directions ($h_u = 0.25h_x$ for our setup), for all x grid points and keeping the maximum in the x direction. The first sum involves only ingoing and the second only outgoing variables. When, as will be the case in what follows, we have $h_x = h_z = h$ we label the norm simply with h . Our discrete approximation to the lopsided norm is,

$$\|\mathbf{u}\|_{\mathbf{q}(h_u, h_x, h_z)}^2 = \sum_{x,z} \psi^2 h_x h_z + \max_x \sum_{u,z} \left(\phi^2 + \psi_v^2 + (D_z \phi)^2 \right) h_u h_z, \quad (7.2)$$

where D_z is the second order accurate, centered, finite difference operator that replaces the continuum operator ∂_z , by

$$D_z f_h(x_i) = \frac{f_h(x_{i+1}) - f_h(x_{i-1}))}{2h_z}, \quad (7.3)$$

for a grid function f_h on a grid with spacing h_z . When the two grid spacings are equal we again label the norm simply with h . This approximation to the continuum lopsided norm is not unique. If we were attempting to prove that a particular discretization converged, it might be necessary to take another. Denoting by f the solution to the continuum system and as f_h the numerical approximation at resolution h provided by a convergent finite difference scheme of accuracy n , then

$$f = f_h + O(h^n), \quad (7.4)$$

and hence

$$\|f - f_h\| = O(h^n), \quad (7.5)$$

in some appropriate norm $\|\cdot\|$ on the grid, with the understanding that the exact solution should be evaluated on said grid. Full definitions of the notions of consistency, stability and convergence for the IVP can be found, for example, in [103, 152, 157].

We use a second order accurate numerical approximation, so that $n = 2$. Considering numerical evolutions with coarse, medium and fine grid spacings h_c , h_m and h_f respectively, we can construct a useful quantity for these tests

$$Q \equiv \frac{h_c^n - h_m^n}{h_m^n - h_f^n}, \quad (7.6)$$

which we call *convergence factor*. In our convergence tests we solve the same discretized PDE problem for different resolutions and every time we want to increase resolution we halve the grid-spacing in all directions i.e.

$$h_m = h_c/2, \quad h_f = h_c/4.$$

Following this approach the convergence factor is $Q = 4$. Combining (7.4) and (7.6) one can obtain the relation

$$f_{h_c} - f_{h_c/2} = Q \left(f_{h_c/2} - f_{h_c/4} \right), \quad (7.7)$$

understood on shared grid-points in the obvious way, which is used to investigate pointwise convergence. In what follows the different resolutions are denoted as

$$h_q = h_0/2^q.$$

The lowest resolution h_0 has $N_x = 17$ points in the x -grid and $N_z = 16$ in the z -grid. We work in units of the code in the entire section.

Smooth data

For the simulations with smooth given data the initial and final times are $u_0 = 0$ and $u_f = 1$ respectively. For both toy models we provide as initial data

$$\psi(0, x, z) = e^{-100(x-1/2)^2} \sin(z),$$

and as boundary data

$$\phi(u, 0, z) = 3 e^{-100(u-1/2)^2} \sin(z),$$

and

$$\psi_v(u, 0, z) = e^{-100(u-1/2)^2} \sin(z).$$

For the SH model we choose the following source terms

$$-S_\phi = \psi, \quad -S_{\psi_v} = \phi + \psi, \quad -S_\psi = \phi, \quad (7.8)$$

and for the WH model we choose the homogeneous case. As discussed in Sec. 2.3, well-posedness of the SH model is unaffected by lower order source terms, so the specific choice of source terms here is not vital. However, we choose to work with the homogeneous WH model, because weakly well-posed problems are sensitive to lower order perturbations.

Runs with resolutions h_0, h_1, h_2, h_3, h_4 and h_5 were performed. In Fig. 7.1 the basic dynamics are plotted with each model. To first verify that the numerical scheme is implemented successfully we performed pointwise convergence tests for both models. We focus specifically here on the highest three resolutions. The algorithm is the following:

1. Consider h_3, h_4 and h_5 as coarse, medium and fine resolutions, respectively.
2. Calculate $\psi_{h_3} - \psi_{h_4}$ and $\psi_{h_4} - \psi_{h_5}$ for the gridpoints of h_3 , for the final timestep of

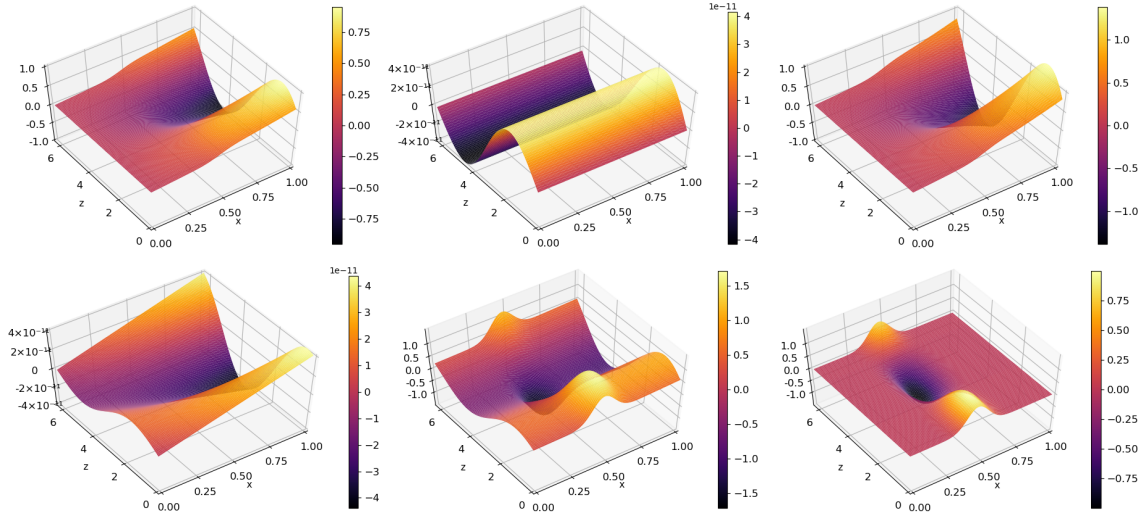


Figure 7.1: The fields ϕ , ψ_v and ψ at final evolution time $u = 1$, for the SH model (top) and the homogeneous WH model (bottom), with the same smooth given data. Observe that the fields ϕ and ψ_v in the WH case are still of the same magnitude $\sim 10^{-11}$ as the boundary data at the retarded time $u = 1$. This is not true once generic source terms are taken.

the evolution.

3. Plot simultaneously $\psi_{h_3} - \psi_{h_4}$ and $Q(\psi_{h_4} - \psi_{h_5})$. As indicated from (7.7), for a convergent numerical scheme the two quantities should overlap, when multiplying the latter with the appropriate convergence factor.

In Fig. 7.2 we illustrate the results of this test for the aforementioned smooth given data for both models. At this resolution one clearly observes perfect pointwise convergence in both cases.

We also wish to examine convergence of our numerical solutions in discrete approximations of the aforementioned norms. Given that the exact solution to the PDE problem is unknown and that each time we increase resolution we decrease the grid spacing in all directions by a factor of d , we can build the following useful quantity

$$\mathcal{C}_{\text{self}} = \log_d \frac{\|\mathbf{u}_{h_c} - \perp_{h_c}^{h_c/d} \mathbf{u}_{h_c/d}\|_{h_c}}{\|\perp_{h_c}^{h_c/d} \mathbf{u}_{h_c/d} - \perp_{h_c}^{h_c/d^2} \mathbf{u}_{h_c/d^2}\|_{h_c}}, \quad (7.9)$$

which we call *self-convergence ratio*, with $\mathbf{u} = (\phi, \psi_v, \psi)^T$ the state vector of the PDE system and ϕ , ψ_v , ψ grid functions. Here $\perp_{h_c}^{h_c/d}$ denotes the projection (in our setup injection) operator from the h_c/d grid onto the h_c grid. We calculate $\mathcal{C}_{\text{self}}$ for a discrete analog of the L^2 -norm. However, if one wishes to examine convergence in a different norm, L^2 can be replaced with that. The theoretical value of $\mathcal{C}_{\text{self}}$ equals the accuracy n of the numerical

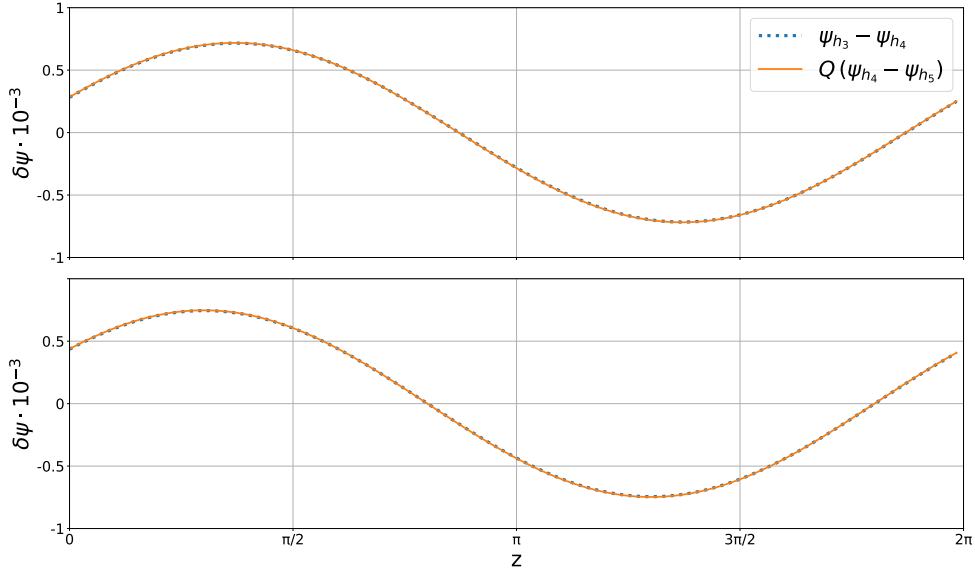


Figure 7.2: Here we plot simultaneously $\psi_{h_3} - \psi_{h_4}$ and $Q(\psi_{h_4} - \psi_{h_5})$, for the SH (top) and the WH (bottom) toy models. We fix $x = 0.5$. Since our scheme is second order and we are doubling resolution we effectively fix $Q = 4$. The results for fixed z are similar. The plot is compatible with perfect second order pointwise convergence.

scheme, and in our specific setup

$$\mathcal{C}_{\text{self}} = \log_2 \frac{\|\mathbf{u}_{h_c} - \perp_{h_c}^{h_c/2} \mathbf{u}_{h_c/2}\|_{h_c}}{\|\perp_{h_c}^{h_c/2} \mathbf{u}_{h_c/2} - \perp_{h_c}^{h_c/4} \mathbf{u}_{h_c/4}\|_{h_c}} = 2. \quad (7.10)$$

We obtain numerical solutions for the same smooth given data for both models at the various resolutions mentioned before. For triple resolution, double resolution and quadruple resolution, we project all gridfunctions onto the coarse grid, and compute $\mathcal{C}_{\text{self}}$ at its timesteps. In the left panel of Fig. 7.3 we collect the results of these norm convergence tests. Both models show similar behavior. At low resolutions curve drifts from the desired rate at early times, but the situation improves as we increase resolution, with $\mathcal{C}_{\text{self}}$ approaching the expected value. The trend with increasing resolution is the essential behavior we are looking at in these tests. By limiting ourselves to convergence tests with smooth given data we could be misled that the WH toy model provides a well-posed CIBVP in the L^2 -norm, since the numerical solutions appear to converge in this norm during our simulations. In other words, were we ignorant of the hyperbolicity of the system, it would be impossible to distinguish strongly and weakly hyperbolic PDEs with this test.

Noisy data

One can also perform norm convergence tests with random noise as given data, which is a strategy to simulate numerical error in an exaggerated form. Since it is expected that

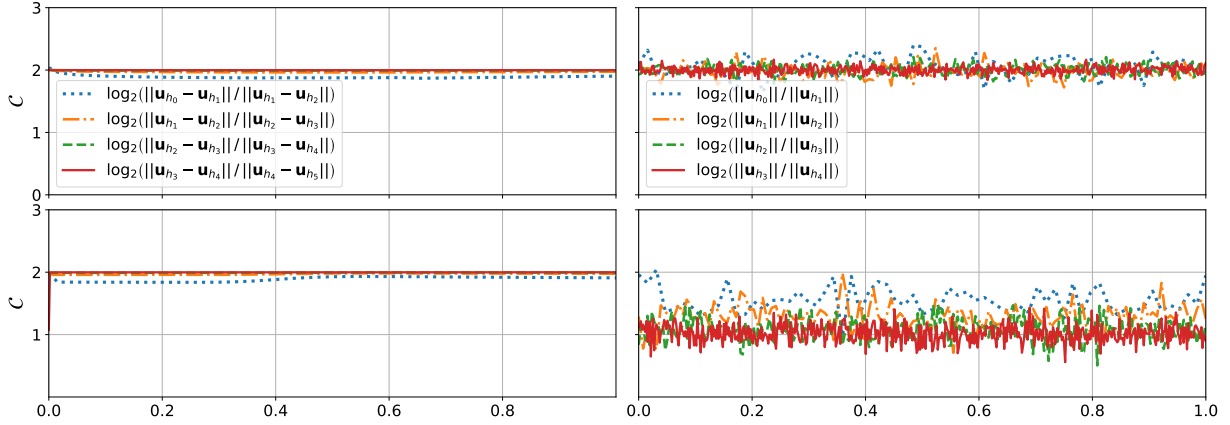


Figure 7.3: The convergence ratio in the L^2 -norm, for the strongly (above) and the weakly (below) toy models, for smooth (left) and noisy (right) given data, as a function of the simulation time. All plots have the same scale on the y -axis. For smooth given data we consider the self convergence ratio (7.10) while for noisy given data the exact convergence ratio (7.11). If we consider the self convergence ratio also for the noisy case the results are qualitatively the same.

numerical error decreases as resolution increases, when performing simulations for these tests one must scale appropriately the amplitude of the noise as resolution improves. This scaling is important to construct a sequence of initial data that converges in a suitable norm to initial data appropriate for the continuum system. The choice of norm here is essential, and should be one which, if possible, provides a bound for the solution of a (weakly) well-posed PDE problem, in the sense of (2.12) and (2.14).

For these tests we perform simulations where the smooth part of the given data is trivial (zero), and hence the exact solution for every PDE problem based on our models vanishes identically. Knowing the exact solution, in addition to the self convergence rate (7.9), we can also construct the exact convergence ratio

$$\mathcal{C}_{\text{exact}} = \log_d \frac{\|\mathbf{u}_{h_c} - \mathbf{u}_{\text{exact}}\|_{h_c}}{\|\perp_{h_c}^{h_c/d} \mathbf{u}_{h_c/d} - \mathbf{u}_{\text{exact}}\|_{h_c}}, \quad (7.11)$$

where we decrease grid spacing by a factor of d when increasing resolution. $\mathcal{C}_{\text{exact}}$ is cheaper numerically than $\mathcal{C}_{\text{self}}$ since only two different resolutions are required to build it, and again the exact solution is understood to be evaluated on the grid itself. It is possible for a scheme to be self-convergent but fail to be convergent, for example if one were to implement the wrong field equations. Therefore one would like to compare the numerical solution to an exact solution wherever (rarely) possible. To calculate $\mathcal{C}_{\text{exact}}$ we compute the discretized approximation to a suitable continuum norm at two resolutions, one twice the other. Each are computed on the naturally associated grid. We then take the ratio of the two at shared timesteps, corresponding to those of the coarse grid h_c . In our setup $\mathbf{u}_{\text{exact}} = \mathbf{0}$ and $d = 2$,

hence

$$\mathcal{C}_{\text{exact}} = \log_2 \frac{\|\mathbf{u}_{h_c}\|_{h_c}}{\|\perp_{h_c}^{h_c/2} \mathbf{u}_{h_c/2}\|_{h_c}}, \quad (7.12)$$

which again equals two for perfect convergence. As previously mentioned appropriate scaling of the random noise amplitude is crucial and is determined by the norm in which we wish to test convergence. To realize the proper scaling in our setup, let us consider the exact convergence ratio (7.12) and denote as A_{h_c} and $A_{h_c/2}$ the amplitude of the random noise for simulations with resolution h_c and $h_c/2$ respectively

$$\mathcal{C}_{\text{exact}} = \log_2 \frac{\|\mathbf{u}_{h_c}\|_{h_c}}{\|\perp_{h_c}^{h_c/2} \mathbf{u}_{h_c/2}\|_{h_c}} \sim \log_2 \frac{O(A_{h_c})}{O(A_{h_c/2})}.$$

The above suggests that to construct noisy data that converge in the discretized version of the L^2 -norm (7.1) for our second order accurate numerical scheme, we need to drop the amplitude of the random noise by a quarter every time we double resolution. For convergence tests in the lopsided norm the scaling factor is different, due to the $D_z\phi$ term that appears in the discretized version of the lopsided norm (7.2). By replacing the L^2 with the lopsided norm in (7.12) we get

$$\mathcal{C}_{\text{exact}} = \log_2 \frac{\|\mathbf{u}_{h_c}\|_{q(h_c)}}{\|\perp_{h_c}^{h_c/2} \mathbf{u}_{h_c/2}\|_{q(h_c)}} \sim \log_2 \frac{O(A_{h_c})}{2O(A_{h_c/2})},$$

where now the norm estimate is dominated by the $D_z\phi$ term. Hence, to construct noisy data that converge in the lopsided norm for our second order accurate numerical scheme, we need to multiply the amplitude of the random noise with a factor of one eighth every time we double resolution. This discussion would be more complicated if we were using either pseudospectral approximation or some hybrid scheme, which is why we focus exclusively on a straightforward finite differencing setup.

The results for norm convergence tests with appropriately scaled noisy data for the L^2 -norm, for both SH and WH models, are collected in the right column of Fig. 7.3. As illustrated there, the inhomogeneous SH model still exhibits convergence since with increasing resolution the exact convergence ratio tends closer to the desired value of two at all times of the evolution. On the contrary, the homogeneous WH model does not converge, and it becomes clear that with increasing resolution the exact convergence ratio of this model moves further away from two at all times.

To appreciate *intuitively* why noisy data allow us to diagnose a lack of strong hyperbolicity, consider the systems in frequency space as in Sec. 2.3, which we may think of as momentum space. In practical terms, Eq. (6.7) states that the homogeneous WH model does not satisfy condition (2.12), and so high frequency modes can grow arbitrarily fast. Considering smooth data however, predominantly low frequency modes are excited, and so using our discretized

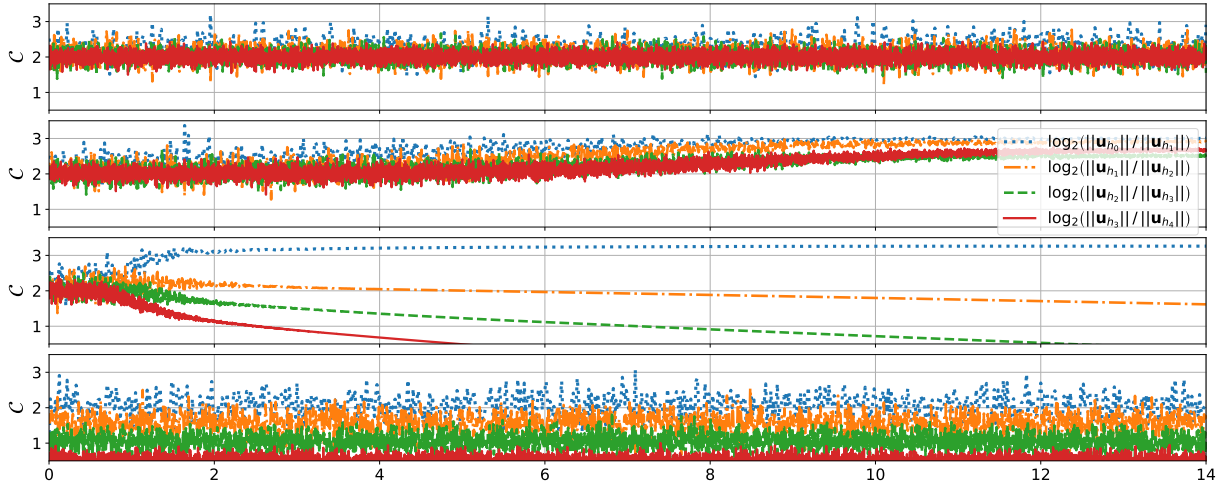


Figure 7.4: The exact convergence ratio in the lopsided norm (7.2) for the different WH models. From top to bottom we plot the homogeneous WH model, then the inhomogeneous adjustments, in order B_1, B_2 and B_3 . Overall we conclude that the homogeneous model and B_1 models are converging in the limit of infinite resolution, with the others failing to do so. Of these, all but the third panel, with source B_2 , agree with our expectation from continuum considerations. In this one case our method appears to have an honest numerical instability, which could be understood properly by careful consideration of the scheme.

approximation the violation of inequality (2.12) is not visible at the limited resolutions we employ. Noisy data on the contrary excite substantially both high and low frequency modes, with the former crucial to illustrate the violation.

We also perform convergence tests in the lopsided norm (7.2) to examine the behavior of the different WH models. As in the previous setup, in these tests we monitor the exact convergence ratio as a function of the simulation time. As illustrated in Fig. 7.4, our expectations from Sec. 2.3 for the homogeneous model are verified. The homogeneous WH model converges at all times in the lopsided norm, provided of course that the given data are restricted to converge at second order to the trivial solution in the same norm. As also expected, the inhomogeneous case with B_3 fails to converge whatsoever during the evolution, exhibiting behavior similar to the homogeneous WH model in the L^2 -norm tests. In fact, in this test the exact convergence ratio diverges further from two with increasing resolution and at earlier times. The discussion for the inhomogeneous WH models with sources B_1 and B_2 is more subtle. Both cases initially exhibit convergence, with the B_1 case maintaining this behavior for longer. The difference lies in their late time behavior and their trend with increasing resolution. In particular, the B_1 case converges for longer with increasing resolution whereas B_2 does the opposite. At late times in the B_1 case C_{exact} reaches a plateau that converges to two with increasing resolution, which is not true with sources B_2 . Thus our numerical evidence seems to indicate that the B_1 inhomogeneous WH

model converges in the lopsided norm, but to disagree with the theoretical expectation at the continuum that the B_2 case does so too. This is not in contradiction with our earlier calculations however, because, as a careful examination of the approximation could reveal, purely algorithmic shortcomings may render a scheme nonconvergent.

7.2 GR in the Bondi-Sachs proper gauge

Similarly to the previous section, here we present convergence tests of the publicly available characteristic code `PITNULL` [43] which employs the Bondi-Sachs formalism and is part of the `Einstein Toolkit` [158]. Although similar tests have been successfully performed in the past [39, 43, 159, 160], the novelty here is that we examine convergence of solutions to the full discretized PDE problem and not just the individual grid functions. The motivation for this comes from the fact that well-posedness is a property of the full PDE problem. We examine the practical consequence of the foregoing results by performing convergence tests in a discretized version of the L^2 -norm. The specific form of that norm plays a key role, depends on the geometric setup and is inspired by a hyperbolicity analysis of the PDE system solved. The details of this analysis can be found in the ancillary files of [2]. The data illustrated in Figs. 7.5 and 7.6 can be found in [161].

7.2.1 The setup

Here we collect the fundamental elements on which the `PITNULL` code is based. The interested reader can find more details e.g. in [38, 43]. The Bondi-Sachs metric ansatz [110, 128] used has the form

$$ds^2 = - \left(e^{2\beta} \frac{V}{r} - r^2 h_{AB} U^A U^B \right) du^2 - 2e^{2\beta} du dr - 2r^2 h_{AB} U^B du dx^A + r^2 h_{AB} dx^A dx^B, \quad (7.13)$$

where $h^{AB} h_{BC} = \delta_C^A$, $\det(h_{AB}) = \det(q_{AB}) = q$, with q_{AB} the metric on the unit sphere. The sphere is parameterized using the stereographic coordinates $x^A = (q, p)$ following [38], though see [52, 162] for a different but equivalent choice. The metric of the unit sphere reads

$$q_{AB} dx^A dx^B = \frac{4}{P^2} (dq^2 + dp^2),$$

where $P = 1 + q^2 + p^2$. One can introduce a complex basis vector q^A (dyad)

$$q^A = \frac{P}{2} (1, i),$$

and then the metric of the unit sphere can be written as

$$q_{AB} = \frac{1}{2} (q_A \bar{q}_B + \bar{q}_A q_B).$$

Using the complex dyad, a tensor field $F_{A_1 \dots A_n}$ on the sphere can be represented as

$$F = q^{A_1} \dots q^{A_p} \bar{q}^{A_{p+1}} \dots \bar{q}^{A_n} F_{A_1 \dots A_n},$$

which obeys the relation $F \rightarrow e^{is\psi} F$, with spin weight $s = 2p - n$. The eth operators for this quantity are defined as

$$\begin{aligned} \eth F &\equiv q^A \nabla_A F = q^A \partial_A F + \Gamma s F, \\ \bar{\eth} F &\equiv \bar{q}^A \nabla_A F = \bar{q}^A \partial_A F - \bar{\Gamma} s F, \end{aligned}$$

with spin $s \pm 1$ respectively and ∇_A the covariant derivative associated with q_{AB} i.e. $\Gamma = -\frac{1}{2} q^a \bar{q}^b \nabla_a q_b$. In the chosen stereographic coordinates the above reads

$$\begin{aligned} \eth F &= \frac{P}{2} \partial_q F + i \frac{P}{2} \partial_p F + (q + ip) s F, \\ \bar{\eth} F &= \frac{P}{2} \partial_q F - i \frac{P}{2} \partial_p F - (q - ip) s F. \end{aligned}$$

It is convenient to introduce the following complex spin-weighted quantities

$$J \equiv \frac{h_{AB} q^A q^B}{2}, \quad K \equiv \frac{h_{AB} q^A \bar{q}^B}{2}, \quad U \equiv U^A q_A,$$

as well as the real variable

$$W \equiv \frac{V - r}{r^2}.$$

Due to the determinant condition $\det(h_{AB}) = \det(q_{AB})$ the quantities K and J are related via $1 = K^2 - J\bar{J}$. J has spin-weight two, U one and K, W, β zero. The spin-weight of the complex conjugate is equal in magnitude and opposite in sign. To eliminate second radial derivatives of U the following intermediate quantity is introduced

$$Q_A \equiv r^2 e^{-2\beta} h_{AB} U_{,r}^B.$$

Using these variables, the implemented vacuum EFE consist of the hypersurface equations

$$\beta_{,r} = N_\beta, \tag{7.14a}$$

$$(r^2 Q)_{,r} = -r^2 (\bar{\eth} J + \eth K)_{,r} + 2r^4 \eth (r^{-2} \beta)_{,r} + N_Q, \tag{7.14b}$$

$$U_{,r} = r^{-2} e^{2\beta} Q + N_U, \tag{7.14c}$$

$$W_{,r} = \frac{1}{2} e^{2\beta} \mathcal{R} - 1 - e^\beta \eth \bar{\eth} e^\beta + \frac{1}{4} r^{-2} \left[r^4 (\eth \bar{U} + \bar{\eth} U) \right]_{,r} + N_W, \tag{7.14d}$$

where $Q \equiv Q_A q^A$ and

$$\mathcal{R} = 2K - \bar{\partial}\bar{\partial}K + \frac{1}{2}(\bar{\partial}^2 J + \partial^2 \bar{J}) + \frac{1}{4K}(\bar{\partial}\bar{J}\partial J - \bar{\partial}J\partial\bar{J}),$$

the curvature scalar for surfaces of constant u and r . The evolution equation of the system is

$$2(rJ)_{,ur} - \left[\frac{r+W}{r} (rJ)_{,r} \right]_{,r} = -r^{-1} (r^2 \bar{\partial}U)_{,r} + 2r^{-1} e^\beta \bar{\partial}^2 e^\beta - J (r^{-1}W)_{,r} + N_J. \quad (7.15)$$

The complete form of N_β, N_Q, N_U, N_J in terms of the eth formalism can be found in [163]. The system (7.14), (7.15) corresponds to the main equations (3.3) in the Bondi-Sachs proper gauge (7.13). A pure gauge analysis of this system was presented in Sec. 5.2. For comparison purposes we employ also the following *artificial* symmetric hyperbolic system

$$\beta_{,r} = N_\beta, \quad (7.16a)$$

$$(r^2 Q)_{,r} = 0, \quad (7.16b)$$

$$U_{,r} = r^{-2} e^{2\beta} Q + N_U, \quad (7.16c)$$

$$W_{,r} = 0, \quad (7.16d)$$

$$2(rJ)_{,ur} = \left[\frac{r+W}{r} (rJ)_{,r} \right]_{,r}. \quad (7.16e)$$

Equations (7.14d) and (7.15) involve the conjugate variables \bar{U} and \bar{J} , for which the system (7.14), (7.15) does not explicitly possess evolution equations. For the hyperbolicity analysis provided in the ancillary files we need to complete the system in the sense of having one equation for each variable. We obtain the equations for \bar{U}, \bar{Q} and \bar{J} by taking the complex conjugate of (7.14b), (7.14c) and (7.15), respectively. The state vector of the linearized about Minkowski and first order reduced system is

$$\mathbf{u} = \left(\beta, \beta_q, \beta_p, Q, \bar{Q}, U, U_q, U_p, \bar{U}, \bar{U}_q, \bar{U}_p, W, J, J_r, J_q, J_p, \bar{J}, \bar{J}_r, \bar{J}_q, \bar{J}_p \right)^T,$$

where

$$\beta_q \equiv \partial_q \beta, \quad \beta_p \equiv \partial_p \beta, \quad U_q \equiv \partial_q U, \quad U_p \equiv \partial_p U, \quad J_q \equiv \partial_q J, \quad J_p \equiv \partial_p J, \quad J_r \equiv \partial_r J,$$

and the complex conjugates are defined in the obvious way. In the ADM coordinates (t, ρ, p, q) with

$$u = t - \rho, \quad r = \rho,$$

the system can be written in the form

$$\partial_t \mathbf{u} + \mathbf{B}^\rho \partial_\rho \mathbf{u} + \mathbf{B}^q \partial_q \mathbf{u} + \mathbf{B}^p \partial_p \mathbf{u} + \mathcal{S} = 0,$$

and it is only WH due to the non-diagonalizability of the principal symbol along the angular directions q and p . This result is expected from the analysis of Sec. 5.2, since the only difference here is the parameterization of the two-sphere. The characteristic variables along the radial direction with speed -1 are ingoing and consist of

$$\frac{J}{r} + J_r,$$

and its complex conjugate. The outgoing variables are those with speed 1, namely

$$-\frac{J}{r}, \quad J_q, \quad J_p, \quad U, \quad U_q, \quad U_p, \quad Q, \quad W, \quad \beta, \quad \beta_q, \quad \beta_p,$$

and their appropriate complex conjugates.

As for the toy models earlier, we perform norm convergence tests where the ingoing variables are integrated over a null hypersurface and the outgoing ones over a worldtube of constant radius. The code works with the compactified radial coordinate

$$z = \frac{r}{R_E + r},$$

where R_E is a constant that denotes the extraction radius and for our tests we set it equal to one. If the grid spacing is denoted as h_z, h_q, h_p for the coordinates z, q, p respectively and the timestep as h_u , then the discretized version of the L^2 -norm that we use is

$$\begin{aligned} \|\mathbf{u}_h\| &= \left\{ \sum_{z,q,p} \left[\left(\frac{J}{r} + J_r \right) \left(\frac{\bar{J}}{r} + \bar{J}_r \right) \right] h_z h_q h_p \right\}^{1/2} + \\ \max_z &\left\{ \sum_{u,q,p} \left(\beta^2 + \beta_q^2 + \beta_p^2 + W^2 + Q\bar{Q} + U\bar{U} + U_q\bar{U}_q + U_p\bar{U}_p + \frac{J\bar{J}}{r^2} + J_q\bar{J}_q + J_p\bar{J}_p \right) h_u h_q h_p \right\}^{1/2}, \end{aligned} \quad (7.17)$$

where the functions in the sums are to be understood as grid functions. All the outgoing variables of the artificial SH system (7.16) satisfy advection equations towards future null infinity. We further introduce

$$U_q, \quad U_p, \quad \beta_q, \quad \beta_p,$$

as well as the appropriate complex conjugates as independent variables, even though it is not necessary, in order to include in the norm terms with angular derivatives. These variables are also outgoing and their equations of motion are obtained by acting with the appropriate derivatives to those of U, \bar{U} and β . Consequently, the appropriate L^2 -norm for this system is (7.17) without the terms $J_q\bar{J}_q$ and $J_p\bar{J}_p$.

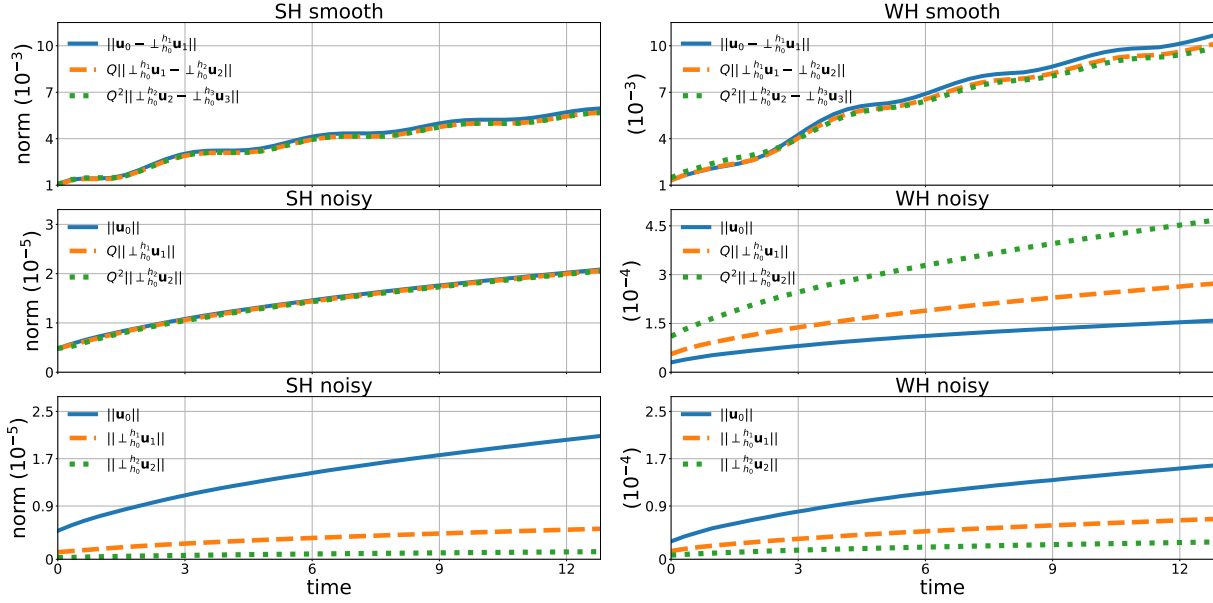


Figure 7.5: Self (above) and exact (below) convergence tests for the artificial SH system and the full Bondi-Sachs system that is WH. In the top and middle rows the rescaled norms are shown, with rescaling factor $Q = 4$. The overlap of the rescaled norms is understood as convergence and the lack of overlap as non-convergence. The tests are performed in the norm (7.17) for the WH and the norm (7.17) without the $J_q \bar{J}_p + J_p \bar{J}_q$ term for the SH system. The self convergence tests with smooth data are passed by both systems. The exact convergence tests with noisy data are passed only by the SH system. In the middle right subfigure we see the failure of convergence of the full Bondi-Sachs system, as expected by theory. In the bottom row the original norms without rescaling are shown. This illustrates that even though the numerical error converges to zero with increasing resolution also for the WH case, the rate at which this happens is not the expected one and this is understood as loss of convergence.

7.2.2 Convergence tests

In the convergence tests we solve the same PDE problem with increasing resolution and we monitor the behavior of the numerical error. The numerical domain is

$$u \in [0, 12.8], \quad z \in [0.45, 1], \quad p, q \in [-2, 2],$$

where u denotes time, z is the compactified radial coordinate, and p, q the angular coordinates. The two-sphere is covered by overlapping north and south patches. In the parameter files included in the supplementary material of [2] the variables y, x correspond to the p, q angular coordinates. These variables refer to the Einstein Toolkit thorn `CartGrid3D` and their domain size is different. The grid they provide corresponds to the grid for p, q . As described

in [159], the p, q grid points are

$$p_i = -1 + \Delta(i - O - 1), \quad q_j = -1 + \Delta(j - O - 1),$$

where O denotes the number of overlapping points beyond the equator. The range of the indices is

$$1 \leq i, j \leq M + 1 + 2O,$$

where M^2 is the total number of p, q grid points inside the equator and $\Delta = 2/M$ is the grid spacing. The physical part of the stereographic domain consists of the grid points for which

$$p^2 + q^2 \leq 1,$$

and these are the only points considered in our tests. We label the different resolutions as h_0, h_1, h_2, h_3 with

$$\begin{aligned} h_0 : \quad N_z, N_p, N_q = 33, \quad h_u = 0.04, \quad h_1 : \quad N_z, N_p, N_q = 65, \quad h_u = 0.02, \\ h_2 : \quad N_z, N_p, N_q = 129, \quad h_u = 0.01, \quad h_3 : \quad N_z, N_p, N_q = 257, \quad h_u = 0.005, \end{aligned}$$

and N_z, N_p, N_q the number of points in the z, p, q numerical grids. N_p, N_q refer to the total number of grid points (overlapping and non-overlapping regions together). By construction the grid points and timesteps of h_0 are common for all resolutions.

We perform convergence tests using both smooth and noisy given data. The former are based upon the linearized gravitational wave solutions derived in [164] and adapted to the notation used here in [159, 165], namely

$$\begin{aligned} J &= \sqrt{(l-1)l(l+1)(l+2)} {}_2R_{lm} \Re(J_l(r)e^{i\nu u}), & U &= \sqrt{l(l+1)} {}_1R_{lm} \Re(U_l(r)e^{i\nu u}), \\ \beta &= R_{lm} \Re(\beta_l e^{i\nu u}), & W_c &= R_{lm} \Re(W_{cl}(r)e^{i\nu u}), \end{aligned}$$

where W_c gives the perturbation to V and for $l = 2$

$$\begin{aligned} \beta_2 &= \beta_0 \\ J_2(r) &= \frac{24\beta_0 + 3i\nu C_1 - i\nu^3 C_2}{36} + \frac{C_1}{4r} - \frac{C_2}{12r^3}, \\ U_2(r) &= \frac{-24i\nu\beta_0 + 3\nu^2 C_1 - \nu^4 C_2}{36} + \frac{2\beta_0}{r} + \frac{C_1}{2r^2} + \frac{i\nu C_2}{3r^3} + \frac{C_2}{4r^4}, \\ W_{c2}(r) &= \frac{24i\nu\beta_0 - 3\nu^2 C_1 + \nu^4 C_2}{6} - \frac{\nu^2 C_2}{r^2} + \frac{3i\nu C_1 - 6\beta_0 - i\nu^3 C_2}{3r} + \frac{i\nu C_2}{r^3} + \frac{C_2}{2r^4}. \end{aligned}$$

We fix the parameters of these solutions to

$$\nu = 1, \quad l = 2, \quad m = 0, \quad C_1 = 3 \cdot 10^{-3}, \quad C_2 = 10^{-3}, \quad \beta_0 = i \cdot 10^{-3}.$$

The constant ν controls the frequency of the solution, l, m refer to the spin-weighted spherical harmonics and C_1, C_2, β_0 are integration constants.

For the noisy tests we set all the initial and boundary data to their Minkowski values, perturbed with random noise of amplitude A with

$$A(h_0) = 4096 \cdot 10^{-10}, \quad A(h_1) = 512 \cdot 10^{-10}, \quad A(h_2) = 64 \cdot 10^{-10},$$

on all the given data. The scaling of the amplitude by a factor of eight every time we double resolution is due to the first order derivatives in the norm (7.17), as explained in Subsec. 7.1.2. The amplitude of the noise is low enough for the non-linear terms to be negligible with the precision at which we work. The complete parameter files used in the simulations can be found in the ancillary files of [2]. We call self convergence the tests in which we obtain an error estimate by taking the difference between two numerical solutions. This is useful when an exact solution is not known, as for instance for the artificial SH system (7.16) when smooth data are given. Hence, we perform self convergence tests in the smooth setup for both WH and SH systems. On the contrary, the noisy tests consist of random noise on top of vanishing given data for both systems and zero is a solution for both cases. So, for this case we perform exact convergence tests, i.e. the error estimate is provided by a comparison between the numerical and the exact solution. We use the operator $\perp_{h_0}^{h_i}$ to denote that we consider only the common grid points of the resolution h_i with the coarse resolution h_0 , as well as the common time steps. For the self convergence tests we monitor

$$\|\mathbf{u}_{h_0} - \perp_{h_0}^{h_1} \mathbf{u}_{h_1}\|, \quad \|\perp_{h_0}^{h_1} \mathbf{u}_{h_1} - \perp_{h_0}^{h_2} \mathbf{u}_{h_2}\|, \quad \|\perp_{h_0}^{h_2} \mathbf{u}_{h_2} - \perp_{h_0}^{h_3} \mathbf{u}_{h_3}\|,$$

and for the exact convergence

$$\|\mathbf{u}_{h_0}\|, \quad \|\perp_{h_0}^{h_1} \mathbf{u}_{h_1}\|, \quad \|\perp_{h_0}^{h_2} \mathbf{u}_{h_2}\|.$$

The code uses finite difference operators that are second order accurate. This, combined with the doubling of grid points every time we increase resolution provides again a convergence factor $Q = 4$.

In Fig. 7.5 the rescaled norms for both smooth and noisy tests, for the artificial SH (7.16) and the full Bondi-Sachs system (7.14), (7.15) that is WH are illustrated. The overlap of the rescaled norms indicates good second order convergence, whereas the lack of overlap suggests non-convergence. For smooth given data both the SH and WH systems exhibit good second order convergence. However, for noisy given data only the SH has the appropriate convergence. This feature is expected, as noisy given data are important to demonstrate

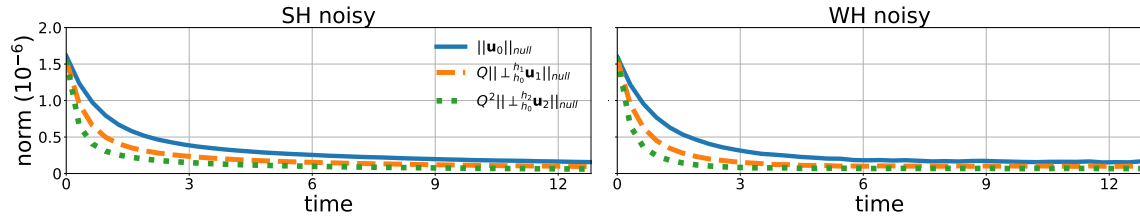


Figure 7.6: Exact convergence test with noisy data for both PDE systems, using only the null part of the norm (7.17). The WH system does not manifest a clear loss of convergence. Similarly to [43] there is no evidence of exponential growth.

WH in numerical experiments [1, 151]. These results are compatible with earlier tests with random noise that demonstrated the lack of exponential growth in the solution [43]. In Fig. 7.6 the sum only over the null hypersurface from (7.17) is shown, that is similar to earlier tests. The loss of convergence in the WH system is less severe than for the full norm (7.17) and there is no sign of exponential growth in the solution. This fact alone may be evidence for numerical stability in the colloquial sense that the code does not crash but, as we demonstrate in Fig. 7.5, is not enough evidence for convergence. It becomes apparent then that the choice of norm in which the convergence tests are performed is crucial. A norm that is compatible with the PDE system under consideration should be used.

7.3 Conclusions

A numerical approximation cannot converge to the exact solution of these PDE problems in any discrete approximation to L^2 , if the PDE systems is only WH. We demonstrated this shortcoming numerically using our toy models and adapting the well-known robust-stability test. Spotting this shortcoming in practice is subtle because smooth data may, and often does, give misleading results.

For our WH toy model, if the nested structure is broken by the source terms, it becomes ill-posed in any sense, as shown in Sec. 6.2. Using random noise for initial data, our numerical experiments are consistent with this analytic result. There is one case in which convergence is not apparent in our approximation, despite the well-posedness of the continuum equations in the lopsided norm. This is our only example of a *pure* numerical instability, and is important as it highlights the fact that for weakly hyperbolic systems numerical methods are not well-developed, and are not guaranteed to converge, even when using appropriate lopsided norms.

When the numerical experiments are performed in full GR, the same conclusions carry over; ill-posedness of the continuum PDE (in the natural equivalent of L^2) for the characteristic problem serves as an obstruction to convergence of the numerics (in a discrete approximation to the same norm). The implication of weak hyperbolicity is that the CIVP and CIBVP

of GR are ill-posed in the natural equivalent of L^2 on these geometric setups. Therefore we carried out convergence tests in a discretized version of such a norm. The tests are performed on the Bondi-Sachs gauge system (7.14), (7.15) implemented in the `PITTNu11` thorn of the `Einstein Toolkit`, as well as on the artificial strongly hyperbolic system (7.16). The norm used is compatible with the strongly hyperbolic model in the characteristic domain. The tests are performed with smooth and with noisy given data. For smooth data both the strongly and weakly hyperbolic systems exhibit good convergence. But with noisy data only the strongly hyperbolic model retains this behavior. This highlights again that noisy given data are essential to reveal weak hyperbolicity in numerical experiments. We have furthermore seen that even with noisy data one might overlook this behavior if tests are performed in a norm that is not suited to the particular problem.

PART II:

APPLICATIONS TO HOLOGRAPHY

This part is based on Refs. [3, 4]

CHAPTER 8

Numerical holography with Jecco

Contents

8.1	Jecco: a new characteristic code for numerical holography	117
8.1.1	Equations	117
8.1.2	Implementation	127
8.2	Testing the code	130
8.2.1	Analytical black brane	130
8.2.2	Comparison with SWEAC	132
8.2.3	Convergence tests	132
8.3	Simulating strongly coupled systems	136
8.3.1	Spinodal instability	138
8.3.2	Bubbles	141

The first part of the thesis focused on the hyperbolicity and well-posedness of characteristic formulations of GR and implications to accurate gravitational waveform modeling. In this part we discuss applications of these formulations in the study of out-of-equilibrium strongly coupled systems via holography. Note that the main standpoint of the thesis is gravity and more specifically the interplay of PDE analysis and numerical simulations. Hence, we cannot do full justice to the vast and growing topic of holography and we rather discuss it as a tool to model strongly coupled systems by solving the equations of motion of appropriate gravitational setups.

By the term *holography* here we mean the duality between a strongly coupled, non-Abelian, four-dimensional gauge theory on fixed Minkowski background and a gravitational theory coupled to a scalar field that resides in a five-dimensional asymptotically AdS spacetime [70, 166]. We call *numerical holography* the process of 1) using standard numerical relativity techniques to obtain approximate solutions to the complicated and dynamical gravitational dual setups of interest and 2) mapping them to quantities of the strongly coupled gauge theory via the holographic dictionary [127]. The specific dictionary we use here is given in Eq. (8.22).

We consider gravitational setups in the Poincaré patch of AdS spacetimes and always include a non-compact planar horizon. The latter is effectively acting as an infrared cut-off, which removes caustic formation from the computational domain. Gravitational constructions of this type have facilitated through holography the study of far-from-equilibrium dynamics of strongly coupled gauge theories, allowing for studies of isotropization [167–169], collisions of gravitational shockwaves (used as models for heavy-ion collisions) [170–172], momentum relaxation [173], turbulence [174, 175], collisions in non-conformal theories [176, 177], phase transitions and dynamics of phase separation [5, 7, 178–182], collisions in theories with phase transitions [183], dynamical instabilities [184], and even applications to gravitational-wave physics [185–189] and bubble dynamics [6, 190–192]. Characteristic formulations have also been employed to study the superradiant instability in asymptotically AdS spacetimes [96, 193]. See [127] for more references and a comprehensive overview of the techniques involved. Cauchy-type evolutions in asymptotically AdS spacetimes can provide an alternative approach for numerical holography; see for example [78, 79, 194]. This approach comes with its own complications, which are not discussed in this thesis.

This chapter presents a new 3+1 code called Jecco (Julia Einstein Characteristic Code) that solves Einstein’s equations in the characteristic formulation in asymptotically AdS spaces. Jecco is written in the Julia programming language and comes with several tools (such as arbitrary-order finite-difference operators as well as Chebyshev and Fourier differentiation matrices) useful for generic numerical evolutions. The code is publicly available and can be obtained from github <https://github.com/mzilhao/Jecco.jl> and Zenodo [195]. To the best of our knowledge, this is the first such freely available code apart from the PittNull code used in Sec. 7.2 for convergence tests in asymptotically flat spacetimes.

In Subsec. 8.1.1 we introduce the class of models to which our code can currently be applied, as well as the corresponding equations of motion. In Subsec. 8.1.2 we discuss the implementation of these equations in the code and the numerical methods that we use. In Sec. 8.2 we present validation tests of the code. In particular, Subsec. 8.2.1 discusses numerical error estimates of the code when reproducing a static configuration, Subsec. 8.2.2 compares Jecco against SWEC, its precursor introduced in [177] and used also in [5–7]. In Subsec. 8.2.3 convergence tests solely within Jecco are presented. More validation tests of the code can be found in [4]. Finally, in Sec. 8.3 we present simulations of the dynamics of phase transitions in some of our models. The results may be relevant for primordial GW production scenarios. In addition to the geometric units $G = c = 1$, we also set $\hbar = 1 = L$, where the latter is the AdS radius.

8.1 Jecco: a new characteristic code for numerical holography

8.1.1 Equations

In this section we outline the theoretical background and equations that are implemented in Jecco. Our approach is similar to that of [127] and generalizes the code presented in [177] to the 3+1 dimensional case. See also [53] for an overview of the approaches and codes used in the asymptotically flat setting.

Equations of motion and characteristic formulation

We consider a five-dimensional action consisting of gravity coupled to a scalar field ϕ with a non-trivial potential $V(\phi)$. The action for this Einstein-scalar model is

$$S = \frac{2}{\kappa} \int d^5x \sqrt{-g} \left[\frac{1}{4} R - \frac{1}{2} (\partial\phi)^2 - V(\phi) \right], \quad (8.1)$$

where $\kappa = 8\pi$ in our units. The resulting dynamical equations of motion read

$$\begin{aligned} E_{\mu\nu} &\equiv R_{\mu\nu} - \frac{R}{2} g_{\mu\nu} - 8\pi T_{\mu\nu} = 0, \\ \Phi &\equiv \square\phi - \partial_\phi V(\phi) = 0, \end{aligned} \quad (8.2)$$

where

$$8\pi T_{\mu\nu} = 2 \partial_\mu\phi \partial_\nu\phi - g_{\mu\nu} \left(g^{\alpha\beta} \partial_\alpha\phi \partial_\beta\phi + 2V(\phi) \right).$$

Our potential $V(\phi)$ comes from a superpotential $W(\phi)$ with the form

$$W(\phi) = -\frac{3}{2} - \frac{\phi^2}{2} + \lambda_4 \phi^4 + \lambda_6 \phi^6, \quad (8.3)$$

and its explicit expression can be derived via

$$V = -\frac{4}{3} W^2 + \frac{1}{2} W'^2,$$

resulting in

$$\begin{aligned} L^2 V(\phi) &= -3 - \frac{3}{2} \phi^2 - \frac{1}{3} \phi^4 + \left(\frac{4\lambda_4}{3} + 8\lambda_4^2 - 2\lambda_6 \right) \phi^6 + \left(-\frac{4\lambda_4^2}{3} + \frac{4}{3} \lambda_6 + 24\lambda_4 \lambda_6 \right) \phi^8 \\ &\quad + \left(18\lambda_6^2 - \frac{8}{3} \lambda_4 \lambda_6 \right) \phi^{10} - \frac{4}{3} \lambda_6^2 \phi^{12}. \end{aligned} \quad (8.4)$$

In these equations λ_4 and λ_6 are freely specifiable dimensionless parameters related to the parameters ϕ_M and ϕ_Q used in e.g. [5, 196] through

$$\lambda_4 = -\frac{1}{4\phi_M^2} \quad \lambda_6 = \frac{1}{\phi_Q}. \quad (8.5)$$

This potential has a maximum at $\phi = 0$, where it admits an exact AdS solution of radius L , here set equal to 1. The holographic dual field theory corresponds to a 3+1 dimensional conformal field theory which is deformed by a source Λ for the dimension-three scalar operator \mathcal{O}_ϕ dual to the scalar field ϕ . The thermodynamical and near-equilibrium properties of this model were presented in [176, 178, 197] for $\lambda_6 = 0$ and in [5, 196] for $\lambda_6 \neq 0$.

Let us point out that even if here we will always make use of the particular potential (8.4), the code implementation is such that more generic potentials can be used provided that, for low values of the scalar field, they behave as

$$L^2V(\phi) = -3 - \frac{3}{2}\phi^2 - \frac{\phi^4}{3} + \mathcal{O}(\phi^6). \quad (8.6)$$

The constant term is fixed by the 4+1 dimensional AdS asymptotics and the quadratic one is in correspondence with the scaling dimension of the dual scalar operator \mathcal{O}_ϕ . The quartic term, determined by the other two in our case, ensures the absence of a conformal anomaly, which would give rise to logarithms in the asymptotic expansions. A change in this near boundary behavior of the potential would alter the hard-coded asymptotic expansions and variable redefinitions that are introduced later.

We consider the following 5-dimensional ansatz for the metric in ingoing Eddington-Finkelstein (EF) coordinates, which falls into the affine null class as described in Sec. 3.1, with the line element

$$ds^2 = g_{\mu\nu}dx^\mu dx^\nu = -Adt^2 + 2dt(dr + F_x dx + F_y dy) + S^2 \left[e^{-B_1 - B_2} \cosh(G) dx^2 + e^{B_1 - B_2} \cosh(G) dy^2 + 2e^{-B_2} \sinh(G) dx dy + e^{2B_2} dz^2 \right], \quad (8.7)$$

where all functions depend on the radial coordinate r , time t and transverse directions x and y . Nothing depends on the coordinate z , so this is effectively a 3+1 system. Physically, this means that in the gauge theory we impose translation invariance along the z -direction but allow for completely general dynamics in the (t, x, y) -directions. Note that hypersurfaces of constant t are ingoing null. This coordinate is often labeled by v in EF coordinates. This particular gauge choice is the affine null since $g_{tr} = 1$ in these coordinates, but now in five spacetime dimensions. At the boundary, t becomes the usual Minkowski time coordinate. The spatial part of the metric is written such that S encodes the area of constant t and r slices,

$$\sqrt{g|_{dt, dr=0}} = S^3.$$

We can recover the 2+1 system of [177] by setting

$$\begin{aligned} F_y = G = 0, \quad B_1 = \frac{3}{2}B, \quad B_2 = \frac{1}{2}B, \quad \text{or} \\ F_x = G = 0, \quad B_1 = -\frac{3}{2}B, \quad B_2 = \frac{1}{2}B, \end{aligned} \tag{8.8}$$

for non-trivial dependence only along the x or y direction respectively.

Notice that the latter returns the weakly hyperbolic system analyzed in Subsec. 5.1.4 and so we expect the resulting system here to be only weakly hyperbolic as well. Even though our main goal with numerical holography is to obtain qualitative results and universal behaviors for the strongly coupled models we analyze, it is desirable to work with strongly or even symmetric hyperbolic characteristic setups, such that we can have robust error estimates. Since there are no such characteristic constructions at the moment—to the best of our knowledge—we work with the standard Bondi-like setups and aim to provide better alternatives in the future. In fact, part of the results presented in [5] have been obtained by fully non-linear numerical evolutions of the setup of Sec. 5.1.4. The end states of these dynamical scenarios match the near-equilibrium configurations computed with completely different methods and presented also in [5]. This compatibility suggests that possible errors due to the weak hyperbolicity of the system would affect the validity of the error estimates of the numerical solutions, but not their qualitative behavior. Of course further investigation is needed in order to address this expectation and alternative characteristic formulations would be necessary. The setup of Sec. 5.1.4 has also been used for the non-linear numerical evolutions presented in [6, 7].

The metric (8.7) is invariant under

$$\begin{aligned} r &\rightarrow \bar{r} = r + \xi(t, x, y), \\ S &\rightarrow \bar{S} = S, \\ B_1 &\rightarrow \bar{B}_1 = B_1, \\ B_2 &\rightarrow \bar{B}_2 = B_2, \\ A &\rightarrow \bar{A} = A + 2\partial_t \xi(t, x, y), \\ F_x &\rightarrow \bar{F}_x = F_x - \partial_x \xi(t, x, y), \\ F_y &\rightarrow \bar{F}_y = F_y - \partial_y \xi(t, x, y). \end{aligned} \tag{8.9}$$

Plugging the ansatz (8.7) into (8.2) results in a nested system of equations, where some of them can be effectively viewed as ODEs in the radial (holographic) direction r at each constant t that can be solved sequentially. As discussed in Sec. 3.1 however, to determine the degree of hyperbolicity of the full system we still need to treat it as an actual PDE in its entirety.

We illustrate the system solved here in Table 8.1. Each row in the table represents an

Table 8.1: Nested structure of the equations of motion.

Function	Combination
S	E_{rr}
F_x	$E_{rx} - g_{tx}E_{rr}$
F_y	$E_{ry} - g_{ty}E_{rr}$
\dot{S}	$E_{tr} - \frac{1}{2}g_{tt}E_{rr}$
$\dot{\phi}$	Φ
A	$\frac{E_{zz}}{g_{zz}} + (g^{ry}g_{ty} + g^{rx}g_{tx})E_{rr} + 2g^{rx}(E_{rx} - g_{tx}E_{rr}) + 2g^{ry}(E_{ry} - g_{ty}E_{rr})$ $-4\left(E_{tr} - \frac{1}{2}g_{tt}E_{rr}\right) + 2\frac{E_{xy}}{g_{xy}} + g_{xx}g^{xx}\left(\frac{E_{yy}}{g_{yy}} + \frac{E_{xx}}{g_{xx}} - 2\frac{E_{xy}}{g_{xy}}\right)$
\dot{B}_2	E_{zz}
\dot{G}	E_{xy}
\dot{B}_1	E_{yy}
\dot{S}	$E_{tt} - \frac{1}{2}g_{tt}E_{tr} - \frac{1}{2}g_{tt}\left(E_{tr} - \frac{1}{2}g_{tt}E_{rr}\right)$
\dot{F}_x	$E_{tx} - \frac{1}{2}g_{tt}E_{rx} - g_{tx}\left(E_{tr} - \frac{1}{2}g_{tt}E_{rr}\right)$
\dot{F}_y	$E_{ty} - \frac{1}{2}g_{tt}E_{ry} - g_{ty}\left(E_{tr} - \frac{1}{2}g_{tt}E_{rr}\right)$

equation, obtained from the particular combination of the equations of motion (8.2) as indicated, that takes the form

$$\left[A_f(t, u, x, y)\partial_u^2 + B_f(t, u, x, y)\partial_u + C_f(t, u, x, y)\right]f(t, u, x, y) = -S_f(t, u, x, y), \quad (8.10)$$

where $u \equiv 1/r$, f is the corresponding function to be solved for and the coefficients A_f , B_f , C_f and S_f are fully determined once the preceding equations have been solved. *Dotted* functions denote an operation defined as

$$\dot{f} \equiv \left(\partial_t + \frac{A}{2}\partial_r\right)f, \quad (8.11)$$

which are necessary to obtain this nested structure.

There are three sets of (two) coupled equations, indicated in the table by the absence of a separating line. These still take the form of (8.10), but now f should be thought of as a vector of the two functions involved, as is the source term S_f , while A_f , B_f and C_f become 2×2 matrices. The equations themselves are lengthy and given in Eqs. (B.2)-(B.10). These equations need to be supplemented with boundary conditions specified at the AdS boundary $u \equiv 1/r = 0$, which are made explicit later. In addition, the functions $B_1(t_0, u, x, y)$, $B_2(t_0, u, x, y)$, $G(t_0, u, x, y)$ and $\phi(t_0, u, x, y)$ should be thought of as initial data which can be freely specified provided they are consistent with AdS asymptotics.

Asymptotic expansions

The study of the near-boundary behavior ($u \rightarrow 0$) of the functions is relevant for two reasons. The first is that, as usually for AAdS spacetimes, some metric components diverge as one approaches the boundary, and their expansion in powers of u is useful to redefine the variables in terms of new, finite ones. The second is that it allows us to understand which boundary conditions to impose on the Eqs. (8.10).

For this purpose, we start with an ansatz that is compatible with the AAdS condition

$$\begin{aligned}
A(t, u, x, y) &= \frac{1}{u^2} + \sum_{n=-1}^{\infty} a_{(2n)}(t, x, y)u^n, & B_1(t, u, x, y) &= \sum_{n=1}^{\infty} b_{1n}(t, x, y)u^n, \\
B_2(t, u, x, y) &= \sum_{n=1}^{\infty} b_{2n}(t, x, y)u^n, & G(t, u, x, y) &= \sum_{n=1}^{\infty} g_n(t, x, y)u^n, \\
S(t, u, x, y) &= \frac{1}{u} + \sum_{n=0}^{\infty} s_n(t, x, y)u^n, & F_x(t, u, x, y) &= \sum_{n=0}^{\infty} f_{xn}(t, x, y)u^n, \\
F_y(t, u, x, y) &= \sum_{n=0}^{\infty} f_{yn}(t, x, y)u^n, & \phi(t, u, x, y) &= \sum_{n=1}^{\infty} \phi_{n-1}(t, x, y)u^n.
\end{aligned} \tag{8.12}$$

Substituting into Eqs. (B.2)-(B.10) and solving order by order, we obtain

$$\begin{aligned}
A(t, u, x, y) &= \frac{1}{u^2} + \frac{2}{u}\xi + \xi^2 - 2\partial_t\xi - \frac{2\phi_0^2}{3} + u^2a_4 - \\
&\quad \frac{2}{3}u^3(3\xi a_4 + \partial_x f_{x2} + \partial_y f_{y2} + \phi_0\partial_t\phi_2) + \mathcal{O}(u^4), \tag{8.13a}
\end{aligned}$$

$$B_1(t, u, x, y) = u^4b_{14} + \mathcal{O}(u^5), \tag{8.13b}$$

$$B_2(t, u, x, y) = u^4b_{24} + \mathcal{O}(u^5), \tag{8.13c}$$

$$G(t, u, x, y) = u^4g_4 + \mathcal{O}(u^5), \tag{8.13d}$$

$$\begin{aligned}
S(t, u, x, y) &= \frac{1}{u} + \xi - \frac{\phi_0^2}{3}u + \frac{1}{3}\xi\phi_0^2u^2 + \frac{1}{54}u^3(-18\xi^2\phi_0^2 + \phi_0^4 - 18\phi_0\phi_2) + \\
&\quad \frac{\phi_0}{90}u^4(30\xi^3\phi_0 - 5\xi\phi_0^3 + 90\xi\phi_2 - 24\partial_t\phi_2) + \mathcal{O}(u^5), \tag{8.13e}
\end{aligned}$$

$$\begin{aligned}
F_x(t, u, x, y) &= \partial_x\xi + u^2f_{x2} - \\
&\quad \frac{2}{15}u^3(15\xi f_{x2} + 6\partial_x b_{14} + 6\partial_x b_{24} - \partial_y g_4 - 2\phi_0\partial_x\phi_2) + \mathcal{O}(u^4), \tag{8.13f}
\end{aligned}$$

$$\begin{aligned}
F_y(t, u, x, y) &= \partial_y\xi + u^2f_{y2} - \\
&\quad \frac{2}{15}u^3(15\xi f_{y2} - 6\partial_y b_{14} + 6\partial_y b_{24} - \partial_x g_4 - 2\phi_0\partial_y\phi_2) + \mathcal{O}(u^4), \tag{8.13g}
\end{aligned}$$

$$\begin{aligned}
\phi(t, u, x, y) &= \phi_0u - \xi\phi_0u^2 + u^3(\xi^2\phi_0 + \phi_2) + \\
&\quad u^4(\partial_t\phi_2 - 3\xi\phi_2 - \xi^3\phi_0) + \mathcal{O}(u^5), \tag{8.13h}
\end{aligned}$$

where ϕ_2 is *not* the one in (8.12), but redefined as

$$\phi_2(t, x, y) \rightarrow \phi_2(t, x, y) + \xi^2(t, x, y)\phi_0. \quad (8.14)$$

Note that ϕ_0 is a constant, while the remaining variables in this expansion are functions of (t, x, y) . Furthermore, note that the redefinitions must be modified if (8.6) does not hold.

We also need the expansions of dotted variables, defined in Eq. (8.11), which take the form

$$\dot{B}_1(t, u, x, y) = -2b_{14}u^3 + \mathcal{O}(u^4), \quad (8.15a)$$

$$\dot{B}_2(t, u, x, y) = -2b_{24}u^3 + \mathcal{O}(u^4), \quad (8.15b)$$

$$\dot{G}(t, u, x, y) = -2g_4u^3 + \mathcal{O}(u^4), \quad (8.15c)$$

$$\dot{S}(t, u, x, y) = \frac{1}{2u^2} + \frac{\xi}{u} + \frac{\xi^2}{2} - \frac{\phi_0^2}{6} + \frac{1}{36}u^2(10a_4 - 5\phi_0^4 + 18\phi_0\phi_2) + \mathcal{O}(u^3), \quad (8.15d)$$

$$\dot{F}_x(t, u, x, y) = \partial_t\partial_x\xi - uf_{x2} + \mathcal{O}(u^2), \quad (8.15e)$$

$$\dot{F}_y(t, u, x, y) = \partial_t\partial_y\xi - uf_{y2} + \mathcal{O}(u^2), \quad (8.15f)$$

$$\dot{\phi}(t, u, x, y) = -\frac{\phi_0}{2} + u^2\left(\frac{\phi_0^3}{3} - \frac{3}{2}\phi_2\right) + \mathcal{O}(u^3). \quad (8.15g)$$

The function $\xi(t, x, y)$ encodes our residual gauge freedom, and the functions $a_4(t, x, y)$, $f_{x2}(t, x, y)$, $f_{y2}(t, x, y)$ are further constrained to obey

$$\partial_t a_4 = -\frac{4}{3}(\partial_x f_{x2} + \partial_y f_{y2} + \phi_0 \partial_t \phi_2), \quad (8.16a)$$

$$\partial_t f_{x2} = -\frac{1}{4}\partial_x a_4 - \partial_x b_{14} - \partial_x b_{24} + \partial_y g_4 + \frac{1}{3}\phi_0 \partial_x \phi_2, \quad (8.16b)$$

$$\partial_t f_{y2} = -\frac{1}{4}\partial_y a_4 + \partial_y b_{14} - \partial_y b_{24} + \partial_x g_4 + \frac{1}{3}\phi_0 \partial_y \phi_2, \quad (8.16c)$$

where $b_{14}(t, x, y)$, $b_{24}(t, x, y)$, $g_4(t, x, y)$, $\phi_2(t, x, y)$, and $\partial_t \phi_2(t, x, y)$ are understood to be read off from the asymptotic behavior of $B_1(t, r, x, y)$, $B_2(t, r, x, y)$, $G(t, r, x, y)$, and $\phi(t, r, x, y)$ in Eqs. (8.13b), (8.13c), (8.13d) and (8.13h). The functions $a_4(t_0, x, y)$, $f_{x2}(t_0, x, y)$, $f_{y2}(t_0, x, y)$, and $\xi(t_0, x, y)$ should also be thought of as initial data, which can be freely specified. ϕ_0 is a parameter that must also be specified and corresponds to the energy scale Λ of the dual boundary theory.

Field redefinitions and boundary conditions

For the numerical implementation we split the numerical grid in two parts: the outer grid region (deep bulk) and the inner grid region. The latter includes the AdS boundary, where boundary conditions are imposed and the gauge-theory variables are read off. Since some of the metric functions diverge at the AdS boundary while others vanish, we employ field redefinitions inspired by the asymptotic field behavior so that the variables employed in the

inner grid remain of order unity. For the outer grid we choose to make simpler redefinitions, which is helpful for the equation used to fix the gauge variable ξ . Denoting with the $g1$ ($g2$) subscript the variables defined in the inner (outer) grid, the redefinitions that we choose to make are

$$\begin{aligned}
A(t, u, x, y) &= \frac{1}{u^2} + \frac{2}{u}\xi(t, x, y) + \xi^2(t, x, y) - 2\partial_t\xi(t, x, y) - \frac{2\phi_0^2}{3} + u^2A_{g1}(t, u, x, y) \\
&= -2\partial_t\xi(t, x, y) + A_{g2}(t, u, x, y), \\
B_1(t, u, x, y) &= u^4B_{1g1}(t, u, x, y) = B_{1g2}(t, u, x, y), \\
B_2(t, u, x, y) &= u^4B_{2g1}(t, u, x, y) = B_{2g2}(t, u, x, y), \\
G(t, u, x, y) &= u^4G_{g1}(t, u, x, y) = G_{g2}(t, u, x, y), \\
S(t, u, x, y) &= \frac{1}{u} + \xi(t, x, y) - \frac{\phi_0^2}{3}u + \frac{1}{3}\xi\phi_0^2u^2 + u^3S_{g1}(t, u, x, y) = S_{g2}(t, u, x, y), \\
F_x(t, u, x, y) &= \partial_x\xi(t, x, y) + u^2F_{xg1}(t, u, x, y) = \partial_x\xi(t, x, y) + F_{xg2}(t, u, x, y), \\
F_y(t, u, x, y) &= \partial_y\xi(t, x, y) + u^2F_{yg1}(t, u, x, y) = \partial_y\xi(t, x, y) + F_{yg2}(t, u, x, y), \\
\phi(t, u, x, y) &= \phi_0u - \xi(t, x, y)\phi_0u^2 + u^3\phi_0^3\phi_{g1}(t, u, x, y) = \phi_{g2}(t, u, x, y), \\
\dot{B}_1(t, u, x, y) &= u^3\dot{B}_{1g1}(t, u, x, y) = \dot{B}_{1g2}(t, u, x, y), \\
\dot{B}_2(t, u, x, y) &= u^3\dot{B}_{2g1}(t, u, x, y) = \dot{B}_{2g2}(t, u, x, y), \\
\dot{G}(t, u, x, y) &= u^3\dot{G}_{g1}(t, u, x, y) = \dot{G}_{g2}(t, u, x, y), \\
\dot{S}(t, u, x, y) &= \frac{1}{2u^2} + \frac{\xi(t, x, y)}{u} + \frac{\xi^2(t, x, y)}{2} - \frac{\phi_0^2}{6} + u^2\dot{S}_{g1}(t, u, x, y) = \dot{S}_{g2}(t, u, x, y), \\
\dot{F}_x(t, u, x, y) &= \partial_t\partial_x\xi(t, x, y) + u\dot{F}_{xg1}(t, u, x, y) = \partial_t\partial_x\xi(t, x, y) + \dot{F}_{xg2}(t, u, x, y), \\
\dot{F}_y(t, u, x, y) &= \partial_t\partial_y\xi(t, x, y) + u\dot{F}_{yg1}(t, u, x, y) = \partial_t\partial_y\xi(t, x, y) + \dot{F}_{yg2}(t, u, x, y), \\
\dot{\phi}(t, u, x, y) &= -\frac{\phi_0}{2} + u^2\phi_0^3\dot{\phi}_{g1}(t, u, x, y) = \dot{\phi}_{g2}(t, u, x, y).
\end{aligned} \tag{8.17}$$

After substituting these redefined variables into Eqs. (B.2)-(B.10), we obtain two versions of the nested system, one for the near boundary region (inner grid), and one for the bulk region (outer grid). The boundary conditions are provided on the timelike boundary of the asymptotically AdS spacetime which is part of the inner grid ($g1$) and are given by

$$S_{g1}|_{u=0} = \frac{1}{54} \left(-18\xi^2\phi_0^2 + \phi_0^4 - 18\phi_0\phi_2 \right), \tag{8.18a}$$

$$\partial_u S_{g1}|_{u=0} = \frac{\phi_0}{90} \left(30\xi^3\phi_0 - 5\xi\phi_0^3 + 90\xi\phi_2 - 24\partial_t\phi_2 \right), \tag{8.18b}$$

$$F_{xg1}|_{u=0} = f_{x2}, \tag{8.18c}$$

$$\partial_u F_{xg1}|_{u=0} = -\frac{2}{15} \left(15\xi f_{x2} + 6\partial_x b_{14} + 6\partial_x b_{24} - \partial_y g_4 - 2\phi_0\partial_x\phi_2 \right), \tag{8.18d}$$

$$F_{yg1}|_{u=0} = f_{y2}, \tag{8.18e}$$

$$\partial_u F_{yg1}|_{u=0} = -\frac{2}{15} (15\xi f_{y2} + 6\partial_y b_{14} + 6\partial_y b_{24} - \partial_x g_4 - 2\phi_0 \partial_y \phi_2), \quad (8.18f)$$

$$\dot{S}_{g1}|_{u=0} = \frac{1}{36} (10a_4 - 5\phi_0^4 + 18\phi_0 \phi_2), \quad (8.18g)$$

$$\dot{B}_{1g1}|_{u=0} = -2b_{14}, \quad (8.18h)$$

$$\dot{B}_{2g1}|_{u=0} = -2b_{24}, \quad (8.18i)$$

$$\dot{G}_{g1}|_{u=0} = -2g_4, \quad (8.18j)$$

$$\dot{\phi}_{g1}|_{u=0} = \frac{1}{3} - \frac{3\phi_2}{2\phi_0^3}, \quad (8.18k)$$

$$A_{g1}|_{u=0} = a_4, \quad (8.18l)$$

$$\partial_u A_{g1}|_{u=0} = -\frac{2}{3} (3\xi a_4 + \partial_x f_{x2} + \partial_y f_{y2} + \phi_0 \partial_t \phi_2). \quad (8.18m)$$

The functions B_1 , B_2 , G , ϕ , a_4 , f_{x2} , f_{y2} and ξ encode the freely-specifiable initial and boundary data. Once the inner grid system is integrated, we evaluate each function at the interface of the inner and outer grids to obtain the boundary conditions for the $g2$ variables and subsequently integrate the corresponding equations.

Gauge fixing

To fully close our system we still need to fix the residual gauge freedom as described in Eq. (8.9). It is advantageous for the numerical implementation to have the Apparent Horizon (AH) lie at constant radial slice $r = r_H$ for the whole numerical evolution, and this guides our choice of gauge fixing. More specifically, we impose that $\Theta|_{r=r_H} = 0$ at all times, where Θ is the expansion of outgoing null rays. The explicit expression for our metric ansatz (8.7) is given in App. B.2.

A simple way to enforce $\Theta|_{r=r_H} = 0$ at all times during the numerical evolution is to impose a diffusion-like equation of the form

$$(\partial_t \Theta + \kappa \Theta)|_{u=u_H} = 0 \quad (8.19)$$

with $\kappa > 0$, ensuring that the expansion Θ is driven towards the fix point $\Theta|_{u=u_H} = 0$ as the time evolution runs, pushing the AH surface to $u = u_H = \text{constant}$. To implement this, we expand Eq. (8.19) using (B.19) as well as the equations of motion for \ddot{S} and $\dot{F}_{x,y}$, to get rid of these variables. Then, the variables \dot{F}' and \dot{F} vanish and for every time step we need to solve the nested system until the equation for A to be able to solve Eq. (8.19). Then, we substitute all the variables by the outer grid redefinitions, and evaluate them at $u = u_H$. We obtain a linear PDE for $\partial_t \xi$ of the type

$$\left(A_{xx}^{(\xi)} \partial_x^2 + A_{xy}^{(\xi)} \partial_x \partial_y + A_{yy}^{(\xi)} \partial_y^2 + B_x^{(\xi)} \partial_x + B_y^{(\xi)} \partial_y + C^{(\xi)} \right) \partial_t \xi(t, x, y) = -S^{(\xi)}, \quad (8.20)$$

which can be readily integrated with periodic boundary conditions in x and y .

Evolution algorithm

After integrating the intrinsic nested system (B.2)-(B.10), we use the definition of the “dot” operator (B.1) to write

$$\partial_t B_1(t, u, x, y) = \dot{B}_1(t, u, x, y) + \frac{u^2}{2} A(t, u, x, y) \partial_u B_1(t, u, x, y), \quad (8.21)$$

and analogously for B_2 , G and ϕ , which are all quantities that need to be specified by the initial data. This tells us how to march them forward in time. In practice we write explicitly the evolution equations in terms of the redefined $g1$ and $g2$ functions. Schematically, the evolution algorithm is the following:

1. Initial conditions $B_1(t_0, u, x, y)$, $B_2(t_0, u, x, y)$, $G(t_0, u, x, y)$, $\phi(t_0, u, x, y)$, $a_4(t_0, x, y)$, $f_{x2}(t_0, x, y)$, $f_{y2}(t_0, x, y)$ and $\xi(t_0, x, y)$ are provided for some initial time t_0 on an ingoing null hypersurface.
2. The intrinsic nested system (B.2)-(B.10) is solved for the redefined variables in the inner grid $g1$, imposing the boundary conditions (8.18).
3. The value of the $g1$ variables at the outer end of the inner grid is used as boundary condition to solve the nested system in the outer grid. The nested system is integrated again in the outer grid for the $g2$ variables.
4. Eq. (8.20) is solved to find $\partial_t \xi(t_0, x, y)$. Eq. (8.21) is then used to evaluate $\partial_t B_1(t_0, u, x, y)$, $\partial_t B_2(t_0, u, x, y)$, $\partial_t G(t_0, u, x, y)$, $\partial_t \phi(t_0, u, x, y)$.
5. Obtain $\partial_t a_4(t_0, x, y)$, $\partial_t f_{x2}(t_0, x, y)$ and $\partial_t f_{y2}(t_0, x, y)$ through Eq. (8.16).
6. Advance B_1 , B_2 , G , ϕ , a_4 , f_{x2} , f_{y2} and ξ to time t_1 .

In Fig. 8.1 an illustration of the geometric setup of the evolution algorithm can be found.

Gauge theory expectation values

The gauge theory expectation values can be obtained from the asymptotic behavior of the bulk variables in a way similar to [177]. These relations are what we call the holographic

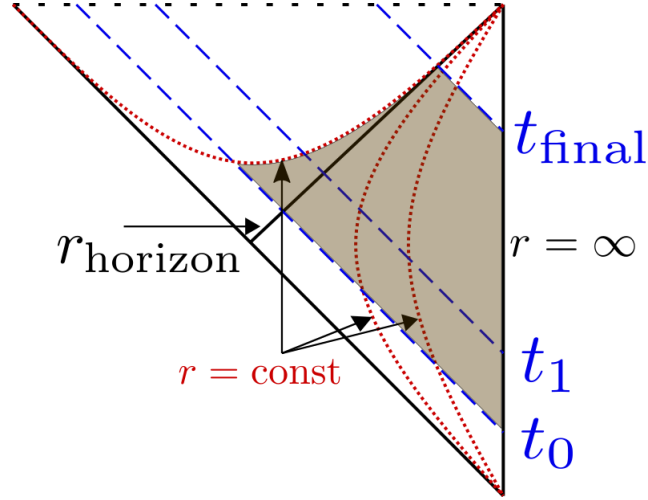


Figure 8.1: The conformal diagram of the evolution procedure, at constant x, y slices. The shaded region represents the region covered by the computational domain.

dictionary here and their derivation is beyond the scope of this thesis. The result is:

$$\begin{aligned}
\mathcal{E} &= \frac{\kappa}{2L^3} \langle T^{tt} \rangle = -\frac{3}{4}a_4 - \phi_0\phi_2 + \left(\frac{7}{36} - \lambda_4\right)\phi_0^4, \\
\mathcal{P}_x &= \frac{\kappa}{2L^3} \langle T^{xx} \rangle = -\frac{a_4}{4} - b_{14} - b_{24} + \frac{\phi_0\phi_2}{3} + \left(\frac{-5}{108} + \lambda_4\right)\phi_0^4, \\
\mathcal{P}_{xy} &= \frac{\kappa}{2L^3} \langle T^{xy} \rangle = -g_4, \\
\mathcal{P}_y &= \frac{\kappa}{2L^3} \langle T^{yy} \rangle = -\frac{a_4}{4} + b_{14} - b_{24} + \frac{\phi_0\phi_2}{3} + \left(\frac{-5}{108} + \lambda_4\right)\phi_0^4, \\
\mathcal{P}_z &= \frac{\kappa}{2L^3} \langle T^{zz} \rangle = -\frac{a_4}{4} + 2b_{24} + \frac{\phi_0\phi_2}{3} + \left(\frac{-5}{108} + \lambda_4\right)\phi_0^4, \\
\mathcal{J}_x &= -\frac{\kappa}{2L^3} \langle T^{tx} \rangle = f_{x2}, \\
\mathcal{J}_y &= -\frac{\kappa}{2L^3} \langle T^{ty} \rangle = f_{y2}, \\
\mathcal{V} &= \frac{\kappa}{2L^3} \langle \mathcal{O}_\phi \rangle = -2\phi_2 + \left(\frac{1}{3} - 4\lambda_4\right)\phi_0^3.
\end{aligned} \tag{8.22}$$

For an $SU(N)$ gauge theory the prefactor $\kappa/2L^3$ in these equations typically scales as N^{-2} , whereas the stress tensor scales as N^2 . The rescaled quantities are therefore finite in the large- N limit. The stress tensor and the expectation of the scalar operator are related through the Ward identity

$$\langle T_\mu^\mu \rangle = -\Lambda \langle \mathcal{O}_\phi \rangle. \tag{8.23}$$

8.1.2 Implementation

The evolution algorithm presented earlier is implemented in a new numerical code called `Jecco` [195], written in Julia [198]. Julia is a dynamically-typed language with good support for interactive use and with runtime performance approaching that of statically-typed languages such as C or Fortran. Even though a relative newcomer to the field of scientific computing, its popularity has been steadily growing in the last few years. It boasts a friendly community of users and developers and a rapidly growing package ecosystem.

`Jecco` was developed as a Julia module and is freely available at <https://github.com/mzilhao/Jecco.jl>. This code is a generalization of the 2+1 C code introduced in [177], and completely written from scratch. The codebase is neatly divided into generic infrastructure, such as general derivative operators, filters, and input/output routines (which are defined in the main `Jecco` module) and physics, such as initial data, evolution equations, and diagnostic routines (which are defined in submodules).

In `Jecco` we have implemented finite-difference operators of arbitrary order through the Fornberg algorithm [199] as well as Chebyshev and Fourier differentiation matrices. These methods are completely general and can be used with any Julia multidimensional array. We have also implemented output methods that roughly follow the openPMD standard [200] for writing data.

Discretization

For the numerical implementation we have discretized the x and y directions on uniform grids where periodic boundary conditions are imposed, while along the u direction we break the computational domain into several (touching) subdomains with N_u points. In each subdomain a *Lobatto-Chebyshev* grid is used where the collocation points, given by

$$X_{i+1} = -\cos\left(\frac{\pi i}{N_u}\right) \quad (i = 0, 1, \dots, N_u - 1), \quad (8.24)$$

are defined in the range $[-1 : +1]$, and can be mapped to the physical grid by

$$u_i = \frac{u_R + u_L}{2} + \frac{u_R - u_L}{2} X_i \quad (i = 1, \dots, N_u), \quad (8.25)$$

where u_L and u_R are the limits of each subdomain. For the subdomain that includes the AdS boundary ($u = 0$), the inner grid variables of Eq. (8.17) are used; all remaining subdomains use the outer grid variables.

Derivatives along the x and y directions are approximated by (central) finite differences. Although in `Jecco` operators of arbitrary order are available, we have mostly made use of fourth-order accurate ones for our applications. In the radial direction u , the use of the Chebyshev-Lobatto grid allow us to use pseudo-spectral collocation methods [201]. These methods are based on approximating solutions in a basis of Chebyshev polynomials $T_n(X)$

but, in addition to the spectral basis, we have an additional *physical* representation—the values that functions take on each grid point—and therefore we can perform operations in one basis or the other depending on our needs. Discretization using the pseudo-spectral method consists in the exact imposition of our equations at the collocation points of the Chebyshev-Lobatto grid.

The radial equations that determine our grid functions have the schematic form of equation (8.10), where f represents the metric coefficients and scalar field ϕ . Once our coordinate u is discretized, the differential operator becomes an algebraic one acting over the values of the functions in the collocation points taking the form (at every point in the transverse directions x, y)

$$\sum_{j=1}^{N_u} \left[A_f^i(t, x, y) \mathcal{D}_{uu}^{ij} + B_f^i(t, x, y) \mathcal{D}_u^{ij} + C_f^i(t, x, y) \mathbb{1}^{ij} \right] f^j(t, x, y) = -S_f^i(t, x, y) \quad (8.26)$$

(no sum in i), where \mathcal{D}_{uu} , \mathcal{D}_u represent the derivative operators for a Chebyshev-Lobatto grid in the physical representation (see for instance [202] for the explicit expression) and i, j indices in the u coordinate. Boundary conditions are imposed by replacing full rows in this operator by the values we need to fix: at the inner grid $g1$, we impose the boundary conditions in (8.18); at the outer grids these are read off from the obtained values in the previous subdomain.

The resulting operators are then factorized through an LU decomposition and the linear systems (8.26) are subsequently solved using Julia’s left division (`ldiv!`) operation. Recall that we need to solve one such radial equation per grid point in the x, y transverse directions. Since these equations are independent of each other, we can trivially parallelize the procedure using Julia’s `Threads.@threads` macro.

Equation (8.20) for $\partial_t \xi$ is a linear PDE in x, y . To solve it, after discretizing in a $N_x \times N_y$ grid, we flatten the solution vector using lexicographic ordering

$$\mathbf{g} \equiv \begin{pmatrix} \partial_t \xi(t, x_1, y_1) \\ \partial_t \xi(t, x_2, y_1) \\ \vdots \\ \partial_t \xi(t, x_{N_x}, y_1) \\ \partial_t \xi(t, x_1, y_2) \\ \vdots \\ \partial_t \xi(t, x_{N_x}, y_{N_y}) \end{pmatrix}$$

and introduce enlarged differentiation matrices, which can be conveniently built as Kronecker

products

$$\begin{aligned}\hat{\mathcal{D}}_x &= \mathbb{1}_{N_y \times N_y} \otimes \mathcal{D}_x, & \hat{\mathcal{D}}_y &= \mathcal{D}_y \otimes \mathbb{1}_{N_x \times N_x}, \\ \hat{\mathcal{D}}_{xx} &= \mathbb{1}_{N_y \times N_y} \otimes \mathcal{D}_{xx}, & \hat{\mathcal{D}}_{yy} &= \mathcal{D}_{yy} \otimes \mathbb{1}_{N_x \times N_x},\end{aligned}\quad (8.27)$$

where \mathcal{D}_x , \mathcal{D}_y , \mathcal{D}_{xx} , \mathcal{D}_{yy} are the first and second derivative finite-difference operators. The cross derivative operator is built as a matrix product, $\hat{\mathcal{D}}_{xy} = \hat{\mathcal{D}}_x \hat{\mathcal{D}}_y$. The PDE (8.20) then takes the algebraic form

$$\sum_{J=1}^{N_x \times N_y} \left[A_{xx}^I \hat{\mathcal{D}}_{xx}^{IJ} + A_{xy}^I \hat{\mathcal{D}}_{xy}^{IJ} + A_{yy}^I \hat{\mathcal{D}}_{yy}^{IJ} + B_x^I \hat{\mathcal{D}}_x^{IJ} + B_y^I \hat{\mathcal{D}}_y^{IJ} + C^I \mathbb{1}^{IJ} \right] \mathbf{g}^J = -S_{\mathbf{g}}^I \quad (8.28)$$

(no sum in I), where $I, J = 1, \dots, N_x \times N_y$. The x and y directions are periodic, so no boundary conditions need to be imposed. See for example [203] for a pedagogical overview of these techniques.

As before, the operator defined inside the square brackets is factorized through an LU decomposition and the linear system (8.28) is then solved with the left division operation. Since all the matrices are sparse, we store them in the Compressed Sparse Column format using the type `SparseMatrixCSC`.

Time evolution

For the time evolution we use a method of lines procedure, where we find it convenient to pack all evolved variables (across all subdomains) into one single state vector. This state vector is then marched forward in time with the previously described evolution algorithm using the `ODEProblem` interface from the `DifferentialEquations.jl` Julia package [149]. This package provides a very long and complete list of integration methods. For our applications, since evaluating the time derivative of our state vector is an expensive operation, we find it convenient for reasons of speed and accuracy to use the Adams-Bashforth and Adams-Moulton family of multistep methods. Depending on the application, we find that the (third order) fixed step method `AB3` and the adaptive step size ones `VCAB3` and `VCABM3` seem to work particularly well. The integration package automatically takes care of the starting values by using a lower-order method initially.

We use Kreiss-Oliger dissipation [204] to remove spurious high-frequency noise common to finite-difference schemes. In particular, when using finite-difference operators of order $p - 1$, we add Kreiss-Oliger dissipation of order p to all evolved quantities f as

$$f \leftarrow f + \sigma \frac{(-1)^{(p+3)/2}}{2^{p+1}} \left(h_x^{p+1} \frac{\partial^{(p+1)}}{\partial x^{(p+1)}} + h_y^{p+1} \frac{\partial^{(p+1)}}{\partial y^{(p+1)}} \right) f, \quad (8.29)$$

after each time step, where h_x and h_y are the grid spacings and σ is a tuneable dissipation parameter which we typically set to 0.2 unless explicitly stated otherwise. This procedure effectively works as a low-pass filter.

Along the u -direction we can damp high order modes directly in the spectral representation. After each time step, we apply an exponential filter to the spectral coefficients of our u -dependent evolved quantities f (see for instance [205]). The complete scheme is

$$\{f_i\} \xrightarrow{\text{FFT}} \{\hat{f}_k\} \longrightarrow \{\hat{f}_k e^{-\alpha(k/M)^\gamma}\} \xrightarrow{\text{FFT}} \{f_i\}, \quad (8.30)$$

where $M \equiv N_u - 1$, $k = 0, \dots, M$, $\alpha = \log \epsilon$ where ϵ is the machine epsilon (for the standard choice of $\epsilon = 2^{-52}$, $\alpha = 36.0437$) and γ is a tuneable parameter which we typically fix to $\gamma = 8$. This effectively dampens the coefficients of the higher-order Chebyshev polynomials.

8.2 Testing the code

To gauge the performance, accuracy and reliability of Jecco we conduct a number of tests. These tests include comparing the data from numerical simulations against known analytical results, as well as those from the 2+1 SWEC code introduced in [177] and convergence tests solely within Jecco. We note that the PDE system we solve is expected to be only weakly hyperbolic. We thus restrict our tests to smooth data, where the effect of weak hyperbolicity is not expected to be manifested. In [4] we perform more tests where we contrast obtained results against expected physical quantities and properties of our model systems, such as the black brane entropy density and the frequencies of its quasi-normal modes.

8.2.1 Analytical black brane

In these tests the code is initiated in a homogeneous black brane configuration, which is a static exact solution of the equations of motion with $\phi_0 = 0$ (conformal case). The functions specified in the initial data vanish and the only non-vanishing boundary data are $a_4 = -4/3$. For most of these tests, we do not perform a time evolution but instead we just solve the whole nested system at $t = 0$ and compare the last bulk function to be computed, that is A , against its analytic form:

$$A = \frac{1}{u^2} + \frac{2\xi}{u} + \xi^2 + \frac{a_4 u^2}{1 + 2\xi u + \xi^2 u^2}, \quad (8.31)$$

using the field redefinitions of Eq. (8.17) appropriately. From (8.31) we see that the gauge fixing can be performed via

$$\xi = (-a_4)^{-1/4} - 1/u_H, \quad (8.32)$$

with $u_H = 1$ the gauge fixed position of the apparent horizon for the tested configuration. Since Jecco provides us with the possibility of multiple outer spectral domains, we wish to understand to what extent faster configurations compromise the accuracy of the numerical solution. We vary the number of nodes in the u -domains, as well as the number of outer u -domains, to examine the accuracy of the code for different configurations of the spectral

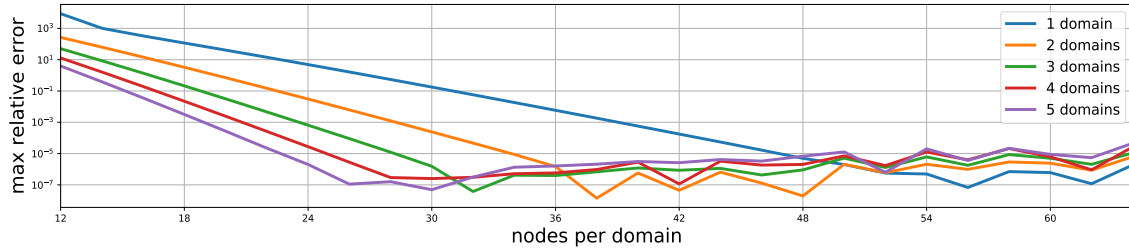


Figure 8.2: The maximum relative errors for the bulk function A , in the outer radial domains, for different configurations of the test against the analytical homogeneous black brane static solution. The same accuracy for this test is achieved e.g. by three outer radial domains with 32 nodes per domain, and a single domain with 56 nodes. The former configuration is faster.

grid. The inner u -domain discretizes the region $[0, 0.1]$ and the outer one the region $[0.1, 1.0]$. The domain of both the transverse directions x and y is $[-5, 5]$ and is discretized uniformly with 128 nodes in each case.

The maximum relative error of A for the inner spectral domain remains below $O(10^{-10})$ for a range of nodes between 12 and 36. The respective error for different configurations of outer spectral domains is shown in Fig. 8.2. A maximum relative error below $O(10^{-5})$ in the outer region can be achieved with one or multiple domains, where the latter typically provides faster configurations. The orders of magnitude difference between the maximum relative error of the inner and outer domains is due to the near boundary field redefinition. This redefinition factors out the near boundary radial dependence of the field and allows for a more accurate numerical solution. For completeness, we perform a time evolution for one of the aforementioned configurations, even if the evolution is expected to be trivial since we are investigating a static setup. For a configuration with 12 nodes in the inner domain and 28 nodes on each of the three outer domains we have verified that the maximum error maintains its expected value even after 550 timesteps, which corresponds to $t_f = 2$ in code units. For the time integration the third order Adams-Moulton method with adaptive step is used.

For a generic physical setup we find that some experimentation may be required to find the optimal numerical parameters, like the number of outer domains and nodes per domain, the choice of time integrator, etc. For instance, if accuracy of temporal derivatives of the solution is important one might consider choosing a fixed timestep integrator with a small timestep instead of an adaptive one. If the main focus is the late-time behavior of the solution, perhaps an adaptive step integrator is preferable.

8.2.2 Comparison with SWEc

For this test the code is initialized with an x -dependent perturbation on top of a homogeneous black brane configuration. The initial data are

$$\begin{aligned} B_1(0, u, x, y) &= 0.01u^4, \\ a_4(0, x, y) &= -\frac{3}{4} \left[1 + \delta a_4 \cos \left(2\pi k_x \frac{x - x_{\text{mid}}}{x_{\text{max}} - x_{\text{min}}} \right) \right], \\ \xi(0, x, y) &= \left(\frac{4}{3} \right)^{1/4} - 1, \end{aligned} \tag{8.33}$$

where $\delta a_4 = 5 \cdot 10^{-4}$, and the remaining free data functions ($B_2, G, \phi, f_{x2}, f_{y2}$) are set to zero. We compare the error of the numerical solution provided by Jecco against that of the SWEc code used in [177], for the same setup.

We use one inner radial domain spanning the region $u \in [0, 0.1]$ discretized with 12 grid points, and another (outer) domain spanning the region $u \in [0.1, 1.01]$ with 48 grid points. The transverse direction x spans $x \in [-10, 10)$, which is discretized with 128 grid points, while the y has trivial dynamics for this setup (and 6 grid points are used so that the finite difference operator fits in the domain). The time evolution is performed using the fourth-order accurate Adams-Bashforth method. The evolution is performed for a total of 2000 time steps. The choice of a single outer radial domain in Jecco is made for a more explicit comparison against SWEc, since the latter does not offer the possibility of multiple outer radial domains. It is worth noticing, however, that there are still differences between the setups in the two codes. For instance, the inner and outer domains of Jecco share only one common radial point, whereas in SWEc there is an overlapping u -region between them.

We show relative differences between the a_4 and ξ functions obtained in the two codes in Fig. 8.3. The pattern observed was similar for the metric function B_1 . To compare the output of the two codes exactly on the same grid points we perform cubic spline interpolation on the data and use the values of the interpolated functions for the comparison. It is reassuring that the results from the two codes agree so well.

8.2.3 Convergence tests

We now show *convergence* tests using numerical solutions obtained only from Jecco. For this, we solve the same physical setup with increasing resolution and inspect the rate at which the numerical solution tends to the exact one. The rate at which numerical error tends to zero with increasing resolution is determined by the approximation *accuracy*. The latter is the degree to which a discretized version of a PDE system approximates the correct continuum PDE system, and such a discretized version is called *consistent*. If its numerical solution is bounded at some arbitrary finite time by the given data of the problem in a discretized version of a suitable norm, it is furthermore called *stable*. The Lax equivalence

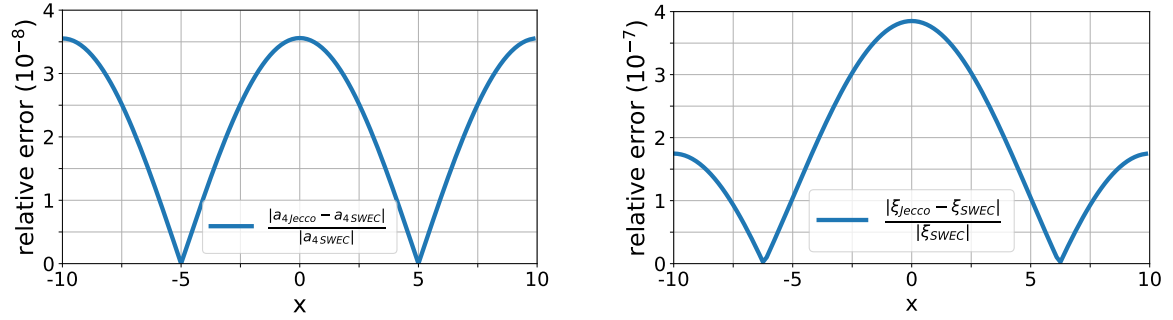


Figure 8.3: Relative errors for the a_4 and ξ functions at the end of the evolution. Results obtained with the SWEC code are used as benchmark.

theorem states that consistency of the finite difference scheme and stability with respect to a specific norm guarantee convergence for linear problems (and the converse) [206].

For our present case, since the spatial discretization is performed with a mixture of finite-difference and pseudo-spectral techniques, we fix the number of grid points along the spectral direction and vary only the number of grid points in the uniform grid along the transverse directions x, y . The finite-difference operators dominate the numerical error, so the expected convergence rate is controlled by the rate at which we increase the resolution in the uniform grid, as well as the approximation order of the operators.

As in Chap. 7 we denote by f the solution to the continuum PDE problem and by f_h its numerical approximation. We have

$$f = f_h + O(h^n), \quad (8.34)$$

where h is the grid spacing and n the accuracy of the finite-difference operators. Performing numerical evolutions with coarse and medium resolutions h_c and h_m respectively, we construct again the exact convergence factor

$$Q = \frac{f_{h_c} - f}{f_{h_m} - f},$$

which informs us about the rate at which the numerical error induced by the finite-difference scheme converges to zero. Comparison of grid functions corresponding to different resolutions is to be understood by the use of the common grid points among the different resolutions.

Using a physical setup with known exact solution provides a clear benchmark to compare with, and we can prepare such a setup by evolving a homogeneous black brane where the apparent horizon is *not* fixed at a constant position u_H but is allowed to move, with only gauge dynamics. This can be achieved by using a different choice for the evolution of the gauge function ξ than the one specified earlier. In particular, we impose the advection

equation

$$\partial_t \xi(t, x, y) = -v_x \partial_x \xi(t, x, y), \quad (8.35)$$

which introduces non-trivial dynamics to the numerical evolution. We choose this function to be a sine with small enough amplitude, such that the apparent horizon is guaranteed to remain within the computational domain. Furthermore, ξ satisfies an advection equation along the transverse direction x , which makes the numerical solution time dependent and the comparison between exact and numerical values non-trivial for later simulation times.

The only non-vanishing initial data for this setup is the boundary function a_4 , which we set to $a_4(t, x, y) = -1$, and the gauge function ξ , which we initialize to

$$\xi(0, x, y) = \xi_0 + A_x \sin\left(\frac{2\pi n_x}{L_x} (x_{\max} - x)\right), \quad (8.36)$$

where $L_x \equiv x_{\max} - x_{\min}$. For such a configuration, the solution to equation (8.35) is

$$\xi(t, x, y) = \xi_0 + A_x \sin\left(\frac{2\pi n_x}{L_x} (x_{\max} - x + v_x t)\right), \quad (8.37)$$

and the exact solution of the metric function A is given by (8.31), where ξ is now provided by (8.37).

For the tests presented herein we have fixed

$$\xi_0 = 0, \quad A_x = 0.1, \quad n_x = 1, \quad x_{\max} = 5 \quad x_{\min} = -5.$$

For the numerical discretization we have employed one inner radial domain with 12 grid points (spanning the region $u \in [0, 0.1]$) and three equal-sized outer domains for the region $u \in [0.1, 1.2]$ with 28 grid points each. For the transverse directions we use 16, 32, and 64 grid points for coarse, medium and fine resolution respectively. The time integration is performed with the third-order accurate Adams-Moulton method, with adaptive timestep. The (periodic) finite difference operators are second order accurate and Kreiss-Oliger dissipation is used with the prescription of equation (8.29) with $\sigma = 0.01$. We run the tests on a laptop with 16GB RAM memory and Intel Core i7-10510U at 1.80GHz CPU. For the fourth order accurate finite difference case, the coarse resolution is performed with a single thread and is completed within 36 minutes. For the same finite difference accuracy, the medium and high resolution tests are performed with two threads running in parallel and are completed within 66 and 271 minutes, respectively.

Convergence tests for the A metric function can be seen in Fig. 8.4. As mentioned above, the comparison of the grid functions against the exact solution is performed only on grid points that are common to all three resolutions. The expected convergence factor for this setup is $Q = 4$ for second order finite difference operators and $Q = 16$ for fourth order, which

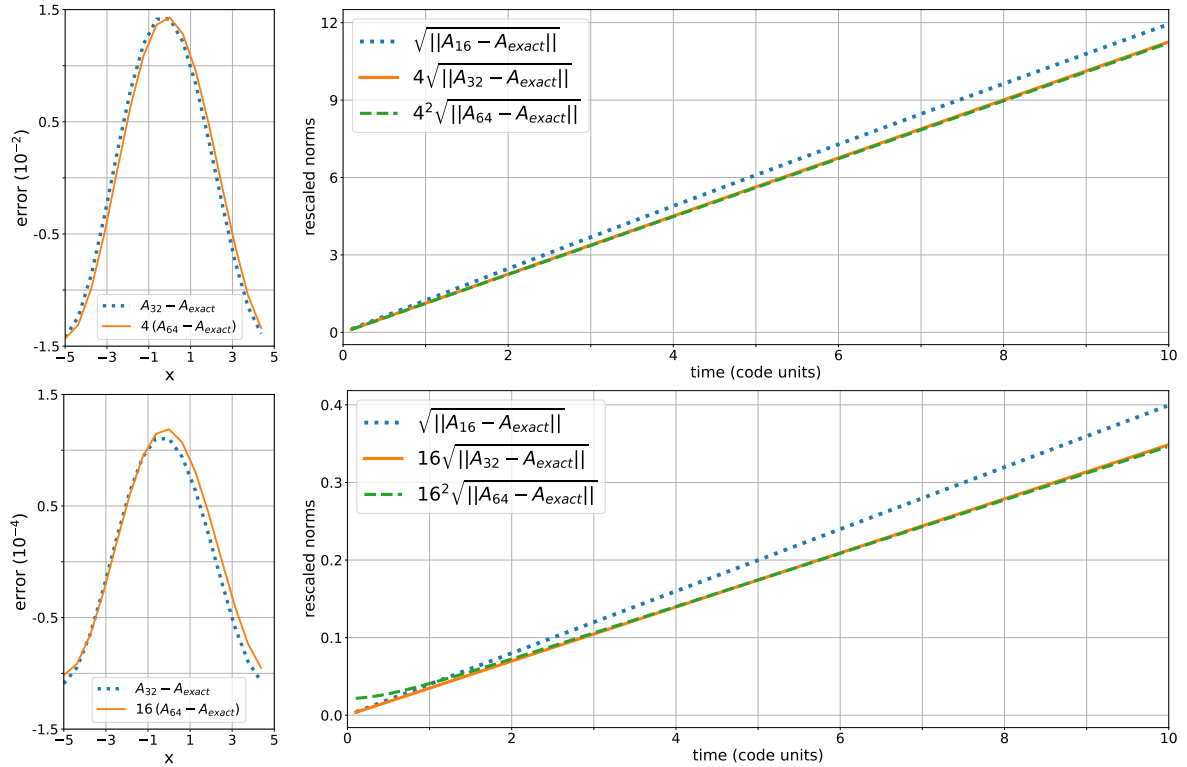


Figure 8.4: (Left) Pointwise convergence of the metric function A along the x direction, at $t = 9.98$ (code units), $u = 0.83$ and $y = 0.625$, for the medium and fine resolutions. (Right) Convergence rate for the metric function A in terms of rescaled norms. Perfect overlap of curves should be understood as perfect convergence. Second order finite difference approximation corresponds to the top and forth order to the bottom row. The ideal convergence factor for the former is $Q = 4$ and the latter $Q = 16$ for the specific tests.

is indeed what we observe in the left column. The same convergence rate is expected when we perform a norm comparison. The discretized version of the L^2 -norm that we employ here is simply the square root of the sum of the squared grid function under consideration (over all domains). In the right column of the figure we again see very good agreement for the norm convergence rate.

Finally, the total energy of the boundary theory is expected to be constant throughout the numerical evolution, which is indeed the case up to numerical errors, as illustrated in Fig. 8.5. The case illustrated corresponds to the setup used for the convergence tests of Fig. 8.4, namely the gauge dynamics of ξ as described by the exact solution of Eq. (8.37). By box we mean the region of the boundary theory is understood to reside, given the periodic boundary conditions in the x, y directions.

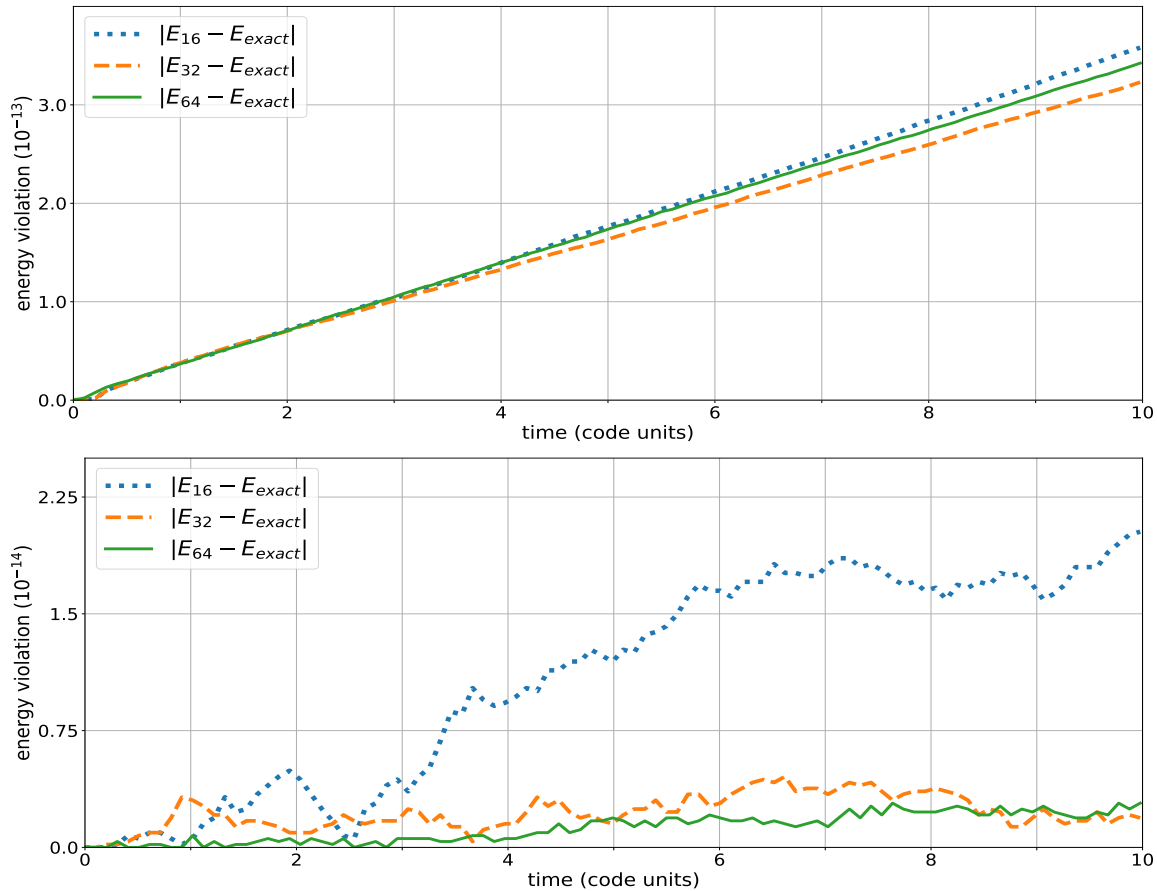


Figure 8.5: The relative error of the total energy of the box for the numerical simulations of the gauge dynamics described by Eq. (8.37). The total energy of the gauge theory for this setup is 75 in code units. The numerical violation is within accepted numerical error as illustrated here. The top figure corresponds to second order finite difference operators, whereas the bottom to fourth order. As expected the numerical violation is smaller when higher order operators are used.

8.3 Simulating strongly coupled systems

By strongly coupled systems here we mean matter under extremely high pressure and temperature. Such scenarios can occur for instance during the early universe or inside neutron stars, as well as in terrestrial experiments that mimic these conditions e.g. heavy ion collisions. For these conditions the fundamental force of the strong interactions is dominant and the theory that describes it is Quantum Chromodynamics (QCD). The gauge theory we study here is not QCD however, but it is a strongly coupled, non-Abelian, gauge theory that exhibits phase transitions. The gravitational dual setups that we construct and evolve allow us to follow the dynamics of these phase transitions. We hope that these models can provide us with valuable insights for the qualitative behavior of strongly coupled matter in similar

physical scenarios.

A very promising arena where this type of studies can be fruitful is in GWs. GW detectors like LISA [74] may be able to observe signals that carry distinct imprints of phase transitions, either originating from the early universe [73] or from events that involve Neutron stars [207]. Such imprints would inform us about the behavior of matter under extreme conditions. Regarding early universe scenarios, within the Standard Model of particle physics the universe cools down from its original hot dense state via a smooth crossover [208–211]. This process is not expected to produce any GWs. However, several beyond the Standard Model scenarios predict that this cooling down can happen via different channels that involve more abrupt phase transitions, which could produce GWs [212–222]. Detection of such patterns in primordial GWs would strongly suggest paths to expand our picture of the fundamental interactions.

SWEC is the code progenitor of Jecco that was introduced in [177] and used among others in [5–7]. Studying GW production scenarios was not possible with SWEC due to the high symmetry along the spatial directions of the boundary theory. In Jecco translational invariance is imposed only along one of the three spatial directions and thus we can simulate processes that can produce GWs. The equations of motion for fully $3 + 1$ dynamical setups of the boundary theory are not yet implemented, but is a desired feature for the future.

In addition to the lower degree of symmetry, another aspect that improves our ability to simulate the dynamics of phase transitions is the scalar potential implemented. In [176, 178, 197] the scalar potential (8.4) with $\lambda_6 = 0$ was chosen. Even though the model still exhibited phase transitions, the separation between the high and low energy density states was very large, which resulted in very slow dynamics. Consequently, more computational time was necessary in order to capture the evolution of the phase transition. Including a non-vanishing λ_6 parameter in the scalar potential allows for a smaller separation of scales between the different phases, and thus in faster dynamics. With this setup it is more convenient to explore the parameter space of the model and search for interesting phenomena. To understand whether the model exhibits phase transitions, a phase diagram has to be constructed. For a scalar potential with non-vanishing λ_6 parameter this is done in detail in [5, 196] and includes the construction of various static black brane configurations. A typical shape of a phase diagram with a phase transition is shown in Fig. 8.6.

The dynamical scenarios that have so far been explored with Jecco are the evolution of the spinodal instability and bubbles of low energy density phase within a bath of high energy density phase. In Subsec. 8.3.1 we provide further details on the former and present a brief overview of its study in [3]. In Subsec. 8.3.2 we give a short description of the holographic bubble dynamics as presented in [4]. Work is already undergoing into implementing different types of initial data generating routines such as those relevant for gravitational shockwaves, which are used to model heavy ion collisions.

In the following figures, all quantities are shown in units of Λ , which is a characteristic energy scale of the dual theory and is tuned by the choice of the scalar quantity ϕ_0 .

8.3.1 Spinodal instability

The thermodynamics of the gauge theory are extracted by building various homogeneous black brane configurations on the gravitational side of the duality (see e.g. [223]). In thermal equilibrium all the pressures \mathcal{P} are equal and the free energy density is $\mathcal{F} = -\mathcal{P}$. The free parameters of the scalar potential (8.4) are fixed to

$$\phi_M = 1, \quad \phi_Q = 10.$$

The discontinuity of the free energy as a function of temperature as seen in the top of Fig. 8.6 is indicative of a first-order phase transition. This behavior leads to multivaluedness for the energy density as a function of the temperature, as seen in the bottom of Fig. 8.6. The critical temperature $T_c = 0.396 \Lambda$ is defined as the point in the top of Fig. 8.6 where the two curves cross. There, the state that minimizes the free energy changes branch. The solid blue curves indicate the thermodynamically stable branches and the difference in their energy density is called the latent heat. These are the high and low energy density phases and both correspond to deconfined plasma phases and are dual to homogeneous black brane geometries. The dashed brown curves are metastable, which means that they are locally thermodynamically stable, but not globally. Finally, the dashed-dotted red curve is locally unstable and defines the spinodal region. Initial states within this region are affected by the spinodal instability, where small amplitude and long wavelength perturbations grow exponentially with time.

In Fig. 8.7 we demonstrate the evolution of the energy density for a state initially within the spinodal region. The exact state chosen is represented as the black dot in Fig. 8.6. This initial homogeneous configuration is slightly perturbed. The evolution of the perturbation has a short initial regime described well by a linearized analysis around the homogeneous configuration, where some modes of the perturbation decay while others grow. After the unstable modes grow large enough, the evolution enters a non-linear regime where the dynamics become richer. A thorough discussion of these different regimes can be found in [180]. In short, the growth of the perturbation creates peaks and valleys in the energy density profile. The initial separation of these structures depends on the unstable modes that dominate the first part of the dynamics. They subsequently merge to eventually form a single low energy domain within a high energy bath, as shown in the last subfigure of Fig. 8.7. If the box where the dynamics takes place is large enough, this state is homogeneous with temperature $T = T_c$ and the energy density for the low and high phase is \mathcal{E}_{low} and \mathcal{E}_{high} as shown in Fig. 8.6, respectively. This process can produce a GW spectrum that is distinct from that of a phase transition which takes place via bubble nucleation and collision, as discussed in detail in [3]. The conditions under which the spinodal channel may be favored

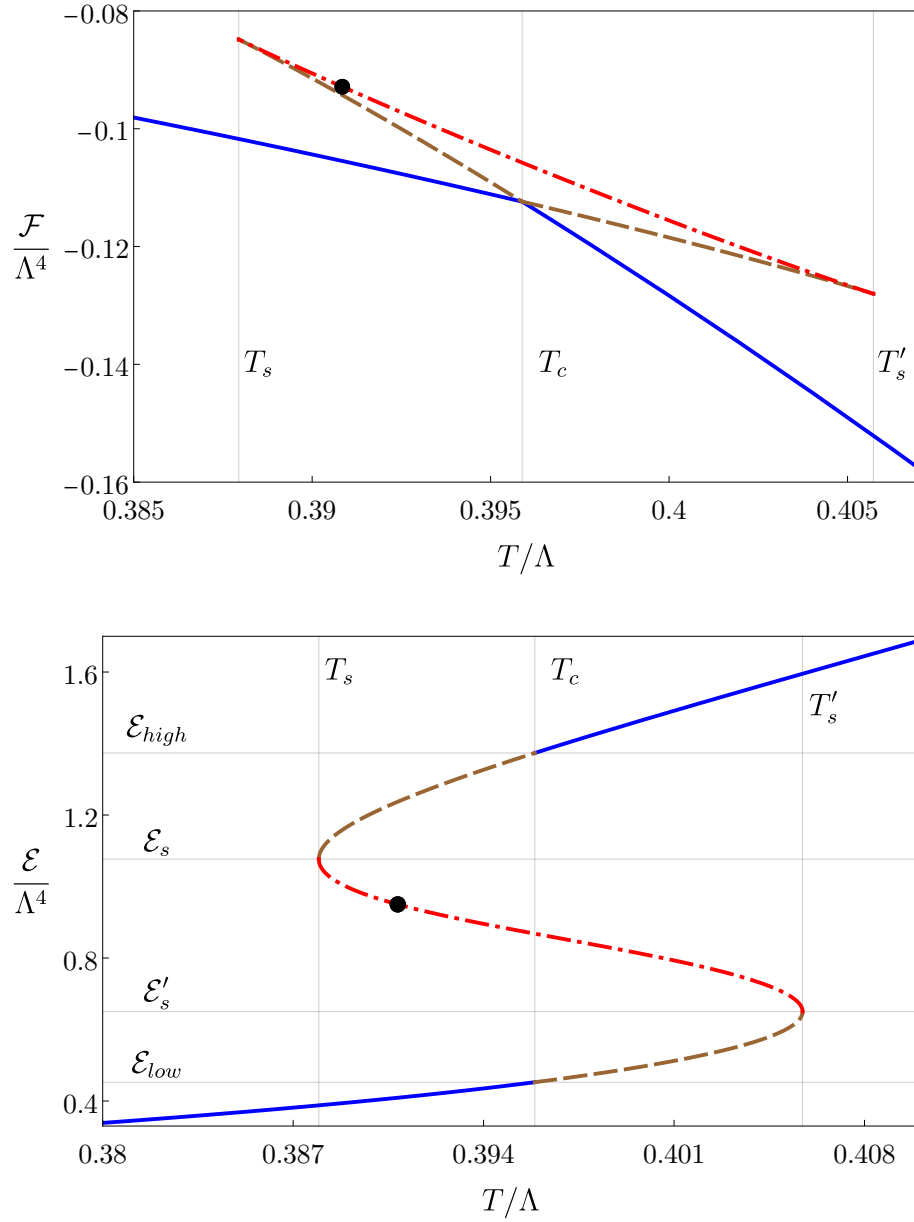


Figure 8.6: Free energy density (top) and energy density (bottom) of the four-dimensional gauge theory dual. States on the solid, blue curves are thermodynamically stable. States on the dashed, brown curves are metastable. States on the dashed-dotted, red curve are unstable. The black dot with $T = 0.3908\Lambda$ indicates the initial state on which we will focus here and is within the spinodal unstable region.

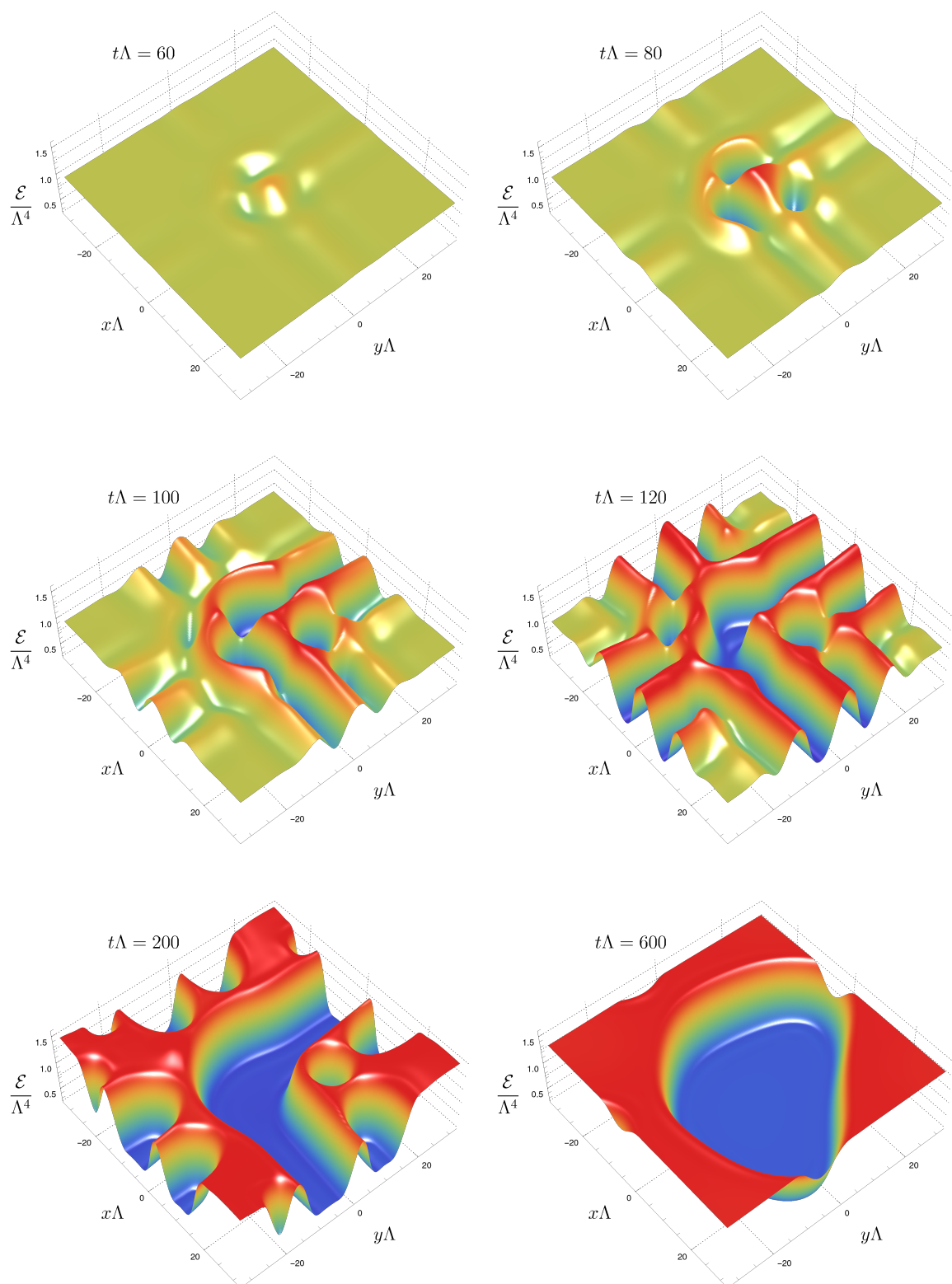


Figure 8.7: Spacetime evolution of the energy density for the initial homogeneous state in the spinodal region, perturbed with small fluctuations. A video of the evolution can be found at <https://www.youtube.com/watch?v=qIhbpchr3gE>.

over the bubble one, are also discussed there.

8.3.2 Bubbles

The phase transitions we study are expected to mostly take place via bubble nucleation, expansion and collision. To accurately predict the GW spectrum of this process, knowledge of several parameters is required, like critical temperature and strength of the transition which are thermodynamic in nature and bubble wall velocity that highly depends on the out-of-equilibrium physics. For the first class of parameters, holographic calculations have been performed e.g. in [5, 178, 180, 183, 185–188, 190, 196, 224], whereas for the bubble wall velocity a holographic calculation from first principles was presented in [6]. This study used **SWEC** and so the bubbles are planar, in the sense that they are invariant along two out of the three spatial direction of the gauge theory. The focus of this study is on the interface between the low and high energy density phases and the velocity of this wall and surface tension is neglected.

In [4] this line of research is expanded by allowing for bubbles with translational invariance only in one spatial direction, which we call cylindrical. With **Jecco** we explore different types of bubbles: the expanding, collapsing and critical ones. The reason for this richness is due to the surface tension that is included in the analysis. In particular, the critical bubble is one where the inward-pointing surface tension force balances the outward-pointing coming from the pressure difference between the inside and outside regions of the bubble. In this study, the free parameters of the scalar potential are fixed to

$$\phi_M = 0.85, \quad \phi_Q = 10.$$

In Fig. 8.8 snapshots of the energy density for three different cylindrical bubbles constructed and evolved with **Jecco** are shown. To construct them we utilize the end-state of the spinodal instability and through a series of manipulations that are described in detail in [4] we build bubbles with different radii. To find the region of criticality we construct various subcritical and supercritical bubbles and gradually move towards the radius of criticality. The subcritical bubbles collapse and the supercritical ones expand. The latter are important for the GW production scenarios discussed earlier and in [4] we also study their bubble wall velocity, their profile at late times and the applicability of hydrodynamics in the description of the phenomenon. A video of an expanding cylindrical bubble simulated with **Jecco** can be found [here](#).

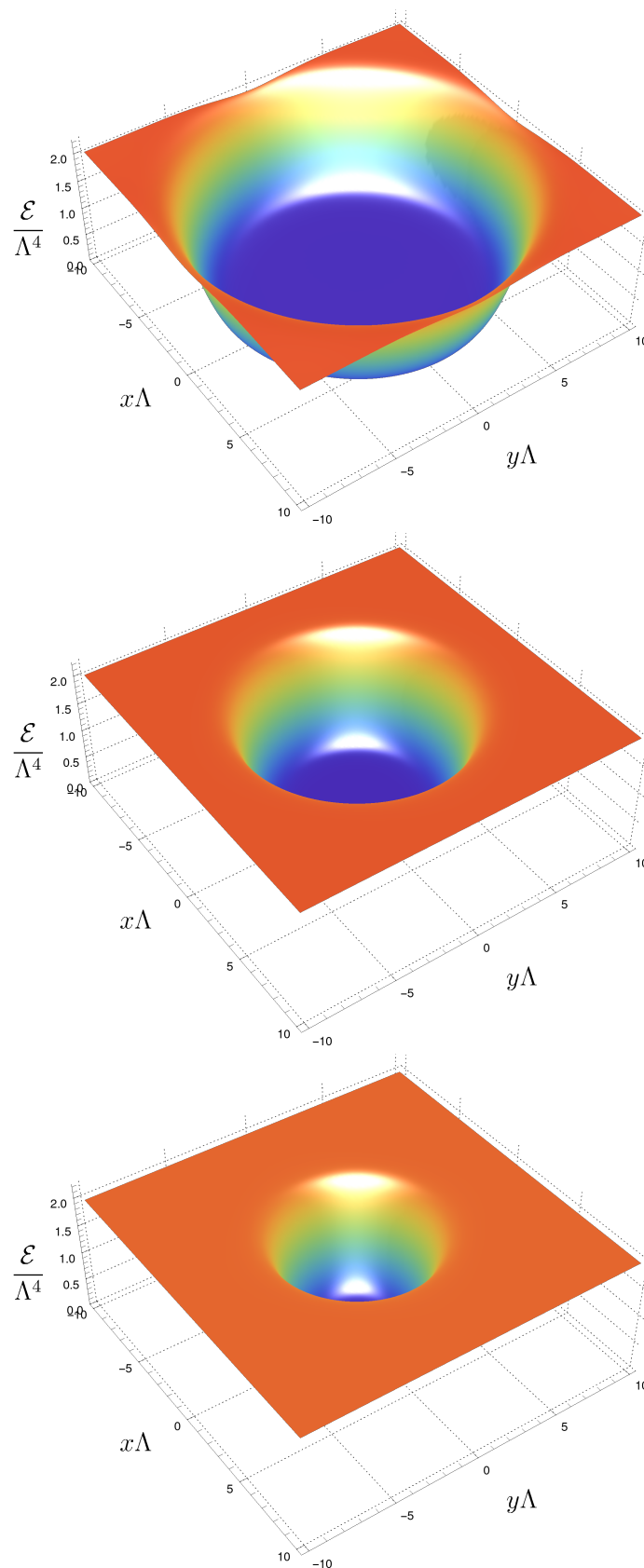


Figure 8.8: Phase-separated configurations in a box of size $L_x\Lambda = L_y\Lambda = 20$ with average energy densities $\bar{\mathcal{E}}/\Lambda^4 = 1.0$ (top), $\bar{\mathcal{E}}/\Lambda^4 = 1.6$ (middle) and $\bar{\mathcal{E}}/\Lambda^4 = 1.8$ (bottom).

CHAPTER 9

Final remarks

Characteristic formulations of GR are used in a number of cases such as gravitational waveform modeling, critical collapse and applications to holography. These formulations are most commonly built upon Bondi-like gauges.

Despite their extensive use, relatively little attention has been paid to well-posedness of the resulting PDE problems, which serves as an obstacle to the construction of rigorous error estimates from computational work. Motivated by this, we analyzed the EFE in some popular Bondi-like gauges and demonstrated that the resulting PDE systems are only weakly hyperbolic. In addition, we showed that this weak hyperbolicity is caused by the gauge condition $g^{uA} = 0$ common to all Bondi-like gauges and identified the resulting PDE structure as a pure gauge effect. To achieve the latter, we had to jump through a number of technical hoops. We mapped the characteristic free evolution system to an ADM setup so that the results of [101, 115] could easily be used. This allowed us to distinguish among the gauge, constraint, and physical degrees of freedom in the linear, constant coefficient approximation. Crucially it is known that weakly hyperbolic pure gauges give rise to weakly hyperbolic formulations. We were able to show the former in a number of cases. Specifically, we have studied three Bondi-like setups: the affine null, the Bondi-Sachs proper and the double null gauges. All three have the same degenerate structure rendering the pure gauge subsystem weakly hyperbolic. We have thus argued that when the EFE are written in a Bondi-like gauge with at most second derivatives of the metric and there are nontrivial dynamics in at least two spatial directions, then, due to the weak hyperbolicity of the pure gauge subsystem, the resulting PDE system is only WH.

All the hyperbolicity analyses are performed in the linear, frozen coefficient approximation and we demand that for a system to be characterized as WH or SH, the definitions of Sec. 2.2 are satisfied at each point in the domain of interest. The latter provides the basis to show well-posedness for the IVP of variable-coefficient SH systems, as well as non-linear systems with a SH linearization. Consequently, obtaining a SH linearization in the frozen coefficient approximation of the original characteristic systems analyzed here, is the minimum requirement for the original characteristic system to be SH.

The implication of weak hyperbolicity is that the CIVP and CIBVP of GR are ill-posed in

the natural equivalent of the L^2 -norm on these geometric setups. The obvious approach to circumvent weak hyperbolicity in characteristic formulations of GR that include up to second order derivatives of the metric, is to adopt a different gauge. For applications in CCM this may be necessary, since it is otherwise not at all clear how a well-posedness result for the composite PDE problem could be obtained. Building different characteristic gauges that are strongly hyperbolic could have positive impact not only in CCM, but also in other dynamical strong gravity scenarios, as for instance gravitational collapse. So, an interesting research avenue is to explore different approaches in constructing strongly hyperbolic characteristic setups, investigate their behavior in numerical applications and compare their results to known ones from Bondi-like formulations.

Concerning purely characteristic evolution, symmetric hyperbolic formulations of GR employing Bondi-like gauges are known [131, 132, 135, 136]. At first sight this seems to contradict the claim that any formulation of GR inherits the pure gauge principal symbol within its own. But these formulations all promote the curvature to be an evolved variable, so practically they include higher than second order derivatives of the metric and hence the results of [101] do not apply. We saw that by taking an outgoing null derivative of the affine null pure gauge subsystem, we obtain a strongly hyperbolic PDE. It is thus tempting to revisit the model of [101] to investigate the conjecture that formulations of GR with evolved curvature can be built that inherit specific derivatives of the pure gauge subsystem. A deeper understanding of the relation between the latter and the Bondi-like formulations analyzed in this thesis could suggest norms in which they are actually well-posed. Obtaining such a proof would help validate error estimates for numerical solutions so relevant for applications in gravitational wave astronomy. Work in this last direction is ongoing and we reported here some preliminary calculations.

To demonstrate the effect of weak hyperbolicity in practice, we performed numerical experiments with toy models, as well as in full GR. In all cases we confirmed that ill-posedness of the continuum PDE (in the natural equivalent of L^2) for the characteristic problem serves as an obstruction to convergence of the numerics (in a discrete approximation to the same norm). For WH toy models that mimic Bondi-like systems, we found and tested a lopsided norm that is not equivalent to L^2 in which we recovered well-posedness, but in a weak form. We found an explicit example for that model where lower order source terms break this weak well-posedness, as well as a purely numerically unstable case which highlights that standard numerical methods are not well developed for WH problems. The tests were performed with smooth and with noisy given data. For smooth data both the strongly and weakly hyperbolic systems exhibited good convergence. But with noisy data only the strongly hyperbolic model retained this behavior. These findings are compatible with previous results [151, 156], namely that noisy given data are essential to reveal weak hyperbolicity in numerical experiments. We furthermore saw that even with noisy data one might overlook this behavior if tests are performed in a norm that is not suited to the particular problem.

Finally, we described in detail `Jecco`, a new open source code that solves the EFE in a characteristic setup. `Jecco` is a modular code written in the Julia programming language. At this stage the code can provide solutions to gravitational setups in asymptotically AdS spacetimes in five dimensions and with trivial dynamics along one of the dimensions of the timelike AdS boundary. These setups are useful to investigate the out-of-equilibrium dynamics of model strongly coupled plasmas via holography. We briefly presented examples where we simulated the evolution of a phase transition for such models. The channels through which the phase transition can evolve are bubble nucleation or the spinodal instability. Both could be relevant for primordial GW production that might be detected by future GW detectors. The PDE systems currently solved are expected to be only WH since they are based on Bondi-like gauges. However, through holography we aim to primarily understand the qualitative behavior of these strongly coupled systems. To perform rigorous error estimates we would need alternative SH characteristic formulations adapted to AAdS, which is a possible research direction. Another possible future task is to enrich the code with more initial data generating routines, such that we can simulate e.g. gravitational shockwave collisions that are used to model heavy ion collisions that take place in terrestrial experiments.

PART III:

APPENDIX

APPENDIX A

Appendix for part I

A.1 The divergence theorem

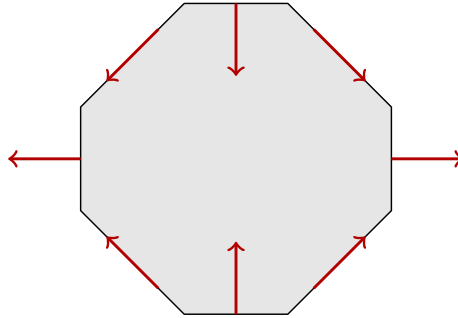


Figure A.1: The orientation of the vector N^μ that is normal to the boundary ∂M : for spacelike ∂M , N^μ points inwards, for timelike ∂M it points outwards and for null ∂M , N^μ consists of a timelike part that points inwards and a spacelike part that points outwards.

The version of the divergence theorem we apply is based on Sec. 5.1 of [25]. In brief, given a spacetime M with boundary ∂M and a spacetime vector X^μ the divergence theorem reads

$$\int_M \nabla_\mu X^\mu dV = \int_{\partial M} X^\mu N_\mu d\sigma,$$

where dV and $d\sigma$ the volume elements of M and ∂M respectively and N^μ the spacetime vector normal to ∂M , with its orientation illustrated in Fig. A.1.

A.2 The Grönwall inequality

We use the integral version of the *Grönwall inequality* which states:

Let I denote an interval of the real line of the form $[a, \infty)$, $[a, b]$ or $[a, b)$, with $a < b$. Let furthermore α, β and u be real-valued functions defined on I and assume that β and u are continuous and that the negative part of α is integrable on every closed and bounded subinterval of I . Then

1. If β is non-negative and u satisfies the integral inequality

$$u(t) \leq \alpha(t) + \int_a^t \beta(s)u(s)ds, \quad \forall t \in I,$$

then

$$u(t) \leq \alpha(t) + \int_a^t a(s)\beta(s)\exp\left(\int_s^t \beta(r)dr\right) ds,$$

with $t \in I$.

2. If in addition $\alpha(t)$ is non-decreasing, then

$$u(t) \leq \alpha(t) \exp\left(\int_a^t \beta(s)ds\right).$$

A.3 A symmetric hyperbolic affine null PDE system

The symmetric hyperbolic characteristic system of [132] is reviewed.

Setup and formalism

The metric ansatz is

$$ds^2 = V du + 2du dr - h_{ab}(d\theta^a + W^a du)(d\theta^b + W^b du), \quad (\text{A.1})$$

where r is an affine parameter for outgoing null geodesics. The chosen tetrad basis is $l^\mu, n^\mu, m^\mu, \bar{m}^\mu$, with

$$l^\mu \partial_\mu = \partial_r \equiv D, \quad (\text{A.2a})$$

$$n^\mu \partial_\mu = \partial_u + P \partial_r + R^a \partial_a \equiv \Delta, \quad (\text{A.2b})$$

$$m^\mu \partial_\mu = Q \partial_r + S^a \partial_a \equiv \delta, \quad (\text{A.2c})$$

where Q and S^a are complex valued functions. Henceforth, the coordinates on the two-sphere may be labeled as $\theta^a = (\theta, \phi)$. The metric and the tetrad are related via the identities

$$g^{\mu\nu} = l^\mu n^\nu + n^\mu l^\nu - m^\mu \bar{m}^\nu - \bar{m}^\mu m^\nu, \quad (\text{A.3a})$$

$$g_{\mu\nu} = l_\mu n_\nu + n_\mu l_\nu - m_\mu \bar{m}_\nu - \bar{m}_\mu m_\nu, \quad (\text{A.3b})$$

which lead to

$$g^{rr} = -V = 2(P - Q\bar{Q}), \quad (\text{A.4a})$$

$$g^{ra} = -W^a = R^a - \bar{S}^a Q - S^a \bar{Q}, \quad (\text{A.4b})$$

$$g^{ab} = -h^{ab} = -S^a \bar{S}^b - S^b \bar{S}^a. \quad (\text{A.4c})$$

The tetrad calculus yields [225]

$$l_\mu l^\mu = n_\mu n^\mu = m_\mu m^\mu = \bar{m}_\mu \bar{m}^\mu = 0, \quad (\text{A.5a})$$

$$l_\mu n^\mu = -m_\mu \bar{m}^\mu = 1, \quad (\text{A.5b})$$

$$l_\mu m^\mu = l_\mu \bar{m}^\mu = n_\mu m^\mu = n_\mu \bar{m}^\mu = 0. \quad (\text{A.5c})$$

In addition to the derivative operators $D, \Delta, \delta, \bar{\delta}$ defined in (A.2), the operators introduced by Geroch-Held-Penrose (GHP) [226] may also be used for convenience:

$$\mathfrak{D}f \equiv (D - p\epsilon - q\bar{\epsilon})f, \quad \mathfrak{D}'f \equiv (\Delta - p\gamma - q\bar{\gamma})f, \quad (\text{A.6a})$$

$$\bar{\mathfrak{D}}f \equiv (\delta - p\beta - q\bar{\alpha})f, \quad \bar{\mathfrak{D}}'f \equiv (\bar{\delta} - p\alpha - q\bar{\beta})f, \quad (\text{A.6b})$$

where f is a scalar of weight (p, q) .

The PDE system

The system of [132] consists of the evolution equations for the metric components, the Ricci rotation coefficients and the Weyl scalars. The first set is obtained by the tetrad commutation relations and reads

$$DP + \gamma + \bar{\gamma} - \bar{\tau}Q - \tau\bar{Q} = 0, \quad (\text{A.7a})$$

$$DR^a - \bar{\tau}S^a - \tau\bar{S}^a = 0, \quad (\text{A.7b})$$

$$DQ + \bar{\alpha} + \beta - \bar{\rho}Q - \rho\bar{Q} = 0, \quad (\text{A.7c})$$

$$DS^a - \bar{\rho}S^a - \rho\bar{S}^a = 0. \quad (\text{A.7d})$$

The second set comes from the Ricci identities

$$D\rho - \rho^2 + \sigma\bar{\sigma} = 0, \quad (\text{A.8a})$$

$$D\sigma - \rho\sigma - \bar{\rho}\bar{\sigma} - \Psi_0 = 0, \quad (\text{A.8b})$$

$$D\tau - \rho\tau - \sigma\bar{\tau} - \Psi_1 = 0, \quad (\text{A.8c})$$

$$D\alpha - \rho\alpha - \bar{\sigma}\beta = 0, \quad (\text{A.8d})$$

$$D\beta - \sigma\alpha - \bar{\rho}\beta - \Psi_1 = 0, \quad (\text{A.8e})$$

$$D\gamma - \tau\alpha - \bar{\tau}\beta - \Psi_2 = 0, \quad (\text{A.8f})$$

$$D\lambda - \rho\lambda - \bar{\sigma}\mu = 0, \quad (\text{A.8g})$$

$$D\mu - \bar{\rho}\mu - \sigma\lambda - \Psi_2 = 0, \quad (\text{A.8h})$$

$$D\nu - \bar{\tau}\mu - \tau\lambda - \Psi_3 = 0. \quad (\text{A.8i})$$

Notice that these two sets involve equations that in the principal part are advections purely along l^μ . This is not true for the Weyl scalars though. Using the Bianchi identities one can

obtain

$$(\mathfrak{p}' + \mu)\Psi_0 - (\mathfrak{d} - 4\tau)\Psi_1 - 3\sigma\Psi_2 = 0, \quad (\text{A.9a})$$

$$(D + \mathfrak{p}' + 2\mu - 4\rho)\Psi_1 - (\mathfrak{d} - 3\tau)\Psi_2 - (\mathfrak{d}' + \nu)\Psi_0 - 2\sigma\Psi_3 = 0, \quad (\text{A.9b})$$

$$(D + \mathfrak{p}' + 3\mu - 3\rho)\Psi_2 - (\mathfrak{d} - 2\tau)\Psi_3 - (\mathfrak{d}' + 2\nu)\Psi_1 + \lambda\Psi_0 - \sigma\Psi_4 = 0, \quad (\text{A.9c})$$

$$(D + \mathfrak{p}' + 4\mu - 2\rho)\Psi_3 - (\mathfrak{d} - \tau)\Psi_4 - (\mathfrak{d}' + 3\nu)\Psi_2 + 2\lambda\Psi_1 = 0, \quad (\text{A.9d})$$

$$(D - \rho)\Psi_4 - \mathfrak{d}'\Psi_3 + 3\lambda\Psi_2 = 0. \quad (\text{A.9e})$$

The spin and boost weights (p, q) of the Weyl scalars are $(4, 0)$, $(2, 0)$, $(0, 0)$, $(-2, 0)$, $(-4, 0)$ for $\Psi_0, \Psi_1, \Psi_2, \Psi_3, \Psi_4$ respectively [225].

The unknowns of the system can be collected in the state vector $\mathbf{v} \equiv (\Psi, \Gamma, \mathbf{g})^T$ with

$$\begin{aligned} \Psi &\equiv (\Psi_0, \Psi_1, \Psi_2, \Psi_3, \Psi_4)^T, \\ \Gamma &\equiv (\rho, \sigma, \tau, \alpha, \beta, \gamma, \lambda, \mu, \nu), \\ \mathbf{g} &\equiv (P, R^\theta, R^\phi, Q, S^\theta, S^\phi). \end{aligned} \quad (\text{A.10})$$

The source terms involve coupling between the above terms and their complex conjugates. The principal part $\mathcal{A}^\mu \partial_\mu \mathbf{v} \simeq 0$ of the system (A.9), (A.8), (A.7) has the structure

$$\mathcal{A}^\mu = \begin{pmatrix} \mathcal{D}_\Psi^\mu & 0 & 0 \\ 0 & \mathcal{D}_\Gamma^\mu & 0 \\ 0 & 0 & \mathcal{D}_\mathbf{g}^\mu \end{pmatrix}, \quad (\text{A.11})$$

with

$$\mathcal{D}_\Psi^\mu \equiv \begin{pmatrix} n^\mu & -m^\mu & 0 & 0 & 0 \\ -\bar{m}^\mu & l^\mu + n^\mu & -m^\mu & 0 & 0 \\ 0 & -\bar{m}^\mu & l^\mu + n^\mu & -m^\mu & 0 \\ 0 & 0 & -\bar{m}^\mu & l^\mu + n^\mu & -m^\mu \\ 0 & 0 & 0 & -\bar{m}^\mu & l^\mu \end{pmatrix}, \quad (\text{A.12a})$$

$$\mathcal{D}_\Gamma^\mu \equiv id_9 \times l^\mu, \quad (\text{A.12b})$$

$$\mathcal{D}_\mathbf{g}^\mu \equiv id_6 \times l^\mu, \quad (\text{A.12c})$$

where id_n denotes the $n \times n$ identity matrix. The matrix \mathcal{A}^μ is Hermitian and positive

definite with respect to the timelike direction $t^\mu \equiv l^\mu + n^\mu$ i.e.

$$\mathcal{A}^t \equiv \mathcal{A}^\mu t_\mu = \text{diag}(1, 2, 2, 2, d_{16}), \quad (\text{A.13})$$

where $d_n \equiv \text{diag}(id_n)$. This system is symmetric hyperbolic with respect to the timelike direction t^μ [132].

To understand the propagation speed of the variables let us consider the spacelike direction $\rho^\mu \equiv l^\mu - n^\mu$. With respect to this direction the principal part reads

$$\mathcal{A}^\rho \equiv \mathcal{A}^\mu \rho_\mu = \text{diag}(1, 0, 0, 0, -d_{16}). \quad (\text{A.14})$$

This yields that Ψ_0 is ingoing at the speed of light, Ψ_1, Ψ_2, Ψ_3 have vanishing propagation speed (static) and $\Psi_4, \Gamma, \mathbf{g}$ are outgoing at the speed of light. For completeness

$$\mathcal{A}^l \equiv \mathcal{A}^\mu l_\mu = \text{diag}(d_4, 0 \times d_{16}), \quad (\text{A.15a})$$

$$\mathcal{A}^n \equiv \mathcal{A}^\mu n_\mu = \text{diag}(0, d_{19}), \quad (\text{A.15b})$$

where the tetrad calculus (A.5) has been applied.

APPENDIX B

Appendix for part II

B.1 Radial equations

For completeness, here we list the radial equations obtained from the metric ansatz (8.7). It is convenient to introduce the following operators to make the expressions more compact

$$\begin{aligned}
 f' &\equiv \partial_r f, \\
 \dot{f} &\equiv \left(\partial_t + \frac{A}{2} \partial_r \right) f, \\
 \tilde{f} &\equiv (\partial_x - F_x \partial_r) f, \\
 \hat{f} &\equiv (\partial_y - F_y \partial_r) f, \\
 \bar{f} &\equiv \left(\partial_x^2 - 2F_x \partial_r \partial_x + F_x^2 \partial_r^2 \right) f, \\
 f^* &\equiv \left(\partial_y^2 - 2F_y \partial_r \partial_y + F_y^2 \partial_r^2 \right) f, \\
 f^\times &\equiv \left(\partial_x \partial_y - F_x \partial_r \partial_y - F_y \partial_r \partial_x + F_x F_y \partial_r^2 \right) f.
 \end{aligned} \tag{B.1}$$

As shown in Table 8.1, by combining Einstein's equations (8.2) in a particular way we obtain a nested system of radial effective ODEs where one can sequentially solve for the different variables. For this particular case, some of these intrinsic equations are coupled.

$$6S'' + S \left(\cosh^2(G) (B_1')^2 + 3(B_2')^2 + (G')^2 + (\phi')^2 \right) = 0, \tag{B.2}$$

$$\begin{aligned}
 &2e^{B_1} S^2 F_x'' + e^{B_1} \left(S^2 \left(-2 \left(\cosh^2(G) (\tilde{B}_1' - B_1' F_x') + B_2' (3\tilde{B}_2 - F_x') + \right. \right. \right. \\
 &\quad \left. \left. \left. \tilde{G} (B_1' \sinh(2G) + G') + \tilde{B}_2' + 4\tilde{\phi}\phi' \right) - 2\tilde{B}_1 B_1' \cosh^2(G) \right) + S \left(-6\tilde{S} \left(B_1' \cosh^2(G) + B_2' \right) - \right. \\
 &\quad \left. 8\tilde{S}' + 2S' F_x' \right) + 8\tilde{S} S' \right) + S^2 \left(-2G' \left(\hat{B}_1 + F_y' \right) + \sinh(2G) \left(\hat{B}_1' - B_1' \left(\hat{B}_1 + F_y' \right) \right) + \right. \\
 &\quad \left. 2\hat{G} B_1' \cosh(2G) + 2\hat{G}' \right) + 3\hat{S} S \left(B_1' \sinh(2G) + 2G' \right) = 0,
 \end{aligned} \tag{B.3}$$

$$\begin{aligned}
& 2S^2 F_y'' + e^{B_1} \left(S^2 \left(2 \left(G' \left(\tilde{B}_1 - F_x' \right) + \tilde{G}' \right) - \sinh(2G) \left(B_1' \left(\tilde{B}_1 - F_x' \right) + \tilde{B}_1' \right) - \right. \right. \\
& \quad \left. \left. 2\tilde{G}B_1' \cosh(2G) \right) - 3S\tilde{S} \left(B_1' \sinh(2G) - 2G' \right) \right) + 2S^2 \left(\cosh^2(G) \left(\hat{B}_1' - B_1' F_y' \right) + \right. \\
& \quad \left. B_2' \left(F_y' - 3\hat{B}_2 \right) + \hat{G} \left(B_1' \sinh(2G) - G' \right) - \hat{B}_1 B_1' \cosh^2(G) - \hat{B}_2' - 4\hat{\phi}\phi' \right) + \\
& \quad S \left(6\hat{S} \left(B_1' \cosh^2(G) - B_2' \right) + 2S' F_y' - 8\hat{S}' \right) + 8\hat{S}S' = 0, \tag{B.4}
\end{aligned}$$

$$\begin{aligned}
& 12e^{B_1} S^3 \dot{S}' + e^{B_1+B_2} \left(S^2 \left(2 \cosh(G) \left(-\hat{G} \left(\tilde{B}_1 + \tilde{B}_2 - F_x' \right) + \tilde{G} \left(\hat{B}_1 - \hat{B}_2 + F_y' \right) + \right. \right. \right. \\
& \quad \left. \left. G' \left(\tilde{F}_y + \hat{F}_x \right) - 2G^\times \right) + 2 \sinh(G) \left(B_2' \left(\tilde{F}_y + \hat{F}_x \right) + F_y' \left(\tilde{B}_2 - F_x' \right) + \hat{B}_2 \left(F_x' - 4\tilde{B}_2 \right) - \right. \right. \\
& \quad \left. \left. 2B_2^\times + \tilde{F}_y' - 2\hat{G}\tilde{G} - 4\hat{\phi}\tilde{\phi} + \hat{F}_x' \right) \right) + S \left(2 \sinh(G) \left(\hat{S} \left(F_x' - 4\tilde{B}_2 \right) + \tilde{S} \left(F_y' - 4\hat{B}_2 \right) + \right. \right. \\
& \quad \left. \left. 4S' \left(\tilde{F}_y + \hat{F}_x \right) - 8S^\times \right) - 8 \cosh(G) \left(\hat{S}\tilde{G} + \hat{G}\tilde{S} \right) \right) + 8\hat{S}\tilde{S} \sinh(G) + \\
& \quad e^{2B_1+B_2} \left(S^2 \left(2 \sinh(G) \left(\tilde{G} \left(2\tilde{B}_1 + \tilde{B}_2 - F_x' \right) - G' \tilde{F}_x + \tilde{G} \right) + \right. \right. \\
& \quad \left. \left. \cosh(G) \left(2 \left(- \left(B_1' + B_2' \right) \tilde{F}_x + \tilde{B}_1 + \tilde{B}_2 - \tilde{F}_x' + \tilde{G}^2 + 2\tilde{\phi}^2 \right) - 2 \left(\tilde{B}_1 + \tilde{B}_2 \right) F_x' + \right. \right. \right. \\
& \quad \left. \left. 2 \left(\tilde{B}_1^2 + \tilde{B}_2 \tilde{B}_1 + 2\tilde{B}_2^2 \right) + \left(F_x' \right)^2 \right) \right) + S \left(2 \cosh(G) \left(\tilde{S} \left(4 \left(\tilde{B}_1 + \tilde{B}_2 \right) - F_x' \right) + 4 \left(\tilde{S} - S' \tilde{F}_x \right) \right) + \right. \\
& \quad \left. 8\tilde{G}\tilde{S} \sinh(G) \right) - 4\tilde{S}^2 \cosh(G) + e^{B_2} \left(S^2 \left(2 \sinh(G) \left(\hat{G} \left(-2\hat{B}_1 + \hat{B}_2 - F_y' \right) - \hat{F}_y G' + G^\star \right) + \right. \right. \\
& \quad \left. \left. \cosh(G) \left(2 \left(\left(B_1' - B_2' \right) \hat{F}_y - B_1^\star + B_2^\star - \hat{F}_y' + \hat{G}^2 + 2\hat{\phi}^2 \right) + 2 \left(\hat{B}_1 - \hat{B}_2 \right) F_y' + \right. \right. \right. \\
& \quad \left. \left. 2 \left(\hat{B}_1^2 - \hat{B}_2 \hat{B}_1 + 2\hat{B}_2^2 \right) + \left(F_y' \right)^2 \right) \right) + S \left(8\hat{G}\hat{S} \sinh(G) - 2 \cosh(G) \left(\hat{S} \left(4\hat{B}_1 - 4\hat{B}_2 + F_y' \right) + \right. \right. \\
& \quad \left. \left. 4\hat{F}_y S' - 4S^\star \right) \right) - 4\hat{S}^2 \cosh(G) + e^{B_1} \left(8S^4 V(\phi) + 24\dot{S}S^2 S' \right) = 0, \tag{B.5}
\end{aligned}$$

$$\begin{aligned}
& 12e^{B_1} S^4 \dot{B}_1' + e^{B_1+B_2} \left(6S^2 \operatorname{sech}(G) \left(\hat{G} \left(F_x' - \tilde{B}_2 \right) + \tilde{G} \left(\hat{B}_2 - F_y' \right) + G' \left(\tilde{F}_y - \hat{F}_x \right) \right) + \right. \\
& \quad \left. 6S \operatorname{sech}(G) \left(\hat{S}\tilde{G} - \hat{G}\tilde{S} \right) \right) + e^{2B_1+B_2} \left(-3S^2 \operatorname{sech}(G) \left(-2B_2' \tilde{F}_x - 2\tilde{B}_2 F_x' + 4\tilde{B}_2^2 + 2\tilde{B}_2 - 2\tilde{F}_x' + \right. \right. \\
& \quad \left. \left. 4\tilde{\phi}^2 + \left(F_x' \right)^2 \right) - 6S \operatorname{sech}(G) \left(\tilde{S} \left(\tilde{B}_2 + 2F_x' \right) - S' \tilde{F}_x + \tilde{S} \right) + 12\tilde{S}^2 \operatorname{sech}(G) \right) + \\
& \quad e^{B_2} \left(3S^2 \operatorname{sech}(G) \left(-2B_2' \hat{F}_y - 2\hat{B}_2 F_y' + 4\hat{B}_2^2 + 2B_2^\star + \left(F_y' \right)^2 - 2\hat{F}_y' + 4\hat{\phi}^2 \right) + \right. \\
& \quad \left. 6S \operatorname{sech}(G) \left(\hat{S} \left(\hat{B}_2 + 2F_y' \right) - \hat{F}_y S' + S^\star \right) - 12\hat{S}^2 \operatorname{sech}(G) \right) + e^{B_1} \left(12S^4 \tanh(G) \left(\dot{B}_1 G' + \dot{G} B_1' \right) + \right. \\
& \quad \left. 18S^3 \left(\dot{B}_1 S' + \dot{S} B_1' \right) \right) = 0 \tag{B.6}
\end{aligned}$$

$$\begin{aligned}
& 12e^{B_1} S^4 \dot{G}' + e^{B_1+B_2} \left(6S^2 \cosh(G) \left(B_1' (\hat{F}_x - \tilde{F}_y) - B_2' (\tilde{F}_y + \hat{F}_x) + (\hat{B}_1 - F_y') (\tilde{B}_2 - F_x') - \right. \right. \\
& \hat{B}_2 (\tilde{B}_1 - 4\tilde{B}_2 + F_x') + \tilde{B}_1 F_y' + 2B_2^\times - \tilde{F}_y' + 4\hat{\phi}\tilde{\phi} - \hat{F}_x' \left. \right) + 6S \cosh(G) \left(\hat{S} (-\tilde{B}_1 + \tilde{B}_2 + 2F_x') + \right. \\
& \tilde{S} (\hat{B}_1 + \hat{B}_2 + 2F_y') - S' (\tilde{F}_y + \hat{F}_x) + 2S^\times \left. \right) - 24\hat{S}\tilde{S} \cosh(G) \left. \right) + \\
& e^{2B_1+B_2} \left(-3S^2 \sinh(G) \left(-2B_2' \tilde{F}_x - 2\tilde{B}_2 F_x' + 4\tilde{B}_2^2 + 2\tilde{B}_2 - 2\tilde{F}_x' + 4\tilde{\phi}^2 + (F_x')^2 \right) - \right. \\
& 6S \sinh(G) \left(\tilde{S} (\tilde{B}_2 + 2F_x') - S' \tilde{F}_x + \tilde{S} \right) + 12\tilde{S}^2 \sinh(G) \left. \right) + e^{B_2} \left(-3S^2 \sinh(G) \left(-2B_2' \hat{F}_y - \right. \right. \\
& 2\hat{B}_2 F_y' + 4\hat{B}_2^2 + 2B_2^\times + (F_y')^2 - 2\hat{F}_y' + 4\hat{\phi}^2 \left. \right) - 6S \sinh(G) \left(\hat{S} (\hat{B}_2 + 2F_y') - \hat{F}_y S' + S^\times \right) + \\
& 12\hat{S}^2 \sinh(G) \left. \right) + e^{B_1} \left(18S^3 (\dot{S}G' + \dot{G}S') - 6\dot{B}_1 S^4 B_1' \sinh(2G) \right) = 0 \tag{B.7}
\end{aligned}$$

$$\begin{aligned}
& 12e^{B_1} S^4 \dot{B}_2' + e^{B_1+B_2} \left(S^2 \left(2 \cosh(G) \left(\hat{G} (\tilde{B}_1 - 2\tilde{B}_2 - F_x') - \tilde{G} (\hat{B}_1 + 2\hat{B}_2 + F_y') - \right. \right. \right. \\
& G' (\tilde{F}_y + \hat{F}_x) + 2G^\times \left. \right) + 2 \sinh(G) \left(2B_2' (\tilde{F}_y + \hat{F}_x) + F_y' (2\tilde{B}_2 + F_x') + 2\hat{B}_2 (F_x' - \tilde{B}_2) - \right. \\
& 4B_2^\times - \tilde{F}_y' + 2\hat{G}\tilde{G} + 4\hat{\phi}\tilde{\phi} - \hat{F}_x' \left. \right) \left. \right) + S \left(2 \sinh(G) \left(2 \left(\hat{S} (F_x' - \tilde{B}_2) + \tilde{S} (F_y' - \hat{B}_2) + S^\times \right) - \right. \right. \\
& S' (\tilde{F}_y + \hat{F}_x) \left. \right) + 2 \cosh(G) \left(\hat{S}\tilde{G} + \hat{G}\tilde{S} \right) - 8\hat{S}\tilde{S} \sinh(G) \left. \right) + \\
& e^{2B_1+B_2} \left(S^2 \left(2 \sinh(G) \left(\tilde{G} (-2\tilde{B}_1 + 2\tilde{B}_2 + F_x') + G' \tilde{F}_x - \tilde{G} \right) - \right. \right. \\
& \cosh(G) \left(2 \left(-(B_1' - 2B_2') \tilde{F}_x + \tilde{B}_1 - 2\tilde{B}_2 - \tilde{F}_x' + \tilde{G}^2 + 2\tilde{\phi}^2 \right) - 2 \left(\tilde{B}_1 - 2\tilde{B}_2 \right) F_x' + \right. \\
& 2 \left(\tilde{B}_1^2 - 2\tilde{B}_2 \tilde{B}_1 - \tilde{B}_2^2 \right) + (F_x')^2 \left. \right) \left. \right) + S \left(-2 \cosh(G) \left(\tilde{S} (\tilde{B}_1 - 2\tilde{B}_2 + 2F_x') - S' \tilde{F}_x + \tilde{S} \right) - \right. \\
& 2\tilde{G}\tilde{S} \sinh(G) \left. \right) + 4\tilde{S}^2 \cosh(G) \left. \right) + e^{B_2} \left(S^2 \left(2 \sinh(G) \left(\hat{G} \left(2 \left(\hat{B}_1 + \hat{B}_2 \right) + F_y' \right) + \hat{F}_y G' - G^\times \right) - \right. \right. \\
& \cosh(G) \left(2 \left((B_1' + 2B_2') \hat{F}_y - B_1^\times - 2B_2^\times - \hat{F}_y' + \hat{G}^2 + 2\hat{\phi}^2 \right) + 2 \left(\hat{B}_1 + 2\hat{B}_2 \right) F_y' + \right. \\
& 2 \left(\hat{B}_1^2 + 2\hat{B}_2 \hat{B}_1 - \hat{B}_2^2 \right) + (F_y')^2 \left. \right) \left. \right) + S \left(2 \cosh(G) \left(\hat{S} (\hat{B}_1 + 2\hat{B}_2 - 2F_y') + \hat{F}_y S' - S^\times \right) - \right. \\
& 2\hat{G}\hat{S} \sinh(G) \left. \right) + 4\hat{S}^2 \cosh(G) \left. \right) + 18e^{B_1} S^3 (\dot{B}_2 S' + \dot{S} B_2') = 0 \tag{B.8}
\end{aligned}$$

$$\begin{aligned}
& 8e^{B_1} S^3 \dot{\phi}' + e^{B_1+B_2} \left(S \left(4 \sinh(G) \left(\hat{\phi} (F_x' - \tilde{B}_2) + \tilde{\phi} (F_y' - \hat{B}_2) + \phi' (\tilde{F}_y + \hat{F}_x) - 2\phi^\times \right) - \right. \right. \\
& 4 \cosh(G) \left(\hat{\phi}\tilde{G} + \hat{G}\tilde{\phi} \right) - 4 \sinh(G) \left(\hat{\phi}\tilde{S} + \hat{S}\tilde{\phi} \right) \left. \right) + e^{2B_1+B_2} \left(4S \left(\cosh(G) \left(\tilde{\phi} (\tilde{B}_1 + \tilde{B}_2 - F_x') - \right. \right. \right. \\
& \phi' \tilde{F}_x + \tilde{\phi} \left. \right) + \tilde{G}\tilde{\phi} \sinh(G) \left. \right) + 4\tilde{S}\tilde{\phi} \cosh(G) \left. \right) + e^{B_2} \left(S \left(4\hat{G}\hat{\phi} \sinh(G) - 4 \cosh(G) \left(\hat{\phi} (\hat{B}_1 - \right. \right. \right. \\
& \hat{B}_2 + F_y') + \hat{F}_y \phi' - \phi^\times \left. \right) \left. \right) + 4\hat{S}\hat{\phi} \cosh(G) \left. \right) + e^{B_1} \left(12S^2 (\dot{\phi}S' + \dot{S}\phi') - 4S^3 V'(\phi) \right) = 0 \tag{B.9}
\end{aligned}$$

$$\begin{aligned}
& 6e^{B_1} S^4 A'' + e^{B_1+B_2} \left(S^2 \left(6 \cosh(G) \left((\hat{B}_2 - \hat{B}_1) \tilde{G} + \hat{G} (\tilde{B}_1 + \tilde{B}_2) - G' (\tilde{F}_y + \hat{F}_x) + 2G^\times \right) + \right. \right. \\
& 6 \sinh(G) \left(-B_2' (\tilde{F}_y + \hat{F}_x) + 2B_2^\times + 4\hat{B}_2 \tilde{B}_2 + 2\hat{G} \tilde{G} + 4\hat{\phi} \tilde{\phi} - F_x' F_y' \right) \left. \right) + 24S \left(\sinh(G) \left(\hat{B}_2 \tilde{S} + \right. \right. \\
& \hat{S} \tilde{B}_2 - S' (\tilde{F}_y + \hat{F}_x) + 2S^\times \left. \right) + \cosh(G) \left(\hat{S} \tilde{G} + \hat{G} \tilde{S} \right) \left. \right) - 24\hat{S} \tilde{S} \sinh(G) \left. \right) + \\
& e^{2B_1+B_2} \left(S^2 \left(3 \cosh(G) \left((F_x')^2 - 2 \left(- (B_1' + B_2') \tilde{F}_x + \tilde{B}_1^2 + 2\tilde{B}_2^2 + \tilde{B}_1 + \tilde{B}_2 + \tilde{B}_1 \tilde{B}_2 + \tilde{G}^2 + \right. \right. \right. \right. \\
& \left. \left. \left. 2\tilde{\phi}^2 \right) \right) - 6 \sinh(G) \left((2\tilde{B}_1 + \tilde{B}_2) \tilde{G} - G' \tilde{F}_x + \tilde{G} \right) \right) + S \left(-24 \cosh(G) \left((\tilde{B}_1 + \tilde{B}_2) \tilde{S} - S' \tilde{F}_x + \right. \right. \\
& \left. \left. \tilde{S} \right) - 24\tilde{G} \tilde{S} \sinh(G) \right) + 12\tilde{S}^2 \cosh(G) \left. \right) + e^{B_2} \left(S^2 \left(6 \sinh(G) \left((2\hat{B}_1 - \hat{B}_2) \hat{G} + \hat{F}_y G' - G^\times \right) + \right. \right. \\
& \left. \left. 3 \cosh(G) \left((F_y')^2 - 2 \left((B_1' - B_2') \hat{F}_y + \hat{B}_1^2 + 2\hat{B}_2^2 - B_1^\times + B_2^\times - \hat{B}_1 \hat{B}_2 + \hat{G}^2 + 2\hat{\phi}^2 \right) \right) \right) + \\
& S \left(24 \cosh(G) \left((\hat{B}_1 - \hat{B}_2) \hat{S} + \hat{F}_y S' - S^\times \right) - 24\hat{G} \hat{S} \sinh(G) \right) + 12\hat{S}^2 \cosh(G) \left. \right) + \\
& e^{B_1} \left(S^4 \left(6 \left(\dot{B}_1 B_1' \cosh^2(G) + 3\dot{B}_2 B_2' + \dot{G} G' + 4\dot{\phi} \phi' + 4 \right) - 2(4V(\phi) + 12) \right) - 72S^2 \dot{S} S' \right) = 0
\end{aligned} \tag{B.10}$$

The following equations (to be solved for \tilde{S} and $\dot{F}_{x,y}$) are not needed for our evolution scheme, but they are used in the equation for the gauge condition $\partial_t \xi$:

$$\begin{aligned}
& 6e^{B_1} \tilde{S} S^3 + e^{B_1+B_2} \left(S^2 \left(\sinh(G) \left(-A' (\tilde{F}_y + \hat{F}_x) + \hat{B}_2 (\tilde{A} + 2\dot{F}_x) + \tilde{B}_2 (\hat{A} + 2\dot{F}_y) + 2A^\times + \right. \right. \right. \\
& \left. \left. \left. 2\tilde{F}_y + 2\hat{F}_x \right) + \cosh(G) \left(\hat{G} (\tilde{A} + 2\dot{F}_x) + \tilde{G} (\hat{A} + 2\dot{F}_y) \right) \right) + S \sinh(G) \left(\hat{S} (\tilde{A} + 2\dot{F}_x) + \right. \right. \\
& \left. \left. \tilde{S} (\hat{A} + 2\dot{F}_y) \right) \right) + e^{2B_1+B_2} \left(S^2 \left(\tilde{G} \sinh(G) \left(-(\tilde{A} + 2\dot{F}_x) \right) - \cosh(G) \left(-A' \tilde{F}_x + \right. \right. \right. \\
& \left. \left. (\tilde{B}_1 + \tilde{B}_2) (\tilde{A} + 2\dot{F}_x) + \tilde{A} + 2\tilde{F}_x \right) \right) - S \tilde{S} \cosh(G) (\tilde{A} + 2\dot{F}_x) - e^{B_1+2B_2} (\hat{F}_x - \tilde{F}_y)^2 + \\
& e^{B_2} \left(S^2 \left(\cosh(G) \left(A' \hat{F}_y + (\hat{B}_1 - \hat{B}_2) (\hat{A} + 2\dot{F}_y) - A^\times - 2\hat{F}_y \right) - \hat{G} \sinh(G) (\hat{A} + 2\dot{F}_y) \right) - \\
& S \hat{S} \cosh(G) (\hat{A} + 2\dot{F}_y) \right) + e^{B_1} \left(S^4 \left(\dot{B}_1^2 \cosh^2(G) + 3\dot{B}_2^2 + \dot{G}^2 + 4\dot{\phi}^2 \right) - 3S^3 \dot{S} A' \right) = 0
\end{aligned} \tag{B.11}$$

$$\begin{aligned}
& 4e^{B_1} S^3 \dot{F}_x' + e^{B_1} \left(2S^3 \left((\tilde{A} + 2\dot{F}_x) \left(B_1' \cosh^2(G) + B_2' \right) + 2\tilde{A}' + 2\tilde{B}_1 \cosh^2(G) + \right. \right. \\
& \left. \left. 2\dot{B}_1 \left(\tilde{B}_1 \cosh^2(G) + \tilde{G} \sinh(2G) \right) + 2\dot{B}_2 + 6\dot{B}_2 \tilde{B}_2 + 2\dot{G} \tilde{G} + 8\dot{\phi} \tilde{\phi} - A' F_x' \right) + \right. \\
& \left. 4S^2 \left(-S' (\tilde{A} + 2\dot{F}_x) + 3\tilde{S} \left(\dot{B}_1 \cosh^2(G) + \dot{B}_2 \right) + 4\tilde{S}' + 3\dot{S} F_x' \right) - 16\dot{S} S \tilde{S} \right) + \\
& e^{B_1+B_2} \left(4S \sinh(G) \left(\hat{F}_x \left(F_x' - 2\tilde{B}_2 \right) + 2\tilde{B}_2 \tilde{F}_y - \tilde{F}_x F_y' - F_x^\times + \tilde{F}_y \right) + 4\tilde{S} \sinh(G) \left(\hat{F}_x - \tilde{F}_y \right) \right) + \\
& e^{B_2} \left(4S \cosh(G) \left(2\hat{B}_2 \left(\hat{F}_x - \tilde{F}_y \right) + \tilde{F}_y F_y' - F_y^\times - \hat{F}_y F_x' + F_x^\times \right) + 4\hat{S} \cosh(G) \left(\tilde{F}_y - \hat{F}_x \right) \right) + \\
& S^3 \left(-(\hat{A} + 2\dot{F}_y) \left(B_1' \sinh(2G) + 2G' \right) + 4\hat{B}_1 \dot{G} - 2\hat{B}_1 \sinh(2G) + 2\dot{B}_1 \left(\hat{B}_1 \sinh(2G) - \right. \right. \\
& \left. \left. 2\hat{G} \cosh(2G) \right) - 4\hat{G} \right) - 6\hat{S} S^2 \left(\dot{B}_1 \sinh(2G) + 2\dot{G} \right) = 0
\end{aligned} \tag{B.12}$$

$$\begin{aligned}
& 4S^3 \dot{F}_y' + e^{B_1} \left(S^3 \left((\tilde{A} + 2\dot{F}_x) (B_1' \sinh(2G) - 2G') - 4\dot{G}\tilde{B}_1 + 2\tilde{B}_1 \sinh(2G) + \right. \right. \\
& \left. \left. 2\dot{B}_1 (\tilde{B}_1 \sinh(2G) + 2\tilde{G} \cosh(2G)) - 4\tilde{G} \right) + 6S^2 \tilde{S} (\dot{B}_1 \sinh(2G) - 2\dot{G}) \right) + \\
& e^{B_2} \left(4S \sinh(G) \left(2\hat{B}_2 (\hat{F}_x - \tilde{F}_y) + \tilde{F}_y F_y' - F_y^\times - \hat{F}_y F_x' + F_x^* \right) + 4\hat{S} \sinh(G) (\tilde{F}_y - \hat{F}_x) \right) + \\
& e^{B_1+B_2} \left(4S \cosh(G) \left(\hat{F}_x (F_x' - 2\tilde{B}_2) + 2\tilde{B}_2 \tilde{F}_y - \tilde{F}_x F_y' - F_x^\times + \tilde{F}_y \right) + 4\tilde{S} \cosh(G) (\hat{F}_x - \tilde{F}_y) \right) + \\
& 2S^3 \left(-A' F_y' - (\hat{A} + 2\dot{F}_y) (B_1' \cosh^2(G) - B_2') + 2\hat{A}' - 2\hat{B}_1 \cosh^2(G) + 2\dot{B}_1 (\hat{B}_1 \cosh^2(G) - \right. \\
& \left. \hat{G} \sinh(2G)) + 2\hat{B}_2 + 6\dot{B}_2 \hat{B}_2 + 2\dot{G}\hat{G} + 8\dot{\phi}\hat{\phi} \right) + 4S^2 \left(-S' (\hat{A} + 2\dot{F}_y) + \right. \\
& \left. 3\hat{S} (\dot{B}_2 - \dot{B}_1 \cosh^2(G)) + 3\dot{S} F_y' + 4\hat{S} \right) - 16\dot{S}\hat{S}S = 0
\end{aligned} \tag{B.13}$$

B.2 Apparent horizon finder

In order to find the AH we need to compute the expansion of the outgoing null rays. We can construct the tangent vector to the outgoing rays using the ingoing null rays, n , together with the form perpendicular to the AH, s ,

$$\begin{aligned}
s &= N_s (-\partial_t \sigma dt - \partial_y \sigma dy - \partial_y \sigma dy + dr) \\
n &= -N_n \partial_r,
\end{aligned} \tag{B.14}$$

from where we can compute the vector s by simply raising the indices. The normalization factors, N_s and N_n , can be computed by imposing $s^2 = 1$ and $s \cdot n = -1/\sqrt{2}$. Combining these two vectors we can construct another vector tangent to outgoing trajectories,

$$l^\mu = \sqrt{2}s^\mu + n^\mu, \tag{B.15}$$

so that it is null, $l^2 = 0$, and properly normalized, $l \cdot n = -1$. The expansion of these rays can be computed as

$$\theta_l = h^{\mu\nu} \nabla_\mu l_\nu, \tag{B.16}$$

where

$$h_{\mu\nu} = g_{\mu\nu} + l_\mu n_\nu + l_\nu n_\mu \tag{B.17}$$

is the induced metric over hypersurfaces normal to both in- and out-going null rays. The AH location is given by the condition $\theta_l = 0$. Imposing it at a generic surface, $r = \sigma(x, y)$,

we obtain the following equation:

$$\begin{aligned}
& 2e^{B_2} (F_y + \partial_y \sigma) \left(S \left(e^{B_1} \cosh(G) \left(\tilde{G} + G' (F_x + \partial_x \sigma) \right) + e^{B_1} \sinh(G) \left(\tilde{B}_2 + B'_2 (F_x + \partial_x \sigma) \right) + \right. \right. \\
& \left. \left. \cosh(G) \left(B'_1 (F_y + \partial_y \sigma) + \hat{B}_1 \right) - \cosh(G) \left(B'_2 (F_y + \partial_y \sigma) + \hat{B}_2 \right) - \sinh(G) \left(G' (F_y + \partial_y \sigma) + \hat{G} \right) \right) + e^{B_1} \sinh(G) \left(\tilde{S} - 2S' (F_x + \partial_x \sigma) \right) - \cosh(G) \left(S' (F_y + \partial_y \sigma) + \hat{S} \right) \right) - 2e^{B_1+B_2} (F_x + \\
& \partial_x \sigma) \left(S \left(e^{B_1} \left(\cosh(G) \left(\tilde{B}_1 + B'_1 (F_x + \partial_x \sigma) \right) + \cosh(G) \left(\tilde{B}_2 + B'_2 (F_x + \partial_x \sigma) \right) + \right. \right. \right. \\
& \left. \left. \sinh(G) \left(\tilde{G} + G' (F_x + \partial_x \sigma) \right) \right) - \sinh(G) \left(B'_2 (F_y + \partial_y \sigma) + \hat{B}_2 \right) - \cosh(G) \left(G' (F_y + \partial_y \sigma) + \hat{G} \right) \right) + e^{B_1} \cosh(G) \left(\tilde{S} + S' (F_x + \partial_x \sigma) \right) - \sinh(G) \left(S' (F_y + \partial_y \sigma) + \hat{S} \right) \right) + \\
& S \left(e^{B_1} \left(2e^{B_2} \sinh(G) \left(\tilde{F}_y + F'_y (F_x + \partial_x \sigma) + \partial_{xy} \sigma \right) - 2e^{B_1+B_2} \cosh(G) \left(\tilde{F}_x + F'_x (F_x + \partial_x \sigma) + \right. \right. \right. \\
& \left. \left. \partial_{xx} \sigma \right) + 6S\dot{S} \right) + 2e^{B_1+B_2} \sinh(G) \left(F'_x (F_y + \partial_y \sigma) + \hat{F}_x + \partial_{xy} \sigma \right) - 2e^{B_2} \cosh(G) \left(F'_y (F_y + \right. \\
& \left. \partial_y \sigma) + \hat{F}_y + \partial_{yy} \sigma \right) \left. \right) + 3e^{2B_1+B_2} \cosh(G) S' (F_x + \partial_x \sigma)^2 + 3e^{B_2} \cosh(G) S' (F_y + \partial_y \sigma)^2 = 0, \tag{B.18}
\end{aligned}$$

where every function is evaluated at the $r = \sigma(x, y)$ surface defining the AH. When the AH is located surfaces of constant radius, which is what we impose to find the evolution equation for the gauge function ξ , then Eq. (B.18) reduces to

$$\begin{aligned}
\Theta \equiv & -2e^{B_1+B_2} F_x \left(S \left(e^{B_1} \left(\cosh(G) \left(\tilde{B}_1 + B'_1 F_x \right) + \cosh(G) \left(\tilde{B}_2 + B'_2 F_x \right) + \right. \right. \right. \\
& \left. \left. \sinh(G) \left(\tilde{G} + F_x G' \right) \right) - \sinh(G) \left(B'_2 F_y + \hat{B}_2 \right) - \cosh(G) \left(F_y G' + \hat{G} \right) \right) + e^{B_1} \cosh(G) \left(\tilde{S} + \right. \\
& \left. F_x S' \right) - \sinh(G) \left(F_y S' + \hat{S} \right) \left. \right) + 2e^{B_2} F_y \left(S \left(e^{B_1} \cosh(G) \left(\tilde{G} + F_x G' \right) + e^{B_1} \sinh(G) \left(\tilde{B}_2 + \right. \right. \right. \\
& \left. \left. B'_2 F_x \right) + \cosh(G) \left(B'_1 F_y + \hat{B}_1 \right) - \cosh(G) \left(B'_2 F_y + \hat{B}_2 \right) - \sinh(G) \left(F_y G' + \hat{G} \right) \right) + \\
& e^{B_1} \sinh(G) \left(\tilde{S} - 2F_x S' \right) - \cosh(G) \left(F_y S' + \hat{S} \right) \left. \right) + S \left(e^{B_1} \left(2e^{B_2} \sinh(G) \left(\tilde{F}_y + F_x F'_y \right) - \right. \right. \\
& \left. \left. 2e^{B_1+B_2} \cosh(G) \left(\tilde{F}_x + F_x F'_x \right) + 6S\dot{S} \right) + 2e^{B_1+B_2} \sinh(G) \left(F_y F'_x + \hat{F}_x \right) - \right. \\
& \left. 2e^{B_2} \cosh(G) \left(F_y F'_y + \hat{F}_y \right) \right) + 3e^{2B_1+B_2} F_x^2 \cosh(G) S' + 3e^{B_2} F_y^2 \cosh(G) S' = 0. \tag{B.19}
\end{aligned}$$

To start with initial data that satisfies $\Theta|_{r=\text{const}} = 0$ we first need to find the AH and adjust ξ accordingly. Solving the Eq. (B.18) provides us the location of the AH at a given time slice t . Contrary to what we have found so far this equation is non-linear, with the form

$$\begin{aligned}
\mathcal{L} \left(\sigma, \partial \sigma, \partial^2 \sigma \right) = & \alpha_{xx}(t, \sigma, x, y) \partial_{xx} \sigma + \alpha_{xy}(t, \sigma, x, y) \partial_{xy} \sigma + \alpha_{yy}(t, \sigma, x, y) \partial_{yy} \sigma \\
& + \beta_{xx}(t, \sigma, x, y) (\partial_x \sigma)^2 + \beta_{xy}(t, \sigma, x, y) \partial_x \sigma \partial_y \sigma + \beta_{yy}(t, \sigma, x, y) (\partial_y \sigma)^2 \\
& + \gamma_x(t, \sigma, x, y) \partial_x \sigma + \gamma_y(t, \sigma, x, y) \partial_y \sigma + \delta(t, \sigma, x, y) = 0, \tag{B.20}
\end{aligned}$$

where

$$\alpha_{xx} = -e^{B_1+B_2} S \cosh(G),$$

$$\begin{aligned}
\alpha_{xy} &= 2e^{B_2} S \sinh(G), \\
\alpha_{yy} &= -e^{B_2-B_1} S \cosh(G), \\
\beta_{xx} &= \frac{1}{2} e^{B_1+B_2} (\cosh(G)S' - 2S (B_1' \cosh(G) + B_2' \cosh(G) + G' \sinh(G))), \\
\beta_{xy} &= e^{B_2} (2S (B_2' \sinh(G) + G' \cosh(G)) - \sinh(G)S'), \\
\beta_{yy} &= \frac{1}{2} e^{B_2-B_1} (2S (B_1' \cosh(G) - B_2' \cosh(G) + G'(-\sinh(G))) + \cosh(G)S'), \\
\gamma_x &= e^{B_2} \left(S \left(-e^{B_1} \tilde{G} \sinh(G) - e^{B_1} \tilde{B}_1 \cosh(G) - e^{B_1} \tilde{B}_2 \cosh(G) - 2e^{B_1} F_x G' \sinh(G) \right. \right. \\
&\quad \left. \left. - 2e^{B_1} B_1' F_x \cosh(G) - 2e^{B_1} B_2' F_x \cosh(G) - e^{B_1} \cosh(G) F_x' + 2B_2' F_y \sinh(G) + \hat{B}_2 \sinh(G) \right. \right. \\
&\quad \left. \left. + 2F_y G' \cosh(G) + \sinh(G) F_y' + \hat{G} \cosh(G) \right) - e^{B_1} \tilde{S} \cosh(G) + e^{B_1} F_x \cosh(G) S' \right. \\
&\quad \left. - F_y \sinh(G) S' + \hat{S} \sinh(G) \right), \\
\gamma_y &= e^{B_2-B_1} \left(S \left(e^{B_1} \tilde{B}_2 \sinh(G) + e^{B_1} \tilde{G} \cosh(G) + 2e^{B_1} F_x G' \cosh(G) + 2e^{B_1} B_2' F_x \sinh(G) \right. \right. \\
&\quad \left. \left. + e^{B_1} \sinh(G) F_x' + 2B_1' F_y \cosh(G) - 2B_2' F_y \cosh(G) + \hat{B}_1 \cosh(G) - \hat{B}_2 \cosh(G) \right. \right. \\
&\quad \left. \left. - 2F_y G' \sinh(G) - \cosh(G) F_y' - \hat{G} \sinh(G) \right) + e^{B_1} \tilde{S} \sinh(G) - e^{B_1} F_x \sinh(G) S' \right. \\
&\quad \left. + F_y \cosh(G) S' + \hat{S}(-\cosh(G)) \right), \\
\delta &= -e^{B_2-B_1} S \left(-F_y \left(e^{B_1} \tilde{B}_2 \sinh(G) + e^{B_1} \tilde{G} \cosh(G) + 2e^{B_1} F_x G' \cosh(G) + 2e^{B_1} B_2' F_x \sinh(G) \right. \right. \\
&\quad \left. \left. + e^{B_1} \sinh(G) F_x' + \hat{B}_1 \cosh(G) - \hat{B}_2 \cosh(G) - \cosh(G) F_y' - \hat{G} \sinh(G) \right) + e^{B_1} F_x \left(e^{B_1} \tilde{G} \sinh(G) \right. \right. \\
&\quad \left. \left. + e^{B_1} \tilde{B}_1 \cosh(G) + e^{B_1} \tilde{B}_2 \cosh(G) + e^{B_1} \cosh(G) F_x' - \hat{B}_2 \sinh(G) - \sinh(G) F_y' - \hat{G} \cosh(G) \right) \right. \\
&\quad \left. + e^{2B_1} \cosh(G) \tilde{F}_x - e^{B_1} \sinh(G) \tilde{F}_y + e^{2B_1} F_x^2 (B_1' \cosh(G) + B_2' \cosh(G) + G' \sinh(G)) \right. \\
&\quad \left. + F_y^2 (-B_1' \cosh(G) + B_2' \cosh(G) + G' \sinh(G)) - e^{B_1} \hat{F}_x \sinh(G) + \hat{F}_y \cosh(G) \right) \\
&\quad + \frac{1}{2} e^{B_2-B_1} \left(-2F_y \left(\hat{S} \cosh(G) - e^{B_1} \sinh(G) (\tilde{S} - F_x S') \right) + e^{B_1} F_x \left(2\hat{S} \sinh(G) \right. \right. \\
&\quad \left. \left. - e^{B_1} \cosh(G) (2\tilde{S} - F_x S') \right) + F_y^2 \cosh(G) S' \right) + 3\dot{S} S^2.
\end{aligned}$$

We solve equation (B.20) with the Newton-Kantorovich method by linearizing the equation around an guessed solution $\sigma_0(x, y)$. Expanding the operator \mathcal{L} we obtain

$$\begin{aligned}
\mathcal{L}(\sigma, \partial\sigma, \partial^2\sigma) &= \left(\mathcal{L} + \frac{\partial\mathcal{L}}{\partial\sigma} + \frac{\partial\mathcal{L}}{\partial(\partial_x\sigma)} \partial_x + \frac{\partial\mathcal{L}}{\partial(\partial_y\sigma)} \partial_y + \frac{\partial\mathcal{L}}{\partial(\partial_{xx}\sigma)} \partial_{xx} + \frac{\partial\mathcal{L}}{\partial(\partial_{xy}\sigma)} \partial_{xy} \right. \\
&\quad \left. + \frac{\partial\mathcal{L}}{\partial(\partial_{yy}\sigma)} \partial_{yy} \right)_{\sigma=\sigma_0} \delta\sigma + \mathcal{O}(\delta\sigma^2) = 0,
\end{aligned} \tag{B.21}$$

where $\delta\sigma = \sigma(x, y) - \sigma_0(x, y)$. The associated linear problem for the correction $\delta\sigma$ is then

$$\begin{aligned}
&[\alpha_{xx}(\sigma_0) \partial_{xx} + \alpha_{xy}(\sigma_0) \partial_{xy} + \alpha_{yy}(\sigma_0) \partial_{yy} + (\gamma_x(\sigma_0) + 2\beta_{xx}(\sigma_0) \partial_x \sigma_0 + \beta_{xy}(\sigma_0) \partial_y \sigma_0) \partial_x \\
&\quad + (\gamma_y(\sigma_0) + 2\beta_{yy}(\sigma_0) \partial_y \sigma_0 + \beta_{xy}(\sigma_0) \partial_x \sigma_0) \partial_y + \partial_\sigma \mathcal{L}(\sigma_0)] \delta\sigma = -\mathcal{L}(\sigma_0, \partial\sigma_0, \partial^2\sigma_0),
\end{aligned} \tag{B.22}$$

which has the same functional form as that of equation (8.20) and that we solve in the same fashion. For the purpose of implementing this into the code, what remains is the rewriting of the coefficients in terms of the outer grid redefinitions.

References

- [1] T. Giannakopoulos, D. Hilditch, and M. Zilhão, “Hyperbolicity of General Relativity in Bondi-like gauges,” *Phys. Rev. D* **102**, 064035 (2020), [arXiv:2007.06419](#).
- [2] T. Giannakopoulos, N.T. Bishop, D. Hilditch, D. Pollney, and M. Zilhão, “Gauge structure of the Einstein field equations in Bondi-like coordinates,” *Phys. Rev. D* **105**, 084055 (2022), [arXiv:2111.14794](#).
- [3] Y. Bea, J. Casalderrey-Solana, T. Giannakopoulos, A. Jansen, S. Krippendorf, D. Mateos, M. Sanchez-Garitaonandia, and M. Zilhão, “Spinodal Gravitational Waves,” (2021), [arXiv:2112.15478](#).
- [4] Y. Bea, J. Casalderrey-Solana, T. Giannakopoulos, A. Jansen, D. Mateos, M. Sanchez-Garitaonandia, and M. Zilhão, “Holographic Bubbles with Jecco: Expanding, Collapsing and Critical,” (2022), [arXiv:2202.10503](#).
- [5] Y. Bea, O.J.C. Dias, T. Giannakopoulos, D. Mateos, M. Sanchez-Garitaonandia, J.E. Santos, and M. Zilhao, “Crossing a large- N phase transition at finite volume,” *JHEP* **02**, 061 (2021), [arXiv:2007.06467](#).
- [6] Y. Bea, J. Casalderrey-Solana, T. Giannakopoulos, D. Mateos, M. Sanchez-Garitaonandia, and M. Zilhão, “Bubble wall velocity from holography,” *Phys. Rev. D* **104**, L121903 (2021), [arXiv:2104.05708](#).
- [7] Y. Bea, J. Casalderrey-Solana, T. Giannakopoulos, D. Mateos, M. Sanchez-Garitaonandia, and M. Zilhão, “Domain collisions,” *JHEP* **06**, 025 (2022), [arXiv:2111.03355](#).
- [8] A. Einstein, “Zur allgemeinen relativitätstheorie,” *Preuss. Akad. Wiss. Berlin, Sitzungsber.*, 778 (1915).
- [9] A. Einstein, “The Foundation of the General Theory of Relativity,” *Einstein Papers Project (English translation supplement)* **6**, 146 (1916), translation from H. A. Lorentz et al.
- [10] B.P. Abbott *et al.*, “Observation of Gravitational Waves from a Binary Black Hole Merger,” *Phys. Rev. Lett.* **116**, 061102 (2016), [arXiv:1602.03837](#).
- [11] B. Abbott *et al.* (LIGO Scientific, Virgo), “GW170817: Observation of Gravitational Waves from a Binary Neutron Star Inspiral,” *Phys. Rev. Lett.* **119**, 161101 (2017), [arXiv:1710.05832](#).

-
- [12] B. Abbott *et al.* (LIGO Scientific Collaboration and Virgo Collaboration), “Binary black hole mergers in the first advanced ligo observing run,” *Phys. Rev. X* **6**, 041015 (2016).
- [13] B. Abbott *et al.* (LIGO Scientific Collaboration and Virgo Collaboration), “Gwtc-1: A gravitational-wave transient catalog of compact binary mergers observed by ligo and virgo during the first and second observing runs,” *Phys. Rev. X* **9**, 031040 (2019).
- [14] R. Abbott *et al.* (LIGO Scientific, VIRGO, KAGRA), “GWTC-3: Compact Binary Coalescences Observed by LIGO and Virgo During the Second Part of the Third Observing Run,” (2021), [arXiv:2111.03606](https://arxiv.org/abs/2111.03606).
- [15] K. Akiyama *et al.* (Event Horizon Telescope), “First M87 Event Horizon Telescope Results. I. The Shadow of the Supermassive Black Hole,” *Astrophys. J. Lett.* **875**, L1 (2019), [arXiv:1906.11238](https://arxiv.org/abs/1906.11238).
- [16] K. Akiyama *et al.* (Event Horizon Telescope), “First Sagittarius A* Event Horizon Telescope Results. I. The Shadow of the Supermassive Black Hole in the Center of the Milky Way,” *Astrophys. J. Lett.* **930**, L12 (2022).
- [17] M.M. D. Kramer, H. Stephani and E. Herlt, *Exact Solutions of Einstein’s Field Equations* (Cambridge University Press, Cambridge, 1980).
- [18] K. Schwarzschild, “Über das Gravitationsfeld eines Massenpunktes nach der Einsteinschen Theorie,” *Sitzungsber. Dtsch. Akad. Wiss. Berlin, Kl. Math. Phys. Tech.* , 189 (1916).
- [19] R.P. Kerr, “Gravitational field of a spinning mass as an example of algebraically special metrics,” *Phys. Rev. Lett.* **11**, 237 (1963).
- [20] C.W. Misner, K.S. Thorne, and J.A. Wheeler, *Gravitation* (W. H. Freeman, San Francisco, 1973).
- [21] R.M. Wald, *General Relativity* (University of Chicago Press, Chicago, 1984).
- [22] S.M. Carroll, *Spacetime and Geometry: An Introduction to General Relativity* (Benjamin Cummings, 2003).
- [23] E. Poisson, *A Relativist’s Toolkit: The Mathematics of Black-Hole Mechanics* (Cambridge University Press, 2004).
- [24] R. Penrose, “Asymptotic properties of fields and spacetimes,” *Phys. Rev. Lett.* **10**, 66 (1963).
- [25] J. Natário, “Mathematical relativity,” (2020), [arXiv:2003.02855](https://arxiv.org/abs/2003.02855).
- [26] J. Aasi *et al.* (LIGO Scientific), “Advanced LIGO,” *Class. Quant. Grav.* **32**, 074001 (2015), [arXiv:1411.4547](https://arxiv.org/abs/1411.4547).

- [27] F. Acernese *et al.* (VIRGO), “Advanced Virgo: a second-generation interferometric gravitational wave detector,” *Class. Quant. Grav.* **32**, 024001 (2015), [arXiv:1408.3978](#).
- [28] T. Akutsu *et al.* (KAGRA), “Overview of KAGRA : KAGRA science,” (2020), [10.1093/ptep/ptaa120](#), [arXiv:2008.02921](#).
- [29] J. Luo *et al.* (TianQin), “TianQin: a space-borne gravitational wave detector,” *Class. Quant. Grav.* **33**, 035010 (2016), [arXiv:1512.02076](#).
- [30] W.H. Ruan, Z.K. Guo, R.G. Cai, and Y.Z. Zhang, “Taiji program: Gravitational-wave sources,” *Int. J. Mod. Phys. A* **35**, 2050075 (2020), [arXiv:1807.09495](#).
- [31] P. Amaro-Seoane *et al.*, “Laser interferometer space antenna,” (2017).
- [32] M. Maggiore *et al.*, “Science Case for the Einstein Telescope,” *JCAP* **03**, 050 (2020), [arXiv:1912.02622](#).
- [33] A. Buonanno and T. Damour, “Effective one-body approach to general relativistic two-body dynamics,” *Phys. Rev. D* **59**, 084006 (1999), [gr-qc/9811091](#).
- [34] P. Ajith, S. Babak, Y. Chen, M. Hewitson, B. Krishnan, J.T. Whelan, B. Brügmann, P. Diener, J.A. González, M. Hannam, S. Husa, M. Koppitz, D. Pollney, L. Rezzolla, L. Santamaria, A.M. Sintes, U. Sperhake, and J. Thornburg, “Phenomenological template family for black-hole coalescence waveforms,” *Class. Quantum Grav.* **24**, S689 (2007), [arXiv:0704.3764](#).
- [35] S.E. Field, C.R. Galley, J.S. Hesthaven, J. Kaye, and M. Tiglio, “Fast prediction and evaluation of gravitational waveforms using surrogate models,” (2013), [arXiv:1308.3565](#).
- [36] N.T. Bishop and L. Rezzolla, “Extraction of gravitational waves in numerical relativity,” *Living Reviews in Relativity* **19**, 2 (2016).
- [37] N.T. Bishop, R. Gómez, L. Lehner, and J. Winicour, “Cauchy-characteristic extraction in numerical relativity,” *Phys. Rev. D* **54**, 6153 (1996).
- [38] N.T. Bishop, R. Gómez, L. Lehner, M. Maharaj, and J. Winicour, “High-powered gravitational news,” *Phys. Rev. D* **56**, 6298 (1997), [gr-qc/9708065](#).
- [39] Y. Zlochower, R. Gómez, S. Husa, L. Lehner, and J. Winicour, “Mode coupling in the nonlinear response of black holes,” *Phys. Rev. D* **68**, 084014 (2003).
- [40] R. Gomez, W. Barreto, and S. Frittelli, “A Framework for large-scale relativistic simulations in the characteristic approach,” *Phys. Rev. D* **76**, 124029 (2007), [arXiv:0711.0564](#).
- [41] C. Reisswig, N.T. Bishop, D. Pollney, and B. Szilagyi, “Unambiguous determination of gravitational waveforms from binary black hole mergers,” *Phys. Rev. Lett.* **103**, 221101 (2009), [arXiv:0907.2637](#).

-
- [42] C. Reisswig, N. Bishop, D. Pollney, and B. Szilagyi, “Characteristic extraction in numerical relativity: binary black hole merger waveforms at null infinity,” *Class. Quant. Grav.* **27**, 075014 (2010), [arXiv:0912.1285](#).
- [43] C.J. Handmer and B. Szilagyi, “Spectral Characteristic Evolution: A New Algorithm for Gravitational Wave Propagation,” *Class. Quant. Grav.* **32**, 025008 (2015), [arXiv:1406.7029](#).
- [44] K. Barkett, J. Moxon, M.A. Scheel, and B. Szilágyi, “Spectral Cauchy-Characteristic Extraction of the Gravitational Wave News Function,” *Phys. Rev. D* **102**, 024004 (2020), [arXiv:1910.09677](#).
- [45] J. Moxon, M.A. Scheel, and S.A. Teukolsky, “Improved Cauchy-characteristic evolution system for high-precision numerical relativity waveforms,” *Phys. Rev. D* **102**, 044052 (2020), [arXiv:2007.01339](#).
- [46] D.A.B. Iozzo *et al.*, “Comparing Remnant Properties from Horizon Data and Asymptotic Data in Numerical Relativity,” *Phys. Rev. D* **103**, 124029 (2021), [arXiv:2104.07052](#).
- [47] K. Mitman *et al.*, “Adding gravitational memory to waveform catalogs using BMS balance laws,” *Phys. Rev. D* **103**, 024031 (2021), [arXiv:2011.01309](#).
- [48] D.A.B. Iozzo, M. Boyle, N. Deppe, J. Moxon, M.A. Scheel, L.E. Kidder, H.P. Pfeiffer, and S.A. Teukolsky, “Extending gravitational wave extraction using Weyl characteristic fields,” *Phys. Rev. D* **103**, 024039 (2021), [arXiv:2010.15200](#).
- [49] K. Mitman, J. Moxon, M.A. Scheel, S.A. Teukolsky, M. Boyle, N. Deppe, L.E. Kidder, and W. Thrope, “Computation of displacement and spin gravitational memory in numerical relativity,” *Phys. Rev. D* **102**, 104007 (2020), [arXiv:2007.11562](#).
- [50] F. Foucart *et al.*, “High-accuracy waveforms for black hole-neutron star systems with spinning black holes,” *Phys. Rev. D* **103**, 064007 (2021), [arXiv:2010.14518](#).
- [51] J. Moxon, M.A. Scheel, S.A. Teukolsky, N. Deppe, N. Fischer, F. Hébert, L.E. Kidder, and W. Thrope, “The SpECTRE Cauchy-characteristic evolution system for rapid, precise waveform extraction,” (2021), [arXiv:2110.08635](#).
- [52] B. Szilágyi, *Cauchy-Characteristic Matching In General Relativity*, Ph.D. thesis, University of Pittsburgh (2000).
- [53] J. Winicour, “Characteristic evolution and matching,” *Living Rev. Relativity* **15**, 2 (2012), [Online article].
- [54] H.O. Kreiss and J. Winicour, “The Well-posedness of the Null-Timelike Boundary Problem for Quasilinear Waves,” *Class. Quant. Grav.* **28**, 145020 (2011), [arXiv:1010.1201](#).

- [55] M.C. Babiuc, H.O. Kreiss, and J. Winicour, “Testing the well-posedness of characteristic evolution of scalar waves,” *Class. Quant. Grav.* **31**, 025022 (2014), [arXiv:1305.7179](#).
- [56] J.M. Stewart and H. Friedrich, “Numerical relativity I: the characteristic initial value problem,” *Proc. Roy. Soc. Lond. A* **384**, 427 (1982).
- [57] V. Moncrief and O. Rinne, “Regularity of the Einstein Equations at Future Null Infinity,” *Class. Quant. Grav.* **26**, 125010 (2009), [arXiv:0811.4109](#).
- [58] A. Zenginoglu, “Hyperboloidal layers for hyperbolic equations on unbounded domains,” *J. Comput. Phys.* **230**, 2286 (2011), [arXiv:1008.3809](#).
- [59] J.M. Bardeen, O. Sarbach, and L.T. Buchman, “Tetrad formalism for numerical relativity on conformally compactified constant mean curvature hypersurfaces,” *Phys. Rev. D* **83**, 104045 (2011), [arXiv:1101.5479](#).
- [60] A. Vañó-Viñuales, S. Husa, and D. Hilditch, “Spherical symmetry as a test case for unconstrained hyperboloidal evolution,” *Class. Quant. Grav.* **32**, 175010 (2015), [arXiv:1412.3827](#).
- [61] D. Hilditch, E. Harms, M. Bugner, H. Rüter, and B. Brügmann, “The evolution of hyperboloidal data with the dual foliation formalism: Mathematical analysis and wave equation tests,” *Class. Quant. Grav.* **35**, 055003 (2018), [arXiv:1609.08949](#).
- [62] M. Ansorg and R. Panosso Macedo, “Spectral decomposition of black-hole perturbations on hyperboloidal slices,” *Phys. Rev. D* **93**, 124016 (2016), [arXiv:1604.02261](#).
- [63] A. Vañó-Viñuales and S. Husa, “Spherical symmetry as a test case for unconstrained hyperboloidal evolution II: gauge conditions,” *Class. Quant. Grav.* **35**, 045014 (2018), [arXiv:1705.06298](#).
- [64] R. Panosso Macedo, B. Leather, N. Warburton, B. Wardell, and A. Zenginoglu, “Hyperboloidal method for frequency-domain self-force calculations,” *Phys. Rev. D* **105**, 104033 (2022), [arXiv:2202.01794](#).
- [65] P. Hübner, “A scheme to numerically evolve data for the conformal Einstein equation,” *Class. Quantum Grav.* **16**, 2823 (1999).
- [66] G. Doulis and J. Frauendiener, “Global simulations of Minkowski space-time including space-like infinity,” (2016), [arXiv:1609.03584](#).
- [67] G. Doulis, J. Frauendiener, C. Stevens, and B. Whale, “COFFEE – An MPI-parallelized Python package for the numerical evolution of differential equations,” (2019), [arXiv:1903.12482](#).
- [68] G. ’t Hooft, “Dimensional reduction in quantum gravity,” *Conf. Proc. C* **930308**, 284 (1993), [arXiv:gr-qc/9310026](#).

-
- [69] L. Susskind, “The World as a hologram,” *J. Math. Phys.* **36**, 6377 (1995), [arXiv:hep-th/9409089](#).
- [70] J.M. Maldacena, “The Large N limit of superconformal field theories and supergravity,” *Adv. Theor. Math. Phys.* **2**, 231 (1998), [arXiv:hep-th/9711200](#).
- [71] P. Kovtun, D.T. Son, and A.O. Starinets, “Holography and hydrodynamics: Diffusion on stretched horizons,” *JHEP* **10**, 064 (2003), [arXiv:hep-th/0309213](#).
- [72] J. Casalderrey-Solana, H. Liu, D. Mateos, K. Rajagopal, and U.A. Wiedemann, *Gauge/String Duality, Hot QCD and Heavy Ion Collisions* (Cambridge University Press, 2014) [arXiv:1101.0618](#).
- [73] M.B. Hindmarsh, M. Lüben, J. Lumma, and M. Pauly, “Phase transitions in the early universe,” *SciPost Phys. Lect. Notes* **24**, 1 (2021), [arXiv:2008.09136](#).
- [74] C. Caprini *et al.*, “Detecting gravitational waves from cosmological phase transitions with LISA: an update,” *JCAP* **03**, 024 (2020), [arXiv:1910.13125](#).
- [75] L. Del Zanna, V. Chandra, G. Inghirami, V. Rolando, A. Beraudo, A. De Pace, G. Pagliara, A. Drago, and F. Becattini, “Relativistic viscous hydrodynamics for heavy-ion collisions with ECHO-QGP,” *Eur. Phys. J. C* **73**, 2524 (2013), [arXiv:1305.7052](#).
- [76] C. Nonaka and S.A. Bass, “Space-time evolution of bulk QCD matter,” *Phys. Rev. C* **75**, 014902 (2007), [arXiv:nucl-th/0607018](#).
- [77] F. Becattini, G. Inghirami, V. Rolando, A. Beraudo, L. Del Zanna, A. De Pace, M. Nardi, G. Pagliara, and V. Chandra, “A study of vorticity formation in high energy nuclear collisions,” *Eur. Phys. J. C* **75**, 406 (2015), [Erratum: *Eur.Phys.J.C* 78, 354 (2018)], [arXiv:1501.04468](#).
- [78] H. Bantilan, P. Figueras, and D. Mateos, “Real-time Dynamics of Plasma Balls from Holography,” *Phys. Rev. Lett.* **124**, 191601 (2020), [arXiv:2001.05476](#).
- [79] H. Bantilan, P. Figueras, and L. Rossi, “Cauchy Evolution of Asymptotically Global AdS Spacetimes with No Symmetries,” *Phys. Rev. D* **103**, 086006 (2021), [arXiv:2011.12970](#).
- [80] G. Moschidis, “A proof of the instability of AdS for the Einstein–null dust system with an inner mirror,” *Anal. Part. Diff. Eq.* **13**, 1671 (2020), [arXiv:1704.08681](#).
- [81] D. Christoudolou, “The formation of black holes and singularities in spherically symmetric gravitational collapse,” *Communications on Pure and Applied Mathematics* **44**, 339 (1991).
- [82] M. Dafermos, G. Holzegel, I. Rodnianski, and M. Taylor, “The non-linear stability of the Schwarzschild family of black holes,” (2021), [arXiv:2104.08222](#).

- [83] S. Aretakis, “Stability and Instability of Extreme Reissner-Nordström Black Hole Spacetimes for Linear Scalar Perturbations I,” *Commun. Math. Phys.* **307**, 17 (2011), [arXiv:1110.2007](#).
- [84] S. Aretakis, “Horizon Instability of Extremal Black Holes,” *Adv. Theor. Math. Phys.* **19**, 507 (2015), [arXiv:1206.6598](#).
- [85] D. Garfinkle, “Choptuik scaling in null coordinates,” *Phys. Rev. D* **51**, 5558 (1995).
- [86] J.A. Crespo, H.P. de Oliveira, and J. Winicour, “Affine-null formulation of the gravitational equations: Spherical case,” *Phys. Rev. D* **100**, 104017 (2019), [arXiv:1910.03439](#).
- [87] C. Gundlach, T.W. Baumgarte, and D. Hilditch, “Critical phenomena in gravitational collapse with two competing massless matter fields,” *Phys. Rev. D* **100**, 104010 (2019), [arXiv:1908.05971](#).
- [88] F. Siebel, J.A. Font, E. Müller, and P. Papadopoulos, “Axisymmetric core collapse simulations using characteristic numerical relativity,” *Phys. Rev. D* **67**, 124018 (2003).
- [89] M.A. Alcoforado, W.O. Barreto, and H.P. de Oliveira, “The Bondi problem revisited: a spectral domain decomposition code,” (2021), [arXiv:2110.09640](#).
- [90] D. Santos-Olivan and C.F. Sopuerta, “New Features of Gravitational Collapse in Anti-de Sitter Spacetimes,” *Phys. Rev. Lett.* **116**, 041101 (2016), [arXiv:1511.04344](#).
- [91] D. Santos-Olivan, *Numerical Relativity studies in Anti-de Sitter spacetimes: Gravitational Collapse and the AdS/CFT correspondence*, Ph.D. thesis, Barcelona U. (2017).
- [92] P. Papadopoulos and J.A. Font, “Relativistic hydrodynamics on spacelike and null surfaces: Formalism and computations of spherically symmetric spacetimes,” *Phys. Rev. D* **61**, 024015 (1999).
- [93] F. Siebel, J.A. Font, E. Müller, and P. Papadopoulos, “Simulating the dynamics of relativistic stars via a light-cone approach,” *Phys. Rev. D* **65**, 064038 (2002).
- [94] R. Gómez, L. Lehner, R.L. Marsa, and J. Winicour, “Moving black holes in 3d,” *Phys. Rev. D* **57**, 4778 (1998).
- [95] R. Gómez, L. Lehner, R. Marsa, J. Winicour, A.M. Abrahams, A. Anderson, P. Anninos, T.W. Baumgarte, N.T. Bishop, S.R. Brandt, J.C. Browne, K. Camarda, M.W. Choptuik, G.B. Cook, R. Correll, C.R. Evans, L.S. Finn, G.C. Fox, T. Haupt, M.F. Huq, L.E. Kidder, S.A. Klasky, P. Laguna, W. Landry, J. Lenaghan, J. Masso, R.A. Matzner, S. Mitra, P. Papadopoulos, M. Parashar, L. Rezzolla, M.E. Rupright, F. Saied, P.E. Saylor, M.A. Scheel, E. Seidel, S.L. Shapiro, D. Shoemaker, L. Smarr, B. Szilágyi, S.A. Teukolsky, M.H.P.M. van Putten, P. Walker, and J.W. York Jr, “Stable characteristic evolution of generic three-dimensional single-black-hole spacetimes,” *Phys. Rev. Lett.* **80**, 3915 (1998), [gr-qc/9801069](#).

-
- [96] P.M. Chesler, “Hairy black resonators and the AdS4 superradiant instability,” *Phys. Rev. D* **105**, 024026 (2022), [arXiv:2109.06901](#).
- [97] P.J. van der Walt and N.T. Bishop, “Observational cosmology using characteristic numerical relativity: Characteristic formalism on null geodesics,” *Phys. Rev. D* **85**, 044016 (2012), [arXiv:1111.6025](#).
- [98] S. Bhattacharyya, V.E. Hubeny, S. Minwalla, and M. Rangamani, “Nonlinear Fluid Dynamics from Gravity,” *JHEP* **02**, 045 (2008), [arXiv:0712.2456](#).
- [99] M. Rangamani, “Gravity and Hydrodynamics: Lectures on the fluid-gravity correspondence,” *Class. Quant. Grav.* **26**, 224003 (2009), [arXiv:0905.4352](#).
- [100] V.E. Hubeny, S. Minwalla, and M. Rangamani, “The fluid/gravity correspondence,” in *Theoretical Advanced Study Institute in Elementary Particle Physics: String theory and its Applications: From meV to the Planck Scale* (2012) pp. 348–383, [arXiv:1107.5780](#).
- [101] D. Hilditch and R. Richter, “Hyperbolicity of Physical Theories with Application to General Relativity,” *Phys. Rev.* **D94**, 044028 (2016), [arXiv:1303.4783](#).
- [102] H.O. Kreiss and J. Lorenz, *Initial-boundary value problems and the Navier-Stokes equations* (Academic Press, New York, 1989).
- [103] B. Gustafsson, H.O. Kreiss, and J. Olinger, *Time dependent problems and difference methods* (Wiley, New York, 1995).
- [104] J.A. Valiente-Kroon, *Conformal Methods in General Relativity* (Cambridge University Press, Cambridge, 2016).
- [105] D. Hilditch, “An Introduction to Well-posedness and Free-evolution,” *Int. J. Mod. Phys.* **A28**, 1340015 (2013), [arXiv:1309.2012](#).
- [106] O. Sarbach and M. Tiglio, “Continuum and discrete initial-boundary value problems and einstein’s field equations,” *Living Reviews in Relativity* **15** (2012), [arXiv:1203.6443](#).
- [107] S. Frittelli, “Well-posed adm equivalent of the bondi-sachs problem,” *Phys. Rev. D* **73**, 124001 (2006).
- [108] Z. Cao and X. He, “Generalized bondi-sachs equations for characteristic formalism of numerical relativity,” *Phys. Rev. D* **88**, 104002 (2013).
- [109] D. Christodoulou, *The Formation of Black Holes in General Relativity*, EMS monographs in mathematics No. v. 4 (European Mathematical Society Publishing House, 2009).
- [110] H. Bondi, M.G.J. van der Burg, and A.W.K. Metzner, “Gravitational waves in general relativity VII. Waves from axi-symmetric isolated systems,” *Proc. Roy. Soc. A* **269**, 21 (1962).

-
- [111] J. Winicour, “Affine-null metric formulation of Einstein’s equations,” *Phys. Rev.* **D87**, 124027 (2013), [arXiv:1303.6969](#).
- [112] M. Alcubierre, *Introduction to 3+1 Numerical Relativity* (Oxford University Press, Oxford, 2008).
- [113] E.ourgoulhon, “3+1 formalism and bases of numerical relativity,” (2007), [gr-qc/0703035](#).
- [114] T.W. Baumgarte and S.L. Shapiro, *Numerical Relativity: Solving Einstein’s Equations on the Computer* (Cambridge University Press, Cambridge, 2010).
- [115] A.M. Khokhlov and I.D. Novikov, “Gauge stability of 3+1 formulations of general relativity,” *Class. Quantum Grav.* **19**, 827 (2002).
- [116] D. Hilditch, “Dual Foliation Formulations of General Relativity,” (2015), [arXiv:1509.02071](#).
- [117] F. Abalos and O. Reula, “On necessary and sufficient conditions for strong hyperbolicity in systems with constraints,” *Class. Quant. Grav.* **37**, 185012 (2020), [arXiv:1811.05558](#).
- [118] J.F. Abalos, “On constraint preservation and strong hyperbolicity,” (2021), [arXiv:2111.06295](#).
- [119] C. Gundlach and J.M. Martín-García, “Hyperbolicity of second-order in space systems of evolution equations,” *Class. Quantum Grav.* **23**, S387 (2006), [gr-qc/0506037](#).
- [120] D. Hilditch and R. Richter, “Hyperbolicity of High Order Systems of Evolution Equations,” *J. Hyper. Differential Equations* **12** (2015), [arXiv:1412.6034](#).
- [121] T. Giannakopoulos, D. Hilditch, and M. Zilhão, “Hyperbolicity of General Relativity in Bondi-like gauges,” (2020).
- [122] S. Frittelli and L. Lehner, “Existence and uniqueness of solutions to characteristic evolution in Bondi-Sachs coordinates in General Relativity,” *Phys. Rev. D* **59**, 084012 (1999).
- [123] R. Gomez and S. Frittelli, “First order quasilinear canonical representation of the characteristic formulation of the Einstein equations,” *Phys. Rev. D* **68**, 084013 (2003), [arXiv:gr-qc/0303104](#).
- [124] A.D. Rendall, “Reduction of the Characteristic Initial Value Problem to the Cauchy Problem and Its Applications to the Einstein Equations,” *Proceedings of the Royal Society A: Mathematical, Physical and Engineering Sciences* **427**, 221 (1990).
- [125] R.M. Balean, *The null-timelike boundary problem*, [Ph.D. thesis](#), University of New England (1997).

- [126] L. Zhang and X. Wu, “The null-timelike boundary problems of linear wave equations in asymptotically anti-de Sitter spacetime,” *Class. Quant. Grav.* **37**, 165005 (2020).
- [127] P.M. Chesler and L.G. Yaffe, “Numerical solution of gravitational dynamics in asymptotically anti-de Sitter spacetimes,” *JHEP* **07**, 086 (2014), [arXiv:1309.1439](#).
- [128] R.K. Sachs, “Gravitational waves in general relativity,” *Proc. Roy. Soc. A* **270**, 103 (1962).
- [129] S. Frittelli, “Well-posed first-order reduction of the characteristic problem of the linearized Einstein equations,” *Phys. Rev. D* **71**, 024021 (2005), [arXiv:gr-qc/0408035x](#).
- [130] J. Luk, “On the local existence for the characteristic initial value problem in general relativity,” *International Mathematics Research Notices* **2012**, 4625 (2012), [arXiv:1107.0898](#).
- [131] D. Hilditch, J.A.V. Kroon, and P. Zhao, “Revisiting the characteristic initial value problem for the vacuum Einstein field equations,” (2019), [arXiv:1911.00047](#).
- [132] J.L. Ripley, “A symmetric hyperbolic formulation of the vacuum Einstein equations in affine-null coordinates,” *J. Math. Phys.* **62**, 062501 (2021), [arXiv:2104.09972](#).
- [133] A. Schoepe, D. Hilditch, and M. Bugner, “Revisiting Hyperbolicity of Relativistic Fluids,” *Phys. Rev.* **D97**, 123009 (2018), [arXiv:1712.09837](#).
- [134] D. Hilditch and A. Schoepe, “Hyperbolicity of divergence cleaning and vector potential formulations of general relativistic magnetohydrodynamics,” *Phys. Rev. D* **99**, 104034 (2019), [arXiv:1812.03485](#).
- [135] I. Rácz, “Stationary Black Holes as Holographs II,” *Class. Quant. Grav.* **31**, 035006 (2014), [arXiv:1307.1683](#).
- [136] A. Cabet, P.T. Chruściel, and R.T. Wafo, “On the characteristic initial value problem for nonlinear symmetric hyperbolic systems, including Einstein equations,” (2014), [arXiv:1406.3009](#).
- [137] N.T. Bishop, R. Gómez, P.R. Holvorcem, R.A. Matzner, P. Papadopoulos, and J. Winicour, “Cauchy-characteristic matching: A new approach to radiation boundary conditions,” *Phys. Rev. Lett.* **76**, 4303 (1996).
- [138] N.T. Bishop, R. Gómez, P.R. Holvorcem, R.A. Matzner, P. Papadopoulos, and J. Winicour, “Cauchy-characteristic evolution and wave-forms,” *J. Comput. Phys.* **136**, 236 (1997).
- [139] G. Calabrese, “Exact boundary conditions in numerical relativity using multiple grids: Scalar field tests,” *Class. Quant. Grav.* **23**, 5439 (2006), [arXiv:gr-qc/0604034](#).

- [140] T. Giannakopoulos, “Characteristic formulations of general relativity and applications: Phd thesis supplementary material,” (2022), <https://github.com/ThanasisGiannakopoulos/PhD-thesis-supp>.
- [141] H. Ringström, *The Cauchy Problem in General Relativity* (European Mathematical Society, 2009).
- [142] D. Hilditch, J.A.V. Kroon, and P. Zhao, “Improved existence for the characteristic initial value problem with the conformal Einstein field equations,” (2020), [arXiv:2006.13757](https://arxiv.org/abs/2006.13757).
- [143] A. Vañó-Viñuales, *Free evolution of the hyperboloidal initial value problem in spherical symmetry*, Ph.D. thesis, U. Iles Balears, Palma (2015), [arXiv:1512.00776](https://arxiv.org/abs/1512.00776).
- [144] E. Gasperin and D. Hilditch, “The Weak Null Condition in Free-evolution Schemes for Numerical Relativity: Dual Foliation GHG with Constraint Damping,” *Class. Quant. Grav.* **36**, 195016 (2019), [arXiv:1812.06550](https://arxiv.org/abs/1812.06550).
- [145] E. Gasperin, S. Gautam, D. Hilditch, and A. Vañó-Viñuales, “The Hyperboloidal Numerical Evolution of a Good-Bad-Ugly Wave Equation,” (2019), [arXiv:1909.11749](https://arxiv.org/abs/1909.11749).
- [146] F. Beyer, J. Frauendiener, and J. Hennig, “Explorations of the infinite regions of space-time,” (2020), [arXiv:2005.11936](https://arxiv.org/abs/2005.11936).
- [147] C.W. Shu and S.J. Osher, “Efficient Implementation of Essentially Non-Oscillatory Shock-Capturing Schemes, I,” *J. Comput. Phys.* **77**, 439 (1988).
- [148] Bezanson, Jeff and Edelman, Alan and Karpinski, Stefan and Shah, Viral B, “Julia: A fresh approach to numerical computing,” *SIAM Review* **59**, 65 (2017).
- [149] C. Rackauckas and Q. Nie, “Differentials.jl – a performant and feature-rich ecosystem for solving differential equations in julia,” *The Journal of Open Research Software* **5** (2017), 10.5334/jors.151.
- [150] M. Alcubierre, G. Allen, T.W. Baumgarte, C. Bona, D. Fiske, T. Goodale, F.S. Guzmán, I. Hawke, S. Hawley, S. Husa, M. Koppitz, C. Lechner, L. Lindblom, D. Pollney, D. Rideout, M. Salgado, E. Schnetter, E. Seidel, H. aki Shinkai, D. Shoemaker, B. Szilágyi, R. Takahashi, and J. Winicour, “Towards standard testbeds for numerical relativity,” *Class. Quantum Grav.* **21**, 589 (2004), [gr-qc/0305023](https://arxiv.org/abs/gr-qc/0305023).
- [151] G. Calabrese, I. Hinder, and S. Husa, “Numerical stability for finite difference approximations of Einstein’s equations,” *J. Comp. Phys.* **218**, 607 (2005), [gr-qc/0503056](https://arxiv.org/abs/gr-qc/0503056).
- [152] I. Hinder, *Well-posed formulations and stable finite differencing schemes for numerical relativity*, Ph.D. thesis, School of Mathematics, University of Southampton (2005).
- [153] M. Boyle, L. Lindblom, H. Pfeiffer, M. Scheel, and L.E. Kidder, “Testing the Accuracy and Stability of Spectral Methods in Numerical Relativity,” *Phys. Rev.* **D75**, 024006 (2007), [arXiv:gr-qc/0609047](https://arxiv.org/abs/gr-qc/0609047).

- [154] M.C. Babiuc *et al.*, “Implementation of standard testbeds for numerical relativity,” *Class. Quant. Grav.* **25**, 125012 (2008), [arXiv:0709.3559](#).
- [155] H. Witek, D. Hilditch, and U. Sperhake, “Stability of the puncture method with a generalized BSSN formulation,” *Phys. Rev.* **D83**, 104041 (2011), [arXiv:1011.4407](#).
- [156] Z. Cao and D. Hilditch, “Numerical stability of the Z4c formulation of general relativity,” *Phys. Rev. D* **85**, 124032 (2012), [arXiv:1111.2177](#).
- [157] J. Thomas, *Numerical Partial Differential Equations: Finite Difference Methods*, Texts in Applied Mathematics (Springer New York, 1998).
- [158] R. Haas, S.R. Brandt, W.E. Gabella, M. Gracia-Linares, B. Karakaş, R. Matur, M. Alcubierre, D. Alic, G. Allen, M. Ansorg, M. Babiuc-Hamilton, L. Baiotti, W. Bengert, E. Bentivegna, S. Bernuzzi, T. Bode, B. Bruegmann, M. Campanelli, F. Ciolletta, G. Corvino, S. Cupp, R.D. Pietri, P. Diener, H. Dimmelmeier, R. Dooley, N. Dorband, M. Elley, Y.E. Khamra, Z. Etienne, J. Faber, T. Font, J. Frieben, B. Giacomazzo, T. Goodale, C. Gundlach, I. Hawke, S. Hawley, I. Hinder, S. Husa, S. Iyer, T. Kellermann, A. Knapp, M. Koppitz, P. Laguna, G. Lanferman, F. Löffler, J. Masso, L. Menger, A. Merzky, J.M. Miller, M. Miller, P. Moesta, P. Montero, B. Mundim, A. Nerozzi, S.C. Noble, C. Ott, R. Paruchuri, D. Pollney, D. Radice, T. Radke, C. Reisswig, L. Rezzolla, D. Rideout, M. Ripeanu, L. Sala, J.A. Schewtschenko, E. Schnetter, B. Schutz, E. Seidel, E. Seidel, J. Shalf, K. Sible, U. Sperhake, N. Stergioulas, W.M. Suen, B. Szilágyi, R. Takahashi, M. Thomas, J. Thornburg, M. Tobias, A. Tonita, P. Walker, M.B. Wan, B. Wardell, H. Witek, M. Zilhão, B. Zink, and Y. Zlochower, “The einstein toolkit,” (2020), to find out more, visit <http://einstein toolkit.org>.
- [159] M.C. Babiuc, N.T. Bishop, B. Szilágyi, and J. Winicour, “Strategies for the characteristic extraction of gravitational waveforms,” *Phys. Rev. D* **79**, 084011 (2009).
- [160] M.C. Babiuc, B. Szilágyi, J. Winicour, and Y. Zlochower, “Characteristic extraction tool for gravitational waveforms,” *Phys. Rev. D* **84**, 044057 (2011).
- [161] T. Giannakopoulos, N.T. Bishop, D. Hilditch, D. Pollney, and M. Zilhão, “Gauge structure of the Einstein field equations in Bondi-like coordinates: convergence tests data,” (2021).
- [162] R. Gómez, L. Lehner, P. Papadopoulos, and J. Winicour, “The eth formalism in numerical relativity,” *Class. Quantum Grav.* **14**, 977 (1997), [gr-qc/9702002](#).
- [163] C. Reisswig, N.T. Bishop, and D. Pollney, “General relativistic null-cone evolutions with a high-order scheme,” *Gen.Rel.Grav.* **45**, 1069 (2013), [arXiv:1208.3891](#).
- [164] N.T. Bishop, “Linearized solutions of the Einstein equations within a Bondi-Sachs framework, and implications for boundary conditions in numerical simulations,” *Class. Quantum Grav.* **22**, 2393 (2005).

- [165] C. Reisswig, N.T. Bishop, C.W. Lai, J. Thornburg, and B. Szilagyi, “Numerical relativity with characteristic evolution, using six angular patches,” *Class. Quant. Grav.* **24**, S327 (2007), [arXiv:gr-qc/0610019](#).
- [166] E. Witten, “Anti-de Sitter space and holography,” *Adv. Theor. Math. Phys.* **2**, 253 (1998), [arXiv:hep-th/9802150](#).
- [167] P.M. Chesler and L.G. Yaffe, “Horizon formation and far-from-equilibrium isotropization in supersymmetric Yang-Mills plasma,” *Phys. Rev. Lett.* **102**, 211601 (2009), [arXiv:0812.2053](#).
- [168] M.P. Heller, D. Mateos, W. van der Schee, and M. Triana, “Holographic isotropization linearized,” *JHEP* **09**, 026 (2013), [arXiv:1304.5172](#).
- [169] U. Gürsoy, A. Jansen, W. Sybesma, and S. Vandoren, “Holographic Equilibration of Nonrelativistic Plasmas,” *Phys. Rev. Lett.* **117**, 051601 (2016), [arXiv:1602.01375](#).
- [170] P.M. Chesler and L.G. Yaffe, “Holography and colliding gravitational shock waves in asymptotically AdS_5 spacetime,” *Phys. Rev. Lett.* **106**, 021601 (2011), [arXiv:1011.3562](#).
- [171] J. Casalderrey-Solana, M.P. Heller, D. Mateos, and W. van der Schee, “Longitudinal Coherence in a Holographic Model of Asymmetric Collisions,” *Phys. Rev. Lett.* **112**, 221602 (2014), [arXiv:1312.2956](#).
- [172] P.M. Chesler and L.G. Yaffe, “Holography and off-center collisions of localized shock waves,” *JHEP* **10**, 070 (2015), [arXiv:1501.04644](#).
- [173] K. Balasubramanian and C.P. Herzog, “Losing Forward Momentum Holographically,” *Class. Quant. Grav.* **31**, 125010 (2014), [arXiv:1312.4953](#).
- [174] S.R. Green, F. Carrasco, and L. Lehner, “Holographic Path to the Turbulent Side of Gravity,” *Phys. Rev. X* **4**, 011001 (2014), [arXiv:1309.7940](#).
- [175] A. Adams, P.M. Chesler, and H. Liu, “Holographic turbulence,” *Phys. Rev. Lett.* **112**, 151602 (2014), [arXiv:1307.7267](#).
- [176] M. Attems, J. Casalderrey-Solana, D. Mateos, D. Santos-Oliván, C.F. Sopena, M. Triana, and M. Zilhão, “Holographic Collisions in Non-conformal Theories,” *JHEP* **01**, 026 (2017), [arXiv:1604.06439](#).
- [177] M. Attems, J. Casalderrey-Solana, D. Mateos, D. Santos-Oliván, C.F. Sopena, M. Triana, and M. Zilhão, “Paths to equilibrium in non-conformal collisions,” *JHEP* **06**, 154 (2017), [arXiv:1703.09681](#).
- [178] M. Attems, Y. Bea, J. Casalderrey-Solana, D. Mateos, M. Triana, and M. Zilhao, “Phase Transitions, Inhomogeneous Horizons and Second-Order Hydrodynamics,” *JHEP* **06**, 129 (2017), [arXiv:1703.02948](#).

-
- [179] R.A. Janik, J. Jankowski, and H. Soltanpanahi, “Real-Time dynamics and phase separation in a holographic first order phase transition,” *Phys. Rev. Lett.* **119**, 261601 (2017), [arXiv:1704.05387](#).
- [180] M. Attems, Y. Bea, J. Casalderrey-Solana, D. Mateos, and M. Zilhão, “Dynamics of Phase Separation from Holography,” *JHEP* **01**, 106 (2020), [arXiv:1905.12544](#).
- [181] L. Bellantuono, R.A. Janik, J. Jankowski, and H. Soltanpanahi, “Dynamics near a first order phase transition,” *JHEP* **10**, 146 (2019), [arXiv:1906.00061](#).
- [182] R.A. Janik, M. Jarvinen, and J. Sonnenschein, “A simple description of holographic domain walls in confining theories — extended hydrodynamics,” *JHEP* **09**, 129 (2021), [arXiv:2106.02642](#).
- [183] M. Attems, Y. Bea, J. Casalderrey-Solana, D. Mateos, M. Triana, and M. Zilhão, “Holographic Collisions across a Phase Transition,” *Phys. Rev. Lett.* **121**, 261601 (2018), [arXiv:1807.05175](#).
- [184] U. Gürsoy, A. Jansen, and W. van der Schee, “New dynamical instability in asymptotically anti-de Sitter spacetime,” *Phys. Rev. D* **94**, 061901 (2016), [arXiv:1603.07724](#).
- [185] M. Ahmadvand and K. Bitaghsir Fadafan, “Gravitational waves generated from the cosmological QCD phase transition within AdS/QCD,” *Phys. Lett. B* **772**, 747 (2017), [arXiv:1703.02801](#).
- [186] M. Ahmadvand and K. Bitaghsir Fadafan, “The cosmic QCD phase transition with dense matter and its gravitational waves from holography,” *Phys. Lett. B* **779**, 1 (2018), [arXiv:1707.05068](#).
- [187] F. Bigazzi, A. Caddeo, A.L. Cotrone, and A. Paredes, “Dark Holograms and Gravitational Waves,” *JHEP* **04**, 094 (2021), [arXiv:2011.08757](#).
- [188] F.R. Ares, M. Hindmarsh, C. Hoyos, and N. Jokela, “Gravitational waves from a holographic phase transition,” *JHEP* **21**, 100 (2020), [arXiv:2011.12878](#).
- [189] F.R. Ares, O. Henriksson, M. Hindmarsh, C. Hoyos, and N. Jokela, “Gravitational Waves at Strong Coupling from an Effective Action,” (2021), [arXiv:2110.14442](#).
- [190] F. Bigazzi, A. Caddeo, A.L. Cotrone, and A. Paredes, “Fate of false vacua in holographic first-order phase transitions,” *JHEP* **12**, 200 (2020), [arXiv:2008.02579](#).
- [191] F. Bigazzi, A. Caddeo, T. Canneti, and A.L. Cotrone, “Bubble wall velocity at strong coupling,” *JHEP* **08**, 090 (2021), [arXiv:2104.12817](#).
- [192] F.R. Ares, O. Henriksson, M. Hindmarsh, C. Hoyos, and N. Jokela, “Effective actions and bubble nucleation from holography,” (2021), [arXiv:2109.13784](#).
- [193] P. Bosch, S.R. Green, and L. Lehner, “Nonlinear Evolution and Final Fate of Charged

- Anti-de Sitter Black Hole Superradiant Instability,” *Phys. Rev. Lett.* **116**, 141102 (2016), [arXiv:1601.01384](#).
- [194] H. Bantilan, F. Pretorius, and S.S. Gubser, “Simulation of Asymptotically AdS5 Spacetimes with a Generalized Harmonic Evolution Scheme,” *Phys. Rev.* **D85**, 084038 (2012), [arXiv:1201.2132](#).
- [195] M. Zilhao, M. Sanchez-Garitaonandia, and T. Giannakopoulos, “[Jecco.jl](#),” (2022).
- [196] Y. Bea and D. Mateos, “Heating up Exotic RG Flows with Holography,” *JHEP* **08**, 034 (2018), [arXiv:1805.01806](#).
- [197] M. Attems, J. Casalderrey-Solana, D. Mateos, I. Papadimitriou, D. Santos-Oliván, C.F. Sopena, M. Triana, and M. Zilhão, “Thermodynamics, transport and relaxation in non-conformal theories,” *JHEP* **10**, 155 (2016), [arXiv:1603.01254](#).
- [198] Bezanson, Jeff and Edelman, Alan and Karpinski, Stefan and Shah, Viral B, “Julia: A fresh approach to numerical computing,” *SIAM Review* **59**, 65 (2017).
- [199] B. Fornberg, “Classroom note: calculation of weights in finite difference formulas,” *SIAM Review* **40**, 685 (1998), <https://doi.org/10.1137/S0036144596322507>.
- [200] A. Huebl, R. Lehe, J.L. Vay, D.P. Grote, I. Sbalzarini, S. Kuschel, D. Sagan, F. Pérez, F. Koller, and M. Bussmann, “[openPMD 1.1.0: Base paths for mesh- and particle-only files and updated attributes](#),” (2018).
- [201] J.P. Boyd, *Chebyshev and Fourier Spectral Methods (Second Edition, Revised)* (Dover Publications, New York, 2001).
- [202] L.N. Trefethen, *Spectral Methods in MATLAB*, Software, Environments, and Tools (SIAM, Philadelphia, 2000).
- [203] A. Krikun, “Numerical solution of the boundary value problems for partial differential equations. crash course for holographer,” [1801.01483v1](#).
- [204] H.O. Kreiss and J. Olinger, *Methods for the Approximate Solution of Time Dependent Problem* (World Meteorological Organization, Case Postale No. 1, CH-1211 Geneva 20, Switzerland, 1973).
- [205] A. Kanevsky, M.H. Carpenter, and J.S. Hesthaven, “Idempotent filtering in spectral and spectral element methods,” *Journal of Computational Physics* **220**, 41 (2006).
- [206] P.D. Lax and R.D. Richtmyer, “Survey of the stability of linear finite difference equations,” *Communications on Pure and Applied Mathematics* **9**, 267 (1956).
- [207] V. Kalogera *et al.*, “The Next Generation Global Gravitational Wave Observatory: The Science Book,” (2021), [arXiv:2111.06990](#).

- [208] Y. Aoki, G. Endrodi, Z. Fodor, S.D. Katz, and K.K. Szabo, “The Order of the quantum chromodynamics transition predicted by the standard model of particle physics,” *Nature* **443**, 675 (2006), [arXiv:hep-lat/0611014](#).
- [209] K. Kajantie, M. Laine, K. Rummukainen, and M.E. Shaposhnikov, “Is there a hot electroweak phase transition at $m(H)$ larger or equal to $m(W)$?” *Phys. Rev. Lett.* **77**, 2887 (1996), [arXiv:hep-ph/9605288](#).
- [210] M. Laine and K. Rummukainen, “A Strong electroweak phase transition up to $m(H)$ is about 105-GeV,” *Phys. Rev. Lett.* **80**, 5259 (1998), [arXiv:hep-ph/9804255](#).
- [211] K. Rummukainen, M. Tsy-pin, K. Kajantie, M. Laine, and M.E. Shaposhnikov, “The Universality class of the electroweak theory,” *Nucl. Phys. B* **532**, 283 (1998), [arXiv:hep-lat/9805013](#).
- [212] M. Carena, M. Quiros, and C.E.M. Wagner, “Opening the window for electroweak baryogenesis,” *Phys. Lett. B* **380**, 81 (1996), [arXiv:hep-ph/9603420](#).
- [213] D. Delepine, J.M. Gerard, R. Gonzalez Felipe, and J. Weyers, “A Light stop and electroweak baryogenesis,” *Phys. Lett. B* **386**, 183 (1996), [arXiv:hep-ph/9604440](#).
- [214] M. Laine and K. Rummukainen, “The MSSM electroweak phase transition on the lattice,” *Nucl. Phys. B* **535**, 423 (1998), [arXiv:hep-lat/9804019](#).
- [215] S.J. Huber and M.G. Schmidt, “Electroweak baryogenesis: Concrete in a SUSY model with a gauge singlet,” *Nucl. Phys. B* **606**, 183 (2001), [arXiv:hep-ph/0003122](#).
- [216] C. Grojean, G. Servant, and J.D. Wells, “First-order electroweak phase transition in the standard model with a low cutoff,” *Phys. Rev. D* **71**, 036001 (2005), [arXiv:hep-ph/0407019](#).
- [217] S.J. Huber, T. Konstandin, T. Prokopec, and M.G. Schmidt, “Baryogenesis in the MSSM, nMSSM and NMSSM,” *Nucl. Phys. A* **785**, 206 (2007), [arXiv:hep-ph/0608017](#).
- [218] S. Profumo, M.J. Ramsey-Musolf, and G. Shaughnessy, “Singlet Higgs phenomenology and the electroweak phase transition,” *JHEP* **08**, 010 (2007), [arXiv:0705.2425](#).
- [219] V. Barger, P. Langacker, M. McCaskey, M.J. Ramsey-Musolf, and G. Shaughnessy, “LHC Phenomenology of an Extended Standard Model with a Real Scalar Singlet,” *Phys. Rev. D* **77**, 035005 (2008), [arXiv:0706.4311](#).
- [220] M. Laine, G. Nardini, and K. Rummukainen, “Lattice study of an electroweak phase transition at $m_h \simeq 126$ GeV,” *JCAP* **01**, 011 (2013), [arXiv:1211.7344](#).
- [221] G.C. Dorsch, S.J. Huber, and J.M. No, “A strong electroweak phase transition in the 2HDM after LHC8,” *JHEP* **10**, 029 (2013), [arXiv:1305.6610](#).
- [222] P.H. Damgaard, A. Haarr, D. O’Connell, and A. Tranberg, “Effective Field Theory

- and Electroweak Baryogenesis in the Singlet-Extended Standard Model,” *JHEP* **02**, 107 (2016), [arXiv:1512.01963](#).
- [223] S.S. Gubser and A. Nellore, “Mimicking the QCD equation of state with a dual black hole,” *Phys. Rev. D* **78**, 086007 (2008), [arXiv:0804.0434](#).
- [224] M. Ahmadvand, K. Bitaghsir Fadafan, and S. Rezapour, “Gravitational waves of a first-order QCD phase transition at finite coupling from holography,” (2020), [arXiv:2006.04265](#).
- [225] E.T. Newman and R. Penrose, “An approach to gravitational radiation by a method of spin coefficients,” *J. Math. Phys.* **3**, 566 (1962), erratum in *J. Math. Phys.* 4, 998 (1963).
- [226] R. Geroch, A. Held, and R. Penrose, “A space-time calculus based on pairs of null directions,” *Journal of Mathematical Physics* **14**, 874 (1973), publisher: American Institute of Physics.